UNIVERSIDADE D
COIMBRA

Saskia Theresa Maria Ammer

REUNITING THE REMAINS OF UNDOCUMENTED BORDER CROSSERS WITH THEIR FAMILIES THROUGH ISOTOPE ANALYSIS

Tese no âmbito do Doutoramento em Antropologia, Antropologia Forense, orientada pela Professora Doutora Eugénia Cunha, Professor Doutor Bruce Anderson e Professor Doutor Eric Bartelink e apresentada ao Departamento de Ciências da Vida da Faculdade de Ciências e Tecnologia da Universidade de Coimbra.

Novembro de 2020

FACULDADE DE
CIÊNCIAS E TECNOLOGIA
UNIVERSIDADE D
COIMBRA

Saskia Theresa Maria Ammer

Reuniting the remains of undocumented border crossers with their families through isotope analysis

Doctoral Thesis in Anthropology with a Specialization in Forensic Anthropology, supervised by Professor Eugénia Cunha, Doctor Bruce Anderson (Pima County Office of the Medical Examiner and Doctor Eric Bartelink (California State University, Chico), and submitted to the Department of Department of Life Sciences of the Faculty of Sciences and Technology of the University of Coimbra.

November 2020

UNIVERSIDADE DE COIMBRA

Doctoral Thesis

Doctoral Program in Anthropology

Specialization in Forensic Anthropology

Department of Life Sciences
Faculty of Sciences and Technology
University of Coimbra

Reuniting the remains of undocumented border crossers with their families through isotope analysis

Saskia Theresa Maria Ammer

Doctoral Thesis in Anthropology with a Specialization in Forensic Anthropology, supervised by Professor Eugénia Cunha, Doctor Bruce Anderson (Pima County Office of the Medical Examiner and Doctor Eric Bartelink (California State University, Chico), and submitted to the Department of Department of Life Sciences of the Faculty of Sciences and Technology of the University of Coimbra.

August 2020

Dedicated to all families who are missing a loved one and all the individuals who remain missing or unidentified.
You will not be forgotten.

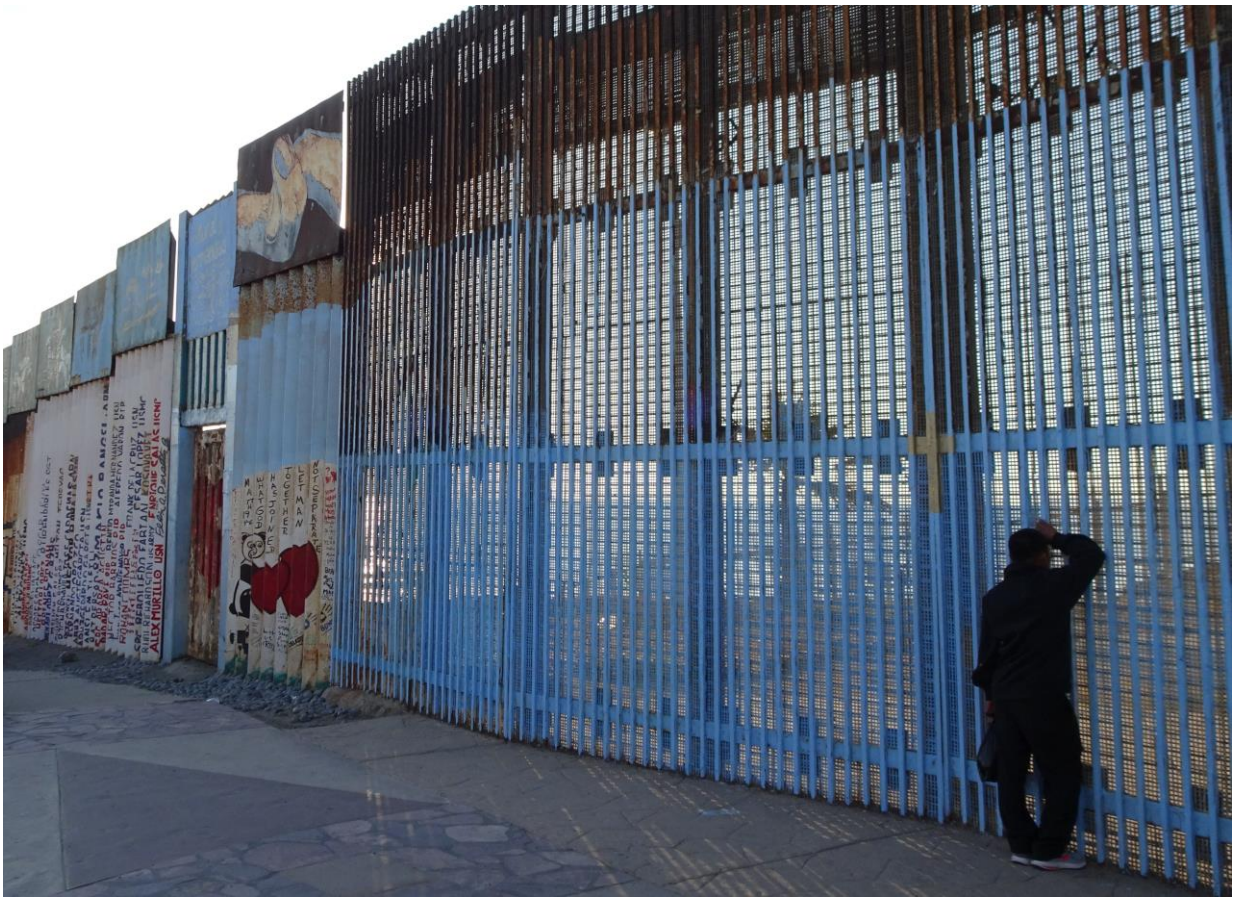

"Migration is an expression of the human aspiration for dignity, safety and a better future. It is part of the social fabric, part of our very make-up as a human family"
~ Ban Ki-moon

"Migrar es amar"
~ Colibri Center for Human Rights

ACKNOWLEDGEMENTS

It takes a village to raise a child- and to write a doctoral thesis.

I would like to thank my supervisors Prof. Eugénia Cunha, Dr. Bruce Anderson and Prof. Eric Bartelink for their commitment to my research and their patience. Eric, thank you for swooping in so late in the game and saving my sanity. Without your feedback, gazillion edits, continuous support and pep-talks, I would not be where I am today. Eugénia, thank you very much for believing in me and investing your time in me.

Thank you very much so the Pima County Office of the Medical Examiner in Tucson Arizona, specifically and especially Dr. Bruce Anderson and Dr. Jennifer Vollner for adopting me for several months and letting me collect the UBC samples used in this research. You two taught me so much and I will always treasure the memories.

I would also like to recognize the Colibrí Center for Human Rights, especially Dr. Robin Reineke and Mirza Monterroso, for imparting in me a deep understanding of the unimaginable situation that keeps unfolding at the border. To the Colibrí Center for Human Rights, keep doing what you are doing. You are amazing!

To the Vrije Universiteit Amsterdam, especially Prof. Gareth Davies and Dr. Lisette Kootker, thank you very much for hosting me and teaching me the dos and don'ts of clean lab work, strontium isotope analysis and believing in me. Thank you to Richard Smeets for teaching me the way around the clean lab and to Dr. Janne Koorneef for teaching me how to run the TIMS Triton. These skills are invaluable and will serve me well into the future aka my post-doc position.

I would also like to express my sincere gratitude to Mexico and its incredible people: Thank you for treating me so well during my journey through your country. Nearly 20.000km in six weeks by way of car, bus, boat, plane and train! It was truly an unforgettable adventure filled with moments that reflected the true heart of this wonderous country and its people. To all the anonymous hair donors and the barbers/ hairdressers that gave their hair to this project: Thank you for just thinking that I was crazy for wanting your hair but not quite crazy enough to send me away. Also, I would like to recognize all the households who let me take some of their precious water: without you, this project would not have been possible. Thank you so Patrick Junkers and Rémi Hernandez.

Last but not least, I want to thank my family and friends from the bottom of my heart. Mama, Papa, as you very well know, none of this would have been possible without you and your continuous support! Thank you for always believing in me and being my biggest cheerleaders. Thank you to my aunt and uncle, Regine and Wolfgang, for their continuous support. Thank you to all my friends from around the world for supporting my craziness and keeping me sane! Special shout out to SPATIAL Room 151: those talks kept me going!

FINANCIAL AND INSTITUTIONAL SUPPORT

I would like to express my sincere gratitude to the following institutions:

- American Academy of Forensic Sciences Humanitarian and Human Rights Resource Center (AAFS HHRRC) Grant, supported by the AAFS and the National Institute of Justice (U.S. Department of Justice)
- J. Lawrence Angel Forensic Anthropology Student Paper Award 2020 for the presentation of the paper *Spatial Distributions of Stable Isotope Ratios in Tap Water from Mexico for Region of Origin Predictions of Unidentified Border Crossers* (AAFS Conference in Baltimore 2019)
- SPATIAL Short Course 2019
- American Academy of Forensic Sciences Forensic Sciences Foundation Student Scholarship for the attendance (AAFS Conference in Baltimore 2019)
- Erasmus+ Scholarship 2018/2019
- Forensic Sciences Foundation Student Travel Grant (AAFS Conference in Seattle 2018)
- Erasmus+ Scholarship 2017

UNIVERSIDADE DE COIMBRA

ABSTRACT

Deceased undocumented border crossers are some of the most difficult individuals to identify due to the inability to narrow down the region-of-origin and therefore to obtain family reference samples for DNA comparison. The isotopic compositions of various body tissues have been demonstrated to be useful biomarkers for tracking locations and movements to aid in the identification of human remains. Thus, together with the forensic anthropological methods used to establish the biological profile and determine other individualizing factors (antemortem trauma, pathological conditions, anatomical variants *etc.*), isotope analysis can provide investigative leads that may aid the identification process.

For the research of the doctoral thesis *Reuniting the Remains of Undocumented Border Crossers with Their Families Through Isotope Analysis,* hair and water samples from across Mexico were analyzed in order to develop reference databases for various isotope systems to aid the identification efforts of undocumented border crosser remains from the Pima County Office of the Medical Examiner (Arizona, United States of America). Carbon, nitrogen, sulfur, lead, strontium, and oxygen isotope ratios were analyzed for the Mexican reference hair, and strontium, oxygen, and hydrogen in the Mexican tap water samples.

Overall, the $^{87}Sr/^{86}Sr$ ratios in the human hair and tap water produced the most promising results. Despite the fact that Mexico is one of the largest bottled water consumers in the world, the $^{87}Sr/^{86}Sr$ ratios of human hair and tap water was strongly correlated ($R^2 = 0.87$ for location averages and $R^2 = 0.80$ when using individual data points).

The $\delta^{13}C$, $\delta^{15}N$, and $\delta^{34}S$ isotopic values showed some distinctive patterns, which are useful for coarsely eliminating regions of origin. This study detected geospatial patterning in the $\delta^{13}C$ values of hair samples from Mexico as well as significant correlations with socioeconomic factors. No geospatial variation was detected in the $\delta^{15}N$ and $\delta^{34}S$ values, however, socioeconomic correlations were found. A $\delta^{13}C$ isoscape was generated using a Geographic Information System (GIS) approach, which could in the future provide a tool to narrow down region-of-origin predictions (in combination with other isotope systems) and to document the travel history of unidentified individuals.

The $\delta^{18}O$ measured in the human reference hair demonstrated how challenging isotopic analyses can be and that there is a dire need for the further development of methods and methodological standardization.

The isotopic values of the tap water show a strong relationship with geography as well as some influences by social and socioeconomic factors. Using $\delta^{2}H$ and $\delta^{18}O$ values, and a GIS

approach, maps of predicted tap water isotope ratios (isoscapes) for Mexico were developed. Clear spatial variation is evident in the developed isoscapes.

Besides the human hair and tap water reference samples, isotope analysis was also conducted on various body tissues (bone, teeth, and hair) of 16 undocumented border crossers recovered from Pima County, Arizona. Using the isotopic reference data and ArcGIS as well as R, several $^{87}Sr/^{86}Sr$ and $\delta^{18}O$ isoscapes were developed, which then served as a reference for assigning possible regions of origins for these undocumented border crossers. Two of the undocumented border crosser cases were recently identified and were used to preliminarily test the effectiveness of these isoscape models. Both isoscapes proved successful in assigning the region-of-origin. While the region-of-origin assignment method used in this research has proven to be effective, it is pertinent to move towards using methods that take the prediction errors into account. This research will serve as a basis for various machine learning regression approaches, which will include multivariate models, and take into consideration various geological covariates, such as the underlying bedrock and weathering regime in order to enable future provenancing studies.

Overall, this research closed the large spatial gap of available human hair and water $^{87}Sr/^{86}Sr$ ratios; human hair $\delta^{13}C$, $\delta^{15}N$ and $\delta^{34}S$ values; and tap water $\delta^{18}O$ and $\delta^{2}H$ values from North America. Nonetheless, it is pertinent to expand the reference samples to other known body tissue samples to establish potential relationships of human hair to body tissues more frequently examined in forensic anthropology casework, such as teeth and bones. This research further illustrates the importance of using a multi-isotope approach when provenancing (e.g. combine Sr and O isotopes).

Keywords: Stable isotopes, Modern human hair, Tap water, Mexico, Forensic provenancing, Undocumented Border Crossers, $^{87}Sr/^{86}Sr$, $\delta^{13}C$, $\delta^{15}N$, $\delta^{34}S$, $\delta^{18}O$, $\delta^{2}H$

RESUMO

Os migrantes mortos indocumentados são indivíduos de difícil identificação devido à incapacidade de restringir a região da qual são provenientes e, consequentemente, de obter amostras de referência da família para comparação de DNA. Contudo, as composições isotópicas de vários tecidos corporais têm demonstrado serem biomarcadores úteis para rastrear localizações e movimentos, auxiliando na identificação de vestígios mortais humanos. Assim, conjuntamente com os métodos antropológicos forenses utilizados na estimativa do perfil biológico e na determinação de factores individualizantes (traumatismos, patologias, variantes anatómicas, entre outros), as análises de isótopos podem auxiliar no processo de identificação.

Para a realização da tese de doutoramento *Reuniting the remains of undocumented border crossers with their families through isotope analysis*, amostras de cabelo e água canalizada de todo o México foram analisadas com o objetivo de criar bases de dados de referência de diversos sistemas de isótopos, e de auxiliar na identificação dos migrantes indocumentados que atualmente se encontram no Pima County Office of the Medical Examiner (Arizona, Estados Unidos da América). Os rácios de isótopos de carbono (C), azoto (N), enxofre (S), chumbo (Pb), estrôncio (Sr) e oxigénio (O) foram analisados em amostras de referência de cabelo de indivíduos mexicanos; Já os rácios de estrôncio, oxigénio e hidrogénio (H) foram examinados com base em amostras de água canalizada mexicana.

No geral, os rácios de $^{87}Sr/^{86}Sr$ no cabelo humano e na água canalizada produziram os resultados mais promissores. Apesar de o México ser um dos maiores consumidores de água engarrafada do mundo, os rácios de $^{87}Sr/^{86}Sr$ no cabelo humano e na água canalizada demonstraram uma forte correlação (R^2 = 0,87 para médias de localização; R^2 = 0,80 ao usar pontos de dados individuais).

Os valores isotópicos de $\delta^{13}C$, $\delta^{15}N$ e $\delta^{34}S$ mostraram padrões distintos e úteis para a exclusão de regiões de origem. O presente estudo detetou ainda padrões geoespaciais nos valores de $\delta^{13}C$ nas amostras de cabelo do México, bem como correlações significativas com fatores socioeconómicos. Apesar de nenhuma variação geoespacial ter sido detetada nos valores de $\delta^{15}N$ e $\delta^{34}S$, foram encontradas correlações socioeconómicas. Um *isoscape* (mapa geológico de distribuição isotópica) de $\delta^{13}C$ foi criado utilizando uma abordagem SIG (Sistema de Informação Geográfica) que poderá, futuramente, ser uma ferramenta útil para restringir regiões de origem (quando combinado com outros sistemas de isótopos), e para documentar o histórico de viagens de indivíduos não-identificados.

Os valores obtidos de $\delta^{18}O$ em amostras de referência de cabelo humano demonstraram o quão desafiantes as análises isotópicas podem ser, bem como a necessidade urgente de uma padronização metodológica.

Os valores isotópicos da água canalizada exibem uma elevada dependência geográfica, bem como algumas dependências sociais/socioeconómicas. Ao utilizar valores de $\delta^{2}H$ e $\delta^{18}O$, bem como uma abordagem SIG, foram desenvolvidos *isoscapes* de água canalizada para o México. A variação espacial é claramente visível nos *isoscapes* criados.

Além das amostras de referência de cabelo humano e água canalizada, a análise isotópica foi também realizada em diferentes tecidos corporais (osso, dentes e cabelo) de dezasseis migrantes indocumentados. Ao empregar os dados de referência isotópica e o *software* ArcGIS, bem como o *software* R, foram desenvolvidos diferentes *isoscapes* ($^{87}Sr/^{86}Sr$ e $\delta^{18}O$), que servem como referência para atribuir regiões de origem aos migrantes indocumentados. Dois dos indivíduos foram recentemente identificados através de outros métodos, podendo estes casos ser utilizados para determinar a eficácia dos *isoscapes* desenvolvidos. Ambos os *isoscapes* foram bem-sucedidos ao atribuir a região de origem. Embora o método de atribuição de região de origem usado nesta investigação se tenha mostrado eficiente, é pertinente empregar métodos que tenham em consideração erros de previsão.

O presente estudo servirá de base para diversas abordagens de *machine learning* que incluirão modelos multivariados, e que terão em consideração diferentes covariáveis geológicas, tal como a rocha-mãe subjacente e o processo de intemperismo, de modo a permitir estudos futuros de comprovação de origem geográfica.

Na sua globalidade, a presente investigação permite combater a grande lacuna espacial de rácios de $^{87}Sr/^{86}Sr$ disponíveis em cabelo humano e água canalizada; valores de $\delta^{13}C$, $\delta^{15}N$ e $\delta^{34}S$ em cabelo humano; e valores de $\delta^{18}O$ e $\delta^{2}H$ em água canalizada da América do Norte. Contudo, é pertinente alargar as amostras de referência para outras amostras conhecidas de tecido corporal, de modo a estabelecer potenciais relações de cabelo humano com tecidos corporais mais frequentemente recolhidos e estudados na Antropologia Forense. O presente estudo ilustra ainda a importância de uma abordagem multi-isotópica na comprovação da origem geográfica (*e.g.*, combinar isótopos Sr e O).

Palavras-chave: Isótopos estáveis; cabelo humano moderno; água canalizada; comprovação forense da origem geográfica; México; imigrantes indocumentados; $^{87}Sr/^{86}Sr$; $\delta^{13}C$; $\delta^{15}N$; $\delta^{34}S$; $\delta^{18}O$; $\delta^{2}H$

TABLE OF CONTENTS

Page Number

TABLE OF TABLES

Page Number

TABLE OF FIGURES

Page Number

Page Number

OVERVIEW OF PUBLICATIONS ASSOCIATED WITH THIS THESIS

Publications:

- Ammer, S.; Kootker, L.; Bartelink, E.; Anderson, B.; Cunha, E. and G. Davies. Comparison of strontium isotope ratios in Mexican human hair and tap water as provenance indicators. Forensic Sciences International 2020. doi: 10.1016/j.forsciint.2020.110422
- Ammer, S.; Bartelink, E.; Vollner, J.; Anderson, B. and E. Cunha. Socioeconomic and Geographic Implications from Carbon, Nitrogen and Sulfur Isotope Ratios in Human Hair from Mexico. Forensic Sciences International 2020. doi: 10.1016/j.forsciint.2020.110455
- In press. Ammer, S.; Kramer, R; and E. Bartelink. *Forensic Isotope Provenancing for Undocumented Border Crosser Human Remains: Application, Overview, and Case Studies*. In: Methodological and Technological Advances in Forensic Science: Application and Case Studies. Editors: Ross, A. and J. Byrd. 1st ed. Elsevier.
- Ammer, S.; Bartelink, E.; Vollner, J.; Anderson, B. and E. Cunha. *Spatial Distributions of Oxygen Stable Isotope Ratios in Tap Water From Mexico for Region of Origin Predictions of Unidentified Border Crossers*. Journal of Forensic Sciences 2020. doi: 10.1111/1556-4029.14283

Conference Presentations:

- Ammer, S. and E. Bartelink (2020, February). *Spatial Distributions of Isotope Ratios in Tap Water, Hair, and Teeth from Latin America for Region of Origin Predictions of Unidentified Border Crosser*. Paper presented at the American Academy of Forensic Sciences 72nd Annual Scientific Meeting, Anaheim, United States.
- Ammer, S. (2020, February). *Isotopes and Isoscapes: Their Potential and Limitations in Aiding the Identification Process of Undocumented Border Crossers from Mexico*. Poster presented at the Humanitarian and Human Rights Resource Center Special Session at the American Academy of Forensic Sciences 72nd Annual Scientific Meeting, Anaheim, United States.
- Ammer, S. (2019, February). *Spatial Distributions of Stable Isotope Ratios in Tap Water From Mexico for Region of Origin Predictions of Unidentified Border Crossers.* Paper presented at the American Academy of Forensic Sciences 71st Annual Scientific Meeting, Baltimore, United States.
    - Supported by the Forensic Sciences Foundation Student Scholarship.
    - J. Lawrence Angel Forensic Anthropology Student Paper Award 2020

Webinar:

- Ammer, S. (2019, February 6th). *Isotopes Aiding Identification Of Undocumented Border Crosser Human Remains.* Forensic Technology Center for Excellence- A program of the National Institute of Justice. Webinar. Available at: https://forensiccoe.org/webinar/isotopes-identification-undocumented-border-crosser-human-remains/

Preamble

Before I present the organization of my doctoral thesis *Reuniting the Remains of Undocumented Border Crossers with Their Families Through Isotope Analysis*, I would like to take a few lines out of this thesis to tell the tale of this massive undertaking.

This research allowed me to live in and travel through five countries over the course of four years. This project came to fruition at the University of Coimbra, Portugal, after I had collected samples at the Texas State University for my M.Sc. dissertation and was able to see the incredible efforts by the forensic anthropologists there to identify undocumented border crossers found in the borderlands of Texas.

Several isotope internships in Munich, Germany and Évora, Portugal later, I was fortunate enough to be allowed to spend three months at the Pima County Office of the Medical Examiner in Tucson, Arizona. At the PCOME, I did not only learn invaluable lessons in forensic anthropology and humanitarian work, I also collected the samples of the 16 undocumented border crossers presented here. While in Arizona, I was also able to tag along with the Colibrí Center for Human Rights, which gave me an even deeper and more versatile understanding of the unimaginable situation that keeps unfolding at the border.

Following the incredible time in Arizona, an equally amazing time followed in Mexico. This research project allowed me to travel nearly 20,000 km in six weeks by way of car, bus, boat, plane, and train from South to North and West to East! This truly unforgettable adventure lead to the collection of 101 human hair and 158 tap water samples which build the core of this research project.

After the completion of the sample collection, I moved to the last destination: Amsterdam, the Netherlands. Here, I was fortunate enough to find an incredible laboratory with even more incredible people who taught me to prepare and analyze all the samples.

The results and lessons learned throughout the journey through the five countries and the various laboratories are presented in the following nearly 300 pages, work that I am incredibly proud of.

Thank you for taking your time to read the fruit of my labor and I am hopeful that it will have a lasting impact on the identification efforts of undocumented border crossers.

Organization of this thesis

This doctoral thesis is organized non-traditionally in an article fashion. Chapters I to IV introduce the subject of the deaths of hundreds of undocumented border crossers in the borderlands of the United States, explain the methodologies of isotope analysis, rectify the human tissues and tap water samples used in this study and lastly present the samples that were taken throughout Mexico and from the undocumented border crossers. Chapter V entails the complete discussions and conclusions of the results of the sample analyses, highlighted by three publications. Chapter VI summarizes the results and discussions of this research project and provides an outlook onto the work to be done in the future.

Chapter I provides the readers with an introduction of the project, specifically the humanitarian issue that causes the deaths of hundreds of individuals each year and the humanitarian response as an effort to identify the deceased undocumented border crossers. The Pima County Office of the Medical Examiner (where the individuals analyzed in this study are housed), and other organizations of importance are presented. Lastly, the issues with DNA typing and the need for isotope analysis is discussed.

Chapter II outlines what isotopes are, and which chemical elements are used in this study. Furthermore, the reader is presented with an introduction into geochemical maps ("isoscapes") and provides an overview of the previous research that has been conducted using isotopes and their forensic applications.

Chapter III outlines and discusses the different human tissue samples used in this study as well as the data that each provide and their limitations. The structure, composition, and remodeling of the various body tissues (bones, teeth, and hair) are presented. Furthermore, the role of diagenesis in forensic human remains is discussed. Lastly, the value of tap water samples in forensic research is considered.

Chapter IV presents an extensive overview of the samples collected by the author. The reference samples, specifically the human hair samples and tap water samples, are presented. An overview is given on the methodology of how and from where the samples were collected. Additionally, the issues which arose during the sample collection process are discussed. Furthermore, the undocumented border crosser samples, collected from current cases housed at the Pima County Office of the Medical Examiner in Tucson, Arizona are summarized.

Chapter V presents the results and discussion of the collected samples. First, the results of the analyses of the reference human hair and tap water samples are presented. These include two publications, *Socioeconomic and Geographic Implications from Carbon, Nitrogen and Sulfur Isotope Ratios in Human Hair from Mexico* and *Comparison of strontium isotope ratios in Mexican human hair and tap water as provenance indicators*. Furthermore, the results of the tap water isotopic analyses are presented. The issues that arose during the oxygen isotope analysis in the human hair samples are discussed in detail. Secondly, the results of the isotopic analyses in the tissues of the undocumented border crossers are presented. These entail the interpretation of the isotope values and ratios as well as various region of origin predictions for the undocumented border crosser cases. This section is highlighted by the published article *Spatial Distribution of Oxygen Stable Isotope Ratios in Tap Water from Mexico for Region of Origin Prediction of Unidentified Border Crossers*, which presents two successful case studies.

Chapter VI concludes this research project, discusses its findings, and gives an outlook on what needs to be done in order to make isotope analysis an even more successful tool in forensic anthropology and in the identification efforts of undocumented border crossers.

CHAPTER I

INTRODUCTION

A main goal of forensic anthropology is assisting the identification of human remains, primarily focusing on establishing a biological profile for the deceased individual in question. The biological profile includes age, ancestry, sex, and stature. Other identifying aspects such as antemortem trauma, pathological conditions, anatomical variants, and other individualizing characteristics are also utilized to facilitate identifications. In some cases, only a limited biological profile can be generated as the remains may be significantly fragmented or degraded due to taphonomic processes, or may be incompletely recovered.

Furthermore, as the world is becoming more and more globalized (and therefore cities, regions and countries more diverse), it is becoming increasingly a challenge to assess the ancestry/population affinity or potential origin of an individual; in fact there have been calls to completely cease ancestry estimation in forensic anthropological examinations (Bethard and DiGangi 2020). Accurate ancestry assessments provide more accurate predictions in the other aspects of the biological profile, *e.g.* the stature estimation (Cunha and Ubelaker 2020). It is also thought to be able to lead to the exclusions of potential missing persons. However, none of the research that has studied morphoscopic cranial traits has attempted to answer the "how" and "why" of these traits (especially in the evolutionary and/or ecogeographic context) (Bethard and DiGangi 2020). The more newly developed methods, such as Fordisc, rely on categorical and generalized labels that depend on both, social-cultural "race" labels and geographical region groupings. Criticism has been voiced that there is no "acknowledgement of the harm of connecting social race to skeletal traits insofar that it only serves to sustain the falsified biological race concept and misinforms the public, to include law enforcement and the medicolegal community, about human variation" (Bethard and DiGangi 2020: 1791). This statement is not only true for Fordisc but also all other methods of skeletal ancestry assessment. Cunha and Ubelaker correctly state that "missing persons are frequently described using racial terminology, [and therefore] forensic anthropologists are guided to use that terminology as well" (Cunha and Ubelaker 2020: 90). Nonetheless, forensic anthropologists are worried that the ancestry assessments potentially even hinder the identification process by putting a label on an individual that does not match their self-identified social label (Bethard and DiGangi 2020). Stull et al. (n.d.) have most recently voiced their concern, stating that "abandoning the estimation of ancestry without proper evaluation within our discipline and consultation with our stakeholders could harm cultural redress in our society and stagnate and dogmatize our discipline".

Overall, the vast majority of undocumented border crossers have a considerable amount of indigenous DNA in their bodies, meaning that an ancestry assessment stating "some level of native American" seldom adds any useful information to the biological profile. Consequently, much of the difficulty associated with identifying deceased individuals stems from an inability to narrow down the search area to more probable options. Therefore, investigators and forensic anthropologists, in particular, need tools that aid the identification in a more sophisticated way, independent of the forensic anthropological ancestry assessment. They are finding the answers by incorporating biomolecular science into their fields of study.

Thus far, the "Holy Grail" in identification efforts has been DNA typing. While DNA is perhaps the fastest growing method of establishing the identity of an individual, it is oftentimes not a practical means for identification. DNA typing is expensive and may be ineffective when remains are too degraded for DNA extraction. Furthermore, DNA is only useful if there is a known reference exemplar (*e.g.*, family reference sample or the decedent's own DNA profile in a database) to compare the samples to, and oftentimes unidentified human remains cases do not have a suitable reference sample available for comparison.

Fortunately, isotope analysis has proven to be a useful and reliable tool for aiding in the identification process by providing additional investigative leads. The isotopic composition of human bone, teeth, and hair have been demonstrated to be useful biomarkers for forensic researchers to narrow region of origin or travel history of individuals, and to aid the identification of remains (Bartelink *et al.* 2018; Ehleringer *et al.* 2008). Even though various disciplines have employed isotope analysis for research, forensic anthropologists have yet to fully embrace the growing significance of the analysis to the field. Furthermore, a large-scale project as the following, combining forensic anthropology with cutting-edge techniques in biogeochemistry to solve a human rights issue, has not been attempted.

While isotope analysis will not identify an individual as DNA or fingerprints do, stable isotopes "create a picture of the person's life and life circumstances" and while "we don't find a needle in a haystack […], we reduce the haystack to a manageable size" as Wolfram Meier-Augenstein puts it (Chant 2012: n.p.).

1. 1. A Historical Perspective on the Humanitarian Issue at Hand

To understand the complexity of this humanitarian issue along the border, it is important to comprehend why the border has become so dangerous. The deaths and disappearance of thousands of migrants are seen as a direct result of border security measures and economic agreements. The North American Free Trade Agreement (NAFTA), a free trade agreement

between Canada, the United States, and Mexico, went into effect 1 January 1994. NAFTA was presented as an initiative to reduce the unauthorized immigration at the Mexico-U.S. border by creating jobs in Mexico. Instead, the implementation of NAFTA had disastrous effects on the economy of Mexico and culminated in the loss of millions of jobs. As the rates of illegal immigration across the border increased, the U.S. Border Patrol ramped up their border security and enforcement policies through initiatives such as Operation Gatekeeper in San Diego, California; Operation Safeguard in southern Arizona; Operation Hold the Line in El Paso, Texas; and Operation Rio Grande in south Texas (de León 2015). Furthermore, enforcement was centralized to larger communities and cities, which created a "funnel effect" (Rubio-Goldsmith *et al.* 2018). Instead of crossing the border into the safe territory (like San Diego or El Paso), the border-crossing movement was funneled into the remote, uninhabited desert. This is a policy referred to as "prevention through deterrence" (de León 2015; Spradley *et al.* 2019), where the harsh environment of the desert acts as a natural deterrent and, would supposedly prevent border crossings. However, these policies had several adverse effects, including an increased risk of death for border crossers.

Due to the economic implications, people had and still have no other choice than to cross, and due to the increased enforcement and militarization in the urban ports of entry, the number of migrant deaths in Arizona increased from an annual average of 12 in the past (prior to the abovementioned enforcement initiatives) up to an average of 170 every year in recent years (with a high of 222 in the year of 2010) (Illingworth 2015; Pima County Office of the Medical Examiner 2018). The funneling of migrants into high risk regions of the Mexico-U.S. border has resulted in a tremendous increase in the number of deaths in the deserts and mountainous regions of border-states.

1. 2. The Humanitarian Response of Identifying Deceased Undocumented Border Crossers

In 1948, the United Nations established the Declaration of Human Rights (United Nations General Assembly 1948). Among the many enumerated rights, the declaration established that it is a human right to be treated with dignity and that "everyone has the right to recognition everywhere as a person before the law" (United Nations General Assembly 1948). Though not explicitly stated by the United Nations, these rights are granted during life and remain in effect after death. Therefore, every person, living or perished, has the right to be recognized and treated with dignity and respect.

Between 1998 and 2017, at least 7,216 people lost their lives attempting to cross the border from Mexico into the United States (Colibrí Center for Human Rights 2018). The total number of

recorded migrant deaths by the humanitarian organization Human Borders' and the Pima County Office of the Medical Examiner's (PCOME) "Arizona Open GIS Initiative for Deceased Migrants" is 3,205 for the time period between 1981 and the end of 2019 (only scarce data is available for the first two decades) (Humane Borders Inc. 2020, Figure 1.1). These numbers represent the undocumented border crosser (UBC) deaths recorded in Arizona and investigated by the Pima County Office of the Medical Examiner as well as to the Maricopa County Office of the Medical Examiner and not the deaths in the other three border states of California, New Mexico, and Texas. Furthermore, the actual number of migrant deaths along the Mexico-U.S. border is likely significantly higher because many missing (and likely deceased) have yet to be found. In 2016, 170 cases were published by Humane Borders and in 2019, 163 cases were documented by the initiative (Figure 1.2 and 1.3). During the years of 2017 and 2018 the numbers were lower, at slightly above 130 per year. Even though border crossings have fallen recently, migrants deaths have increased, meaning the border has become more deadly (Missing Migrants Project by the United Nations International Organization for Migration 2018).

Recently, a volunteer for the organization *No More Deaths/No Mas Muertes* was standing trial for harboring charges after aiding two migrants at the organization's medical camp. The volunteer was found not guilty but, nonetheless, it is expected that this trial will have a negative impact on humanitarian aid and is seen as an intimidation strategy by the government. John Fife, one of the founders of *No More Deaths*, commented that:

> *Since 2013 the Tucson sector of the Border Patrol has had a written agreement with No More Deaths (NMD) that they will respect the NMD camp as a medical facility under the International Red Cross standards, which prohibit government interference with humanitarian aid centers. That agreement now has been violated by the U.S. Border Patrol under the most suspicious circumstances. The Border Patrol acknowledged that they tracked a group for 18 miles, but only after the migrants sought medical treatment did the Border Patrol try to arrest them. The choice to interdict these people only after they entered the No More Deaths' camp is direct evidence that this was a direct attack on humanitarian aid. At the same time, the weather forecast is for record-setting deadly temperatures (No More Deaths/ No Mas Muertes 2017).*

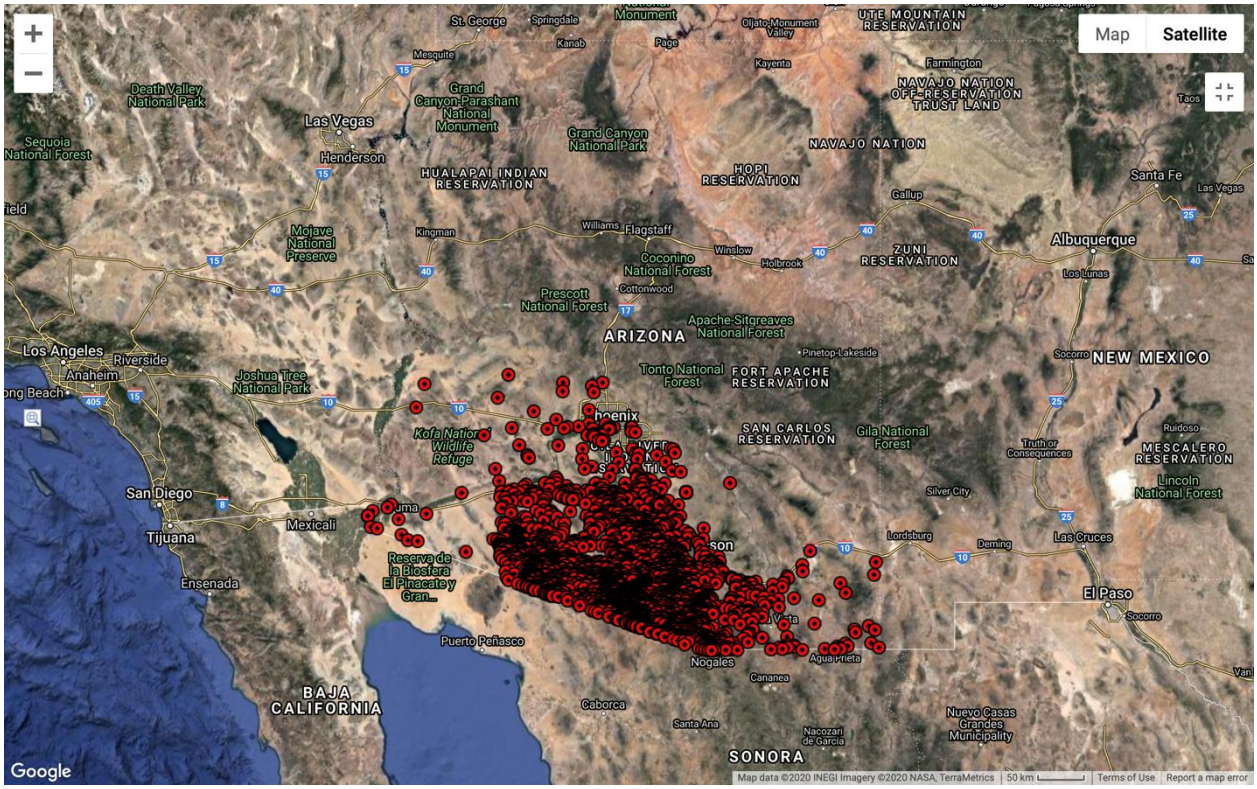

Figure 1.1. Map of Migrant Mortality in Arizona- All recorded deaths since 1981 (Humane Borders 2020).

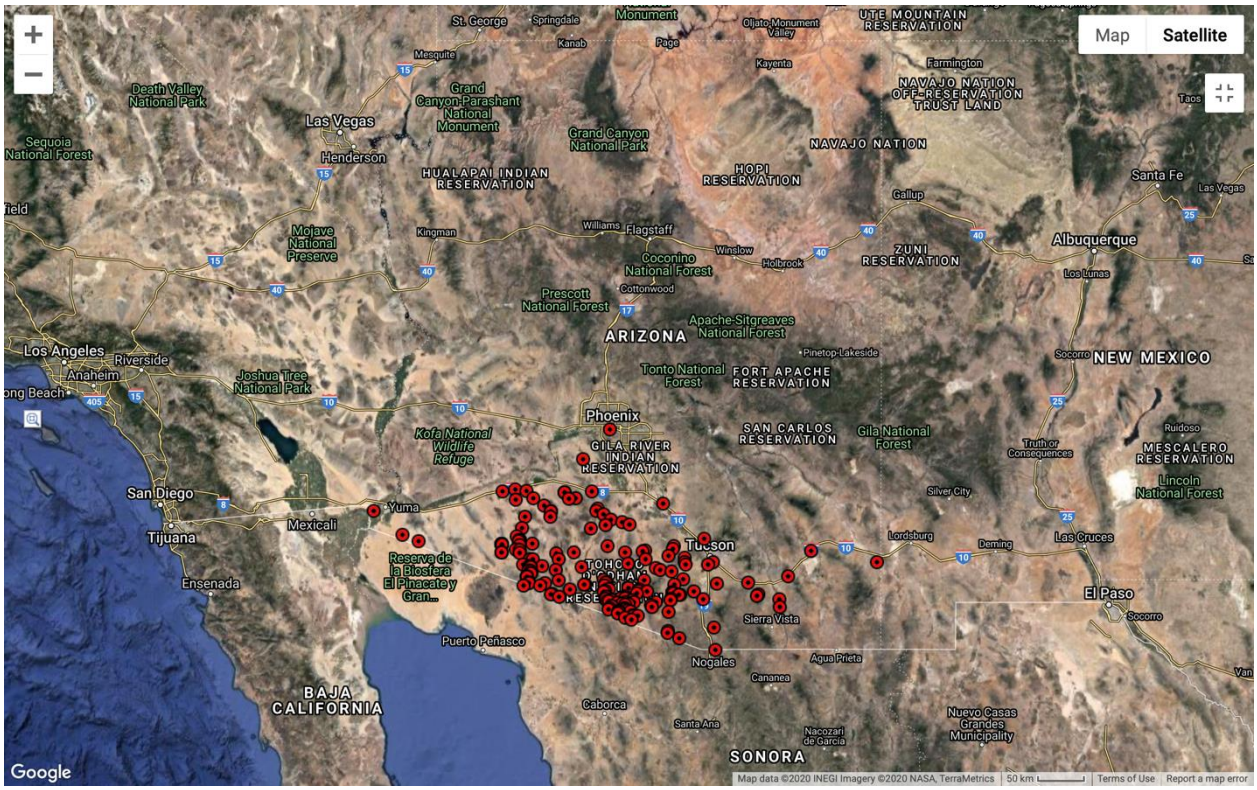

Figure 1.2. Map of Migrant Mortality in Arizona- Recorded Deaths in 2016 (Humane Borders 2020).

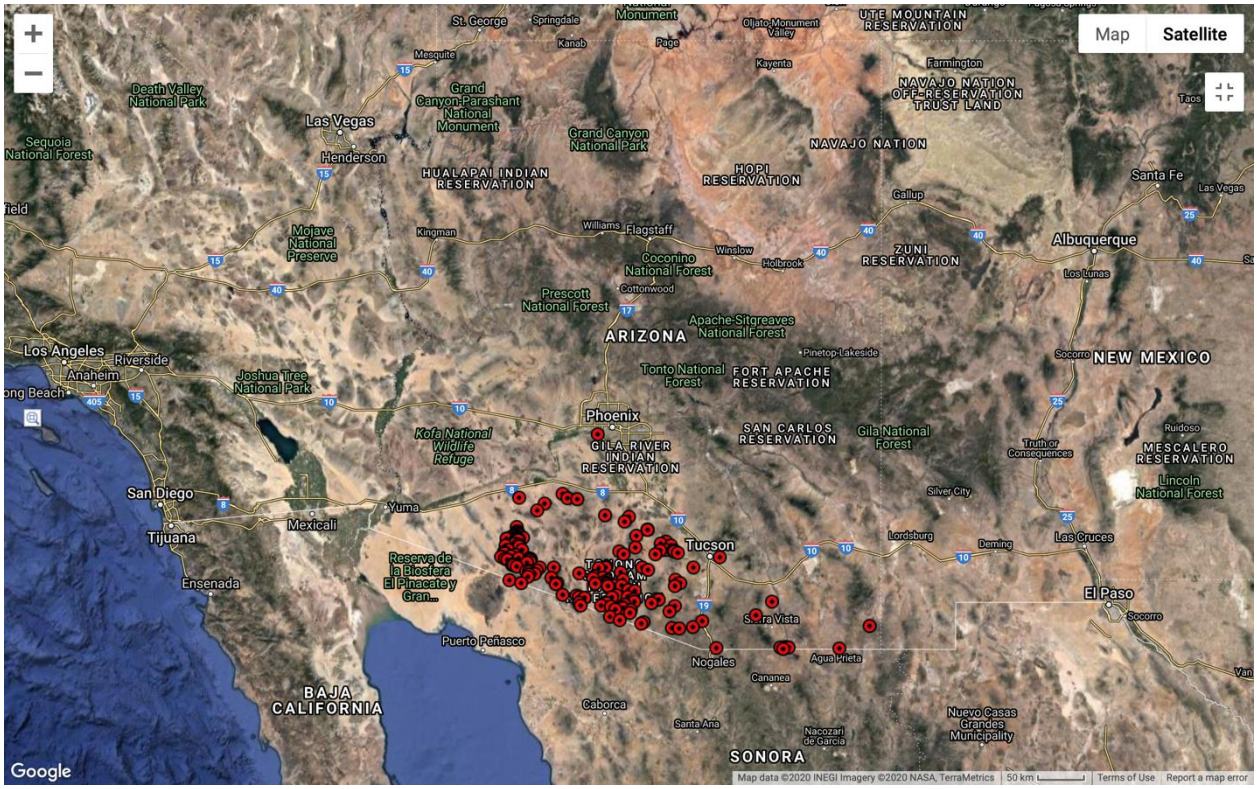

Figure 1.3. Map of Migrant Mortality in Arizona- Recorded deaths in 2019 (Humane Borders 2020).

Predominantly in Texas, many of the remains found in the border region were buried without autopsy, investigation, or identification (Anderson and Spradley 2016). In Arizona, the Pima County Office of the Medical Examiner (PCOME) has attempted to identify individuals who were believed to be foreign nationals since the beginning of the crisis (Anderson and Spradley 2016; Anderson and Parks 2008; Anderson 2008).

Predominantly in Texas, many of the remains found in the border region were buried without autopsy, investigation, or identification (Anderson and Spradley 2016). In Arizona, the PCOME has attempted to identify individuals who were believed to be foreign nationals since the beginning of the crisis in southern Arizona during 2000 (Anderson and Spradley 2016; Anderson and Parks 2008; Anderson 2008).

Previous research has found that a migrant's place of origin can play a major role in the unauthorized crossing experience (Martínez *et al.* 2014). For instance, 86% of all identified decedents recovered in Arizona and identified by the PCOME are Mexican nationals. Among those positively identified, migrants from central Mexico (24%) were the most prevalent, followed by those from southern Mexico (20%), west-central Mexico (16%), and northern Mexico (14%) (Martinez *et al.* 2015; Anderson and Parks 2008; Massey, Durand, and Malone 2002). In contrast, Texas State University's Operation Identification (OpID) reports that more individuals with Central American nationalities were recovered in southern Texas than Mexican nationals

(Spradley *et al.* 2019; Kramer *et al.* 2020). Geographic localities within these different countries also can play a role, as recent research has shown that statistically, more individuals with indigenous ancestry remain unidentified than individuals of European ancestry (Hughes *et al.* 2017).

The leading cause of death recorded by the PCOME is "undetermined" due to advanced decompositional stages (49% of all cases between 2000 and 2019), followed closely by death due to the "exposure" to the harsh environment (39% of all cases between 2000 and 2019) (Pima County Office of the Medical Examiner 2019). The remaining 13% of the deaths recorded by the PCOME are made up of specific injuries and diseases, which include but are not limited to asphyxia, blunt force injury, complications from diabetes, drowning, drug overdose, exposure, exsanguination, gunshot wound, heart disease, lightning strike, motor vehicle accident, nonviable fetus, pregnancy complications, and other injury/homicide. Examples of other injuries are foot injuries, electrocution, mass envenomation, and perforated bowel (Humane Borders Inc. 2020). Recorded homicide cases included entrapment in car trunks, hangings (asphyxia), bound and buried, as well as stab wounds (Humane Borders Inc. 2020).

1. 3. The Pima County Office of the Medical Examiner and Other Organizations of Importance

The PCOME provides death investigation services for Pima County, Arizona as well as for four additional counties, stretching over the entirety of the Arizona-Mexico border. Consequently, this medical examiner's office covers approximately 95% of all reported undocumented migrant deaths in Arizona (Martinez *et al.* 2015). Dr. Bruce Anderson, a forensic anthropologist at the PCOME, has been working for two decades identifying deceased UBCs and over a decade in conjunction with cultural anthropologists (Anderson 2008).

While the forensic anthropologists at the PCOME are an integral part of the identification process of many UBCs, a positive identification is, under normal circumstances, not effected by pure forensic anthropological examination. Specifically, at the intake of the remains, it is decided by the pathologists whether the forensic anthropologists will carry out a secondary examination. This is commonly determined by the state of decomposition of the remains. If possible, fingerprints are recovered from the remains. The forensic anthropologists then carry out the secondary examinations and report their findings. If there are missing persons who may fit the description, the lead is further investigated. If there are no immediate matches, the findings are entered into the NamUs system, and also provided to the Colibrí Center for Human Rights to be compared with the missing persons reports. If there are, at any point in time, probable matches

that cannot be verified through fingerprint comparison or circumstantial evidence, DNA samples will be collected from the family of the missing person and directly compared to the remains of the UBC. Therefore, there are no forensic anthropological identifications, *per se*, at the PCOME but forensic anthropology provides essential investigative leads for a successful identification.

A collaboration with Dr. Robin Reineke led to the founding of the Colibrí Center for Human Rights. Colibrí is a not-for-profit, non-governmental organization dedicated to ending the loss of life and suffering of undocumented migrants on the Mexico-U.S. border. Colibrí is a family advocacy organization that collects missing persons reports and DNA samples from relatives of missing migrants in an attempt to match data, build a community, and help raise consciousness about this human rights crisis (Illingworth 2015, Colibrí Center for Human Rights 2018).

In Texas, forensic anthropologist Dr. Kate Spradley is the director of Operation Identification (OpID), an organization nested within the Forensic Anthropology Center at Texas State University. The major objective of OpID is to identify and repatriate the skeletal remains of undocumented deceased Latin American migrants recovered in south Texas. OpID has performed several exhumations of deceased UBCs that were buried unidentified in cemeteries in south Texas to start identification efforts and eventually repatriate the remains to families.

For all UBC cases, an "Unidentified Persons" profile is established in the National Missing and Unidentified Persons (NamUs) database (https://www.namus.gov/UnidentifiedPersons/). Persons missing someone can not only create a missing persons' profile but can also search the unidentified and unclaimed case reports in NamUs.

Along with a number of other organizations (*e.g.*, Argentine Forensic Anthropology Team and South Texas Human Rights Center), PCOME and OpID have linked up with the Forensic Border Coalition to share information regarding migrant deaths with the goal to increase the number of identifications and to improve the understanding, scope and impact of migrant deaths (Anderson and Spradley 2016; Spradley 2014). Furthermore, wherever applicable, the abovementioned institutions work with foreign consulates and the United States Customs and Border Protection on identification efforts.

Overall, UBCs are among the most difficult individuals to identify due to the common lack of antemortem identification records as well as challenges in obtaining family reference DNA samples. This difficulty is underlined by the fact that approximately one third of the presumed UBC cases (1050 unidentified of 2943 total recoveries) between 2000 and 2018 at the PCOME are currently unidentified (Pima County Office of the Medical Examiner 2018). Therefore, it is essential that isotope provenancing methods continue to advance to provide another important line

of evidence in the identification process of undocumented border crossers and other unidentified individuals.

1. 4. Issues with DNA Typing

DNA typing and comparison is often challenging in investigations of UBCs for various reasons. Until 2012, presumed undocumented border crosser cases in Texas (specifically Brooks County) were sent to funeral homes for identification efforts, consistently without conducting autopsies or consultation of a forensic anthropologist (Anderson and Spradley 2016). Further, DNA samples were not collected or submitted in all cases, for example, because the method is too expensive or time intensive, because the remains are affected by taphonomic conditions, or merely because the person found is a presumed migrant and therefore not an identification priority (Anderson and Spradley 2016). Moreover, the use of multiple DNA genetic databases presents a significant issue. When DNA is analyzed, the genetic profile may be submitted to the Combined DNA Index System, or CODIS, a genetic database run by U.S. Federal Bureau of Investigation (FBI) (Federal Bureau of Investigation 2020a). CODIS is divided into three databases: local (LDIS), state (SDIS), and national (NDIS); and four indices: the Unidentified Index, the Forensic Index, the Offender Index, and the Relatives of the Missing Persons Pedigree Tree Index, which are kept separate to ensure that a person submitting a familial DNA sample is not at risk of arrest if they left their DNA at a crime scene (Federal Bureau of Investigation 2020b). However, many individuals whose loved ones went missing crossing the U.S.-Mexico border may fear a breach of conduct, wish to maintain their anonymity, and thus refrain from allowing their DNA profile to be submitted into the federal database to protect their privacy and their families. It has been found that the more socially marginalized the family of the missing is, the more obstacles the family has to face in order to obtain information about the loved one's whereabouts and to submit data to the appropriate authorities (Reineke 2016). Oftentimes those families missing loved ones do not live in the United States and are therefore not able to submit a DNA sample to CODIS. For migrant-related cases, families of missing persons may reside in the U.S. already and fear deportation if their names and their genetic information are submitted to a federal repository (Spradley *et al.* 2019). Therefore, CODIS often does not contain genetic reference information to identify deceased and missing border crossers. Furthermore, CODIS is not easily cross-referenced with international genetic databases, which means that DNA submitted by families in another country is difficult to compare with the U.S. database. Through 2019 at the PCOME, CODIS associations resulted in 86 matches (24 U.S. citizens and 62 foreign nationals). For the U.S. citizens, six matches were found in the Offender Index, one in the Forensic Index, and seventeen in the Relatives of the Missing Persons Pedigree Tree Index. For the foreign nationals, fifty-five hits

were made in the Offender Index and seven in the Relatives of the Missing Persons Pedigree Tree Index. It is important to note that the matches of foreign nationals (mostly undocumented border crossers) in the Offender Index do not always equate to proper identifications due to inaccurate self-reported information (*e.g.* aliases and dates of birth) and information known to reporting next of kin.

For these reasons, non-governmental organizations and human rights groups are essential to UBC identification efforts because they provide a safe environment for families to report loved ones missing both within the U.S. and in foreign countries as well as an ability to provide reference DNA samples that are analyzed in secure, private labs.

1. 5. Why Isotope Analysis?

Stable isotope analysis has been shown to be an effective geolocation tool (Chesson *et al.* 2018a,c; Lehn *et al.* 2019; Santamaria-Fernandez *et al.* 2009; Huelsemann *et al.* 2009). Isotope analysis provides a record of movement and eating habits of an individual throughout life. Isotope signatures are not altered once incorporated into tissues and can be examined at any point during life or after death, depending on the research question and body tissue used for analysis.

A migrant's place of origin can be essential in the identification process and also plays a major role in shaping the reasons people migrate, how and where along the border they may attempt a crossing, as well as their desired destination (Martínez *et al.* 2014). Isotope analysis may not identify a person to the individual level, but it is a means to identify locations and movements of individuals during various stages of their lives.

Much of the difficulty in identification and the return of deceased UBCs to families results from an inability to restrict the search range to the most probable options. Therefore, isotope analysis of these unidentified individuals will provide investigators with additional information and investigative leads, which could have a tremendous impact on the identification itself as well as the speed of the identification process.

1. 6. Isotope Analysis and Forensic Anthropology

In the 1970s, the initial definitions of forensic anthropology by its founders T. Dale Stewart, Clyde Snow, Ellis Kerley and other active practitioners were more or less the same and stated that forensic anthropology deals with more or less skeletonized (suspected human) remains in order to establish a biological profile in an attempt to identify the deceased individual (Dirkmaat and Cabo 2012).

While the field was formally defined in the 1970s, it then experienced stunted growth in the 1980s. Only few forensic anthropologists were involved in casework and because federal court rulings threatened the credibility of the field and scientific evidence in court settings in general (*e.g.* United States Supreme Court 1993). Since then, the field has developed dramatically, primarily because of the improvements in the methodologies used for biological profile estimations, as well as the addition of forensic taphonomy, forensic archaeology, and trauma analysis to the field (Ubelaker 2018, Dirkmaat *et al.* 2008). The methods for establishing the biological profile, in particular, were greatly improved by establishing modern skeletal collections, forensic anthropological research facilities, and utilizing statistical tools to reduce the errors in the predictions (Dirkmaat and Cabo 2012). All these aspects are part of the solution to keep forensic anthropology a vibrant and innovative field long term. This also led forensic anthropology from being a subfield of physical anthropology and a solely laboratory-based science to be a science that is also focused on the crime scene investigation (Dirkmaat and Cabo 2012).

Interestingly, anthropology and archaeology started adopting the tools of isotope analysis during the same time as forensic anthropology was first formally defined, in the 1970s (Bartelink 2020, Bartelink *et al.* 2016, Bocherens *et al.* 2007, Schoeninger *et al.* 1983). Isotopes have traditionally been used in hydrology, geology, and ecology (Fry 2008). More recently, though, forensic sciences have implemented these methodologies and utilized them for their purposes. From analyzing food for their authenticity to analyzing explosives and provenancing poached wildlife, isotope analysis has been proven useful in many different areas (Chesson *et al.* 2013). This is also the case for forensic anthropology. Forensic anthropology has adopted and adapted original scientific methods, (*e.g.* geometric morphometrics, biomechanics, bone microscopy) as well as methodologies from the related fields of archaeology, bioarchaeology, and paleoanthropology to the discipline of forensic anthropology (Ubelaker 2018, Dirkmaat *et al.* 2008). The two major areas covered by isotope analysis in the field of forensic anthropology are dietary reconstruction and geological residence reconstruction (Ubelaker and Francescutti 2020).

For obvious reasons, forensic anthropologists are the most appropriate experts to conduct and interpret isotopic data on human remains. Forensic anthropologists are experts on the human skeleton, the biology and chemistry of bones and teeth, and the influences of postmortem processes that affect the preservation of remains and their *in vivo* biogeochemical signatures (*e.g.*, the influence of diagenesis). Therefore, forensic anthropologists are able to assess the value of each skeletal element and determine which element serves the purpose of the investigation. Further, the correct interpretation of isotopic data in respect to the skeletal element investigated is

only guaranteed when interpreted by a trained forensic anthropologist with experience in isotope analysis. Additionally, as many forensic anthropologists also have a background in archaeology and bioarchaeology, the principals of isotope analysis are often a component of the formal training and research (Bartelink *et al.* 2016).

As outlined above, forensic anthropology is an ever-developing field that has a history of adding aspects to its repertoire to remain relevant to the identification process. Adding the most recent scientific inventions and discoveries and implementing them into forensic anthropology is, in fact, what keeps the field interesting and stimulating to scientists. Adding isotope analysis is just one of the latest additions to the toolkit that will certainly gain even more importance in the future. While still in its baby shoes, forensic anthropology has started to embrace the value of isotope analysis and has even added special sessions to conferences and journals already. This demonstrates that isotope analysis is now starting to become an integral part of forensic anthropology.

CHAPTER II
ELEMENTS AND ISOTOPES

Stable isotope techniques were first developed in the 1950s to gain an understanding of how different earth elements are chemically altered in kinetic and equilibrium reactions. Later, in the 1970s, they were used to reconstruct dietary and migratory patterns of living and extinct animals. Plants and animals record these isotopic signatures in their tissues. Isotopes are thus useful for reconstructing past environments for various fields of research, such as archaeology and paleoclimatology, and continue to be used in modern contexts in fields such as conservation, ecology, food forensics, and forensic anthropology. Before using isotopes to estimate the geographic origin of deceased unidentified human remains, it is necessary to understand the basic principles of isotopes, including what they are and how they are measured.

There are 90 known chemical elements, which consist of atoms, protons, neutrons, and electrons. Together, these are referred to as subatomic particles. An atom consists of two parts: the nucleus and orbitals. The number of protons and electrons are always equal in an atom of any element, but the number of neutrons may vary (Schoeninger and Moore 1992; Schwarcz and Schoeninger 1991). While the number of protons is referred to as the atomic number, the atomic weight/mass is representative of the sum of protons, electrons, and neutrons. Commonly, electrons are not counted as they do not contribute to a significant enough extent to the mass.

About two-thirds of the 90 chemical elements occur in more than one form and are consequently called isotopes. Isotopes of an element contain the same number of protons but differ in their number of neutrons, which means that isotopes of a chemical element differ in their atomic mass (Hoefs 2015; Schoeninger and Moore 1992; Fry 2008; Katzenberg 2007; McMurry and Fay 2004). For example, oxygen has 17 known isotopes.

Isotopes are divided into two key groups: stable and unstable (Fry 2008). While stable isotopes retain their nuclear configuration, unstable isotopes decay (change their nuclear configuration) over time. Stable isotopes are found in all organic elements. Isotopes that carry too many or too few neutrons (relative to the protons of the element) are unstable and therefore prone to decay into lighter and more stable isotopes (White *et al.* 2011). Therefore, the proportion of the lighter isotope is far more predominant in nature. One of the most widely known unstable isotopes is ^{14}C, which is used in radiocarbon dating to determine the approximate age of organic materials by measuring the amount of ^{14}C present. Unstable isotopes are commonly referred to as radioisotopes. These are radioactive, hence the name, and have half-lives.

Isotopes are measured as ratios of heavy isotopes to light isotopes for an individual element as compared to an international standard using mass spectrometry (Schoeninger and Moore 1992; Katzenberg 2007). Delta (δ), is used to denote the ratio of heavy isotope to the light isotope in the sample compared to that same ratio in the standard (Fry 2008). This equation shows the method used to calculate the δ values for isotopes, in this case oxygen (Fry 2008):

$$\delta^{18}O = [(({}^{18}O/{}^{16}O) \text{ sample} / ({}^{18}O/{}^{16}O) \text{ standard}) - 1]$$

As the ratio-of-ratios calculated is typically small, δ values can be multiplied by 1000 and presented in parts per thousand difference or "per mil," denoted by the ‰ symbol. Calculations using this equation can produce negative or positive values. A negative δ value means that the sample is depleted in the heavy isotope relative to the standard, whereas a positive δ value means that the sample is enriched in the heavy isotope relative to the standard (Fry 2008).

2. 1. Isotopic Variation and Fractionation

While the earth's abundances and ratios of elemental isotopes were fixed when planet Earth was formed and globally have not changed, this is not necessarily the case for regional abundances of isotopes (Hoefs 2015). Contrary to common belief, the stable isotopes of the elements are not uniformly distributed globally. Various isotopes, such as oxygen find themselves in a state of constant partitioning which results in one isotope of oxygen existing in greater abundances than another. This process is referred to as fractionation (Hoefs 2015). During any equilibrium reaction, isotopic fractionation occurs. As it is the case with the transformation for water vapor to liquid precipitation, equilibrium fractionation describes the isotopic exchange reactions that maintain equilibrium while occurring between two different phases of a compound (Meier-Augenstein 2018). The difference between the true amount and the amount in a sample is known as isotope fractionation $\langle_{A\text{-}B} = R_A/R_B$ (West *et al.* 2010).

There are two different types of isotopic fractionation, one occurring in physiochemical processes and the other occurring during (bio-)chemical processes. Both describe processes that affect the relative abundance of isotopes. The fractionation occurring during (bio-)chemical processes is influenced by the reduced mass of a system, primary bond strength (energy) as well as bond length, resulting in the breakage or formation in the rate-determining step of the reaction of the atom or its isotope. The effects associated with this kind of fractionation are called primary or kinetic isotope effects since the degree of fractionation is dependent on the reaction kinetics of the chemical reaction (Meier-Augenstein 2010).

Isotopic fractionation during physiochemical processes refers to fractionation events occurring during diffusion, evaporation, two-phase partitioning, and molecular spectroscopy. This

one is influenced by the reduced mass of a system such as different velocities of isotopic molecules of the same compound in the gas phase or difference in absorption of energy (Meier-Augenstein 2010). The isotopic effects associated with kind of fractionation are called secondary or dynamic isotope effect as the chemical bonds are not broken or formed.

Isotopic fractionation transpires because bonds combining lighter isotopes are weaker than bonds incorporating heavier isotopes and therefore break more easily during chemical exchanges, such as during biosynthesis and respiration (Hoefs 2004; Fry 2007). A classic example of isotopic fractionation, called the Rayleigh distillation, describes the diminishing presence of heavy isotopes, such as ^{18}O, along with increasing latitudes and altitudes, such as mountainous landscapes (Bentley and Knipper 2005). While rain close to the ocean consists of heavier isotopes, lighter isotopes are retained in the atmosphere longer and rained off further inside the land, commonly referred to as isotopic depletion (Fry 2007). Additionally, Brettell and colleagues (2012) have shown that boiled water is isotopically heavier due to preferential loss of ^{16}O to steam as it evaporates off the initial water sample. Therefore, the $\delta^{18}O$ values derived from skeletal remains should reflect the diet and water intake of the individual after fractionation events occur during evaporation, condensation, and precipitation (Bösl *et al.* 2006; Bentley and Knipper 2005).

However, isotopic signatures are not only influenced by nature but also due to physiological influences in living tissues. It has been demonstrated that factors like diet, metabolism, body size, and heat loss mechanisms may have significant fractionation effects (Bryant and Froelich 1995; Kohn *et al.* 1996). Furthermore, stable isotope analysis is sensitive to any changes in diet, excursions from physiological homeostasis and metabolic disorders, such as osteoporosis, diabetes, or protein stress (Reitsema 2015; 2013).

Furthermore, the mechanism called "nursing effect" influences the isotopic signature of humans and other mammals, primarily the dental tissue. The metabolic fractionation that occurs within a nursing mother's body leads to the breast milk's ^{18}O to be enriched by 0.7 ‰ (White *et al.* 2011; Wright and Schwarcz 1998; 1999). This enrichment is passed to the infant through the milk, which leads to the enrichment being incorporated into the teeth, which are mineralizing during the nursing period. This phenomenon is especially prominent in the permanent incisors, canines, and first molars and should therefore be taken into consideration when examining isotopic signatures.

The phrase "you are what you eat and drink" summarizes the effects of nutritional influences on the human body. Anything that is eaten or imbibed will be reflected in bodily fluids and tissues. Longinelli (1984) demonstrated that a linear relationship exists (R=0.98) between the isotopic composition of ingested water from the diet and body water. Thus, it is important to

consider the time of formation and the rate of remodeling for hard and soft tissues that will be sampled for isotope analysis to avoid inherent biases with the interpretation of the results.

Bone remodeling rates (discussed in Chapter III) also influence isotopic composition due to the diverse rates of bone turnover among different skeletal elements and tissue types. Therefore, sampling the same elements and/or tissue types during an isotopic study is a sound research approach and implemented in this project.

Furthermore, nuclear testing has caused isotopic variation. For example, one can measure precisely the age of materials as ^{14}C has very precise half-life, which makes it easy to measure (Shin *et al.* 2004). The year 1950 is used as "year zero" in time and the bomb pulse curve is used to compare analyzed data sets. Bomb pulse refers to the drastic incline of atmospheric ^{14}C during the 1950s and 1960s due to the nuclear weapon tests and usage, which produced levels 100% higher than pre-bomb (Zoppi *et al.* 2004, Wild *et al.* 2000).

In the following section, overviews of dietary isotopes (carbon, nitrogen, and sulfur) and geolocation isotopes (strontium, oxygen, and hydrogen) used in this research project are presented. Further discussion of isotope fractionation can be found throughout the isotope-related literature (Van Klinken *et al.* 2002; Schoeller 1999; Fry 2008).

2. 2. Elements Used in This Study

First, the isotopes most known as "dietary isotopes" are discussed which include carbon, nitrogen, and sulfur. Dietary isotopes are well established and have been used extensively in ecological and archaeological studies. Then, isotopes that are commonly used for geolocation research (hydrogen, oxygen, and strontium) are reviewed because they are particularly useful for region of origin predictions and assignments.

Carbon ($^{13}C/^{12}C$)

Carbon has 15 known isotopes, of which two are stable and have relative abundances of 98.89% and 1.11% on Earth, respectively (Wagner *et al.* 2018; Craig 1953). Carbon isotopes vary in plants as a product of the three different photosynthetic pathways: C_3, C_4, and CAM (Table 1). C_3 plants discriminate more against the heavier isotope of carbon (^{13}C) when incorporating CO_2 into their tissues, resulting in more negative $\delta^{13}C$ values than C_4 plants (White *et al.* 2011). C_3 plants comprise approximately 95% of the earth's plants and include fruits, vegetables, and grains such as wheat and rice (Reitsema 2015). C_4 plants, on the other hand, do not discriminate as much against ^{13}C when incorporating carbon dioxide (CO_2) into their tissues, resulting in less negative $\delta^{13}C$ values (White *et al.* 2011). C_4 plants include corn (maize), sugarcane, amaranth, millet, and

sorghum (Reitsema 2015). The third photosynthetic pathway, crassulacean acid metabolism (CAM), includes plants that can utilize either the C_3 or C_4 pathways depending on environmental factors; CAM plants include pineapples, succulents, and cacti (Reitsema 2015; Schoeninger and Moore 1992) and are not typically major components of the human diet.

Studies have shown that in control-fed animals, dietary protein is the primary contributor to bone collagen whereas products of the entire diet make up bone apatite and tooth enamel (Ambrose and Norr 1993; Tieszen and Fagre 1993). In humans, an estimated fractionation of 9.5 ‰ to as much as 11 ‰ or 12 ‰ in $\delta^{13}C$ values between diet and bone apatite have been found (Ambrose and Norr 1993; Hedges 2003). The differences in photosynthetic pathways of C_3 and C_4 plants and its isotopic effect on skeletal tissues have been outlined by Tykot (2006).
Marine fish, terrestrial animals, and freshwater fish typically display high, intermediate, and low $\delta^{13}C$ values, respectively, owing to fluctuations in atmospheric and aquatic carbon sources (Reitsema 2015).

Table 2.1. Plant classifications according to their produced stable carbon isotope ranges.

Plant type	**$\delta^{13}C$ Values**	**Food examples**
C_3 plants	low $\delta^{13}C$ values	Including fruits, vegetables, and some grains such as wheat and rice
C_4 plants	high $\delta^{13}C$ values	Including corn (maize), sugarcane, millet, sorghum, amaranth
Crassulacean Acid Metabolism (CAM) plants	intermediate and overlapping $\delta^{13}C$ values	Pineapple, succulents, and cacti

(adapted from Reitsema 2015)

Nitrogen ($^{15}N/^{14}N$)

Nitrogen is an element that exists as two stable isotopes (^{14}N and ^{15}N) and fourteen radioisotopes (Cartigny and Busigny 2018). The $\delta^{15}N$ isotope values are useful for interpreting and understanding the sources of animal protein that a person consumes during life. Moving up the food chain, $\delta^{15}N$ values become higher due to fractionation during nitrogen metabolism (Meier-Augenstein 2018; Reitsema 2015; Steele and Daniel 1978; O'Connell *et al.* 2012). Organisms that do not consume animal protein are located on the lower tiers of the food chain and exhibit lower $\delta^{15}N$ values (depleted in ^{15}N), while carnivorous animals are higher in the food chain and exhibit higher $\delta^{15}N$ values (Deniro and Epstein 1981). Additionally, $\delta^{15}N$ values can provide information about the presence of fertilizers used in agricultural products. For example, organic produce typically display higher $\delta^{15}N$ values (Meier-Augenstein 2018). Other factors that can lead

to elevated δ^{15}N values include environmental factors such as aridity as well as metabolic factors such as starvation and wasting.

Culture and social structures, like social status or gender, can play a major role in how food resources (*i.e.* diet, specifically meat resources) are distributed within a society. In other words, δ^{15}N values can be used to make predictions about the influence of cultural phenomenon on the human body (Agarwal and Glencross 2011). Bender and colleagues (2015) demonstrate that δ^{15}N values can reflect differences in low versus high socioeconomic status groups using hair from living humans from Cali Colombia. Furthermore, nitrogen isotopes can be used to differentiate coastal-dwelling populations from inland, terrestrial-dwelling populations. The consumption of marine proteins results in higher δ^{15}N values of organismal tissues compared to organisms subsisting on terrestrial food sources (White *et al.* 2011; Deniro and Epstein 1981).

Sulfur (^{34}S/^{32}S)

Sulfur has four naturally occurring stable isotopes (^{32}S (95.018%), ^{33}S (0.75%), ^{34}S (4.215%), and ^{36}S (0.017%)) as well as one cosmogenic isotope (^{35}S) (Farquhar 2018).
Sulfur isotopes have traditionally been used to establish the geological chronology of sediment stratigraphy (Rickard 2012). Sulfur isotopes vary with the underlying bedrock lithology, microbial activity in the soil, and other environmental factors (Richards *et al.* 2003). Stable sulfur isotope values (δ^{34}S) can reflect diet and geographic residence because δ^{34}S in plants vary with the isotopic values of underlying bedrock and fractionation is essentially non-existent (Meier-Augenstein 2018; Richards *et al.* 2003; Valenzuela *et al.* 2011).

Higher δ^{34}S values are representative of marine water, intermediate δ^{34}S values are illustrative of terrestrial water, and low δ^{34}S values are seen in freshwater (Reitsema 2015). However, it is important to note that the "sea spray effect" can influence coastal δ^{34}S values to mimic marine water signatures (Wadleigh *et al.* 1994). A more recent study by Valenzuela and colleagues (2011) created a sulfur "isotopic landscape" (isoscape) of North America by sampling human hair from 73 cities across the United States. The isoscape model identified geospatial patterning in δ^{34}S values, with considerably lower values occurring in the Great Plains region of the United States and higher δ^{34}S values occurring near the eastern, western, and southern coasts (Valenzuela *et al.* 2011). Therefore, lower δ^{34}S values are found among inland terrestrial ecosystems, while higher δ^{34}S values reflect marine and coastal ecosystems.

Oxygen ($^{18}O/^{16}O$)

Oxygen is an element that exists in three stable isotope forms (^{16}O, ^{17}O and ^{18}O) (Bao, Cao, and Hayles 2016) and is used for isotope analysis because there is a strong linear relationship between the oxygen composition of body tissue and that of the water ingested during the time of that tissue's formation. Furthermore, 60% percent of the human body is composed of oxygen and hydrogen (Emsley 2011). Oxygen isotope ($\delta^{18}O$) values reflect the water that an individual takes into their system during life. Dietary $\delta^{18}O$ is a proxy for environmental $\delta^{18}O$ and is influenced by evaporation, condensation, and precipitation (Figure 2.1, Bentley and Knipper 2005; Knudson *et al.* 2009).

High $\delta^{18}O$ values correspond to colder climates while lower $\delta^{18}O$ values reflect warmer climates. Because $\delta^{18}O$ is heavier than $\delta^{16}O$, it will evaporate later. Thus, the ocean will show high $\delta^{18}O$ values in tropical areas of the world. Lighter isotopes are retained in the atmosphere longer, which means the rain close to the ocean contains more of the heavy isotope compared to the rain further away from the ocean (Figure 2.1). Additionally, as water vapor condenses to create rain, water droplets rich in ^{18}O precipitate first because they are heavier than ^{16}O. Therefore, tropical areas show an abundance in ^{18}O but little ^{16}O, whereas colder regions have less ^{18}O but an abundance of ^{16}O. Obviously, this is not a permanent state as climate changes constantly and even more rapidly nowadays.

The geological signal that is taken up in liquid form through the water is transferred to various tissues, internal and external (Ehleringer *et al.* 2010). Therefore, $\delta^{18}O$ values are an indicator of climate and diet, meaning that probable regions of origin can be predicted for individuals based on their measured isotope values. Consequently, $\delta^{18}O$ values found in humans are most representative of the climate and distance to the sea, with the greatest contribution to the total body water being the drinking water (Reitsema 2015).

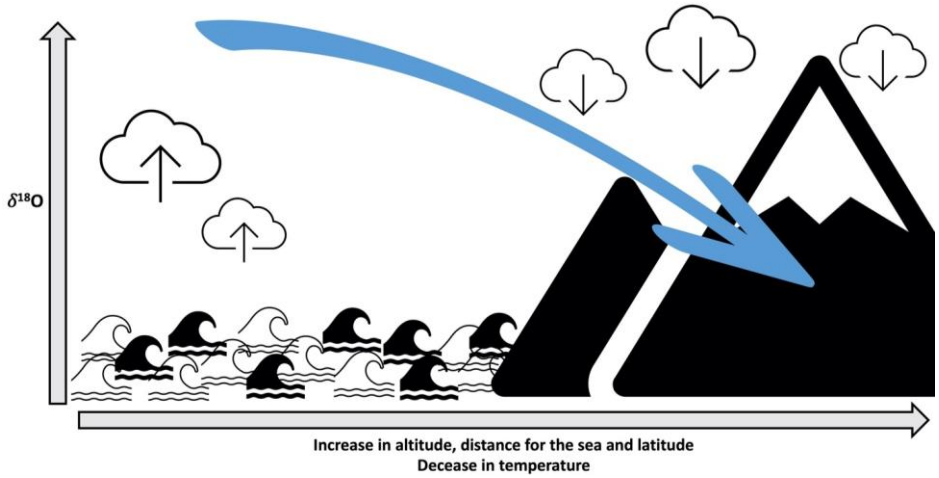

Figure 2.1. Visualization of changes in $\delta^{18}O$ values because of geographic and environmental variables.

Hydrogen ($^{2}H/^{1}H$)

Hydrogen has three naturally occurring isotopes, of which two are stable (^{1}H and ^{2}H) and one is radioactive (^{3}H). ^{1}H is the most abundant on Earth (Schimmelmann and Sauer 2018). Depending on the latitude, altitude, temperature, and distance to the ocean, precipitation (meteoric) $\delta^{2}H$ water values can range from -230 to +20 ‰ (Meier-Augenstein 2018). Hydrogen isotope values in human hair correlate with geography (Ehleringer *et al.* 2008) and are useful for predicting residence patterns in medicolegal contexts over the course of weeks to months prior to death, the time frame dependent on the length of the hair.

As discussed in the section concerning oxygen isotopes, hydrogen isotopes are also representative of climatic patterns and proximity to the oceans. The precipitation patterns that were explained above apply to hydrogen as well, given than oxygen and hydrogen are strongly correlated and form a global meteoric water line. Humans derive their hydrogen values from drinking water (including water used to prepare food), water stored in food (representing the food's place of origin), and the bonded hydrogen within the chemical structures of food resources (Meier-Augenstein 2018).

Strontium ($^{87}Sr/^{86}Sr$)

Strontium has four naturally occurring stable isotopes (^{84}Sr (0.56%), ^{86}Sr (9.86%), ^{87}Sr (7.0%) and ^{88}Sr (82.58%)) (Ropp 2013) and is a naturally occurring alkaline earth metal (Group IIA) with an atomic mass of 87.62 ± 0.01 u (Faure and Powell 1972). ^{87}Sr is formed by the decay of rubidium (Rb), a naturally occurring substance in geologic materials, and the quantity of Sr varies based on the age of a mineral (Faure and Powell 1972; Beard and Johnson 2000; Bentley 2006). Rb and Sr naturally occur in igneous, metamorphic, and sedimentary geological strata (Faure and Powell 1972).

Strontium closely resembles calcium (Ca) and readily substitutes for Ca in the inorganic component of bones and teeth, hydroxyapatite, due to their similar atomic structuring. In provenancing research, the ratio of ^{87}Sr to ^{86}Sr is measured in tissues. For the geo/trace-elements of strontium and lead (as opposed to bio-elements that make up most of organic matter), raw ratios are used because they are meaningful to several decimal places. $^{87}Sr/^{86}Sr$ ratios vary based on the age of the rock, given that ^{87}Sr is a decay product of ^{87}Rb; however, it is not radioactive (it is radiogenic, thus produced by radioactivity instead). Lower $^{87}Sr/^{86}Sr$ ratios are associated with younger rocks, while higher ratios indicate older geological formations. The ratio of $^{87}Sr/^{86}Sr$ is used because of their similar relative abundances (Capo *et al.* 1998).

The $^{87}Sr/^{86}Sr$ ratio of an organism's tissues reflects the intake of environmental $^{87}Sr/^{86}Sr$ values during the time of tissue formation and can be used as an indicator of residency and to track migration (Figure 2.1; Beard and Johnson 2000; Bentley and Knipper 2005; Bentley 2006; Lee-Thorp 2008) due to the fact that there is little to no mass-dependent fractionation occurring during ecological, chemical, or biological processes (Åberg 1995; Capo *et al.* 1998).

In herbivores, the $^{87}Sr/^{86}Sr$ ratios represent an average of the plant material that is ingested from the local landscape. Migration studies using strontium isotopes have been conducted for many regions around the world, such as Europe (Schweissing and Grupe 2003; Bentley and Knipper 2005; Kootker *et al.* 2016; Bol *et al.* 2007; Bentley *et al.* 2004), Africa (Sealy *et al.* 1991; Sillen *et al.* 1995), Central America (Wright 2005; Price *et al.* 2015; Laffoon *et al.* 2017; Thornton 2011; Warner *et al.* 2018; White *et al.* 2007; Wright 2012; Price *et al.* 2000; Price *et al.* 2008; Knudson and Buikstra 2007; Freiwald 2011; Bataille *et al.* 2012), South America (Knudson and Buikstra 2007; Knudson *et al.* 2009; 2005), North America (Ezzo *et al.* 1997; Price *et al.* 1994), and Asia (Regan 2006).

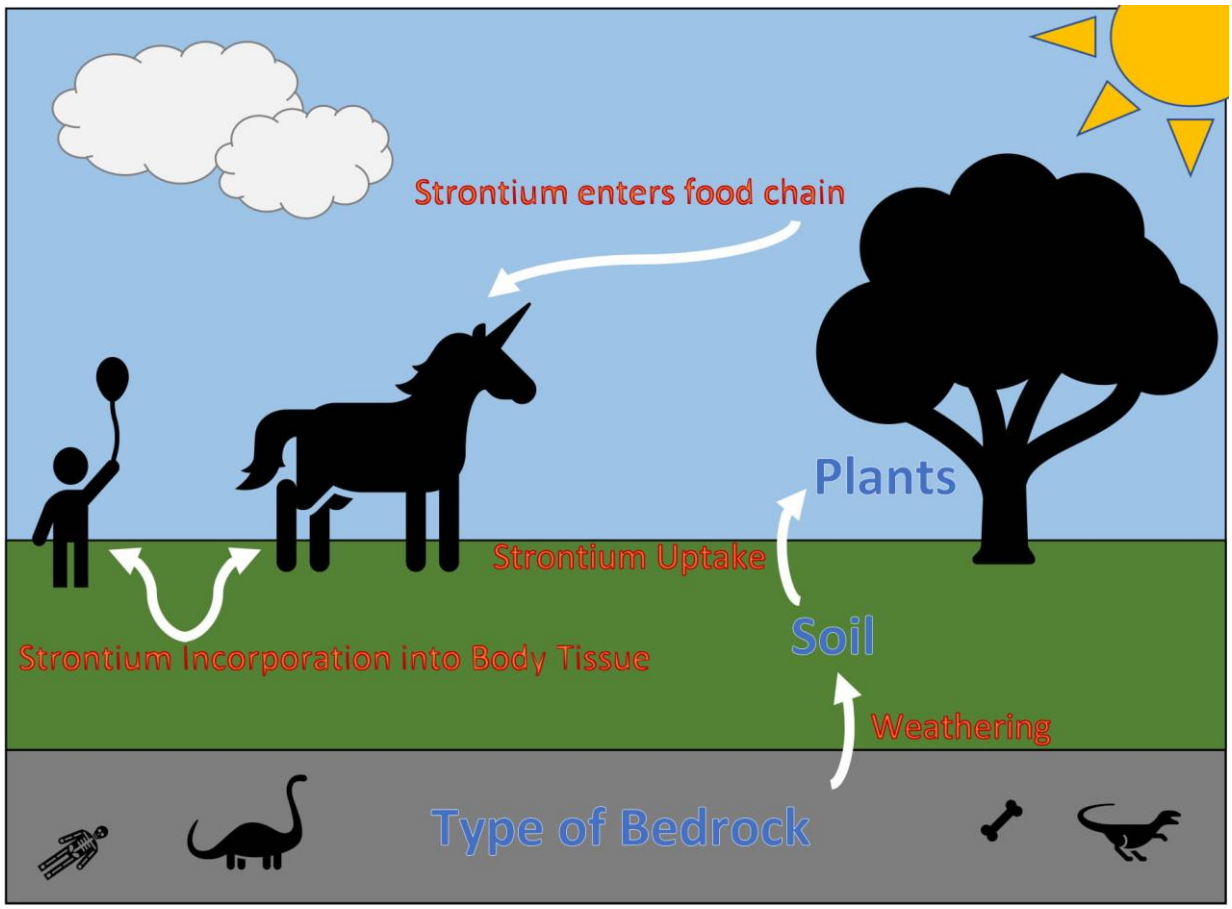

Figure 2.2. Incorporation of strontium into the human skeleton.

2. 3. Isoscapes

According to Bowen (2010) and West *et al.* (2010), the distribution of spatio-temporal isotopes can be mapped and predicted across space and time using "isoscapes", or isotopic landscapes (= maps of spatial isotopic variation). Isoscapes represent spatially explicit predictions of isotope ratios by interpolating natural spatial isotopic distributions to global-scale patterns. These are produced by using process-level models of elemental isotope fractions or distribution in a geographic information system (GIS) (Bowen 2010a). Isoscapes are created by sampling an environmental source, such as soil, plants, water, or local bedrock as well as biological materials like bones, teeth, hair, trees, fruits, or vegetables to characterize the isotope baseline value for a local region.

Using geostatistical methods, isotope values for untested sites can be predicted or inferred using interpolation (Bowen 2010a; 2010b). Interpolation should be employed cautiously because it may not consider the additional sources which contribute to the bioavailability of an isotope, such as the atmosphere, climate, and distribution of soil and bedrock (Bataille and Bowen 2012). The analysis of isoscapes and the comparison of the isoscape predictions with observational data have been used for various purposes, such as to test biogeochemical models, calculate aerially integrated biogeochemical fluxes based on isotope mass balance, and determine spatial connectivity in biogeochemical, ecological, and anthropogenic systems (Bowen 2010a; 2010b).

2. 4. Previous Research and Forensic Applications

Each human being records the so-called isotopic fingerprint of the place she or he lived. Using isotopic composition of body tissues, it is, therefore, possible to trace the location of origin of individuals (Beard and Johnson 2000). Stable isotope ratios are thus helpful in the identification of unknown remains and solving of criminal cases (Lehn and Graw 2014; 2016). Isotope analysis has proven to be a useful method for predicting region-of-origin and tracking changing residence patterns among individuals during various stages of their lives (Benson *et al.* 2006; Regan 2006; Beard and Johnson 2000; Bartelink and Chesson 2019; Bartelink *et al.* 2014b; Bartelink *et al.* 2016; 2018; Warner *et al.* 2018; Kramer *et al.* 2020) and has been used to track migration in archaeological settings around the world: Europe (Schweissing and Grupe 2003; Bentley and Knipper 2005; Kootker *et al.* 2016; Bol *et al.* 2007; Bentley *et al.* 2004), Africa (Sealy *et al.* 1991; Sillen *et al.* 1995), Central America (Price *et al.* 2015; Wright 2012; Laffoon *et al.* 2017; Thornton 2011; Warner *et al.* 2018; White *et al.* 2007; Wright 2005; Price *et al.* 2000; Price *et al.* 2008; Knudson and Buikstra 2007; Freiwald 2011; Bataille *et al.* 2012), South America (Knudson and

Buikstra 2007; Knudson *et al.* 2009; 2005), North America (Ezzo *et al.* 1997; Price *et al.* 1994), and Asia (Regan 2006).

As isotopes are incorporated into the hard (*i.e.*, bones and teeth) and soft tissues (*i.e.*, skin, hair, nails) of organisms, their tissues reflect the isotopic signatures of food and water ingested while that tissue was forming. For example, teeth carry a signature of childhood diet because the dentition is formed during infancy and childhood and does not remodel during life (Hillson 2013). Bones, on the other hand, are constantly remodeling and should reflect the last 1-2 decades of dietary intake based on which bone is sampled (Hill and Orth 1998). Isotopes derived from soft keratinaceous tissues, like hair and fingernails, have been used to track diet and migration months and even weeks before death (Ehleringer *et al.* 2008; Tipple 2015). By targeting different tissues, investigators can infer diet and predict residential location for an individual during specific time periods of their life prior to death. Therefore, isotope analysis can provide investigators with additional lines of evidence that could increase the likelihood of identification for unidentified forensic cases.

Isotope analysis has been used on a small-scale in forensics but has never in large-scale identification efforts (Fraser *et al.* 2006). Examples are the identification of the "Berlin case" (Lehn and Graw 2016), and the waterlogged remains in Amsterdam (Font *et al.* 2015). Various isotopes archived in different body tissues representing different timeframes (hair, rib, femur, enamel, and dentin of premolars and molars) were analyzed to investigate mobility patterns for different periods of life (Alkass *et al.* 2011). Another prominent example of identification of a person through isotope analysis was discussed by Meier-Augenstein and Fraser (2008). Isotope analysis gave the investigating officer the necessary geographic information for the previous movements of the victim as well as the essential lead to conduct DNA analysis on a presumed child of the victim, which ultimately led to the identification. The isotope analysis furthermore more aided the apprehension of the perpetrators, known as the "Scissor Sisters," who dismembered and mutilated the body. Although this review illustrates a variety of archaeological and forensic applications for which isotope analysis has been utilized, it demonstrates that isotope analysis has not been used to solve large-scale disasters such as a migration crisis.

As stressed above, a migrant's region-of-origin is a crucial piece of evidence that can aid the identification process and plays a major role in shaping their reasons for migration, how and where they attempt to cross the Mexico-U.S. border, and their desired final destinations. For example, the majority of deceased migrants recovered in southern Texas and identified by OpID originate from the Central American countries of El Salvador, Honduras, and Guatemala, the so-called Northern Triangle countries (Kramer *et al.* 2020). On the other hand, the PCOME in

Arizona records a larger portion of Mexican nationals among their identified deceased migrant cases (Martínez *et al.* 2014; Anderson and Parks 2008; Massey *et al.* 2002). It is important to understand the nationality profiles of recovered deceased migrants because they can be used to better understand the scope of the issue and potentially bring awareness to the events affecting migration and the humanitarian crisis at the border. Isotope analysis provides a novel approach for predicting region-of-origin for deceased unidentified Latin American migrants and may prove useful in humanitarian crises around the world.

It is furthermore important to note that there are isoscapes of Europe representing the isotopic values of various elements but that there are very limited resources in that regard of Central and South America. Oftentimes, investigators rely on archaeological data, which can potentially skew the investigation and identification of individuals.

CHAPTER III
BODY TISSUES AND TAP WATER

Theoretically, any biological tissue or bodily fluid can be used for isotopic analysis, such as blood, muscle, or nails. However, in forensic anthropology bone, teeth, and hair (especially head hair but also all other types) are most used because they are very durable and do not decompose easily compared to other human tissues. Therefore, the isotope values of bone, dental enamel, and hair reflect the geological origins on which the dietary intake was sourced. Isotope analysis typically focuses on individual molecular compounds and requires a basic comprehension of the compositional differences between biological tissues. Human bones, teeth, hair, and nails are excellent candidates for isotope analysis due to their makeup. A brief overview of these tissues and their structures is provided below. Furthermore, tap water, which is used for hydration, food preparation as well as body hygiene serves as a baseline for region variation in oxygen, hydrogen, and strontium isotopic values. This is the case because, through the direct or indirect consumption, the elements get incorporated into all body tissues, including hair, bones, and teeth.

3. 1. Bone Structure, Composition and Remodeling

There are approximately 206 named bones in the typical adult skeleton that are differentiated by type: long, short, irregular, flat, and sesamoid. Bone functions to provide support and protection of organs, to produce red and white blood cells within the bone marrow, to store minerals, to provide structure and support for the body, and to enable mobility. All bones are made up of two structural components: the compact (cortical) and the spongy (cancellous/trabecular) bone (White *et al.* 2011). The molecular and cellular makeup of both components is identical, only differing in porosity (5-10% and 75-95% porosity respectively) (Martin *et al.* 2015). The compact bone makes up the walls of bone shafts as well as the external bone surfaces. At joints, the compact bone that is covered with cartilage is termed subchondral bone. Other kinds of tissues found in and on human bones are the bone marrow, nerves, blood vessels, endosteum, periosteum as well as cartilage.

Bone is a composite material that is formed of organic protein (primarily collagen) and inorganic apatite mineral (primarily highly substituted and poorly crystalline apatite mineral ($Ca_{10}(PO_4)_6(OH)_2$)). They make up 20-25% and 60% of the dry bone weight respectively (Martin *et al.* 2015). Collagen is the main structural protein in the extracellular spaces in the various connective tissues in the human body. It is the most abundant protein in mammals and is mostly found in fibrous tissues (such as tendons, ligaments, and skin) to provide bone its flexibility. It

can also be found in bones, corneas, cartilage, blood vessels intervertebral discs, the gut, and dentin (Lynnerup and Klaus 2019). The crystals of the mineral biological hydroxyapatite, or bioapatite, infiltrate the collagen matrix, giving the bone its hardness and rigidity (White *et al.* 2011). Isotopically speaking, the collagen will be representative of the dietary protein intake, with the bioapatite being representative of the whole diet (Tykot 2006; Ambrose and Norr 1993; Tieszen and Fagre 1993). Depending on the type of bone, the amount of organic and inorganic material varies as the function of the bone varies as well. A weight-bearing bone, such as the tibia or femur, obviously will contain more compact bone to sustain constant stress.

Growth-related modeling occurs throughout growth and development and ceases for a given bone whenever the epiphysis is fully united with the metaphysis. However, general remodeling occurs during the entire lifespan of an individual. Even though human bone is a very highly durable material, the human body continually replaces damaged or fatigued osseous tissue with new, structurally sound tissue through osteoclastic resorption and osteoblastic activity. Furthermore, remodeling is needed to provide the body with calcium and phosphate that is locked up in the bone (Rodan and Martin 2000; Lynnerup and Klaus 2019).

Remodeling is a cyclical process of bone resorption and deposition at one site (White *et al.* 2011). The remodeling rates, as well as growth times, vary for different tissues. A healthy adult may resorb and replace approximately 3 million new bone remodeling units (BRU, also called basic multicellular units, or BMUs), each one taking 3 to 4 months from activation to completion in one single year (Frost 1999; Ortner 2003). This process consists of four phases: activation, resorption, reversal and formation (Waldron 2008). The standard turnover of bone consists of a balanced act between the destructive action of the osteoclasts and the production capability of the osteoblasts. Osteoclasts resorb bone at a rate of approximately three weeks per site, whereas osteoblasts need three to four months per site for bone constructing (Rodan and Martin 2000; Lynnerup and Klaus 2019). Wolff's Law states that bone is deposited where it is needed and resorbed where it is not neededm based on the stresses that affect the bone.

Osseous elements that consist predominantly of trabecular bone (such as ribs, vertebrae, and the iliac crest) have faster remodeling rates, while bones that are more compact (bones of the extremities and skull) show slower remodeling rates (Hedges *et al.* 2007). Bone remodeling rates vary by bone, *e.g.* the iliac crest has a yearly remodeling rate of approximately 50%, the ribs of 17%, and the femur of 2.9%, depending on the age and sex of the individual (Rummel *et al.* 2007). This faster remodeling rate (~25%) is associated with the support of mineral homeostasis, which is necessary for the maintenance of certain physiological functions (Ortner 2003). Overall, it is thought that ribs remodel completely roughly every 5 years while weight bearing bones, such as

femora and tibiae, remodel every 20-25 years (Frost 1990; Hedges *et al.* 2007; Meier-Augenstein and Fraser 2008; Pearson and Lieberman 2004)

During childhood and adolescence, the remodeling rates can be 2 to 5 times higher than in fully developed bones, which usually occurs in a person's twenties based on the predominantly sampled bones. The skeletons of middle-aged adults contain about 50% of the osseous material from their youth (Lehn and Graw, 2014). Due to the slow remodeling rates, cortical bones can store information for up to 50 years ago (Lehn and Graw, 2014). The mineral component and the collagen of the bone have about the same remodeling rates and therefore the same integration times of the elements (Shin *et al.* 2004; Wild *et al.* 2000). This makes it very elementally stable and therefore ideal for isotope analysis.

3. 2. Tooth Enamel Structure, Composition, and Remodeling

Humans develop two sets of teeth during their lifetime, the deciduous and the permanent teeth. The deciduous teeth begin mineralizing (forming) in utero and erupt from early infancy through early childhood, while some permanent teeth start forming before birth and all by ten years of age (Nelson 2014; Hillson 1996; Smith 1991). Every tooth can be divided into a crown and root portion, consisting of four tissues: enamel, cementum, dentin (referred to as hard tissues), and pulp (which is a soft tissue) (Cunningham *et al.* 2016). While the crown is covered with enamel, the root portion is covered with cementum (Nelson 2014).

Tooth enamel is composed of ~97% inorganic minerals (carbonate rich, hydroxyl-deficient apatite), ~1% organic protein (amelogenin), and ~2% water (Laffoon *et al.* 2017; He and Swain 2007; Hillson 1996). The organic portion of tooth enamel is primarily composed of the protein amelogenin, which has a similar function as collagen in bone, providing a structural matrix for the deposition of inorganic minerals (Hillson 1996). The inorganic mineral portion of tooth enamel functions similarly to bone hydroxyapatite but consists of larger crystals and contains a superior structural organization, a structure that allows for fewer ionic substitutions than in bone (Ross and Pawlina 2010). The inorganic material consists predominantly of calcium phosphate in the form of hydroxyapatite crystals, which are carbonated or fluoridated (Hueb De Menezes Oliveira *et al.* 2010; Gwinnett 1992; ten Cate and Featherstone 1991).

The enamel microstructure comprises crystals that are arranged in prisms or rods, which run roughly perpendicular from the dentin-enamel junction towards the surface of the tooth (Ortner 2003; Fava *et al.* 1997; ten Cate and Featherstone 1991). According to Fejerskov, Josephsen, and Nyvad (1984), the interfacial area between prisms is called inter-prismatic enamel and is protein-rich. In the prism-less enamel layer, the hydroxyapatite crystals are arranged

parallel to one another and perpendicular to the surface of the enamel (Hueb De Menezes Oliveira *et al.* 2010; Fava *et al.* 1997; Stack 1967). Because of its high mineral content, enamel is the hardest tissue found in the human body. Furthermore, unlike bone and dentine, enamel, once it is deposited, does not remodel over the lifetime of the individual (Hillson 1996). Since teeth do not remodel, they maintain the original elemental signature and the encoded information will not change during the lifetime of an individual. This makes teeth the perfect bio-material for isotope analysis (Lee-Thorp 2002). As elaborated above, the first molar starts mineralizing around birth, capturing information from where the person may have lived then. Half of the enamel forming cells (ameloblasts) undergo apoptosis (disappear) during amelogenesis, and the rest die after the maturation stage, *i.e.*, during and after eruption (Giacaman *et al.* 2016; Matalová *et al.* 2015).

3. 3. Hair Structure and Composition

Human scalp hair starts growing from follicles, which are little "pockets" in the skin and are nourished by blood vessels that create more cells, which in return make the hair grow. In total, 80,000 to 150,000 follicles are located on the scalp (Krause and Foitzik 2006). It is the only organ in the mammalian organism that undergoes life-long cycles of rapid growth, regression, and resting periods, referred to as anagen, catagen, and telogen respectively (Krause and Foitzik 2006).

According to Font *et al.* (2012), human hair is composed of keratin, which is a tough structural fibrous protein that comprises of 50% carbon, 21% nitrogen, 17.5% hydrogen, 6.5% oxygen, and 5% sulfur, but also includes trace contents of metals such as strontium. The trace elements are integrated into the hair structure through consumption of food and water and exposure to outside sources such as air and water.

Once hair is long enough to exit the protection of the skin, it dies. Human scalp hair grows at an average of 1 cm per month, and since the elemental exchange between hair and blood ceases when it dies off, it retains the biogenic and dietary information, preserving a longitudinal record of stable isotope signatures (Font *et al.* 2012; Krause and Foitzik 2006). It is important to note, however, that not all hair grows at the same time and therefore, it is essential to choose the hair wisely when it is not analyzed as a bulk but rather used to acquire information from a certain time period (Mekota *et al.* 2006). This method of using human scalp hair strands has been demonstrated on modern individuals as well as for archaeological casework (Chesson *et al.* 2018a,c; Lehn *et al.* 2019; Santamaria-Fernandez *et al.* 2009; Huelsemann *et al.* 2009).

3. 4. Diagenesis and Forensic Material

As used here, diagenesis is any physical, chemical, or biological alteration of biological remains following death and body deposition (Meier-Augenstein 2010). Causes, mechanisms, and effects vary widely depending on the tissue type (Darwent and Lyman 2001). Even though no tissue is completely immune to diagenetic processes, the dense makeup of tooth enamel is very protective of isotopic information. Bone, a more porous tissue, is therefore understandably more prone to exterior influences.

For example, an individual found clothed and in a surface burial context will not have exhibited the same diagenetic changes as an individual found buried subsurface in wet soil. For buried remains, the extent of diagenetic alteration to bone largely depends on the chemistry of the burial context and material culture associated with the body. Furthermore, Hedges (2002) cites a number of intrinsic factors that may determine the diagenetic influences, such as size, shape, condition, and age of the bone.

Forensic anthropology decomposition facilities, commonly known as "body farms", around the world have explored the extrinsic factors (*e.g.*, temperature, aridity, microbial activity, scavenging, etc.) that contribute to differential decomposition rates in hopes of better estimating the postmortem interval for forensic cases. Overall, in most modern forensic anthropology cases, diagenesis will not have a negative effect on the isotopic results unless the remains have been buried or exposed to the elements for long periods of time (longer than months) (Gordon *et al.* 2018; Bartelink *et al.* 2018; Hedges *et al.* 2006).

3. 5. Tap Water

Drinkable tap water resources constitute a significant challenge across the globe, and Mexico is a prime example for the lack of sustainable drinking water resources. This fact is highlighted by the fact that Mexico is one of the highest bottled water consumers per capita in the world (Contreras 2019; Inter-American Development Bank 2011). Bowen *et al.* (2005) found the $\delta^{18}O$ and $\delta^{2}H$ isotopic values of bottled water from around the world to be very similar to the signatures found in the local tap water. It is, however, unknown if this is also the case for Mexico. While Mexican authorities and other institutions such as the Inter-American Development Bank have worked hard in the last couple of years to tackle the contamination problems in the Mexican river and lake systems as well as the deficiency in sanitation, the lack of clean tap water still exists (Inter-American Development Bank 2013). The availability of water. in terms of both quantity and quality. is spatially highly varied and reports show that over 30 million citizens lack high quality water services or have overall limited access to water (World Bank 2018). All factors are

largely dependent on economic prosperity. While the Global Network for Isotopes in Precipitation (GNIP) dataset provides a crucial foundation for establishing global precipitation controlled isotopic landscapes (commonly called isoscapes), it has insufficient spatial coverage in Mexico. There are 39 recording stations in the United States but merely two in Mexico (Veracruz and Chihuahua) in a country of almost 2 million square kilometers (International Atomic Energy Agency and World Meteorological Organization 2018). This spatial deficiency is a major concern when attempting to answer research questions concerning large scale Mexican isotope hydrology, ranging from determining the origins of food (Primrose *et al.* 2010) to reconstructing the travel history or region of origin of an individual (Ehleringer *et al.* 2008). Consequently, this research is a pertinent step towards overcoming the major limitation in the $\delta^{18}O$ and $\delta^{2}H$ isoscape data in Mexico, and therefore the limitations in potentially aiding the identification of human remains through isotope analysis. Furthermore, $^{87}Sr/^{86}Sr$ in water have most commonly been used to examine ecosystem processes and answer various hydrological and geological questions, such as surface and ground water interactions, source mixing, contaminations, provenancing of water, and mineral weathering (Nigro *et al.* 2017; Hogan *et al.* 2000; Capo *et al.* 1998; Négrel and Petelet-Giraud 2005; Frei and Frei 2011). This has, more recently, developed into the possibility of sourcing individuals (Rauch *et al.* 2007).

CHAPTER IV

THE SAMPLES- MATERIALS AND METHODS

Based on the justifications given in Chapter III Body Tissues and Tap Water, the human tissue and tap water samples used in this study will be presented in further detail. First, the human hair samples (Chapter 4.1) and the tap water (Chapter 4.2) samples collected throughout Mexico are reviewed and the sampling locations visually presented. The collection procedures for both sample types are described and discussed. An overview over all collected sample sites can be seen in Figure 4.1. The red dots represent sampling locations from where human hair and tap water samples were collected. The sampling locations from where only water was collected are represented by the blue dots. Furthermore, two locations, from where only hair samples were collected, are shown by the green dots.

In section 4.3, the human tissue samples of UBCs from the Pima County Office of the Medical Examiner (PCOME) are presented. A total of 16 individuals were sampled for this research. For all individuals rib, long bone, and tooth samples were collected. For seven of the 16 individuals, hair samples were available for collection. The standard operating procedures for the cleaning of the hair, bone and tooth samples are outlined in the Supplementary Material of the chapter.

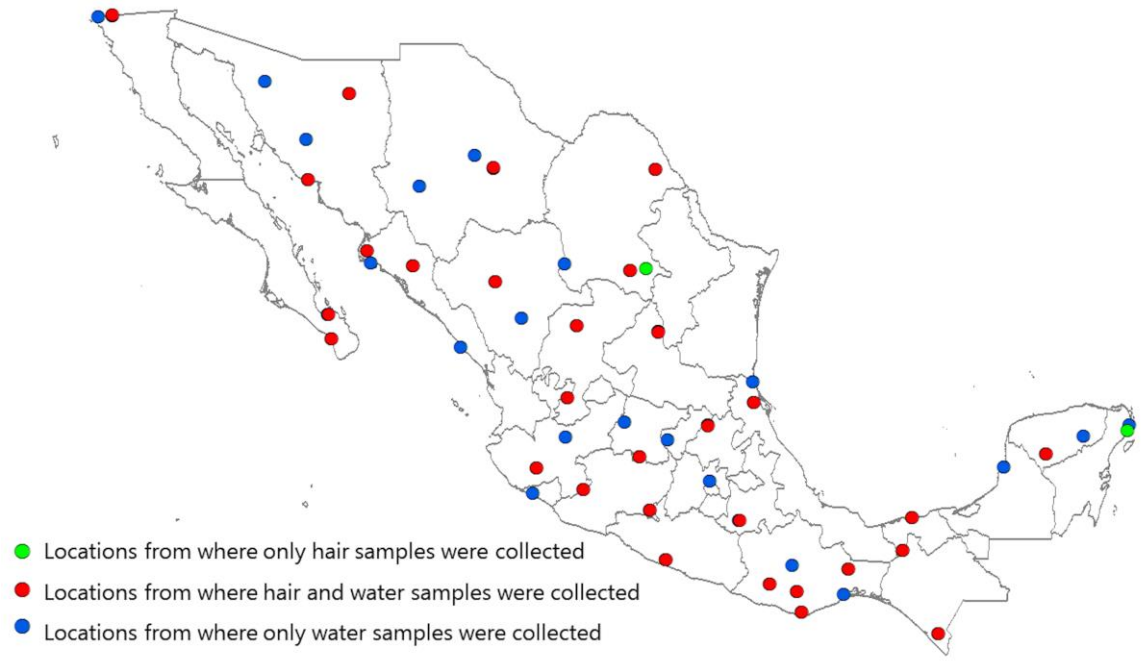

Figure 4.1. Sample Collection Sites in Mexico. Red dots represent the locations from where hair and tap water samples were collected. Blue dots represent the locations from where only tap water samples were collected. Green dots represent locations from where only hair samples were collected.

4. 1. The Human Hair Samples from Mexico

To comply with all ethics concerns, the hair samples are being picked up from the floor, they are considered ‘trash' by the Institutional Review Board and are not subject to protocol requirements. A total of 101 discarded human head hair samples were collected in barbershops and hair salons in 32 towns and cities in Mexico (Figure 4.2) during a six-week period between June and July 2018. Since this hair collection was anonymous, no information regarding sex, age, diet, or travel history was collected from the individuals. Only bunches of hair of the same color and texture were collected to ensure that the discarded hair belonged to one individual and that the sample was not contaminated by other customers of the barbershop. All samples were placed in separate paper envelopes and stored in airtight bags. A minimum of three samples per location were gathered, with the exceptions of La Paz, Baja California Sur and Saltillo, Coahuila, where only one sample was collected. These two locations were disregarded in location average and standard deviation calculations.

Figure 4.2. Map of Mexico showing the sampling locations of human hair.

The following locations were chosen to collect human hair samples from. Two of the locations initially chosen were not accessible

- ☑ Puerto Morelos, Quintana Roo
- ☑ Tekax de Álvaro Obregón, Yucatan
- ☑ Paraíso, Tabasco
- ☒ Tila, Chiapas

  The national road 199 (Ocosingo- San Christóbal de las Casas) was (and still is) blocked near the town of Oxchuc and the Federal Police advised against using it as two tourists have recently been killed and others held for ransom. The samples were collected in the towns of *Plan de Ayala* and *Lindavista*, Chiapas instead.
- ☑ Huixtla, Chiapas
- ☑ San Juan Guichicovi, Oaxaca
- ☑ San Pedro Pochutla, Oaxaca
- ☑ Miahuatlán de Porfirio Díaz, Oaxaca
- ☒ Santa Cruz Zenzontepec, Oaxaca

  The town of Santa Cruz Zenzontepec was blocked off due to a three-way conflict among the municipality and the *communa* and a large corporation. A foreign company wants to use the mountainous region to build a dam as well as search for valuable minerals. This disagrees with the *communa* and municipality and therefore, no foreigners to the region can enter the town. Instead, samples were collected in a community close by: *San Jacinto Tlacotepec*, Oaxaca. Since they are facing similar issues, the local police and community leaders were consulted. They agreed that three police officers would donate hair to this research project.
- ☑ Tehuitzingo, Puebla
- ☑ Atoyac de Álvarez, Guerrero
- ☑ Huetamo de Núñez, Michoacán
- ☑ Tepalcatepec, Michoacán
- ☑ El Grullo, Jalisco
- ☑ Tlaltenango de Sánchez Román, Zacatecas
- ☑ Moroleón, Guanajuato
- ☑ Jacala, Hidalgo
- ☑ Ozuluama de Mascareñas, Veracruz
- ☑Matehuala, San Luis Potosi
- ☑ General Capeda, Coahuila
- ☑ Villa Unión, Coahuila
- ☑ Saltillo, Coahuila → only one sample was collected from this location
- ☑ Pedro Meoqui, Chihuahua
- ☑ Santiago Papasquiaro, Durango

☑ Río Grande, Zacatecas
☑ El Salto, Sinaloa
☑ Villa de Ahome, Sinaloa
☑ Todos Los Santos, Baja California Sur
☑ La Paz, Baja California Sur → only one sample was collected from this location
☑ Guaymas, Sonora
☑ Nacozari de García, Sonora
☑ Tecate, Baja California

Notes to Plan de Ayala and Lindavista, Chiapas: The two towns are one community divided by the Mezcalapa River. A small boat continuously crosses the river and lets the inhabitants commute from one to the other for school, shopping, and work. When talking to the local pharmacist, he informed me that they are having a Hepatitis A epidemic in Lindavista, the smaller community of the two. They have had over 50 new cases in the last year, which is enormous considering Lindavista only has 716 inhabitants. Plan de Ayala only has had very few cases. According to PueblosAmerica.com, not even 4% of the homes have piped water. Since the most prominent ways to transmit the disease is through contaminated food or water, it has to be feared that one of the water sources is contaminated. The two communities have contacted the Mexican government for intervention; however, they have not received any aid.

Notes on Santa Cruz Zenzontepec, Oaxaca: As mentioned above, there have been some recent but ongoing conflicts among government, *communas* and big corporations. The landowners (owners of so-called Haciendas) were expropriated during the revolution and only a larger group of people was allowed to own land together (so-called *communas/ejidos*). Before the revolution, the owner not only owned the land but indirectly also the inhabitants of the land. It was not a rare occurrence that they had their own currency in which they paid their employees. There was no way to change the money into another currency. Nowadays, some towns are both, a *communa* as well as a municipality. The municipality, being part of the public administration and federal government, is responsible for the "town" (security, electricity, public services etc.). The *communa* is in charge for the "earth" (access to soil, water etc.). As one can imagine, this division can cause various issues, especially as big corporations are getting involved as well. Currently, a company is trying to access the land to build a dam and exploit the soil for natural resources. The *communa* is explicitly divided up by family, which means that the families that would be affected by this project would have no space to relocate within the *communa*. Because

of previous conflicts, the representatives of the municipality and the *communa* have established the rule that if one decides "no" on a subject, both will support that standpoint. They furthermore have established that no samples are to be taken on their land, unfortunately that also included hair and water.

4. 2. The Tap Water Samples from Mexico

Towns and cities throughout Mexico were sampled during a six-week period from June to July 2018 to characterize the tap water ratios across the country and explore potential spatial variations (Figure 4.3). During the data collection period, 26 out of 32 states were sampled: Baja California, Baja California Sur, Chiapas, Campeche, Chihuahua, Coahuila, Colima, Durango, Guanajuato, Guerrero, Hidalgo, Jalisco, Mexico City, Michoacán, Oaxaca, Puebla, Querétaro, Quintana Roo, San Luis Potosi, Sinaloa, Sonora, Tabasco, Tamaulipas, Veracruz, Yucatan, Zacatecas. At least three tap water samples were collected from each location to evaluate local variation as well as inter-regional variation within Mexico.

Sample locations were chosen by geographic variation to obtain relatively complete coverage of Mexico. Both large cities as well as rural communities, were sampled. Nonetheless, a major factor was also accessibility. Some municipalities turn off the water source during the day to preserve water or prohibit foreigners from entering their villages due to recent conflicts with big international companies. Some other locations could not be sampled due to roadblocks and safety concerns.

For the oxygen and hydrogen isotopic analyses, the collection yielded a total of 158 tap water samples from fifty-four locations. Unfortunately, one less location was samples for the strontium analyses and therefore only 156 samples were collected. Samples were collected from local tap water sources by running cold water for approximately 10 seconds before filling the clean vials. 4mL glass vial and 30mL LDPE vials were used for the samples for oxygen and hydrogen, and strontium, respectively. 50µL of 6M nitric acid were added to the 30mL tap water samples. It was ensured that no air bubbles were present within the vial to avoid fractionation. After capping, the vials were sealed with Parafilm® to avoid the loosening of the caps and sample evapoconcentration. Prior to shipment as well as at the laboratory, the samples were stored in a cool and dark place. Pictures of the sample collection can be found in Figures 4.4 and 4.5.

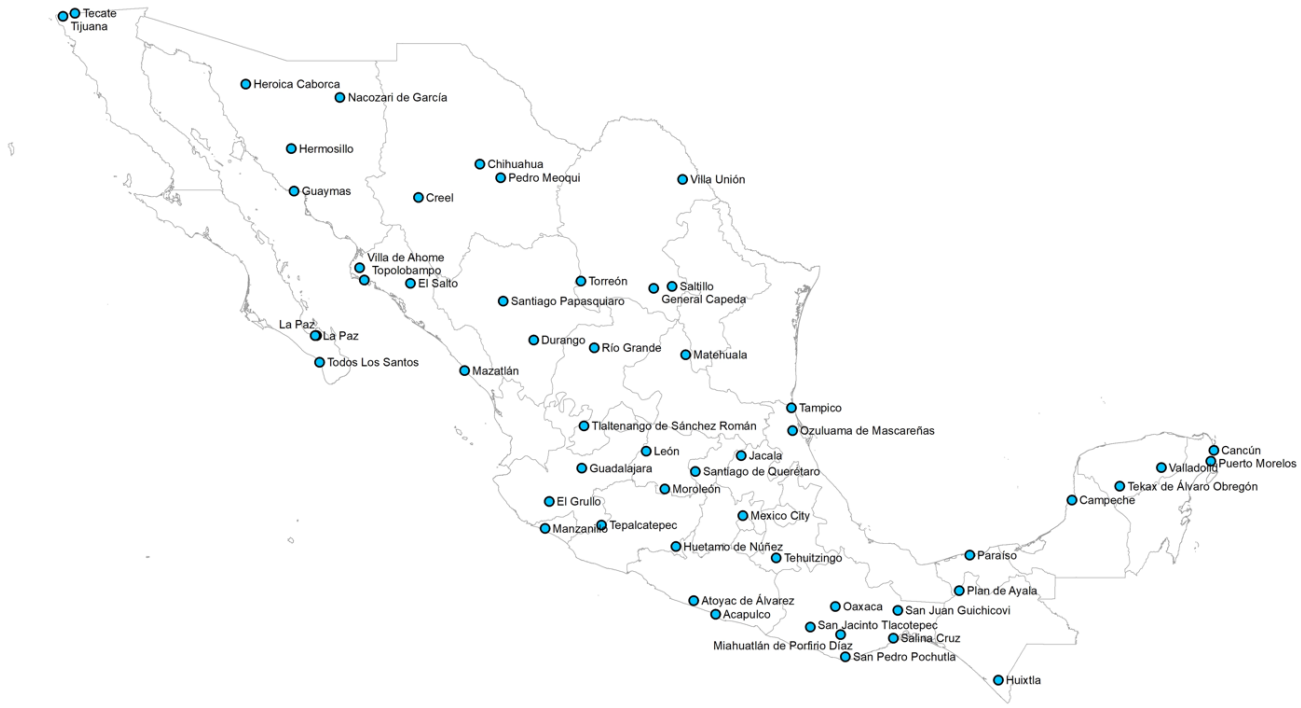

Figure 4.3. Map of Mexico showing the sampling locations of tap water.

Samples were collected from the following locations. The locations were the same as the ones from where hair samples were collected. Additional samples were collected throughout the journey.

- ☑ Cancún, Quintana Roo
- ☑ Puerto Morelos, Quintana Roo
- ☑ Valladolid, Yucatan
- ☑ Campeche, Campeche
- ☑ Lindavista, Chiapas
- ☑ Acapulco, Guerrero
- ☑ Manzanillo, Colima
- ☑ Guadalajara, Jalisco
- ☑ León, Guanajuato
- ☑ Santiago de Querétaro, Querétaro
- ☑ Tampico, Tamaulipas
- ☑ Creel, Chihuahua
- ☑ Mazatlán, Sinaloa
- ☑ Topolobampo, Sinaloa
- ☑ El Salto, Sinaloa
- ☑ Villa de Ahome, Sinaloa
- ☑ Durango, Durango
- ☑ Santiago Papasquiaro, Durango
- ☑ Hermosillo, Sonora
- ☑ Heroica Caborca, Sonora

☑ Nacozari de García, Sonora
☑ La Paz, Baja California Sur
☑ Todos Los Santos, Baja California Sur
☑ Tijuana, Baja California
☑ Mexico City, Mexico
☑ Tehuitzingo, Puebla
☑ Atoyac de Álvarez, Guerrero
☑ Huetamo de Núñez, Michoacán
☑ Tepalcatepec, Michoacán
☑ El Grullo, Jalisco
☑ Tlaltenango de Sánchez Román, Zacatecas
☑ Moroleón, Guanajuato
☑ Jacala, Hidalgo
☑ Ozuluama de Mascareñas, Veracruz
☑ Matehuala, San Luis Potosi
☑ General Capeda, Coahuila
☑ Villa Unión, Coahuila
☑ Torreón, Coahuila
☑ Pedro Meoqui, Chihuahua
☑ Chihuahua, Chihuahua
☑ Río Grande, Zacatecas
☑ Guaymas, Sonora
☑ Tecate, Baja California
☑ Huixtla, Chiapas
☑ San Juan Guichicovi, Oaxaca
☑ San Pedro Pochutla, Oaxaca
☑ San Jacinto Tlacotepec, Oaxaca
☑ Miahuatlán de Porfirio Díaz, Oaxaca
☑ Salina Cruz, Oaxaca
☑ Oaxaca, Oaxaca
☑ Plan de Ayala, Chiapas
☑ Lindavista, Chiapas
☑ Tekax de Álvaro Obregón, Yucatan
☑ Paraíso, Tabasco

In many of the smaller communities, the water supply is cut off during the day. In these cases, water was sampled at the houses that still had water, some houses store the water in airtight tanks on top of their houses. This could, of course, influence the results and will be examined closer in the future.

Figure 4.4. Collection of tap water samples for Oxygen and Hydrogen isotopic analysis.

Figure 4.5. Left photograph: Collection of tap water samples for Strontium isotopic analysis. Right photograph: 50µL of 6M nitric acid were added to conserve the tap water samples.

4. 3. The Samples from the Pima County Office of the Medical Examiner

A total of 16 individuals were sampled to match determine regionality and aid the identification efforts. The bone, tooth and hair samples are part of the ongoing investigations into the deaths of the unidentified persons at the PCOME and therefore are approved for by the chief medical examiner Dr. Hess. An overview over the collected samples can be found in Table 4.1.

As with any study that is at risk for contamination, it was essential to work thoroughly and rigorously to maintain a clean and sterile lab to outside influences. Instruments, equipment, and the surroundings were cleaned between each sample and gloves and a N95 mask were always worn. To minimize the possibility of incorrect isotope readings, cases exhibiting obvious pathology were not considered for this study. Furthermore, all cases showing dramatic postmortem diagenetic alterations were excluded from the research.

Table 4.1. Overview of samples collected at the PCOME.

#	ML #	**Tooth #**	**Femur/ Tibia**	Side	**Rib**	Side	**Hair**
1	17-1681	30 (1st molar right mandible)	Femur	left	yes	right	no
2	17-2186	14 (1st molar left maxilla)	Femur	left	yes	right	no
3	17-2006	3 (1st molar right maxilla)	Femur	right	yes	left	no
4	17-2469	30 (1st molar right mandible)	Femur	left	yes	left	no
5	16-2688	29 (2nd premolar right mandible)	Femur	left	yes	right #6	no
6	16-2623	19 (1st molar left mandible)	Femur	right	yes	right #5	no
7	16-1585	14 (1st molar left maxilla)	Femur	right	yes	right	no
8	17-1466	30 (1st molar right mandible)	Femur	left	yes	left #3	yes
9	17-1944	14 (1st molar left maxilla)	Tibia	right	yes	right #5	no
10	17-1742	30 (1st molar right mandible)	Tibia	right	yes	right #5	yes
11	16-01616	3 (1st molar right maxilla)	Tibia	left	yes	right #7	yes
12	16-1822	6 (canine right maxilla)	Tibia	left	yes	left #3	yes
13	16-01516	19 (1st molar left mandible)	Tibia	right	yes	right #3	yes
14	17-1682	14 (1st molar left maxilla)	Tibia	right	yes	right #2	yes
15	17-1314	19 (1st molar left mandible)	Tibia	right	yes	left #3	yes
16	16-3187	19 (1st molar left mandible)	Femur	right	yes	left #8	no

The sample of the extremity was taken from the bone that the DNA sample was taken from previously. For remains that were in advanced decompositional stages, the femur was usually sampled. If the skin and surrounding tissues were not decomposed yet, the tibia was sampled, as it is generally easier to access when the decedent is fleshed. Specifically, nine femora and seven tibiae were sampled, always from the midshaft, posteriorly or anteriorly, respectively. Photographs of the sample collection procedure can be found in Figure 4.6.

Figure 4.6. Tibia and femur sample collection at the PCOME.

For all except two individuals, the first molar was sampled. For the two exceptions, a second premolar and a canine were extracted, respectively (Figure 4.7).

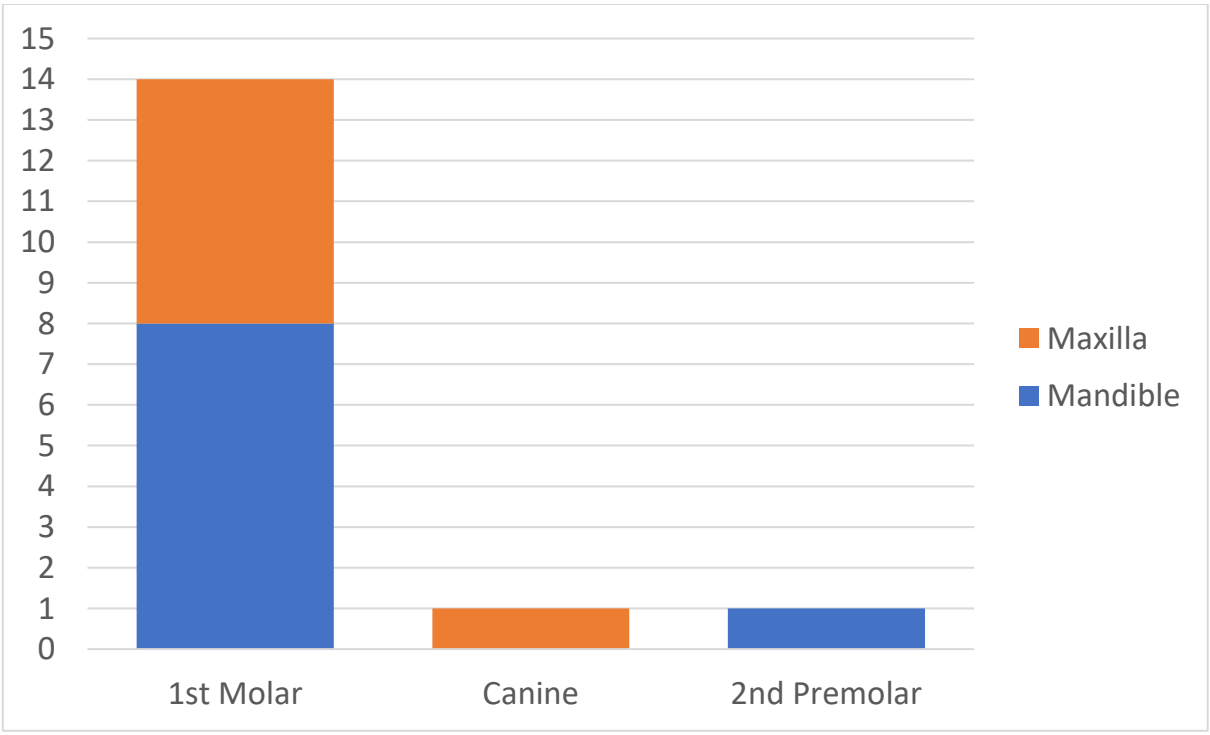

Figure 4.7. Tooth samples.

The ribs were sampled towards the sternal end or an available fragment was selected. An overview of the sampled ribs can be found in Table 4.1 and pictures of the sample collection procedure can be found in Figure 4.8. Depending on the state of decomposition and availability, hair was collected for a total of 7. Photographs of the sample collection procedure can be found in Figure 4.9.

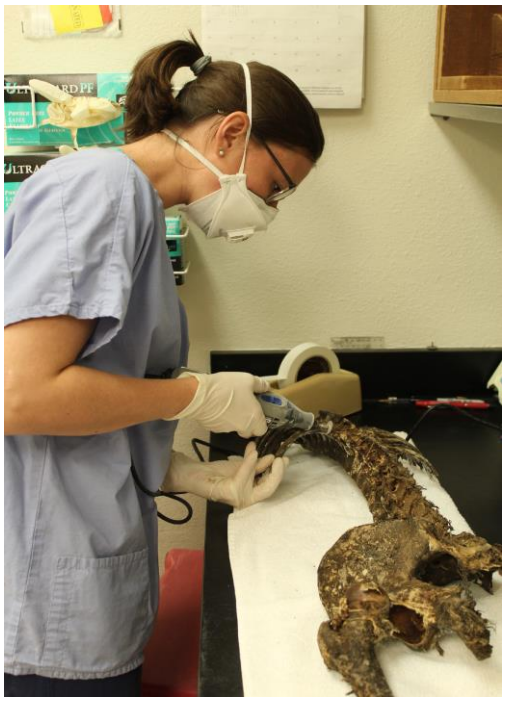

Figure 4.8. Rib Sample Collection at the PCOME.

Figure 4.9. Hair Sample Collection at the PCOME.

4. 4. Summary of the Collected Samples

Overall, a total of 470 samples were collected for this research project, inclduing 101 discarded human head hair samples which were collected throughout Mexico. These samples were used for the strontium, carbon, nitrogen, sulfur, and oxygen isotopic analysis and serve as a baseline for the Mexican population. A visual representation of the cleaned and cut human hair samples in airtight glass vials can be found in Figure 4.10.

Furthermore, 158 tap water samples were collected to create a baseline of oxygen and hydrogen isotopic values from Mexico. Additionally, 156 tap water samples were collected for the strontium isotopic analysis. One location was not sampled, resulting in two less samples. Pictures of the 156 30mL samples can be found in Figure 4.11.

A total of 55 samples were collected from UBCs housed at the PCOME between September and December 2017. The samples originated from 16 individuals, resulting in 16 tooth samples, 16 long bone samples, 16 rib samples, and 7 hair samples. Figure 4.12 shows the airtight sealed samples as well as samples stored in airtight glass vials after being cleaned and cut for sample analysis.

Figure 4.10. Cleaned and cut human hair samples from Mexico.

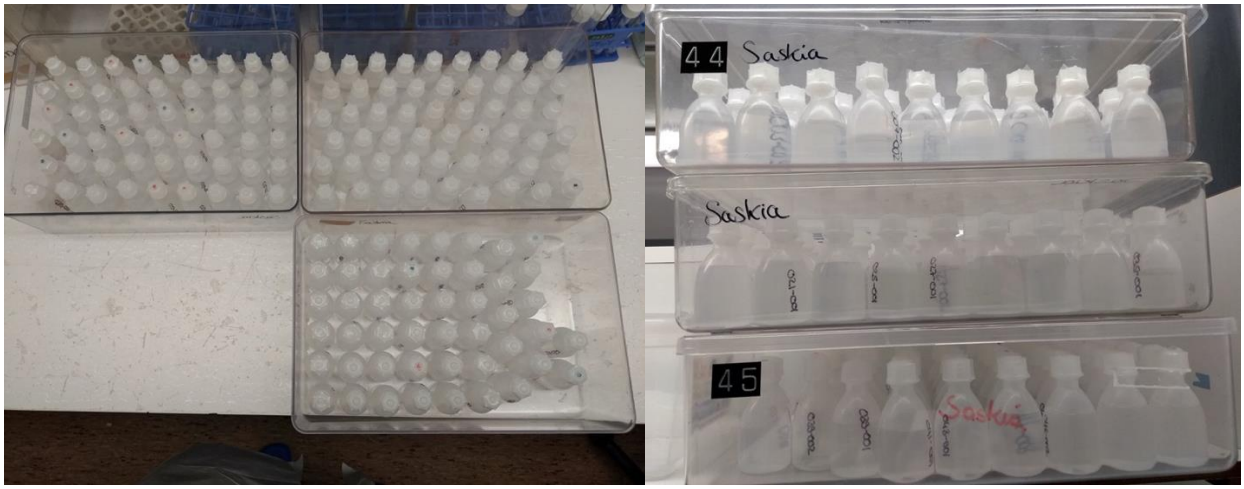

Figure 4.11. 30mL tap water samples from Mexico.

Figure 4.12. Bone, tooth and hair samples from the PCOME. The photograph on the right shows the cleaned and cut samples.

SUPPLEMENTARY MATERIAL. THE SAMPLES CLEANING PROCEDURES

The following sections outline the standard operating procedures for the cleaning of the hair, bone and tooth samples collected throughout Mexico and form the Pima County Office of the Medical Examiner. All sample cleaning took place at the Vrije Universiteit Amsterdam, the Netherlands.

1. Cleaning Procedures of Hair Samples

Items needed: plastic lab coat, safety glasses, hairnet, gloves, plastic sleeves, filter paper, tools (tweezers), 2:1 chloroform/methanol, acetone, ethanol, MilliQ squeeze bottle, aluminum foil

1. Clean 100ml glass beaker with acetone and ethanol.
2. Clean working area with ethanol.
3. Turn on hood.
4. Put waste beaker underneath the vacuum glass:
    a. Clean vacuum glass with acetone by spraying it on the sides of the glass and letting the vacuum suck it through the filter paper,
    b. Repeat step a. with MilliQ water,
    c. Change filter paper after cleaning.
5. Place aluminum foil on working space.
6. Place hair sample onto filter paper inside of vacuum glass.
7. Place hair samples on filter paper and pour chloroform/methanol mixture over the sample, leave to soak for about 20 seconds.
8. Removed mixture through the vacuum and replace with Milli-Q distilled water, leave to soak for about 20 seconds.
9. Repeated four more times.
   (Whenever the filter paper got visibly soiled during these steps, it was replaced by a clean one.)
10. Place hair sample between two new filter papers and wrap with aluminum foil.
11. Opened the foil up on its ends under the laminar flow hood for the samples to dry.
12. Once dry, cut the samples with surgical grade scissors.

2. Cleaning Procedures of Bone Samples

Items needed: clean centrifuge tubes, 1 set of Ezee filters, MilliQ water, EtOH, 2:1 chloroform/methanol, 0.1M NaOH, 0.6M HCl, pH 3 HCl

1. Clean the fume hood and flow hood with NaOCl 10% or H_2O_2 31%. Clean Dremel drill bits by soaking 20 mins in H_2O_2 31%, then 20 minutes in 5% HNO_3. Dry on paper towels.
2. Weigh centrifuge tube and cap. Label.
3. Lay Aluminum foil working surface in fume hood. Cut bone sample, c. 2cm by 1cm. Place in 15mL centrifuge tube, cap. Reweigh.
4. Rinse sample in MilliQ, EtOH, H2O. Sonicate in MilliQ repeatedly until supernatant remains clear. After sonication, shake the sample a bit- it will start bubbling and the liquid discolor. Repeat sonication until no more bubbles and discoloration occur.
5. Add 4mL chloroform/methanol (2:1) mixture; place on rocker for 30 mins.
6. Centrifuge sample, pour off supernatant, rinse in MilliQ x3, centrifuging in between each rinse before supernatant is discarded.
7. Dry down in flow hood on hotplate at 50°C. Reweigh centrifuge tube.

3. Cleaning Procedures of Tooth Samples

Items needed: Ball-tipped diamond drill bit for Dremel, MilliQ, HCl 10%, Ethanol, Weighing Paper, small Eppendorf vials (1.5ml with pop-on lids)

1. Dip drill bit into:
    a. MilliQ,
    b. HCl 10%,
    c. MilliQ,
    d. Ethanol.
2. Clean area on tooth that is supposed to be sampled with drill bit:
    a. DO NOT sample: carious areas, cracked areas, facets.
3. Dip drill bit into again:
    a. MilliQ,
    b. HCl 10%,
    c. MilliQ,
    d. Ethanol.
4. Label Eppendorf Vial with sample number, weigh, record weight.
5. Powder sample with drill bit onto weighing paper.
6. Transfer sample into Eppendorf Vial, weigh vial, record weight.
7. Calculate sample weight.

Repeat powdering with next tooth.

CHAPTER V
RESULTS AND DISCUSSION

Chapters I to IV introduced the project, defined what isotopes are and which chemical elements are used in this study, outlined and discussed the kind of samples that are being used in this study and why, and presented an extensive overview of the samples collected. For this dissertation, human hair and tap water samples from all over Mexico were analyzed to create a database of reference samples that encompass the Mexican population. Furthermore, stable isotope analysis was conducted on 16 undocumented border crossers from the Pima County Office of the Medical Examiner (PCOME) in Tucson, Arizona. An overview was given on the methodology on how those samples were collected as well as from where the samples were collected.

Here, the results of the reference data are presented as well as the results of the isotopic analysis of the undocumented border crossers. The reference data are presented and discussed in Chapters 5.1 to 5.4, featuring two publications from *Forensic Science International*.

- Chapter 5.1: Ammer, Saskia, Eric Bartelink, Jennifer Vollner, Bruce Anderson, and Eugénia Cunha. "Socioeconomic and Geographic Implications from Carbon, Nitrogen, and Sulfur Isotope Ratios in Human Hair from Mexico." *Forensic Science International* (2020): 110455.
- Chapter 5.4: Ammer, Saskia, Lisette Kootker, Eric Bartelink, Bruce Anderson, Eugénia Cunha, and Gareth Davies. "Comparison of strontium isotope ratios in Mexican human hair and tap water as provenance indicators." *Forensic Science International* (2020): 110422.

Chapters 5.2 and 5.3 present the stable isotope ratios of tap water in Mexico and the Oxygen Isotope Ratios in Human Hair Versus Tap Water from Mexico.

Furthermore, this chapter entails the results and discussion of the isotopic analyses of the Undocumented Border Crossers. Specifically, the results of the carbon, nitrogen, sulfur (Chapter 5.5.1), oxygen (Chapter 5.5.2) and strontium (Chapter 5.5.4) isotope analyses in bones, teeth, and hair are presented and discussed. For the oxygen values and the strontium ratios recovered from the human remains, forensic provenancing studies have been developed and are showcased here. Chapter 5.5.3 features the case study published in the Journal of Forensic Sciences:

- Ammer, Saskia TM, Eric J. Bartelink, Jennifer M. Vollner, Bruce E. Anderson, and Eugénia M. Cunha. "Spatial Distributions of Oxygen Stable Isotope Ratios in Tap Water From Mexico for Region of Origin Predictions of Unidentified Border Crossers." *Journal of Forensic Sciences* (2020).

5. 1. Socioeconomic and Geographic Implications from Carbon, Nitrogen and Sulfur Isotope Ratios in Human Hair from Mexico

Paper published in Forensic Science International
Digital Object Identifier:
doi: 10.1016/j.forsciint.2020.110455

Authors:
Saskia T. M. Ammer,[1] M.Sc.; Eric J. Bartelink,[2] Ph.D.; Jennifer M. Vollner,[3] Ph.D.; Bruce E. Anderson,[3] Ph.D.; and Eugénia M. Cunha,[1] Ph.D.

Affiliations:
[1]Laboratory of Forensic Anthropology, Department of Life Sciences Cal"cada Martim de Freitas, University of Coimbra, Coimbra, PT 3000-456.
[2]Department of Anthropology, California State University, Chico, Chico, CA.
[3]Pima County Office of the Medical Examiner, 2825 E District St, Tucson, AZ 85714.

Highlights:
- δ^{13}C, δ^{15}N & δ^{34}S relative isotopic abundances of Mexican human hair were measured
- Value ranges: −18.3 to −12.8 ‰ for δ^{13}C, 6.8 to 10.8 ‰ for δ^{15}N, 2.7 to 8.0 ‰ for δ^{34}S
- δ^{13}C isoscape was generated using a GIS approach
- No significant geospatial distribution was detected in the δ^{15}N and δ^{34}S values
- Carbon showed strong correlations with socioeconomic covariates

Abstract:
This article presents data on carbon (C), nitrogen (N) and sulfur (S) isotope ratios measured in human hair collected throughout Mexico. The recorded values ranged from −18.3‰ to −12.8‰ for δ^{13}C, 6.8‰ to 10.8‰ for δ^{15}N and from 2.7‰ to 8.0‰ for δ^{34}S. The socioeconomic covariates explored in this study showed, in parts strong correlations to the recorded isotope values. Furthermore, these three isotope systems provided records of the dietary preferences and practices and also showed some spatial variation. This study detected geospatial patterning in the δ^{13}C values of hair samples from Mexico as well as significant correlations with socioeconomic factors. No geospatial variation was detected in the δ^{15}N and δ^{34}S values, however, socioeconomic correlations were found. A δ^{13}C isoscape was generated using a GIS approach, which provides a tool to narrow down region-of-origin predictions (in combination with other isotopic systems) and to document the travel history of unidentified individuals.

KEYWORDS: human hair, Mexico, stable isotopes, isoscape, socioeconomic covariates, geographic and environmental covariates

5.1.1. Introduction

Carbon, nitrogen, and sulfur isotopes are routinely used to evaluate the nutritional content of an individual's diet, not just in modern humans but also past populations (Drucker and Bocherens 2004; Katzenberg 2007; Chisholm *et al.* 1982). Isotopic values among modern humans can vary significantly by country and cultural group (*e.g.*, Southeast Asian countries eating predominantly rice vs. many Latin American countries having a corn-based diet). Based on this knowledge, as well as the fact that drinking water oxygen isotope values are geographically predictable (Bowen *et al.* 2007), researchers from around the world have started to explore the spatial variation of $\delta^{13}C$, $\delta^{15}N$, and $\delta^{34}S$ in the hair of modern populations (Hülsemann *et al.* 2015; Valenzuela *et al.* 2011; Thompson *et al.* 2010; Bol and Pflieger 2002). Researchers have applied stable isotopes (including $\delta^{13}C$, $\delta^{15}N$, and $\delta^{34}S$) to forensic cases, including to hair of unidentified individuals (Lehn *et al.* 2015; Remien *et al.* 2014; Kamenov *et al.* 2014; Meier-Augenstein and Fraser 2008). Nonetheless, more research is needed to explore dietary diversity within and between different cultural groups and geographic regions, especially for forensic provenancing studies.

Carbon ($\delta^{13}C$) isotope values are especially informative regarding the source of dietary nutrients of an individual and vary according to the three following photosynthetic pathways used by the plant: C_3, C_4, and CAM plants. Pure C_3 feeders are known to produce more negative isotope values while pure C_4 feeders, discriminating less against ^{13}C when incorporating CO_2 into their tissues, produce less negative values (White *et al.* 2011). Thus, mixed feeders will show values in between C_3 and C_4 consumers (Tykot 2006). CAM plants can employ either one of the photosynthetic pathways depending on the amount of daytime photosynthesis but are generally rare in the human diet compared to C_3 and C_4 plants (Reitsema 2015; Schoeninger and Moore 1992). Additionally, $\delta^{13}C$ values are more elevated in marine ecosystems compared to terrestrial ecosystems due to the influence of dissolved bicarbonate, freshwater inputs containing organic matter, marine algae, phytoplankton, and submerged aquatic plants (Fry 2008).

Nitrogen ($\delta^{15}N$) values are analyzed to understand the types of animal proteins a person consumes. Moving up the food chain, $\delta^{15}N$ become higher by 2-4 ‰ due to the fractionation during nitrogen metabolism, a trophic level effect (Meier-Augenstein 2018; Reitsema 2015; Steele and Daniel 1978; O'Connell *et al.* 2012). $\delta^{15}N$ values reflect whether the person was an omnivore, vegetarian, or vegan. People eating primarily marine food are expected to have higher $\delta^{15}N$ values than those subsisting on terrestrial food sources due to the longer food chains in marine ecosystems (White *et al.* 2011). Not only can $\delta^{15}N$ values can give an indication over a person's dietary habits but also about their nutritional status (*e.g.* stress, health or pregnancy) (Fuller *et al.* 2004; Petzke

et al. 2010; Meier-Augenstein 2018). Elevated δ^{15}N values have been recorded in cases of malnutrition and starvation (Neuberger *et al.* 2013; Mekota *et al.* 2006).

Sulfur isotope values provide insight regarding the consumption of marine protein resources (*e.g.* marine fish), proximity to seawater, and foods consumed from different geological regions. Sulfur isotope ratios (δ^{34}S) reflect both diet and geographic origin because δ^{34}S values in plants vary with the isotopic values of underlying bedrock (Nehlich 2015). High δ^{34}S values reflect marine ecosystems, intermediate δ^{34}S values reflect terrestrial ecosystems, and low δ^{34}S values reflect freshwater ecosystems (Reitsema 2015). Previous research showed geographic variation in the δ^{34}S isotopic values, for example, in the United States and Canada (Valenzuela *et al.* 2011; Katzenberg and Krouse 1989; Krouse and Grinenko 1991).

The average human has 80,000 to 150,000 hair follicles on their head (Krause and Foitzik 2006). A hair dies when it is long enough to exit the skin, at which point the elemental exchange between hair and blood ceases and the hair retains the biogenic dietary information. On average, hair grows 1 cm per month and therefore creates a longitudinal record of isotope signatures (Font *et al.* 2012; Krause and Foitzik 2006). However, it undergoes a life-long cycle of rapid growth, regression, and resting periods (Krause and Foitzik 2006), meaning not all hair strands will be from exactly the same period of time. Made of the structural protein keratin, hair is 50% carbon, 21% nitrogen, 17.5% hydrogen, 6.5% oxygen, and 5% sulfur, but also includes trace contents of metals (Font *et al.* 2012). Various forensic and archaeological studies have demonstrated the value of using human hair in isotopic research (Chesson *et al.* 2018c; Reynard *et al.* 2016; Remien *et al.* 2014; Huelsemann *et al.* 2009; Bowen *et al.* 2009).

Overall, there is a high potential for variation in isotope values recorded in human tissues. While isotope analysis cannot be used to identify an exact region of origin for an individual, it can certainly add important information to the identification process of unidentified decedents. Every year, thousands of people go missing and are recovered deceased along the Mexico-United States border as well as within the country of Mexico (Anderson and Spradley 2016; Secretariado Ejecutivo del Sistema Nacional de Seguridad Pública 2018; Instituto Nacional de Estadística y Geografía 2018). As isotopes have now been recognized as a tool in the identification process of unidentified human remains (Bartelink *et al.* 2018; Chesson *et al.* 2018b; Bartelink *et al.* 2014), such as undocumented border crossers and people forcibly disappeared by their governments, this study works towards developing a baseline database of δ^{13}C, δ^{15}N, and δ^{34}S isotope values for individuals from Mexico. The potential spatial variation and distribution of these isotopic values will be explored. The documented values will be compared to known isotopic values from other continents, namely South America, North America, Europe, and Asia.

5.1.2. Materials and methods

Sample Acquisition

A total of 101 discarded human head hair samples were collected in barbershops and hair salons in 32 towns and cities in Mexico (Figure 1) during a six-week period between June and July 2018. Since this hair collection was anonymous, no information regarding sex, age, diet, health status, nutritional status, or travel history was collected. Only bunches of hair of the same color and texture were collected in order to ensure that the discarded hair belonged to a single individual. All samples were placed in separate paper envelopes and stored in airtight bags. A minimum of three samples per location were gathered, with the exceptions of La Paz, Baja California Sur, and Saltillo, Coahuila, where only one sample was collected. These two locations were disregarded in location average and standard deviation calculations.

Figure 5.1.1. Map of Mexico showing the sampling locations (n=32).

Sample Preparation

The hair samples were cleaned using a vacuum funnel in combination with an extractor hood at the Vrije Universiteit Amsterdam (the Netherlands). Individual hair samples were placed on filter paper within the funnel and a 2:1 chloroform-methanol mixture was poured over the sample and left to soak for ~20 seconds to remove surface contaminants and lipids. After the funnel was evacuated using the vacuum pump, Milli-Q distilled water was poured over the sample and soaked for ~20 seconds. This water rinse and soak step was repeated five times. If the filter paper was soiled, it was replaced with new paper between the soaking steps. After the fifth soak, the sample was placed between two clean filter papers and wrapped in aluminum foil to be

transported to the laminar flow hood where the foil was opened to air-dry the hair. Between the rinsing of each hair sample, the working space, glassware, and utensils were cleaned using acetone, ethanol, and Milli-Q distilled water to avoid contamination. The hair samples were cut into pieces using surgical grade scissors. For the $\delta^{13}C$ and $\delta^{15}N$ analyses 500µg ±10%, and for the $\delta^{34}S$ analyses 900µg ±10% were loaded into tin capsules. Since $\delta^{13}C$ and $\delta^{15}N$ were analyzed in one sample, only one tin capsule was needed for both elements.

Sample Analysis

All samples were analyzed at the University of California Davis Stable Isotope Facility, using an elemental analyzer interfaced to a continuous flow isotope ratio mass spectrometer (IRMS). Three repeats were analyzed for seven samples to ensure reproducibility of the results (average standard deviations for $\delta^{13}C$: 0.12 ‰, $\delta^{15}N$: 0.08 ‰, $\delta^{34}S$: 0.08 ‰). The samples were analyzed for $\delta^{13}C$ and $\delta^{15}N$ isotopes using a Sercon Integra II combined elemental analyzer and isotope ratio mass spectrometer (Sercon Ltd., Cheshire, UK). Stable isotope ratios of $^{34}S/^{32}S$ in solid samples were measured using an Elementar vario ISOTOPE cube interfaced with a SerCon 20-22 IRMS (Sercon Ltd., Cheshire, UK). Several internal laboratory reference materials were measured alongside the samples. These internal standards were previously calibrated using international standards, including: IAEA-600, USGS-40, USGS-41, USGS-42, USGS-43, USGS-61, USGS-64, and USGS-65. The following reference materials were used for $\delta^{13}C$ and $\delta^{15}N$: glutamic acid ($\delta^{13}C$ = −16.62 ‰, $\delta^{15}N$ = −6.82 ‰), bovine liver ($\delta^{13}C$ = −21.77 ‰, $\delta^{15}N$ = 7.68 ‰), enriched alanine ($\delta^{13}C$ = 43.02 ‰, $\delta^{15}N$ = 41.13 ‰) and nylon 6 ($\delta^{13}C$ = −27.76 ‰, $\delta^{15}N$ = −10.54 ‰). For $\delta^{34}S$, six reference materials were employed to ensure the quality of the data: cysteine (34.2 ‰), hair (2.7 ‰), mahi-mahi muscle (19.5 ‰), whale baleen (17.5 ‰), seaweed (20.8 ‰) and taurine (−2.5 ‰).

A sample's provisional isotope ratio was measured relative to a cylinder gas (of known isotopic composition) peak that was analyzed with each sample. These values were finalized by correcting the values for the entire batch based on the known values of the included internal laboratory reference materials. The results for $\delta^{13}C$ values are presented on the Vienna Pee Dee Belemnite (VPDB) scale, for $\delta^{15}N$ values on the AIR scale, and for $\delta^{34}S$ values on the Vienna Canyon Diablo Troilite (VCDT) scale.

The long-term standard deviation for analyses at UC Davis are 0.2 ‰ for $\delta^{13}C$, 0.3 ‰ for $\delta^{15}N$, and 0.4 ‰ for $\delta^{34}S$. In order to better capture the minor differences in stable isotope abundance ratios (R), they were expressed as δ values against an internationally defined standard known as 'per mil' (‰). The calculation is as follows: $\delta = (R_{Samp} / R_{RM} - 1)$, where R_{Samp} is the

ratio of the sample and R_{RM} is the ratio of the internationally agreed scale zero-point (Dunn and Carter 2018).

Statistical and geostatistical analyses

The programming language R was utilized for all statistical analyses (R Core Team 2020). The Pearson's product-moment correlation was used to explore the relationship between the isotopic values found in Mexican hair as well as other metric variables, such as geographic and socioeconomic correlations. Correlations were marked according to their strength of association (Supplementary Material).

Geographic and environmental covariates

Data from a total of eight geographic/environmental covariates were gathered and their correlations to the observed isotopic values calculated. Overall, Mexico has a wide range of different terrains and climates, which are expected to influence isotopic values and therefore create distinctive ranges. Longitude, latitude, and elevation were the three most basic covariates explored. Longitude and latitude have been shown to influence isotopic values in various studies, especially concerning hydrology (Bowen *et al.* 2007; Wassenaar *et al.* 2009). Valenzuela *et al.* (2012) showed that latitude and longitude correlate with isotope ratios of $\delta^{13}C$ and $\delta^{34}S$ in human hair from European countries, something that is likely to be found in the Mexican hair samples as well. Furthermore, the range of elevation found in Mexico is large and a significant factor in the Mexican geography, ranging from -10m below sea level to 5636m above sea level. Since the crops grown vary by altitude, it was hypothesized that especially the carbon isotopes could vary with elevation. The elevation data for the sampling locations was derived from the "North American Elevation 1- Kilometer Resolution" digital elevation model (DEM). GTOPO30's resolution is 30 arc seconds, approximately 1 kilometer (United States Department of the Interior-U.S. Geological Survey 2007). The data for each sampling location was obtained using "Extract Values to Points" from the ArcGIS Spatial Analyst toolbox (Environmental Systems Research Institute (ESRI) 2018).

Mexico is home to a large range of climates, varying from tropical to desert through terrains that cover high rugged mountains, high plateaus, low coastal plains, and deserts. This variety also shows in the average annual temperatures observed throughout the country. Average annual temperatures between 10°C and 26°C are found throughout most of the country (~83% of the territory) in dry, warm-subhumid, very dry and temperate-subhumid climates. The rest of the territory has very warm or cold climates, with annual average temperatures above 26°C or below

10°C (The Food and Agriculture Organization of the United Nations 2014). The maritime influence, which generates humid air masses that infiltrate from the Gulf of Mexico and the Pacific Ocean, contributes to the scarce thermal oscillations throughout the year and to the moderate climate (The Food and Agriculture Organization of the United Nations 2014). Under the assumption that isotopic values are influenced by elevation, temperature is hypothesized to correlate to the various isotopic systems as well, given the fact that temperatures decrease with increasing elevation. Temperature data were derived from the WorldClim- Global Climate Data Version 2 database (Fick and Hijmans 2017). Monthly data for Mexico was extracted from the global raster using the "Extract by Mask" tool (ArcGIS Spatial Analyst toolbox (Environmental Systems Research Institute (ESRI) 2018)). Mean annual temperature was calculated using the Raster Calculator (ArcGIS Spatial Analyst toolbox (Environmental Systems Research Institute (ESRI) 2018)). The "Extract Values to Points" tool was used to determine the temperatures at the sampling locations (ArcGIS Spatial Analyst toolbox (Environmental Systems Research Institute (ESRI) 2018)).

The mean annual amount of precipitation found throughout Mexico vary greatly from frequent droughts in the north to extreme weather events that affect the Pacific coast, Gulf of Mexico, as well as the Caribbean coasts. The rain throughout the year is concentrated mostly in the months of June to October (The Food and Agriculture Organization of the United Nations 2014). Previous studies have found that δ^{15}N values in plants and animals, including humans, exhibit a negative correlation to amount of rainfall because plants from more arid regions tend to have higher δ^{15}N values in this study. Mean annual precipitation averages were calculated using the Raster Calculator. A one-year (July 2017 to June 2018) and a three-year (July 2015 to June 2018) mean annual average was calculated and compared. The monthly precipitation analyses and visualizations used for this research were created with the Giovanni online data system, developed and maintained by the National Aeronautics and Space Administration's Goddard Earth Sciences Data and Information Services Center. The precipitation dataset was extracted from the Tropical Rainfall Measuring Mission (TRMM) satellite product 3B43 version 7. The units of reporting are mm/month for the precipitation amounts, the temporal resolution is monthly, and the spatial resolution is 0.25 degrees (Acker and Leptoukh 2007).

Various studies have demonstrated that the proximity to sea water can have a significant effect on isotopic values (Thompson *et al.* 2010; Mützel *et al.* 2009; Katzenberg and Krouse 1989). As discussed above, higher δ^{34}S and δ^{15}N values are expected to be seen in individuals consuming a high amount of marine foods, something that is commonly associated with residency in proximity to the sea. Therefore, two covariates (Distance to the nearest ocean, Distance to the

nearest ocean excluding the Gulf of California) were explored in this study to determine whether any spatial patterning were of significance to Mexican human hair values. *Distance to the nearest ocean* was measured using the shortest distance from the sampling location points to the boundary polygon for Mexico, which included the Gulf of California. For example, a sampling point in Sonora was measured to the Gulf of California. *Distance to the nearest ocean excluding the Gulf of California* was the measured distance from the sampling point to the Pacific Ocean, disregarding the Gulf of California. For example, a sampling location in Sonora would be measured beyond the Gulf of California to the Pacific Ocean.

Socioeconomic covariates

Data from six socioeconomic covariates were gathered and their correlations to the observed isotopic values calculated. Based on the fact that food consumption habits are influenced by socioeconomic status, various covariates were explored in this study (Pechey and Monsivais 2016; Alkerwi *et al.* 2015). This fact has been utilized in a variety of archaeological and forensic studies examining socioeconomic status of the sampled individuals (Dhaliwal *et al.* 2020; Bender *et al.* 2015; Hülsemann *et al.* 2015).

Population size, indicating the number of inhabitants at the sampling locations was derived from the Instituto Nacional de Estadística y Geografía (2015a; 2010). Previous research showed that isotopic values found in human tissues may be skewed and not representative of the sampling location due to so-called global supermarket diets (Ehleringer *et al.* 2008; Nardoto *et al.* 2006). This phenomenon may lead to greater homogenization of isotopic values in the sampled locations and can potentially overprint the local geological signature. Through correlating the isotopic values to population size, the question was explored whether larger communities show similarities in isotopic values compared to smaller communities who may predominantly rely on local resources. Furthermore, through correlating population size to the standard deviation value so of the sample locations, it was investigated if greater variation in values is found in locations with larger populations.

As indicated above, lower socioeconomic status, *i.e.*, degree of poverty, is linked to food choices. Therefore, two covariates directly related to poverty were explored: The *percent of the population living in poverty per state* as well as the *number of people living in poverty by state* (Consejo Nacional de Evaluación de la Política de Desarrollo Social 2018).

Another covariate that explores poverty in greater detail was correlated to the isotopic values: the *Human Development Index* by state (HDI) (Smits and Permanyer 2019, Figure 2). HDI takes into account the life expectancy, level of education, and standard of living. A higher index

indicates a higher developmental level. It was hypothesized that HDI may be a less informative covariate compared to the two poverty covariates as it takes into account more variables that fall under the umbrella term 'socioeconomic status'.

The 2016 Mexican census concluded that over 70% of Mexicans of indigenous ancestry live in poverty (Consejo Nacional de Evaluación de la Política de Desarrollo Social 2018). Furthermore, the food choices of the indigenous population are expected to vary from those of non-indigenous Mexicans. Therefore, it was hypothesized that the isotopic values recorded in states (and locations) would correlate with covariates measuring the *percentage of indigenous speaking* (of total state population) (Instituto Nacional de Estadística y Geografía 2015a) or *percentage of indigenous ancestry* (of total state population) (Instituto Nacional de Estadística y Geografía 2015b). Both the geographic/environmental and socioeconomic factors were correlated with the entire sample set as well as the location averages. All data were later split into an Atlantic and a Pacific drainage basin dataset to explore potential differences.

A Kruskal-Wallis test in R was used to compare the isotopic data independently for each location to evaluate potential differences (R Core Team 2020). This test determined whether there were significant differences between a continuous dependent variable (*i.e.*, the isotope value) and a categorical independent variable (*i.e.*, the location). Geostatistical analyses were performed using the ArcGIS Geostatistical Analyst toolbox and Geostatistical Wizard (Environmental Systems Research Institute (ESRI) 2018). The Global Moran's I Spatial Autocorrelation tool was used to determine the spatial autocorrelation based on the locations of the data points (hair sampling locations) and their corresponding isotopic values. The resulting index provided information as to whether the isotopic data are spatially clustered, dispersed, or random (Environmental Systems Research Institute (ESRI) 2018).

Isoscapes were generated using ArcGIS ordinary kriging with a semivariogram function. All isotopic level data was employed to achieve the lowest Root Mean Square Error (RMSE). For $\delta^{13}C$, an additional isoscape using location averages was created using the same methodology. Location averages are the averages of all isotopic values recorded in any one sampling location.

Figure 5.1.2. Human Development Indices for the Mexican states where hair samples were collected. The color indicates the strength of the index (green- high HDI, red- low HDI). Grayed out states were not sampled for this study.

5.1.3. Results

A total of 101 hair samples were analyzed for all three isotopes. The sample size per city varied from one to six. All raw data is publicly available on fighare.com (Ammer 2020c) and Table 1 of the Supplementary Materials. The descriptive statistics are reported in Table 1.

Table 5.1.1. Descriptive statistics of the $\delta^{13}C$, $\delta^{15}N$, and $\delta^{34}S$ results for all samples.

	$\delta^{13}C$	$\delta^{15}N$	$\delta^{34}S$
Minimum	−18.3 ‰	6.8 ‰	2.7 ‰
Maximum	−12.8 ‰	10.8 ‰	8.0 ‰
Mean	−15.6 ‰	9.2 ‰	4.5 ‰
Range	5.5 ‰	4.1 ‰	5.3 ‰
Standard Deviation	1.0 ‰	0.6 ‰	1.0 ‰
N	101	101	101

Inter-Element Correlation

The isotopic values recorded yielded a weak relationship between for $\delta^{13}C$ and $\delta^{15}N$ but did not show correlations for $\delta^{13}C$ and $\delta^{15}N$ versus $\delta^{34}S$ (Table 2 Supplementary Material). Averaging the isotopic data for each location improved the correlations for $\delta^{13}C/\delta^{15}N$ and $\delta^{13}C/\delta^{34}S$ but not between $\delta^{15}N$ and $\delta^{34}S$ (Table 2 Supplementary Material). The average $\delta^{34}S$ value for each location correlated strongly to the standard deviation recorded for the respective locations is statistically significant at the 0.05 level ($r = 0.52$, $p = 0.003$).

Inter-City Variance

Carbon, nitrogen, and sulfur isotopes in hair differed significantly between geographic locations ($\delta^{13}C$: $p < 0.001$, $\delta^{15}N$: $p < 0.002$, $\delta^{34}S$: $p < 0.001$). Therefore, the null-hypothesis tested via Kruskal-Wallis analyses was rejected for all three isotope systems.

Standard Deviation Correlations

Table 2 shows the stable isotope variance for the locations sampled; only locations with more than three samples are reported here (n=30). Notably, the average and maximum standard deviations for the $\delta^{13}C$ values were significantly larger than the long-time analytical precision ($1\sigma = 0.2$ ‰). $\delta^{15}N$ and $\delta^{34}S$ did not show the same level of variance (Table 2). The standard deviations were plotted with the respective isotopic value averages for each location (Figure 3). Standard Deviation (SD) correlations determined whether the amount of variation in isotopic values correlated to any geographic/environmental or socioeconomic covariates assessed (Tables 3-16 Supplementary Material).

For the geographic and environmental variables, some correlations to the location SDs were identified. Longitude and latitude showed no relationship with any of the isotope SD values (Tables 3 and 4 Supplementary Material). Elevation and distance to the ocean (including or excluding the Gulf of California) varied directly with SD of $\delta^{13}C$ and values at individual collection sites while temperature varied inversely with $\delta^{13}C$ SD (Tables 5-8 Supplementary Material). Only the correlation of Elevation and isotopic values was significant at $\alpha = 0.05$ level. Carbon Location SDs did not correlate to precipitation factors (Tables 9 and 10 Supplementary Material).

Nitrogen Location SD values did not correlate to any of the geographic and environmental covariates except Distance to the Ocean and the two precipitation covariates, which showed a weak correlation (Tables 3-10 Supplementary Material). Sulfur Location SDs showed weak inverse correlations to Elevation, Distance to Ocean, One-Year Precipitation, and Three-Year Precipitation (Tables 5, 7, 9-10 Supplementary Material).

Overall, the socioeconomic covariates were weakly correlated or uncorrelated with the isotope element location SDs in a significant manner. Population Size did not correlate with the Location SDs of any of the elements (Table 15 Supplementary Material). Carbon Location SD correlations were recorded for the Poverty covariates, the Indigenous covariates, and an inverse correlation was documented for HDI (Tables 11-16 Supplementary Material). Nitrogen Location SDs only showed correlations to the Percentage of the Population living in Poverty and the HDI (Tables 11-16 Supplementary Material). The Sulfur SDs for each location correlated to the

indigenous covariates and HDI, but inversely correlated to the number of people living in poverty (Tables 11-16 Supplementary Material).

Table 5.1.2. Variance by location.

SD by location	δ^{13}C	δ^{15}N	δ^{34}S
Minimum SD	0.1 ‰	0.8 ‰	0.1 ‰
Maximum SD	1.4 ‰	0.9 ‰	1.4 ‰
Mean SD	0.6 ‰	0.3 ‰	0.5 ‰
Number of cities	30		

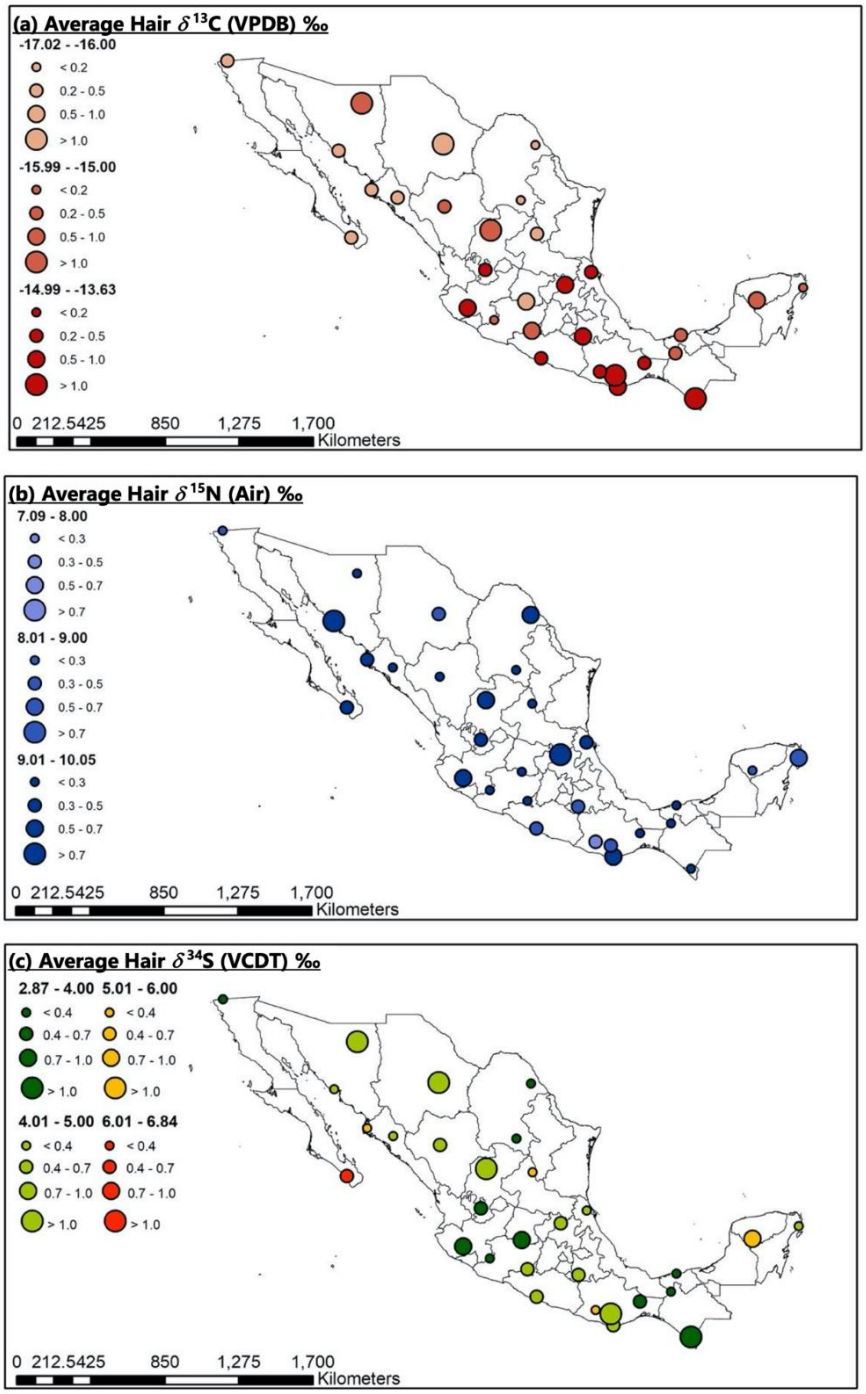

Figure 5.1.3. Map of Mexico showing the average δ^{13}C, δ^{15}N and δ^{34}S isotope ratios as well as the standard deviations for the corresponding locations (n=30).

Geographic and Environmental Correlations

The results for all the Pearson's correlations (Tables 3-10 Supplementary Material) show the detailed relationships between isotope values and the various geographic and environmental covariates described above. The Pearson's correlation coefficients show that the assignment of a drainage basin had a significant influence on the relationship between the isotopic values and the environmental covariates.

Overall, $\delta^{13}C$ had the strongest correlations to the geographic and environmental covariates, particularly to latitude and the precipitation (Tables 4, 9-10 Supplementary Material). Longitude and the distance to the ocean also explain some of the isotopic variation in $\delta^{13}C$ values (Tables 3, 7-8 Supplementary Material). All of these correlations were further improved by using location averages (Tables 3-4, 7-10 Supplementary Material).

$\delta^{15}N$ and $\delta^{34}S$ values were weakly correlated to all geographic and environmental factors explored here. The values of the Pacific drainage basin show higher correlation to the covariates than the values of the Atlantic drainage basin (Tables 3-10 Supplementary Material). Interestingly, for $\delta^{15}N$, the Atlantic and Pacific drainage basins showed inverse correlations for elevation and temperature (Tables 5 and 6 Supplementary Material). Using averaged location values improved the correlations for $\delta^{15}N$ values, while they did not improve for $\delta^{34}S$.

Spatial Autocorrelation

The Moran's Indices were 0.606 (Z-score= 6.7, $p < 0.001$), 0.515 (Z-score= 5.9, $p < 0.001$), and 0.764 (Z-score= 8.6, $p < 0.001$) for $\delta^{13}C$, $\delta^{15}N$ and $\delta^{34}S$, respectively. When plotting the predicted versus measured values for all sample values, the root-mean-square errors (RMSE) for the three isotopes were: RMSE = 0.72 for $\delta^{13}C$, RMSE = 0.48 $\delta^{15}N$, and RMSE = 0.67 for $\delta^{34}S$. The relationship between predicted versus mean location values yielded a significantly lower RMSE of 0.52 for $\delta^{13}C$. Averaging the location values did not impact the performance of the models for $\delta^{15}N$ and $\delta^{34}S$.

The average $\delta^{13}C$ value for 19 of the 30 cities with more than three samples was correctly predicted within the analytical precision (Figure 4). The mean difference between measured and predicted values was −0.006 ‰ (±0.3 ‰).

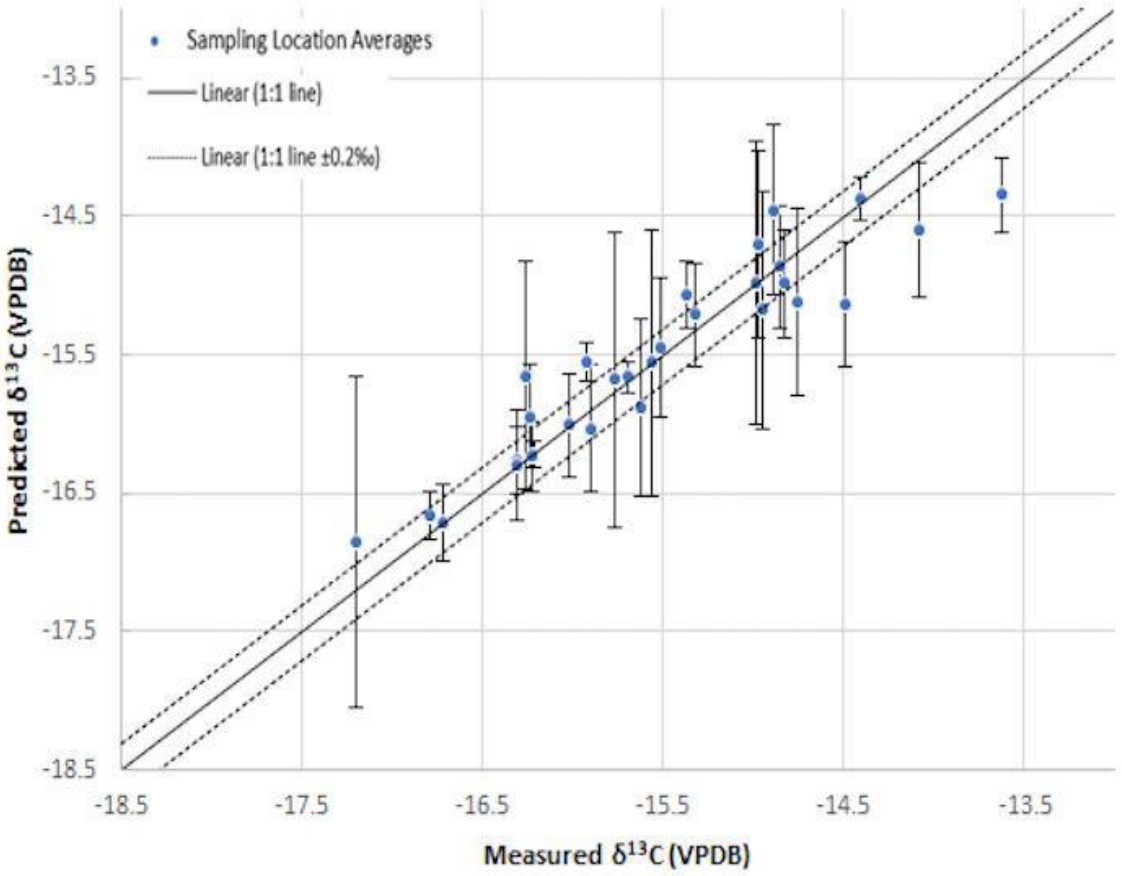

Figure 5.1.4. Measured versus predicted $\delta^{13}C$ for locations with three or more samples (n=30). The blue dots represent the mean $\delta^{13}C$ values for each location ± the standard deviation. The solid black line represents the 1:1 line and the dashed lines represent the estimated analytical error (±0.2 ‰).

Construction of isoscapes

Even though $\delta^{15}N$ and $\delta^{34}S$ showed very weak to non-existing correlations to geographic variables, isoscapes were developed for all three elements (Figure 5, 6 and 7). While these isoscapes cannot be used for region-of-origin assignments, they are a tool to better visualize the collected data and identify any kind of trends that may not be interpretable with correlations to latitude, longitude or elevation.

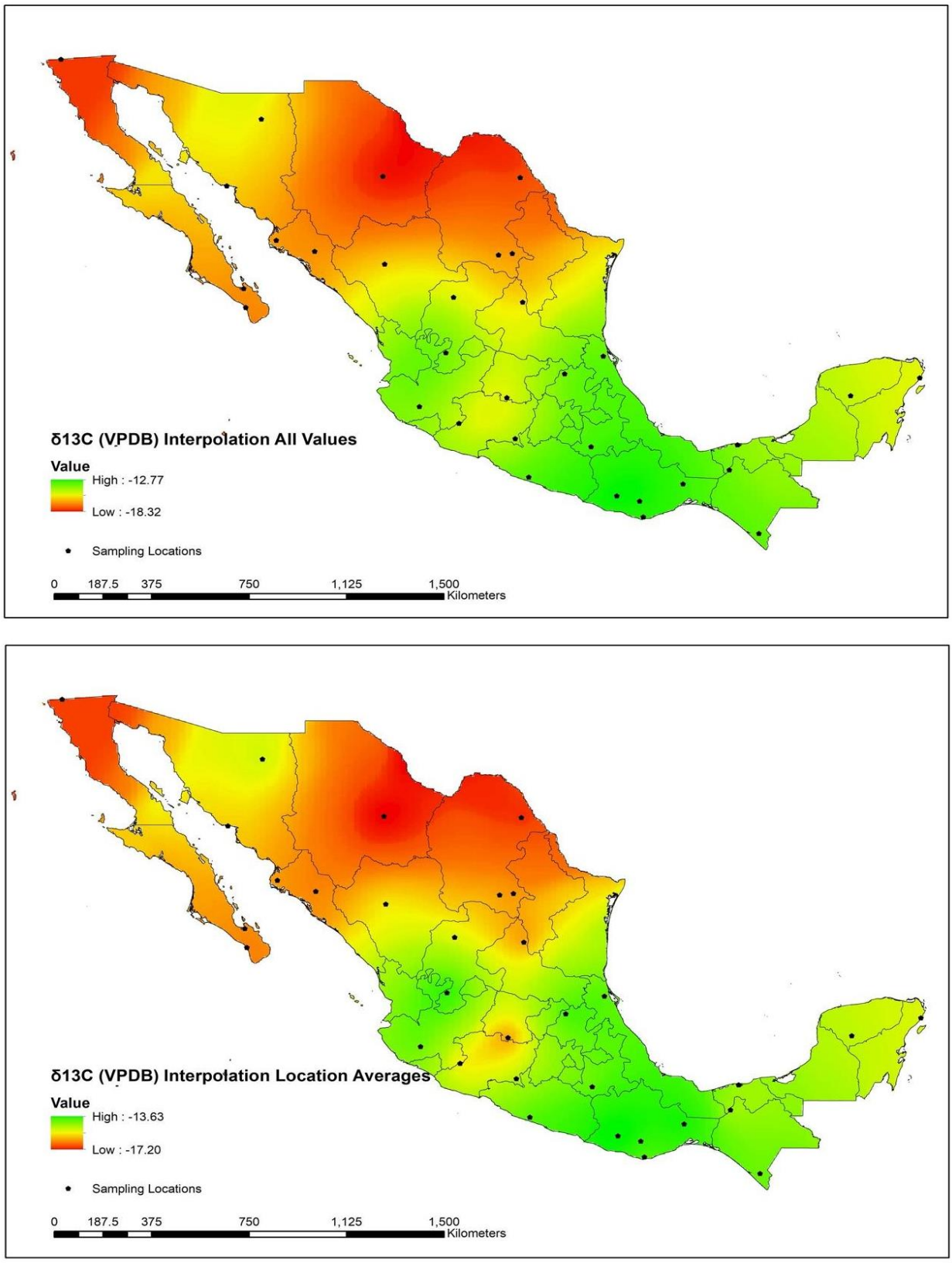

Figure 5.1.5. δ^{13}C isoscape for all values (top) (n=101) and location averages (bottom) (n=30) representing predictions produced using ordinary kriging interpolation.

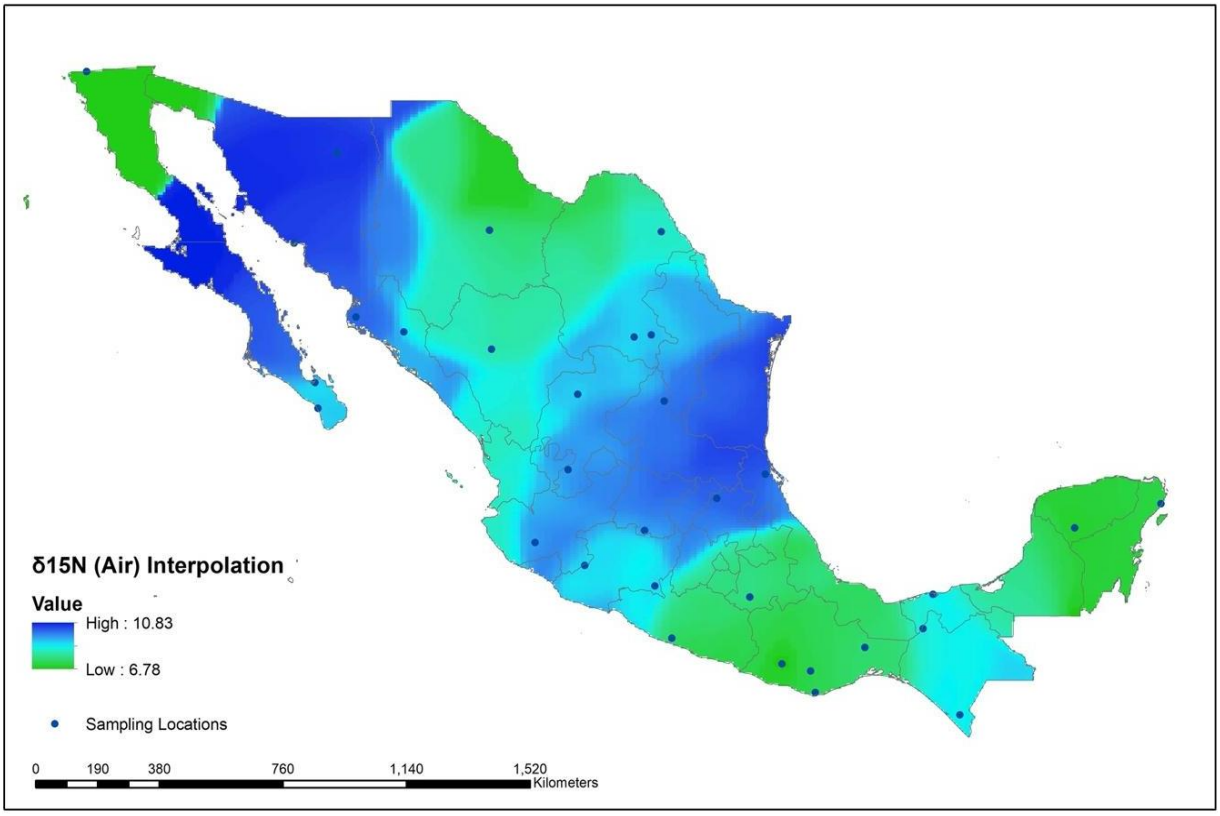

Figure 5.1.6. δ^{15}N isoscape for all values (n=101) representing predictions produced using ordinary kriging interpolation.

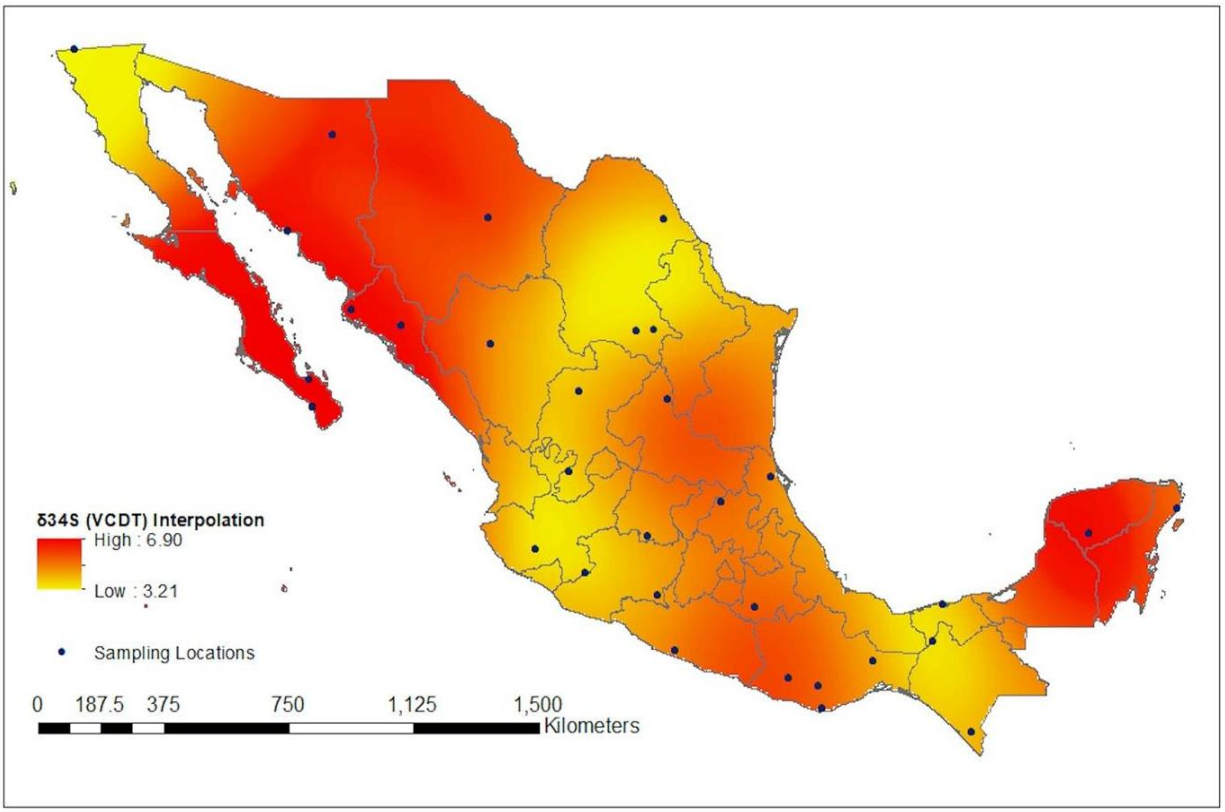

Figure 5.1.7. δ^{34}S isoscape for all values (n=101) representing predictions produced using ordinary kriging interpolation.

Socioeconomic Correlations

The results of the Pearson's correlation analyses between the isotopic factors and the socioeconomic covariates can be found in Tables 11-16 of the Supplementary Material. HDI had the strongest relationship with the isotopic ratios observed for the Mexican hair sample dataset. $\delta^{13}C$ showed again the strongest correlations to all covariates explored here, except Population Size. Population size demonstrated weak correlations to $\delta^{15}N$ and $\delta^{34}S$, but no correlation to $\delta^{13}C$.

$\delta^{13}C$ is strongly related to both poverty factors explored here, but the percentage of the population living in poverty is more correlated to the isotope values than the number of persons living in poverty (Table 11-12 Supplementary Material). Interestingly, for $\delta^{15}N$ and $\delta^{34}S$, the two poverty covariates show opposing results: The percentage is deemed somewhat useful as an indicator for $\delta^{15}N$ isotopic values while the number of people living in poverty shows greater utility when correlating the factor with $\delta^{34}S$ (Table 11-12 Supplementary Material).

The factors related to the indigenous population of Mexico (percent of population speaking an indigenous language and percent of population of indigenous ancestry) yielded strong results for $\delta^{13}C$ and moderate results for $\delta^{15}N$. For $\delta^{13}C$ and $\delta^{15}N$, the correlation coefficients improved by 0.1 when using location averages. $\delta^{34}S$ did not correlate to either variable without averaging but showed a weak correlation when using the average isotope values (Table 13-14 Supplementary Material).

Correlations of Geographic/environmental and Socioeconomic variables

While it is essential to evaluate the correlations of the various geographic/environmental and socioeconomic factors to the recorded isotopic values, it is also important to analyze how the covariates relate to one another (Table 17 Supplementary Material). Overall, some covariates showed strong correlations to one other but none of the covariates were deemed redundant because of their strong relationship.

Population size showed the weakest correlations to all the covariates explored here. The percentage of the population living in poverty and HDI correlated most strongly but HDI does not only take the income levels into consideration but also other factors such as life expectancy and education levels. The poverty factors related correlated strongly to the factors of indigenous ancestry and language.

5.1.4. Discussion

Standard Deviations

Only carbon isotopic values showed correlations with some of the associated standard deviations for the location variables such as Elevation, temperature, and distance to ocean (including and excluding the Gulf of California). Potentially, there is greater variation in diet and farming practices with increased elevation, lower temperatures, and increased distance to the oceans.

Sulfur isotopic location SDs only correlated with one-year precipitation, showing that the amount of precipitation recorded for the locations slightly influenced the amount of variation within a single location. Nitrogen did not show any significant correlations between location SDs and the geographic and environmental variables.

The location SDs of the isotopic values of all elements did not show a significant correlation with the socioeconomic variables explored in this study, showing that the socioeconomic factors did not influence the location variation.

Many of the above correlations failed to show statistical significance ($p > 0.1$ were deemed statistically insignificant) even though they showed strong correlation values (high r values). The presented p-values are most likely underestimated in statistical significance due to the fact that the number of pairs for the Pearson's correlations was only 30 (the 30 locations with more than three samples).

Carbon

Overall, carbon showed the strongest correlations, and therefore the highest coefficients of determination, for both geographic/environmental and socioeconomic factors in comparison to nitrogen and sulfur. Due to the fact that averaging improved the correlations coefficient of the $\delta^{13}C$ isotopic values for the geographic/environmental factors as well as the RMSE significantly, two separate isoscapes (Figure 5) were developed using all data points and averaged location values. However, through visualizing the prediction errors for the two isoscapes, it became clear that the overall RMSE may have improved, but that the prediction merely improved in those areas that were tightly sampled (Figure 8). The hotspots visible in the prediction error map of the averaged location isoscape is likely due to the scarcity of sample locations throughout the country. Therefore, it is more useful to use all values without averaging until more samples can be collected from places that show high predictive errors.

Nonetheless, the clear north-south latitudinal pattern indicated by the correlation and determination coefficient is clearly visible in both isoscapes. Furthermore, the weak longitudinal pattern was also visible. There were visible hotspots in two locations: Moroleón (Guanajuato) and

Nacozari de García (Sonora). Unfortunately, due to the lack of personal information on the subjects, it was not possible to explain this deviation from the values in the surrounding regions. The highest overall values were found in San Jacinto Tlacotepec (Oaxaca) and the lowest in Pedro Meoqui (Chihuahua).

The values obtained from this Mexican sample were, on average, significantly higher than those obtained from the United States, South America, Europe and Asia (Figure 11; Table 3; Bender *et al.* 2015; Lehn *et al.* 2015; Valenzuela *et al.* 2011; Thompson *et al.* 2010). The mean values of the Americas (with the exception of Mexico) were similar and the mean values observed in Europe and Asia were similar. While the Mexican values were distinct from the European countries (Germany, Italy, UK/Ireland, France, Poland and Russia), there was an overlap with the values from the Americas. The highest values observed in Asia overlapped with the lowest values observed in Mexico (with the exception of Pakistan). The most likely explanation for the elevated values seen in the Mexican hair samples are the more prominent consumption of C_4 plants in Mexico, which are associated with higher $\delta^{13}C$ values. In regard to the inter-country variation, the relationship to socioeconomic factors and varying diet among the Mexican population could provide an explanation. Furthermore, it would be interesting to explore the variation of the different kinds of corn and their associated $\delta^{13}C$ values as Mexico has over 50 varieties of indigenous corn that are used to varying degrees across the country.

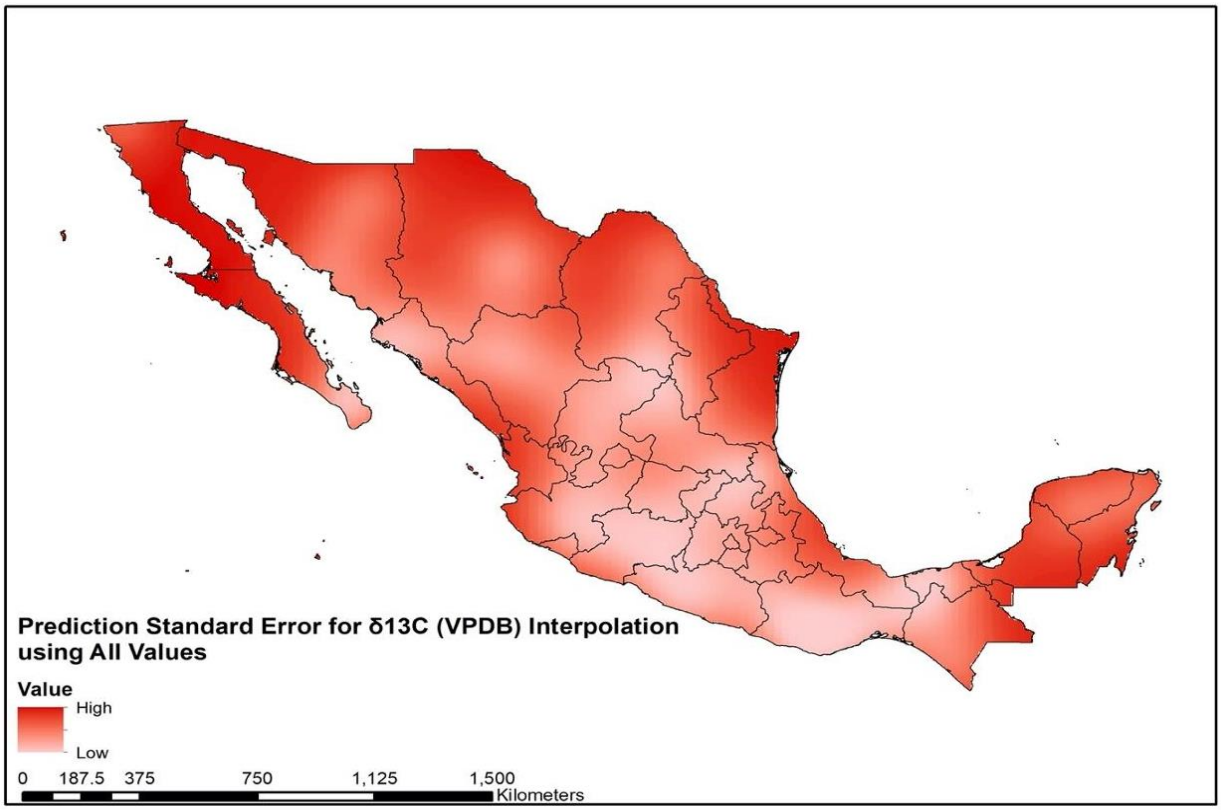

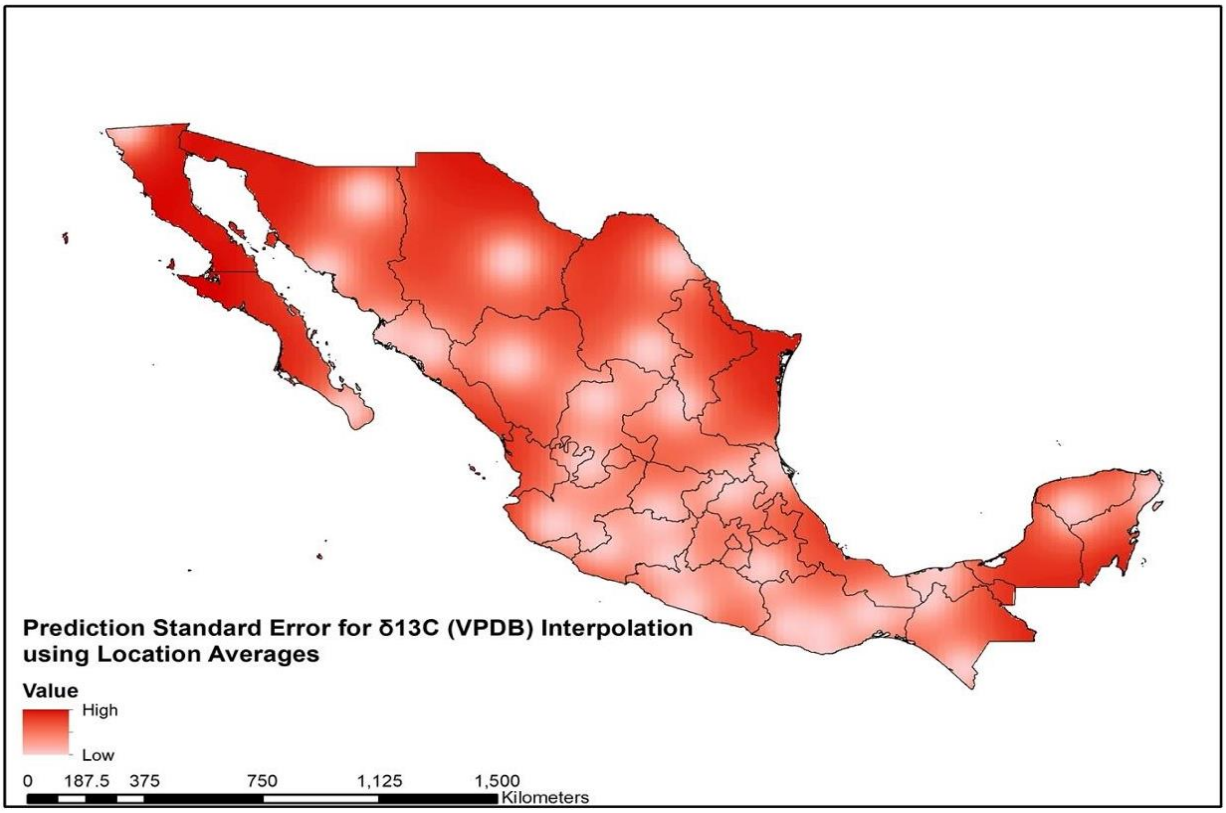

Figure 5.1.8. Prediction Standard Error output for δ^{13}C isoscapes (Figure 5.1.5) for all values (top) and location averages (bottom).

Nitrogen

Geographic and environmental factors seemingly had little to no effect on δ^{15}N values. This was clearly visualized in the isoscape (Figure 6) and the predictive error map (Figure 9). Thus, no clear patterns were observed in the isoscape; however, the predictive error map is relatively accurate in its predictions within the regions of Michoacán, Guerrero, Puebla, and Guanajuato. It is important to note that the correlations for δ^{15}N isotopic values often show the opposite pattern when divided up into an Atlantic and a Pacific drainage basin, likely caused by the East-West divide of the Sierra Madre mountain ranges.

The δ^{15}N values of Europe and the Americas are within the value range observed in this Mexican population. The United States showed slightly lower values but was overall indistinguishable from Mexico. The Asian values show more variance than the European and American (South and North America) values (Figure 11; Table 3; Bender *et al.* 2015; Lehn *et al.* 2015; Valenzuela *et al.* 2011; Thompson *et al.* 2010).

The Mexican values were overall in accordance with an omnivore diet but were more closely aligned with a high meat than a vegan diet (Meier-Augenstein 2018). However, considering that the United States is the highest meat consumer (of the countries evaluated here) with approximately 124 kg/person/year (Food and Agriculture Organization of the United Nations

2017; Ritchie and Roser 2017) and that Mexico's meat consumption only lies at approximately 64 kg/person/year (Food and Agriculture Organization of the United Nations 2017; Ritchie and Roser 2017), other factors that may elevate δ^{15}N isotopic values must be considered. As outlined above, nutritional stress, such as starvation and malnutrition can lead to elevated δ^{15}N values due to breaking down muscle protein to meet the body's amino acid needs (Meier-Augenstein 2018). The data trend seems to indicate that lower δ^{15}N values can be found in places with higher percentages of indigenous ancestry and language. While not strong, all variables showed some correlation, often also showing a divide between the Atlantic and Pacific drainage basin (*e.g.* poverty covariates and HDI). Since the correlations for the drainage basins were inverse, it seemed as if the δ^{15}N values do not correlate to poverty but upon further exploration, it is clear that poverty (and therefore most likely nutritional stress) has an effect on the δ^{15}N values of Mexican hair samples. This is further supported by the elevated δ^{15}N values recorded in India, which has some of the lowest meat consumption in the world (4kg/person/year; Food and Agriculture Organization of the United Nations 2017; Ritchie and Roser 2017), yet has one of the poorest populations worldwide. To explore this observation in greater depth, it would be useful to obtain hair samples with personal information regarding ancestry, dietary practices, and nutritional status.

Interestingly, there was only one location that did not fit the typical omnivore isotope pattern: San Jacinto Tlacotepec, Oaxaca. While the other nine samples from three locations throughout the state averaged around 9.2 ‰, this particular location averaged significantly lower at 7.1 ‰. Following Petzke *et al.* (2005) and Reitsema (2015), these values would represent a diet between vegan and ovo-lacto-vegetarian. There did not seem to be a geographic/environmental or socioeconomic factor that could clearly explain this deviation from the rest of the state and the country. Furthermore, most δ^{15}N values derived from the 101 Mexican hair samples fell within the reported range of low socioeconomic status as reported by Bender *et al.* (2015), who studied isotopic values and their relationship to socioeconomic status in Colombian urban women. This finding was not supported when using all data points without location averaging and therefore needs further exploration.

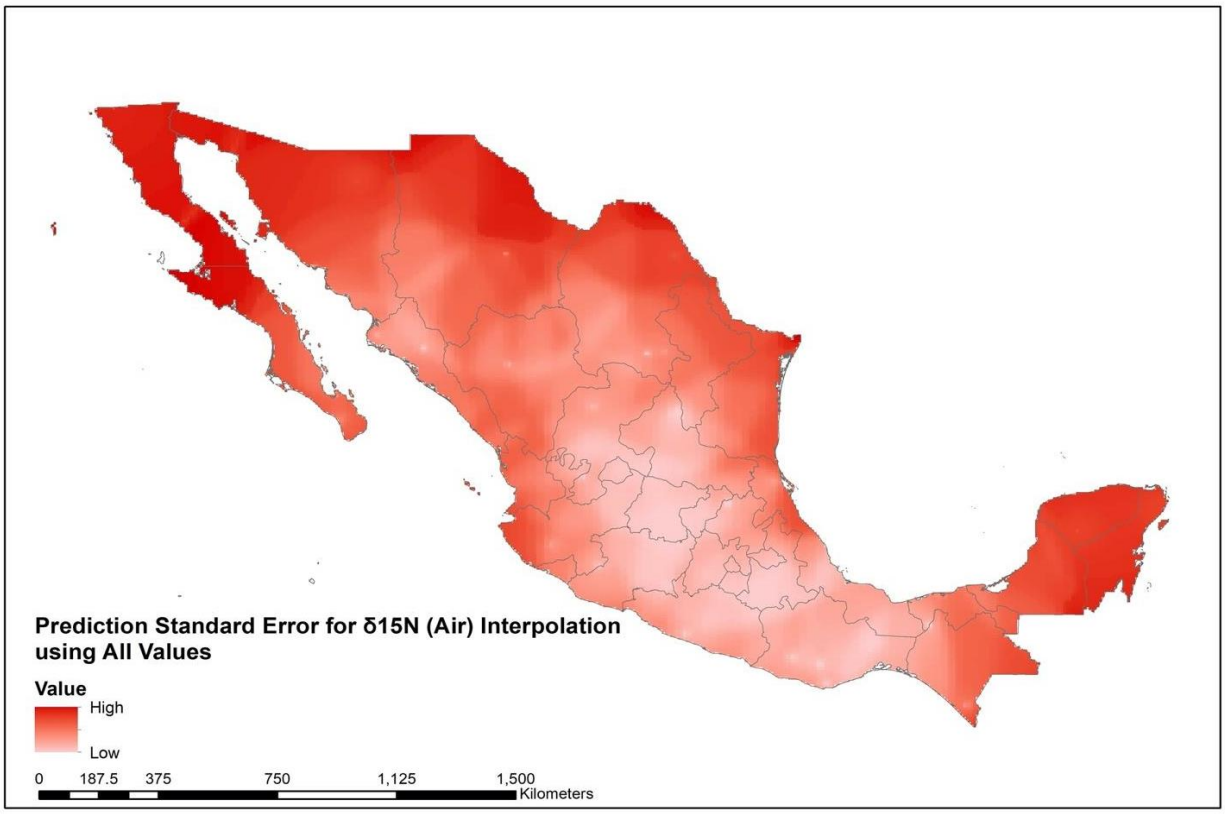

Figure 5.1.9. Prediction Standard Error output for δ^{15}N isoscape (Figure 5.1.6) for all values.

Sulfur

δ^{34}S performed poorly for both geographic and socioeconomic variables. The patterning of the isoscape (Figure 7) can be interpreted as somewhat similar to the pattern seen in the δ^{15}N isoscape. The prediction standard error seems especially elevated along the coastlines of the country and even further elevated on the Baja California and Yucatan peninsulas (Figure 10).

The fact that latitude did not influence the isotopic values was in accordance with the common understanding that δ^{34}S is mainly influenced by the marine environment. The somewhat stronger longitudinal effects reflect the influences of both the Atlantic and Pacific Oceans, which also explains the contrary relationships when dividing the dataset into separate drainage basins. As mentioned above, elevation did not affect isotopic values significantly on the Atlantic side, while the Pacific dataset showed some correlation.

Also, somewhat surprisingly, the distance to closest ocean (with and without considering the Gulf of California) only correlated very weakly and was not statistically significant, meaning the assumed correlation of proximity to the sea and seafood consumption was not supported. However, it is important to note that there was a correlation between isotopic values and elevation on the Atlantic side of the samples. This is especially interesting because one would expect stronger gradients and therefore correlations from the Atlantic side of the dataset. The reason

behind this is that the Pacific side is in the rain shadow and the Atlantic side is facing windward of the rainout gradient, which explains the isotopic gradients observed in the oxygen and hydrogen tap water data collected from Mexico. Potentially, a larger sample size in areas along the coasts could explain what influence the marine environment may have on the isotopic values and potential predictions. Furthermore, the fact that contamination from pollution can be a major issue in sulfur isotopes in modern populations could explain the lack of correlation (Richards, Fuller, and Hedges 2001).

The weak spatial patterning observed in this Mexican sample is contrary to the findings of Valenzuela *et al.* (2011) who discovered a clear north-south gradient in δ^{34}S values of human hair collected throughout the United States. The values observed in this study, nonetheless, are comparable to the observed values from North and South America, Europe, and Asia (Figure 11; Table 3; Bender *et al.* 2015; Lehn *et al.* 2015; Valenzuela *et al.* 2011; Thompson *et al.* 2010). The values of this study overlap with all other countries, except Brazil and Costa Rica. For these two countries, the values are distinctly higher than for Mexico. The values are, on average, lower than those observed in Europe and Asia. The lowest Mexican values are only seen in the United States and not in any of the other countries used here for comparison.

The Mexican δ^{34}S values are slightly elevated in comparison to the United States values but fall within their observed range. The higher values could mean more marine food consumption, but the dietary and locational signals are difficult to distinguish. Further, the lack of correlation between δ^{13}C and δ^{15}N further indicate that marine resources were not key food items among individuals in our sample.

The δ^{34}S values observed in Colombia are overall comparable but show a smaller range than that observed here, most likely explained by the difference in size, and therefore overall spatial range, of the countries. They values are, however, significantly lower than the observed values in China, India, and Mongolia (Table 3; Figure 11; Thompson *et al.* 2010).

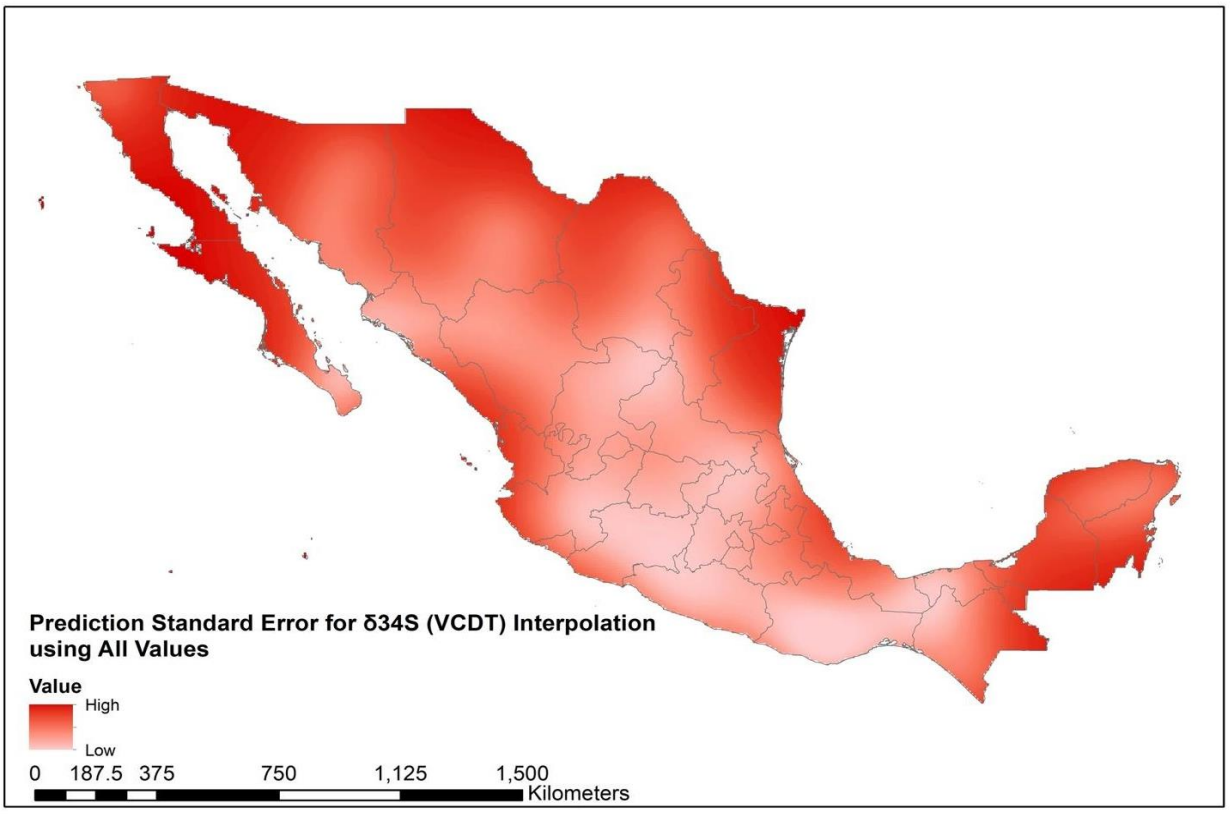

Figure 5.1.10. Prediction Standard Error output for δ^{34}S isoscape (Figure 5.1.7) for all values.

Table 5.1.3. Comparison of descriptive statistics of δ^{13}C, δ^{15}N, and δ^{34}S values from Mexico, United States (Valenzuela *et al.* 2011), Colombia (Bender *et al.* 2015), China, India, Mongolia, Pakistan (Thompson *et al.* 2010), Brazil, Costa Rica, Germany, Italy, UK/Ireland, France, Poland and Russia (Lehn *et al.* 2015). All values in per mil (‰).

	δ^{13}C				δ^{15}N				δ^{34}S			
	Min	**Max**	**Mean**	**N**	**Min**	**Max**	**Mean**	**N**	**Min**	**Max**	**Mean**	**N**
Mexico	-18.3	-12.8	-15.6±1.0	101	6.8	10.8	9.2±0.6	101	2.7	8.0	4.5±1.0	101
USA	-21.6	-14.7	-16.8±0.8	206	6.5	9.7	8.8±0.4	206	-1.2	9.9	3.4±1.1	228
Colombia	-18.5	-15.4	-16.8±0.8	38	8.9	10.8	9.9±0.6	38	3.1	7.4	4.9±0.8	38
Brazil	-22.8	-15.0	-16.6±1.7	22	8.1	10.2	9.0±0.6	22	8.0	10.6	9.5±0.7	22
Costa Rica	-18.8	-15.8	-17.2±1.0	17	8.2	9.8	8.8±0.5	17	1.9	8.1	4.3±1.6	17
Germany*	-22.5	-19.6	-20.8±0.4 -20.9±0.5	143	6.9	9.8	8.5±0.5 8.2±0.6	143	4.7	9.1	6.6±0.8 7.0±0.9	143
Italy	-21.7	-18.9	-20.4±0.6	34	7.2	9.5	8.4±0.7	33	4.9	7.7	6.3±0.7	32
UK/Ireland	-22.0	-20.8	-21.3±0.3	28	8.3	9.9	8.8±0.4	28	5.0	7.3	6.3±0.6	28
France	-21.1	-19.6	-20.3±0.5	24	8.0	10.6	8.9±0.7	24	6.5	9.5	7.5±0.7	24
Poland	-22.0	-20.1	-21.2±0.5	19	7.8	9.3	8.7±0.4	19	4.4	6.8	5.3±0.7	19
Russia	-21.6	-18.7	-20.4±0.6	40	8.3	11.9	9.6±0.7	40	4.2	9.7	7.0±1.0	40
China	-23.8	-17.4	-20.3±1.5	74	5.2	10.6	8.1±1.1	74	3.3	11.8	6.7±2.1	28
India	-22.6	-17.2	-19.8±1.2	38	5.8	12.2	8.1±1.7	38	5.3	13.8	10.1±1.7	26
Mongolia	-21.7	-17.4	-20.0±1.0	20	7.3	13.3	9.6±1.4	20	3.7	7.2	6.0±1.0	19
Pakistan	-21.7	-19.6	-20.6±0.7	11	6.7	9.2	8.2±0.7	11	3.2	5.3	4.0±0.6	12

*Germany mean and SD values refer to Southern Germany and Northern Germany as presented by Lehn *et al.* 2015.

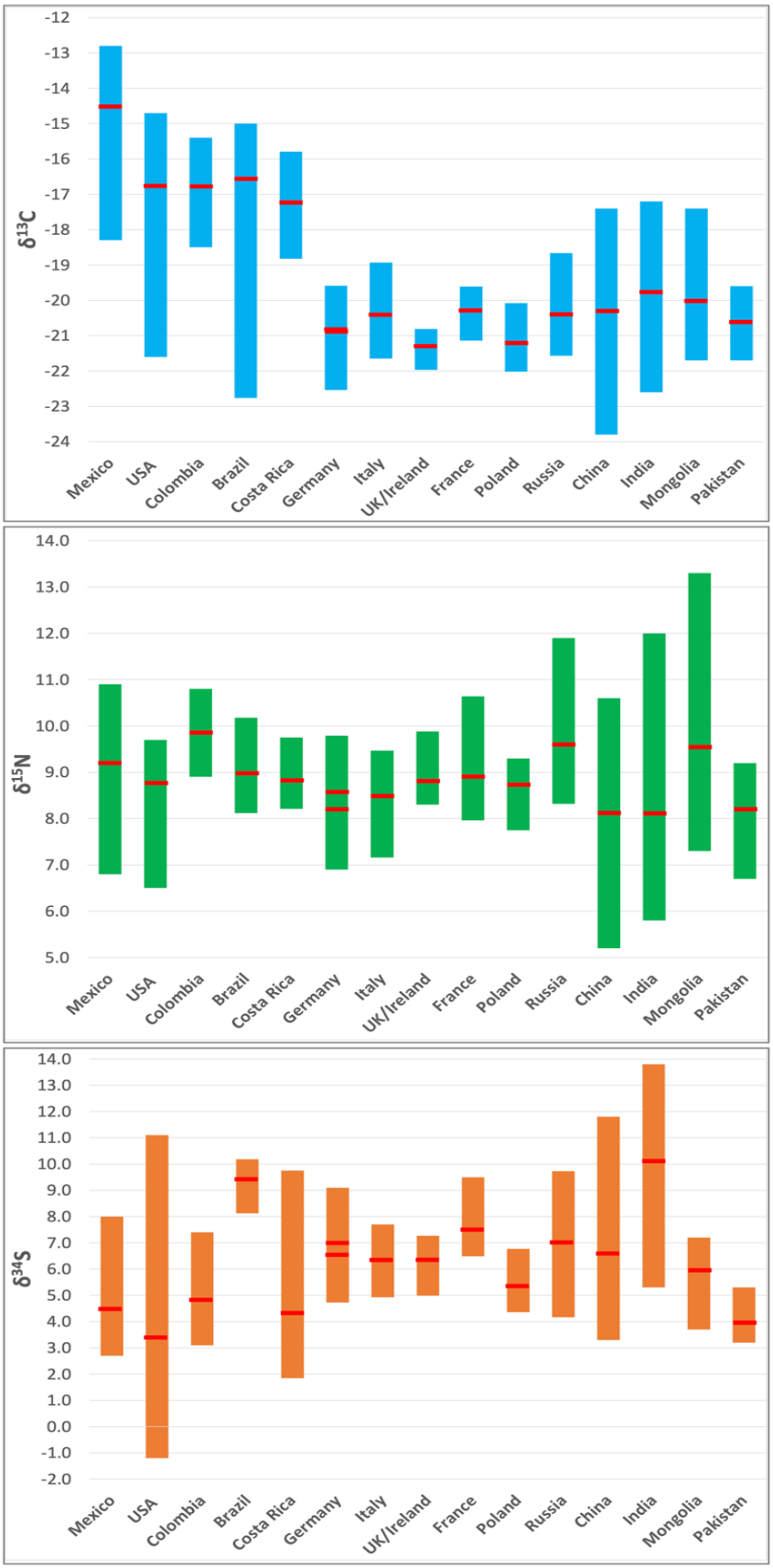

Figure 5.1.11. Boxplot comparing δ^{13}C, δ^{15}N and δ^{34}S values from Mexico, United States (Valenzuela *et al.* 2011), Colombia (Bender *et al.* 2015), China, India, Mongolia, Pakistan (Thompson *et al.* 2010), Brazil, Costa Rica, Germany, Italy, UK/Ireland, France, Poland, and Russia (Lehn *et al.* 2015). All values in per mil (‰).

5.1.5. Conclusion

In this study, 101 hair samples from 32 locations in Mexico were analyzed. The resulting $\delta^{13}C$, $\delta^{15}N$, and $\delta^{34}S$ isotopic values were then examined to study the inter-population variance and potential correlations to geographic/environmental and socioeconomic variables. Another objective was to explore the spatial distribution of carbon, nitrogen, and sulfur isotope ratios in human hair across Mexico and their potential usefulness for forensic applications, such as narrowing down the region of origin of undocumented border crossers. The results and success varied greatly between isotope systems.

While previous research showed geographic patterns in the $\delta^{34}S$ isotopic values in several countries (Valenzuela *et al.* 2011; Katzenberg and Krouse 1989; Krouse and Grinenko 1991), this study was not able to identify similar patterns within Mexico. Further study into the dietary habits of the Mexican population is needed to find potential explanations for these patterns. The findings reinforce the idea that the average Mexican diet is very C_4-plant based as well as meat-heavy. Nonetheless, the observation of geographic patterns in the $\delta^{13}C$ values is somewhat surprising as they had not been previously documented in human hair studies. While the produced isoscape shows clear trends, it is essential to further the research into the farming practices and dietary preferences, especially considering the significant influence of socioeconomic factors on isotope values. A tighter network of samples is needed to strengthen the now established baseline data and employ it in the future as a new tracer from which geographic information can be extracted. Additionally, a more thoroughly documented history of the hair donors would improve the possibility to draw further conclusions.

If used along with other isotopes such as $\delta^{2}H$, $\delta^{18}O$, and $^{87}Sr/^{86}Sr$, there is significant potential for accurate region-of-origin predictions of human hair. Furthermore, the divide for the Atlantic and Pacific drainage basin needs to be considered in future research and in the modeling of isotope values. This finding also shows that ordinary kriging will most likely not be sufficient in the future and that more sophisticated models, which include environmental and geographic variables, are needed when generating isoscapes.

Overall, the lack of correlation between the C-N-S isotopic values and the population size of the locations sampled for this study could indicate that the diet does not vary significantly between rural and more urban locations. Since some of the socioeconomic correlations were greater than the geographic correlations, it is essential to further our knowledge into these factors and their influences.

In conclusion, the C-N-S data show stronger correlations with socioeconomic covariates than with geographic and environmental ones within Mexico. The recorded isotopic values have

the potential to be used in combination with other isotope systems to narrow potential regions of origin. Furthermore, socioeconomic factors may have an even larger impact on the recorded values than previously thought.

Acknowledgements
We would like to thank the 101 anonymous hair donors throughout Mexico for supporting this research. This research was made possible by the American Academy of Forensic Sciences (AAFS) Humanitarian and Human Rights Resource Center (HHRRC) grant, supported by the AAFS and National Institute of Justice (U.S. Department of Justice). We would like to especially thank Dr. Lisette Kootker for her tremendous input and editing of this article.

Supplementary Material

Table 1. Results of Carbon, Nitrogen, Sulfur Isotope Ratios, C%, N% and S%.

Location	δ^{13}C (VPDB)	Total C (µg)	δ^{15}N (Air)	Total N (µg)	δ34S (VCDT)	Total S (µg)
Puerto Morelos, Quintana Roo	-15.6	206	8.6	70	4.0	40
Puerto Morelos, Quintana Roo	-15.7	239	9.5	79	4.1	33
Puerto Morelos, Quintana Roo	-15.8	218	8.5	70	4.1	35
Tekax de Álvaro Obregón, Yucatan	-14.9	209	8.7	70	6.1	35
Tekax de Álvaro Obregón, Yucatan	-15.1	220	8.4	74	6.7	35
Tekax de Álvaro Obregón, Yucatan	-16.7	255	8.5	84	4.0	38
Paraíso, Tabasco	-15.3	213	9.2	69	3.5	34
Paraíso, Tabasco	-15.6	227	9.2	73	3.5	39
Paraíso, Tabasco	-15.6	195	9.2	63	3.2	36
Paraíso, Tabasco	-14.8	215	9.7	70	4.3	28
Plan de Ayala, Chiapas	-15.2	234	9.3	78	4.1	35
Plan de Ayala, Chiapas	-15.6	225	9.3	73	4.3	32
Plan de Ayala, Chiapas	-15.3	230	9.4	75	3.5	40
Huixtla, Chiapas	-14.8	206	9.6	68	4.0	38
Huixtla, Chiapas	-14.1	219	9.1	72	3.9	37
Huixtla, Chiapas	-16.1	201	9.1	67	3.8	36
San Juan Guichicovi, Oaxaca	-14.6	222	9.2	71	3.4	37
San Juan Guichicovi, Oaxaca	-14.1	228	9.0	77	4.0	22
San Juan Guichicovi, Oaxaca	-13.6	188	9.2	64	4.5	27
San Pedro Pochutla, Oaxaca	-15.5	237	9.5	76	4.2	42
San Pedro Pochutla, Oaxaca	-14.8	216	10.3	71	5.6	40
San Pedro Pochutla, Oaxaca	-14.3	249	9.0	78	3.6	37
Miahuatlán de Porfirio Díaz, Oaxaca	-12.8	211	8.4	71	5.0	41
Miahuatlán de Porfirio Díaz, Oaxaca	-15.1	253	8.5	82	4.1	37
Miahuatlán de Porfirio Díaz, Oaxaca	-15.3	221	9.2	70	3.9	36
San Jacinto Tlacotepec, Oaxaca	-13.3	236	7.6	79	5.3	29
San Jacinto Tlacotepec, Oaxaca	-13.8	219	6.9	70	5.0	34
San Jacinto Tlacotepec, Oaxaca	-13.8	187	6.8	61	4.7	34
Tehuitzingo, Puebla	-14.2	209	8.4	70	4.3	35
Tehuitzingo, Puebla	-15.6	245	9.3	77	4.2	34
Tehuitzingo, Puebla	-15.1	221	9.1	73	5.0	35
Atoyac de Álvarez, Guerrero	-15.0	196	9.3	65	4.4	15
Atoyac de Álvarez, Guerrero	-14.6	246	8.6	83	4.4	39
Atoyac de Álvarez, Guerrero	-14.9	204	8.5	66	4.3	41
Atoyac de Álvarez, Guerrero	-14.1	244	8.9	81	4.1	41
Huetamo de Núñez, Michoacán	-15.5	194	9.3	66	4.0	32
Huetamo de Núñez, Michoacán	-15.0	208	9.4	69	4.2	44
Huetamo de Núñez, Michoacán	-16.0	251	9.7	81	4.0	38

Tepalcatepec, Michoacán	-15.9	250	9.5	77	4.5	36
Tepalcatepec, Michoacán	-15.8	200	9.6	63	4.0	39
Tepalcatepec, Michoacán	-16.1	239	9.3	76	3.3	39
El Grullo, Jalisco	-14.5	242	8.9	77	3.5	38
El Grullo, Jalisco	-15.9	227	8.7	74	3.6	36
El Grullo, Jalisco	-14.4	211	9.7	68	4.4	19
Tlaltenango de Sánchez Román, Zacatecas	-14.2	215	8.8	73	3.5	40
Tlaltenango de Sánchez Román, Zacatecas	-15.0	223	8.9	72	3.8	20
Tlaltenango de Sánchez Román, Zacatecas	-14.3	243	9.5	81	3.5	36
Moroleón, Guanajuato	-15.4	234	9.9	79	3.5	26
Moroleón, Guanajuato	-16.5	210	9.8	70	3.3	34
Moroleón, Guanajuato	-17.0	178	9.8	58	5.0	40
Jacala, Hidalgo	-14.0	229	9.1	75	5.5	34
Jacala, Hidalgo	-15.5	214	9.9	69	3.9	39
Jacala, Hidalgo	-15.1	197	9.9	61	4.6	24
Jacala, Hidalgo	-14.4	244	8.1	81	4.3	36
Ozuluama de Mascareñas, Veracruz	-14.7	236	9.9	80	3.9	43
Ozuluama de Mascareñas, Veracruz	-15.3	223	9.4	74	3.9	40
Ozuluama de Mascareñas, Veracruz	-14.5	224	10.2	73	4.2	40
Matehuala, San Luis Potosi	-16.3	225	9.5	76	5.3	42
Matehuala, San Luis Potosi	-15.7	221	9.6	74	5.3	38
Matehuala, San Luis Potosi	-16.3	186	9.5	60	4.5	43
Matehuala, San Luis Potosi	-16.6	249	9.8	80	5.0	37
General Capeda, Coahuila	-16.1	196	9.4	64	3.6	39
General Capeda, Coahuila	-16.2	187	9.0	59	3.4	40
General Capeda, Coahuila	-16.3	231	9.2	77	3.0	41
Saltillo, Coahuila	-16.3	214	9.5	72	3.2	39
Villa Unión, Coahuila	-16.6	235	8.6	77	3.7	43
Villa Unión, Coahuila	-16.8	232	9.6	77	4.2	40
Villa Unión, Coahuila	-16.9	203	9.0	68	3.9	42
Pedro Meoqui, Chihuahua	-15.8	214	8.9	73	4.9	35
Pedro Meoqui, Chihuahua	-18.3	201	8.3	64	4.8	39
Pedro Meoqui, Chihuahua	-18.1	202	8.4	68	5.4	11
Pedro Meoqui, Chihuahua	-16.6	208	8.9	72	4.0	42
Santiago Papasquiaro, Durango	-16.4	235	9.3	75	4.0	77
Santiago Papasquiaro, Durango	-15.4	229	9.6	77	4.4	76
Santiago Papasquiaro, Durango	-16.2	242	9.3	79	4.3	78
Santiago Papasquiaro, Durango	-15.6	206	9.4	69	4.0	80
Río Grande, Zacatecas	-14.7	226	9.6	75	4.0	71
Río Grande, Zacatecas	-15.8	235	9.4	78	4.2	77
Río Grande, Zacatecas	-16.8	213	8.6	70	4.2	73
El Salto, Sinaloa	-16.0	236	9.0	78	5.1	74

El Salto, Sinaloa	-16.4	219	9.4	74	4.8	78
El Salto, Sinaloa	-16.5	214	9.4	72	4.9	75
Villa de Ahome, Sinaloa	-16.3	227	9.7	77	5.8	80
Villa de Ahome, Sinaloa	-16.4	240	9.8	80	4.8	80
Villa de Ahome, Sinaloa	-15.9	246	9.0	81	4.9	73
Todos Los Santos, Baja California Sur	-16.6	234	9.0	78	6.9	74
Todos Los Santos, Baja California Sur	-15.7	204	9.5	69	4.8	70
Todos Los Santos, Baja California Sur	-16.7	213	9.0	69	7.5	75
Todos Los Santos, Baja California Sur	-16.5	225	9.6	74	7.3	77
Todos Los Santos, Baja California Sur	-16.4	188	9.7	61	8.0	74
La Paz, Baja California Sur	-15.9	227	8.9	76	7.0	78
Guaymas, Sonora	-16.0	195	10.8	63	5.7	81
Guaymas, Sonora	-15.6	225	10.2	76	5.3	79
Guaymas, Sonora	-16.4	230	9.1	77	3.9	85
Nacozari de García, Sonora	-14.4	215	9.8	72	4.7	81
Nacozari de García, Sonora	-17.1	232	9.3	78	5.2	76
Nacozari de García, Sonora	-15.3	180	9.5	61	4.4	71
Tecate, Baja California	-17.0	212	8.6	72	4.1	76
Tecate, Baja California	-16.9	226	8.7	77	3.0	82
Tecate, Baja California	-16.3	218	8.7	75	2.7	78
Tecate, Baja California	-16.7	217	8.4	70	3.0	76

> 0.5
0.5 > 0.3
0.3 > 0.1
⚡

Table 2. Pearson's Correlation results for inter-elemental correlations for all data, inter-elemental correlations for location averages, and for element vs. standard deviation.

r	p
Carbon / Nitrogen	
-0.17	= 0.09
Carbon / Sulfur	
⚡	
Nitrogen/ Sulfur	
⚡	
Carbon Location Average / Nitrogen Location Average	
-0.32	= 0.08
Carbon Location Average / Sulfur Location Average	
-0.12	= 0.54
Nitrogen Location Average / Sulfur Location Average	
⚡	
Carbon Location Average / Carbon Location SD	
0.14	= 0.46
Nitrogen Location Average / Nitrogen Location SD	
⚡	
Sulfur Location Average / Sulfur Location SD	
0.52	= 0.003

Geographic and Environmental Covariate Correlations

Table 3. Pearson's Correlations between Longitude and Isotopic factors.

Longitude					
r	**p**	**r**	**p**	**r**	**p**
Carbon		**Nitrogen**		**Sulfur**	
0.44	< 0.001	-0.13	= 0.19	-0.19	= 0.06
Carbon Location Average		**Nitrogen Location Average**		**Sulfur Location Average**	
0.50	= 0.005	-0.20	= 0.29	-0.16	= 0.40
Carbon Location SD		**Nitrogen Location SD**		**Sulfur Location SD**	
⚡		⚡		⚡	
Carbon Atlantic		**Nitrogen Atlantic**		**Sulfur Atlantic**	
0.26	= 0.16	-0.42	= 0.02	0.16	= 0.38
Carbon Pacific		**Nitrogen Pacific**		**Sulfur Pacific**	
0.61	< 0.001	-0.16	= 0.20	-0.23	= 0.05

Table 4. Pearson's Correlations between Latitude and Isotopic factors.

Latitude					
r	**p**	**r**	**p**	**r**	**p**
Carbon		**Nitrogen**		**Sulfur**	
-0.64	< 0.001	0.11	= 0.27	⚡	
Carbon Location Average		**Nitrogen Location Average**		**Sulfur Location Average**	
-0.74	< 0.001	0.17	= 0.36	⚡	
Carbon Location SD		**Nitrogen Location SD**		**Sulfur Location SD**	
⚡		⚡		⚡	
Carbon Atlantic		**Nitrogen Atlantic**		**Sulfur Atlantic**	
-0.64	< 0.001	⚡		-0.11	= 0.56
Carbon Pacific		**Nitrogen Pacific**		**Sulfur Pacific**	
-0.64	< 0.001	0.12	= 0.29	⚡	

Table 5. Pearson's Correlations between Elevation and Isotopic factors.

Elevation					
r	**p**	**r**	**p**	**r**	**p**
Carbon		**Nitrogen**		**Sulfur**	
⚡		⚡		-0.20	= 0.05
Carbon Location Average		**Nitrogen Location Average**		**Sulfur Location Average**	
⚡		⚡		-0.20	= 0.30
Carbon Location SD		**Nitrogen Location SD**		**Sulfur Location SD**	
0.38	= 0.04	⚡		-0.17	= 0.37
Carbon Atlantic		**Nitrogen Atlantic**		**Sulfur Atlantic**	
-0.23	= 0.02	0.23	= 0.21	⚡	
Carbon Pacific		**Nitrogen Pacific**		**Sulfur Pacific**	
⚡		-0.15	= 0.20	-0.31	= 0.009

Table 6. Pearson's Correlations between Temperature and Isotopic factors.

Temperature					
r	**p**	**r**	**p**	**r**	**p**
Carbon		**Nitrogen**		**Sulfur**	
-0.33	= 0002				
Carbon Location Average		**Nitrogen Location Average**		**Sulfur Location Average**	
0.32	= 0.08			0.11	= 0.57
Carbon Location SD		**Nitrogen Location SD**		**Sulfur Location SD**	
-0.24	= 0.20				
Carbon Atlantic		**Nitrogen Atlantic**		**Sulfur Atlantic**	
0.35	= 0.05	-0.25	= 0.18		
Carbon Pacific		**Nitrogen Pacific**		**Sulfur Pacific**	
0.30	= 0.01	0.12	= 0.32	0.12	= 0.33

Table 7. Pearson's Correlations between Distance to ocean and Isotopic factors.

Distance to ocean					
r	**p**	**r**	**p**	**r**	**p**
Carbon		**Nitrogen**		**Sulfur**	
0.31	< 0.001			-0.17	0.09
Carbon Location Average		**Nitrogen Location Average**		**Sulfur Location Average**	
-0.41	= 0.03			-0.16	= 0.41
Carbon Location SD		**Nitrogen Location SD**		**Sulfur Location SD**	
0.25	= 0.18	-0.16	= 0.41	-0.17	= 0.38
Carbon Atlantic		**Nitrogen Atlantic**		**Sulfur Atlantic**	
-0.60	< 0.001				
Carbon Pacific		**Nitrogen Pacific**		**Sulfur Pacific**	
-0.25	= 0.04			-0.20	= 0.10

Table 8. Pearson's Correlations between Distance to ocean excluding gulf and Isotopic factors.

Distance to ocean excluding gulf					
r	**p**	**r**	**p**	**r**	**p**
Carbon		**Nitrogen**		**Sulfur**	
-0.42	< 0.001				
Carbon Location Average		**Nitrogen Location Average**		**Sulfur Location Average**	
-0.52	= 0.003				
Carbon Location SD		**Nitrogen Location SD**		**Sulfur Location SD**	
0.31	= 0.09				
Carbon Atlantic		**Nitrogen Atlantic**		**Sulfur Atlantic**	
-0.60	< 0.001				
Carbon Pacific		**Nitrogen Pacific**		**Sulfur Pacific**	
-0.38	= 0.001				

Table 9. Pearson's Correlations between Three-year precipitation and Isotopic factors.

Three-year precipitation					
r	**p**	**r**	**p**	**r**	**p**
Carbon		**Nitrogen**		**Sulfur**	
0.51	< 0.001	-0.15	= 0.12	-0.23	= 0.02
Carbon Location Average		**Nitrogen Location Average**		**Sulfur Location Average**	
0.59	< 0.001	-0.20	= 0.28	-0.22	= 0.25
Carbon Location SD		**Nitrogen Location SD**		**Sulfur Location SD**	
ϟ		-0.19	= 0.32	-0.22	= 0.24
Carbon Atlantic		**Nitrogen Atlantic**		**Sulfur Atlantic**	
0.50	= 0.004	ϟ		ϟ	
Carbon Pacific		**Nitrogen Pacific**		**Sulfur Pacific**	
0.55	< 0.001	-0.23	= 0.06	-0.28	= 0.02

Table 10. Pearson's Correlations between One-year precipitation and Isotopic factors.

One-year precipitation					
r	**p**	**r**	**p**	**r**	**p**
Carbon		**Nitrogen**		**Sulfur**	
0.54	< 0.001	-0.11	= 0.28	-0.27	= 0.006
Carbon Location Average		**Nitrogen Location Average**		**Sulfur Location Average**	
0.62	< 0.001	-0.15	= 0.43	-0.28	= 0.14
Carbon Location SD		**Nitrogen Location SD**		**Sulfur Location SD**	
ϟ		-0.17	= 0.36	-0.24	= 0.21
Carbon Atlantic		**Nitrogen Atlantic**		**Sulfur Atlantic**	
0.53	= 0.002	ϟ		ϟ	
Carbon Pacific		**Nitrogen Pacific**		**Sulfur Pacific**	
0.59	< 0.001	-0.17	= 0.16	-0.34	= 0.004

Socioeconomic Covariate Correlations

Table 11. Pearson's Correlations between Percentage of population living in poverty and Isotopic factors.

Percentage of population living in poverty					
r	**p**	**r**	**p**	**r**	**p**
Carbon		**Nitrogen**		**Sulfur**	
0.60	< 0.001				
Carbon Location Average		**Nitrogen Location Average**		**Sulfur Location Average**	
0.72	< 0.001	-0.14	= 0.48		
Carbon Location SD		**Nitrogen Location SD**		**Sulfur Location SD**	
0.13	= 0.48	-0.11	= 0.57		
Carbon Atlantic		**Nitrogen Atlantic**		**Sulfur Atlantic**	
0.55	= 0.001	0.29	= 0.11		
Carbon Pacific		**Nitrogen Pacific**		**Sulfur Pacific**	
0.63	< 0.001	-0.22	= 0.07		

Table 12. Pearson's Correlations between Number of people living in poverty and Isotopic factors.

Number of people living in poverty					
r	**p**	**r**	**p**	**r**	**p**
Carbon		**Nitrogen**		**Sulfur**	
0.48	< 0.001			-0.26	= 0.01
Carbon Location Average		**Nitrogen Location Average**		**Sulfur Location Average**	
0.55	= 0.002			-0.25	= 0.18
Carbon Location SD		**Nitrogen Location SD**		**Sulfur Location SD**	
0.12	= 0.53			-0.16	= 0.40
Carbon Atlantic		**Nitrogen Atlantic**		**Sulfur Atlantic**	
0.45	= 0.01	0.40	= 0.03		
Carbon Pacific		**Nitrogen Pacific**		**Sulfur Pacific**	
0.52	< 0.001	-0.16	= 0.20	-0.36	= 0.002

Table 13. Pearson's Correlations between Percentage of state population being of indigenous ancestry and Isotopic factors.

Percentage of state population being of indigenous ancestry					
r	**p**	**r**	**p**	**r**	**p**
Carbon		**Nitrogen**		**Sulfur**	
0.58	< 0.001	-0.31	= 0.001		
Carbon Location Average		**Nitrogen Location Average**		**Sulfur Location Average**	
0.68	< 0.001	-0.40	= 0.03	0.16	= 0.39
Carbon Location SD		**Nitrogen Location SD**		**Sulfur Location SD**	
0.15	= 0.01			0.24	= 0.19
Carbon Atlantic		**Nitrogen Atlantic**		**Sulfur Atlantic**	
0.45	= 0.01	-0.36	= 0.05	0.58	= 0.001
Carbon Pacific		**Nitrogen Pacific**		**Sulfur Pacific**	
0.62	< 0.001	-0.32	= 0.007		

Table 14. Pearson's Correlations between Percentage of state population speaking an indigenous language and Isotopic factors.

Percentage of state population speaking an indigenous language					
r	**p**	**r**	**p**	**r**	**p**
Carbon		**Nitrogen**		**Sulfur**	
0.55	< 0.001	-0.33	< 0.001	ϟ	
Carbon Location Average		**Nitrogen Location Average**		**Sulfur Location Average**	
0.66	< 0.001	-0.41	= 0.02	0.11	= 0.57
Carbon Location SD		**Nitrogen Location SD**		**Sulfur Location SD**	
0.19	= 0.32	ϟ		0.17	= 0.36
Carbon Atlantic		**Nitrogen Atlantic**		**Sulfur Atlantic**	
0.35	= 0.06	-0.28	= 0.12	0.54	= 0.002
Carbon Pacific		**Nitrogen Pacific**		**Sulfur Pacific**	
0.61	< 0.001	-0.36	= 0.003	ϟ	

Table 15. Pearson's Correlations between Population size and Isotopic factors.

Population size					
r	**p**	**r**	**p**	**r**	**p**
Carbon		**Nitrogen**		**Sulfur**	
ϟ		0.21	= 0.04	-0.21	= 0.03
Carbon Location Average		**Nitrogen Location Average**		**Sulfur Location Average**	
-0.13	= 0.50	0.28	= 0.14	= 0.20	= 0.29
Carbon Location SD		**Nitrogen Location SD**		**Sulfur Location SD**	
ϟ		ϟ		ϟ	
Carbon Atlantic		**Nitrogen Atlantic**		**Sulfur Atlantic**	
ϟ		0.24	= 0.20	0.20	= 0.27
Carbon Pacific		**Nitrogen Pacific**		**Sulfur Pacific**	
ϟ		0.22	= 0.07	-0.45	< 0.001

Table 16. Pearson's Correlations between HDI and Isotopic factors.

HDI					
r	**p**	**r**	**p**	**r**	**p**
Carbon		**Nitrogen**		**Sulfur**	
0.62	< 0.001	0.16	= 0.11	0.23	= 0.02
Carbon Location Average		**Nitrogen Location Average**		**Sulfur Location Average**	
-0.72	< 0.001	0.21	= 0.27	0.22	= 0.24
Carbon Location SD		**Nitrogen Location SD**		**Sulfur Location SD**	
-0.14	= 0.47	0.12	= 0.53	0.16	= 0.39
Carbon Atlantic		**Nitrogen Atlantic**		**Sulfur Atlantic**	
-0.45	= 0.01	-0.26	= 0.16	-0.17	= 0.37
Carbon Pacific		**Nitrogen Pacific**		**Sulfur Pacific**	
-0.65	< 0.001	0.26	= 0.03	0.34	= 0.004

Table 17. Pearson's Correlations among socioeconomic covariates and correlations between socioeconomic and geographic covariates.

% of pop. living in poverty		**# of people living in poverty**		**% of state pop. w/ indigenous ancestry**		**% of state pop. speaking ind. language**		**Population Size**		**HDI**	
r	**p**	**r**	**p**	**r**	**p**	**r**	**p**	**r**	**p**	**r**	**p**
		% of pop. living in poverty		% of pop. living in poverty		% of pop. living in poverty		% of pop. living in poverty		% of pop. living in poverty	
		0.74	< 0.001	0.64	< 0.001	0.70	< 0.001	ϟ		-0.89	< 0.001
# of people living in poverty				# of people living in poverty		# of people living in poverty		# of people living in poverty		# of people living in poverty	
0.74	< 0.001			0.46	< 0.001	0.53	< 0.001	ϟ		-0.78	< 0.001
% of state pop. w/ indigenous ancestry		% of state pop. w/ indigenous ancestry				% of state pop. w/ indigenous ancestry		% of state pop. w/ indigenous ancestry		% of state pop. w/ indigenous ancestry	
0.64	< 0.001	0.46	< 0.001			0.94	< 0.001	-0.17	= 0.08	-0.70	< 0.001
% of state pop. speaking ind. language		% of state pop. speaking ind. language		% of state pop. speaking ind. language				% of state pop. speaking ind. language		% of state pop. speaking ind. language	
0.70	< 0.001	0.53	< 0.001	0.94	< 0.001			-0.21	= 0.04	-0.77	< 0.001
Population Size		Population Size		Population Size		Population Size				Population Size	
ϟ		ϟ		-0.17	= 0.08	-0.20	= 0.04			ϟ	
HDI		HDI		HDI		HDI		HDI			
-0.89	< 0.001	-0.78	< 0.001	-0.70	< 0.001	-0.77	< 0.001	ϟ			
Longitude		Longitude		Longitude		Longitude		Longitude		Longitude	
0.53	< 0.001	0.46	< 0.001	0.67	< 0.001	0.66	< 0.001	-0.13	= 0.19	-0.63	< 0.001
Latitude		Latitude		Latitude		Latitude		Latitude		Latitude	
-0.83	< 0.001	-0.64	< 0.001	-0.70	< 0.001	-0.67	< 0.001	ϟ		0.83	< 0.001
Elevation		Elevation		Elevation		Elevation		Elevation		Elevation	
-0.19	= 0.06	-0.15	= 0.13	-0.26	= 0.008	-0.19	= 0.06	ϟ		ϟ	
Temperature		Temperature		Temperature		Temperature		Temperature		Temperature	
0.49	< 0.001	0.43	< 0.001	0.52	< 0.001	0.40	< 0.001	ϟ		-0.41	< 0.001
Distance to ocean		Distance to ocean		Distance to ocean		Distance to ocean		Distance to ocean		Distance to ocean	
-0.42	< 0.001	-0.25	= 0.01	-0.40	< 0.001	-0.32	= 0.001	-0.11	= 0.29	0.22	= 0.03
Distance to ocean w/o gulf		Distance to ocean w/o gulf		Distance to ocean w/o gulf		Distance to ocean w/o gulf		Distance to ocean w/o gulf to ocean		Distance to ocean w/o gulf ocean	
-0.52	< 0.001	-0.32	= 0.001	-0.43	< 0.001	-0.37	< 0.001	ϟ		0.37	= 0.001
Three-year precipitation		Three-year precipitation		Three-year precipitation		Three-year precipitation		Three-year precipitation		Three-year precipitation	
0.74	< 0.001	0.76	< 0.001	0.57	< 0.001	0.66	< 0.001	-0.11	= 0.28	0.76	< 0.001
One-year precipitation		One-year precipitation		One-year precipitation		One-year precipitation		One-year precipitation		One-year precipitation	
0.73	< 0.001	0.75	< 0.001	0.58	< 0.001	0.65	< 0.001	ϟ		0.78	< 0.001

5.2. Stable isotope ratios of tap water in Mexico

Abstract:

This study is the first national-level tap water survey of stable isotope ratios, which includes a spatially distributed sample from many cities and towns across Mexico. Overall, there has been little stable isotope research in Mexico on water. Furthermore, the spatial coverage with Global Network for Isotopes in Precipitation (GNIP) stations is highly insufficient in Mexico (International Atomic Energy Agency World Meteorological Organization (IAEA/WMO) 2018). This work reports a first attempt to overcome the major limitation in the H and O tap water isotopic data for Mexico. The spatial variation in tap water across the country is large, spanning an 82.4‰ range for δ^2H and a 12.0‰ range for δ^{18}O. The isotopic values show a high geographic as well as some social and socioeconomic relationships. Using δ^2H and δ^{18}O values, and a Geographic Information System approach, maps of predicted tap water isotope ratios (isoscapes) for Mexico were developed. Clear spatial variation is visible in the developed isoscapes. These data will be useful to researchers interested in human-hydrological systems as well as forensic scientists interested in establishing the region of origin or the travel history for human remains.

KEYWORDS: Mexico, tap water, isotopes, oxygen, hydrogen, isoscape

5.2.1. Introduction

Drinkable tap water resources constitute a significant challenge across the globe, and Mexico is a prime example of the lack of sustainable drinking water resources. This fact is highlighted by the fact that Mexico is one of the highest bottled water consumers per capita in the world (Contreras 2019; Inter-American Development Bank 2011). Bowen *et al.* (2005) found the $\delta^{18}O$ and $\delta^{2}H$ isotopic values of bottled water from around the world to be very similar to the signatures found in the local tap water. It is, however, unknown if this is also the case for Mexico. While Mexican authorities and other institutions such as the Inter-American Development Bank have worked hard in the last couple of years to tackle the contamination problems in the Mexican river and lake systems as well as the deficiency in sanitation, the lack of clean tap water still exists (Inter-American Development Bank 2013). The availability of water, in terms of both quantity and quality, is highly variable across Mexico and reports show that over 30 million citizens lack high quality water services or have overall limited access to water (World Bank 2018). All factors are largely dependent on prosperity.

Factors such as population growth (especially in megacities such as Mexico City) and climate change play a huge role in understanding and managing the available water supplies. Even though this requires regular and routine monitoring, this large-scale research will provide a starting point for potential long-term monitoring to identify any present or future problems (Bowen *et al.* 2007).

Fortunately, $\delta^{2}H$ and $\delta^{18}O$ isotopic values of water are easily measured and analyzed. Therefore, there are few research limitations into the sources of these waters as well as evaporation losses, which could hold very valuable information for the future of Mexican water management.

While the Global Network for Isotopes in Precipitation (GNIP) dataset provides a crucial foundation for establishing global precipitation controlled isotopic landscapes (isoscapes), it has insufficient spatial coverage in Mexico. There are 39 recording stations in the United States but only two in Mexico (Veracruz and Chihuahua) in a country of almost 2 million square kilometers (International Atomic Energy Agency World Meteorological Organization 2018). Additionally, these two stations are not in operation anymore as they were only operated between 1962 and 1988. This spatial deficiency is a major concern when attempting to answer research questions concerning large scale Mexican isotope hydrology, reaching from determining the origins of food (Primrose *et al.* 2010) to determining the travel history or region of origin of an individual (Ehleringer *et al.* 2008). Consequently, this work reports one of very few recent attempts to overcome the major limitation in the $\delta^{18}O$ and $\delta^{2}H$ isoscape data in Mexico.

5.2.2. Methods

Study Location and Sample Acquisition

The sampling sites comprise tap water sources located across the country of Mexico (Figure 5.2.1). Fifty-four towns and cities throughout Mexico were sampled during a six-week period from June to July 2018 to characterize the tap water ratios across the country and explore potential spatial variations. In total, 26 out of 32 states were sampled: Baja California, Baja California Sur, Chiapas, Campeche, Chihuahua, Coahuila, Colima, Durango, Guanajuato, Guerrero, Hidalgo, Jalisco, Mexico City, Michoacán, Oaxaca, Puebla, Querétaro, Quintana Roo, San Luis Potosi, Sinaloa, Sonora, Tabasco, Tamaulipas, Veracruz, Yucatan, Zacatecas.

At least three tap water samples were collected from each location to evaluate local variation as well as inter-regional variation within Mexico. The collection included a 158 tap water samples.

Sample locations were chosen based on geographic variation in order to obtain relatively complete coverage of Mexico. Both large cities as well as rural communities were sampled. Nonetheless, a major factor was also accessibility. Some municipalities turn off the water source during the day to preserve water or prohibit foreigners from entering their villages due to recent conflicts with big international companies. Some other locations could not be sampled due to roadblocks and safety concerns.

Samples were collected from local tap water sources by running cold water for approximately 10 seconds before filling a clean 4ml vial to avoid air bubbles that could cause fractionation. After capping, the vials were sealed with Parafilm® to avoid the loosening of the caps and sample evapoconcentration. After the completion of the six-week data collection trip, the samples were sent to the Stable Isotope Ratios for Environmental Research (SIRFER) lab at the University of Utah, where they were prepared for analysis. Prior to shipment as well as at the laboratory, the samples were stored in a cool and dark place. Several vials were damaged during transportation. To replace these, aliquots of 30 mL samples, collected from the same taps for strontium analysis, were taken and subsequently submitted to SIRFER for analysis.

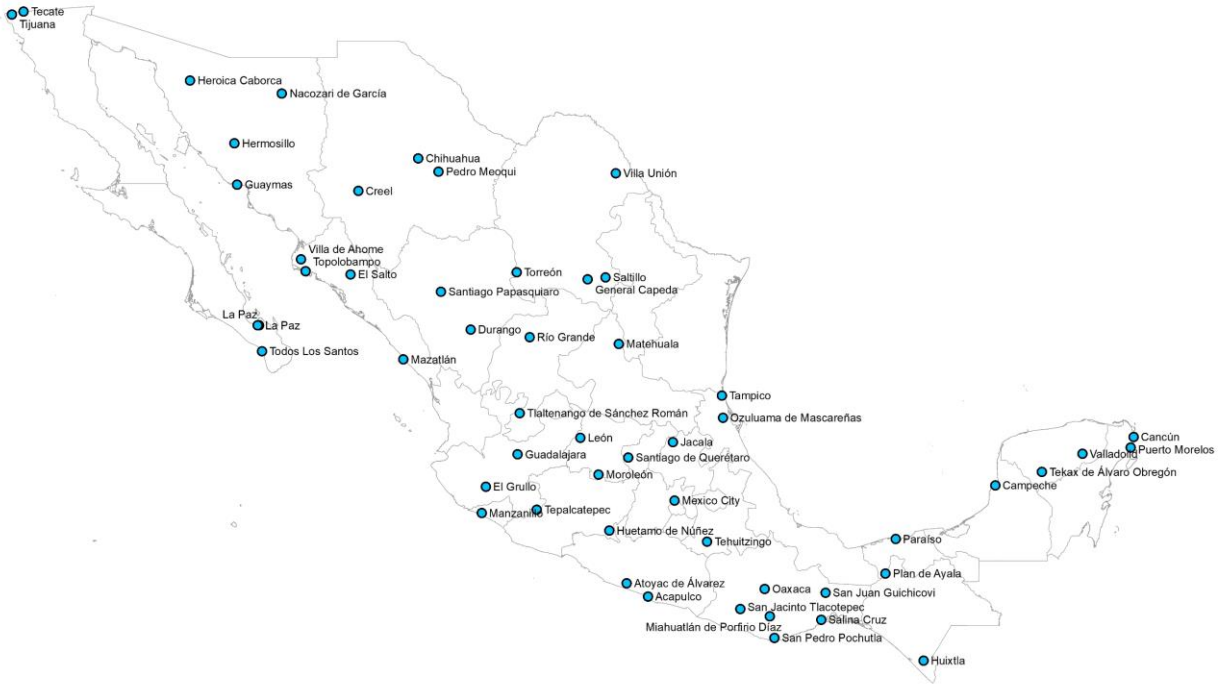

Figure 5.2.1. Map of Mexico showing the sampling locations.

Sample Analysis

Prior to analysis, an aliquot of each sample was transferred to a septum-capped vial. The δ^2H and δ^{18}O values are reported using the δ notation (where $\delta = (R_{sample}/R_{standard} - 1)*1000$, R = ^{2}H/^{1}H or ^{18}O/^{16}O) and normalized on the VSMOW – VSLAP standard scale. The samples were run for their H and O isotopic composition on a Picarro L2130-i analyzer. Three laboratory reference waters were measured and included in each analysis batch to correct the raw data for sample to sample memory effect as well as any drift that may occur during the course of the run (Van Geldern and Barth 2012). The known values of those are reported to be PZ: 16.9‰, 1.65‰; PT: 45.6‰, 7.23‰; UD: 123.1‰, 16.52‰; for δ^2H and δ^{18}O, respectively (Good *et al.* 2014). Cavity ringdown spectroscopy determined the isotopologue concentrations by transferring approximately 1.2 microliters of water from the heated vaporizer into the cavity of the spectroscopic analyzer (Gupta *et al.* 2009). The four measurements of each sample were averaged to obtain uncalibrated sample values. The reference waters were used to calibrate the obtained sample values to the VSMOW-SLAP reference scale using a two-point linear calibration (Good *et al.* 2014). All samples were analyzed between August and September 2018. The analytical precision for oxygen was 0.06‰and 0.22‰ for hydrogen.

Statistical and Geostatistical Analysis

Data analyses and statistical calculations were conducted using the programming language R. The correlations among the tap water isotope values and between the values and other environmental and socioeconomic variables were analyzed using Pearson's product-moment correlation. The strength of the correlations was primarily defined by the strength of association (r-value): large/strong > 0.5, medium/moderate 0.5 > 0.3, small/weak 0.3 > 0.1, 0.1 > 0 non-existent.

The Kruskal- Wallis rank-sum test was used to compare the isotopic data independently for each location in order to evaluate the differences between them. It explored whether there may be a statistically significant difference on a continuous dependent variable (isotope) by a categorical independent variable (location).

Geostatistical analyses were performed using the Geostatistical Analyst toolbox and Geostatistical Wizard (Environmental Systems Research Institute (ESRI) 2018). To quantify spatial autocorrelation and identify robust spatial patterns in the data, Global Moran's I Spatial Autocorrelation tool based on the locations of the data points and their corresponding values were used (Environmental Systems Research Institute (ESRI) 2018). As a mean to interpolate the data, isoscapes were created using ordinary kriging with a stable Semivariogram model optimization (Environmental Systems Research Institute (ESRI) 2018), which also provided the lowest Root Mean Square Error (RMSE).

IsoMAP precipitation model

The collected tap water $\delta^{18}O$ data was compared to a precipitation model, developed using IsoMAP (Bowen *et al.* 2019, Ammer 2019). The following model parametrizations were used: dependent variable- $\delta^{18}O$; independent variables- precipitation, elevation, latitude absolute value, longitude absolute value, latitude squared, longitude squared; latitude range- 9.4 to 36.4; longitude range- -123.9 to -77.2; number of stations 52; year range- 1960 to 2009; months range: 1 to 12. The precipitation model was defined by a R^2 value of 0.80 with a mean square error of 0.83 and an Akaike Information Criterion of 144.17. The cross validation yielded a mean absolute residual of 0.71 and a mean square residual of 1.03. The Moran's Index was -0.092 with a z-Score of -1.14 and p = 0.25. The results of the ANOVA test, the parameter values, QQ plot and residual plot can all be directly accessed through isomap.org (Ammer 2019; Bowen *et al.* 2019).

Comparison of tap water and ground water

The tap water isoscape from this study was further compared to the ground water isoscape previously published by Wassenaar *et al.* (2009). In order to do so, the developed isoscape (*e.g.* δ^{18}O tap water) as well as the sampling locations for the counterpart (consequently δ^{18}O ground water) were projected in ArcGIS (Environmental Systems Research Institute (ESRI) 2018). Using "Extract Values to Points" from the ArcGIS Spatial Analyst toolbox (ESRI 2018), δ^{18}O values were extracted to the ground water sampling locations. This procedure was repeated the other way around using the ground water isoscape to extract δ^{18}O values to tap water sampling locations, as well as for δ^{2}H. Following the extraction, the differences between the recorded and the extracted values were calculated.

Environmental Covariates

Six environmental covariates were explored: latitude, longitude, elevation, distance to water/ocean, precipitation, and temperature. These were chosen because they have traditionally shown to have an influence on isotopic values in water. Dansgaard (1964) previously showed that the δ^{2}H and δ^{18}O isotopic values of precipitation closely relate to mean annual temperature and mean (monthly) precipitation amounts recorded in the sampling location as well as to the distance to the source regions (here the oceans). These findings were supported by Rozanski, Araguás-Araguás and Gonfiantini (1993), who further presented the latitudinal and altitude effect on isotopic values.

Even though the information yielded by analyzing isotopic values in tap water is not expected to be as straightforward as in environmental water sources (*e.g.* ground water or precipitation), there significant information can be discovered in regard to the initial water source and the water transport. Specifically, it is anticipated that tap water reflects the mixed values of various water sources, such as wells, rivers, lakes and springs, integrating hydrological processes and human activities.

The correlations of these covariates with the isotopic values were explored using the entire dataset as well as split into two groups. The dataset was split into Atlantic and Pacific drainage basins to explore the potential of variation due to the geography of the country. Using "Extract Values to Points" from the ArcGIS Spatial Analyst toolbox (ESRI 2018), the elevation data for each sampling point was extracted. The elevation data used for this study was derived from the "North American Elevation 1- Kilometer Resolution" digital elevation model (DEM). GTOPO30's resolution is 30 arc seconds, approximately 1 kilometer (United States Department of the Interior- U.S. Geological Survey 2007).

The distance to the water was first determined using the sampling location points and the boundary polygon for Mexico. This version of analyses included the Gulf of California for the Pacific drainage basin. This means that the distance from sampling point located in, for example, Sonora, were measured to the Gulf of California. However, after determining these correlations, it was decided to also measure the distances to the Pacific Ocean, assuming that the Pacific Ocean (rather than the Gulf of Mexico) is the source region for the water (Dansgaard 1964). Here, the distances were measured from the sampling point across the Gulf of California and the Baja California peninsula to the Pacific Ocean. This adjustment significantly improved the results. Therefore, only the results of the distances to the ocean will be presented in this study.

The monthly precipitation analyses and visualizations used in this study were produced with the Giovanni online data system, developed and maintained by the NASA GES DISC. The precipitation dataset was extracted from the Tropical Rainfall Measuring Mission (TRMM) satellite product 3B43 version 7. The units of reporting are mm/month for the precipitation amounts, the temporal resolution is monthly, and the spatial resolution is 0.25 degrees (Acker and Leptoukh 2007). Mean annual averages were calculated using the Raster Calculator (Figure 5.2.2, (Environmental Systems Research Institute (ESRI), 2018- Spatial Analyst Toolbox). For this study, a one-year (July 2017 to June 2018) and a three-year (July 2015 to June 2018) mean annual averages were calculated and compared.

The mean temperatures used for this study were derived from the WorldClim- Global Climate Data Version 2 database (Fick and Hijmans 2017). WorldClim version 2 contains the monthly average temperature data from 1970 to 2000. The monthly data for Mexico was extracted from the global raster using the “Extract by Mask” tool (Environmental Systems Research Institute (ESRI), 2018- Spatial Analyst Toolbox). The mean annual temperature was calculated using the Raster Calculator, followed by the “Extract Values to Points” tool to determine the temperatures at the sampling points (Environmental Systems Research Institute (ESRI), 2018- Spatial Analyst Toolbox).

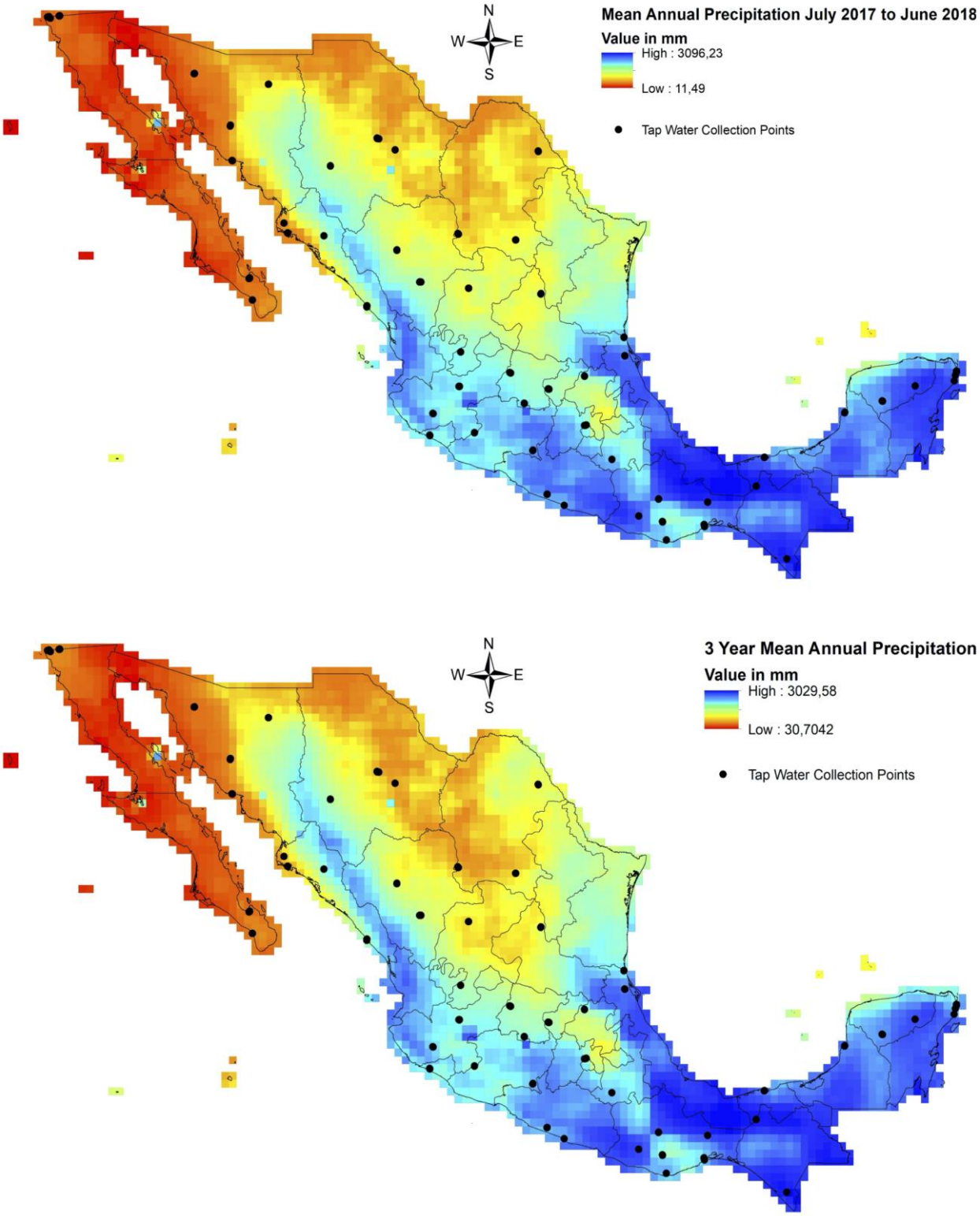

Figure 5.2.2. Tap water collection points sampled in 2018 depicted on visualizations of the mean annual precipitation from July 2017 to July 2018 and 3 year mean annual precipitation (Acker and Leptoukh 2007).

Socioeconomic covariates

Since accessibility to water, especially drinking water, is largely dependent on prosperity, it was decided that several socioeconomic variables should also be analyzed for correlation with the isotopic values measured in the tap water. The five following socioeconomic variables were explored:

The population sizes for each sampling location were recorded to examine if this covariate may have an influence on the variance observed in the data from one location. The numbers were retrieved from the Instituto Nacional de Estadística y Geografía (2010, 2015a). Again, since the access to water is largely dependent on socioeconomic status, two covariates directly representing the degree of poverty were explored in this study: Percent of population living in poverty per state (Consejo Nacional de Evaluación de la Política de Desarrollo Social 2018) and Human Development Index by state (HDI) (Smits and Permanyer 2019; Figure 5.2.3). The HDI is a more sophisticated approach to quantifying the degree of poverty as it takes into account the life expectancy, level of education, and standard of living.

Because 70% of Mexican citizens with indigenous ancestry live in poverty (Consejo Nacional de Evaluación de la Política de Desarrollo Social 2018) (and because, again, access to water is dependent on the degree of poverty), it was decided that two associated covariates would be explored: Percent Indigenous Speaking (of the total state population) (Instituto Nacional de Estadística y Geografía 2015a) and Percent Indigenous Ancestry (of the total state population) (Instituto Nacional de Estadística y Geografía 2015b).

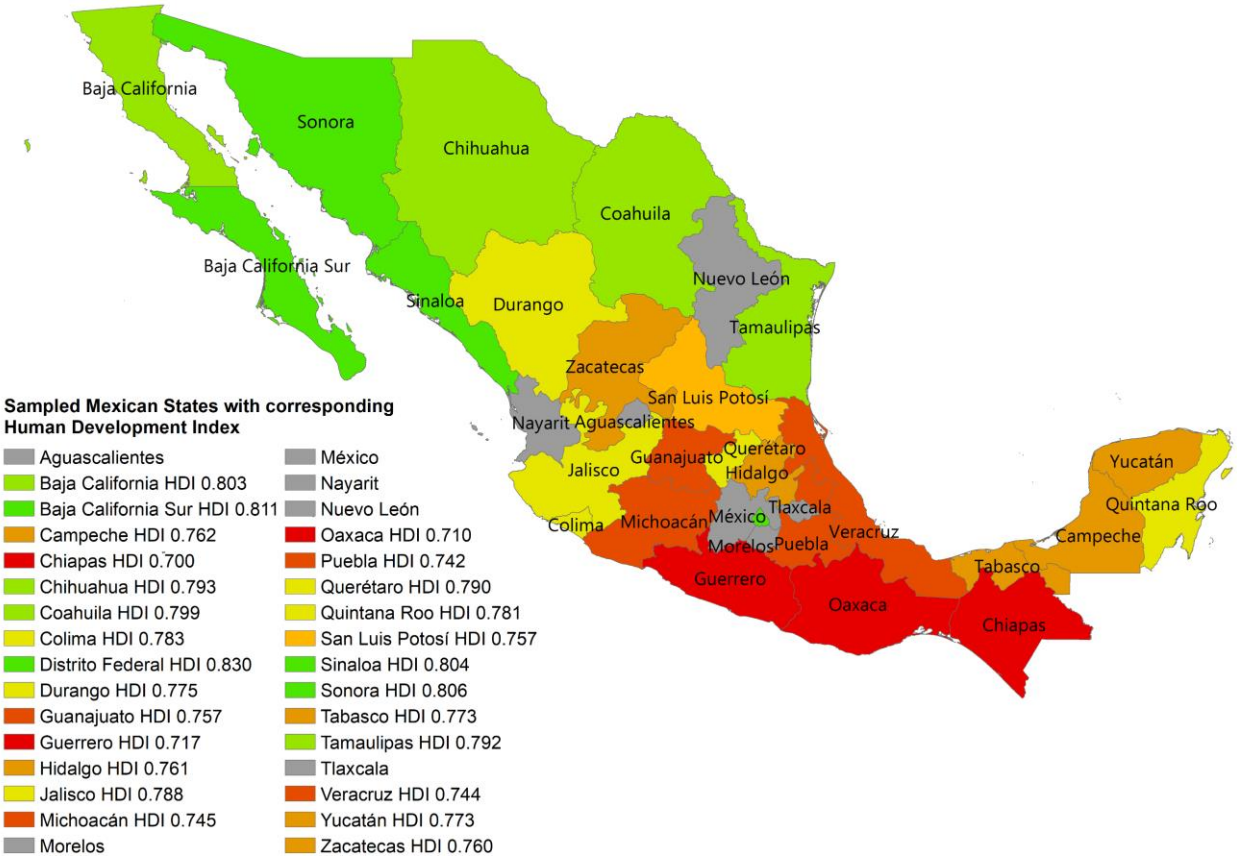

Figure 5.2.3. Human Development Indices for the Mexican states from which water samples were collected. The color indicates the strength of the index (green- high HDI, red- low HDI). States in grey were not sampled for this study. A higher HDI reflects higher socioeconomic development.

5.2.3. Results

Tap Water Results

All tap water δ^2H and $\delta^{18}O$ values are presented in Table 5.2.1. The data are also accessible at waterisotopes.org (Project ID 198- MEX Water). The $\delta^{18}O$ isotopic values ranged from -12.1‰ to -0.2‰, while the δ^2H ranged from -91.3‰ to -8.9‰ and deuterium excess ranged from -14.9‰ to 15.6‰ (Table 5.2.2). The values of deuterium excess (d-excess) were determined through the following calculation: d-excess = δ^2H - 8.0 x $\delta^{18}O$ (Craig 1961). The regression function for the Mexican tap water is defined as $\delta^2H = 7.5\ \delta^{18}O + 2.3$ ($r^2 = 0.93$) (red line in Figure 5.2.10).

When splitting the data into an Atlantic and a Pacific drainage basin, the $\delta^{18}O$ values in the Atlantic drainage basin can be found on a slightly smaller scale than the $\delta^{18}O$ values in the Pacific drainage basin. The δ^2H values appear to be elevated in the Atlantic dataset when compared with the Pacific dataset. The d-excess values in the Pacific dataset show the entirety of the value range while the Atlantic dataset is only represented by positive (>0) values.

Table 5.2.2. Basic descriptive statistics for the $\delta^{18}O$, $\delta^{2}H$ and d-excess results in Mexican tap water. Standard Deviations in the $\delta^{18}O$, $\delta^{2}H$, and d-excess columns represent the standard deviations for all data combined. Standard deviations in the SD columns represent values recorded for multiple samples in one location.

		$\delta^{18}O$	SD	**$\delta^{2}H$**	SD	**d-excess**	SD
All data	**Minimum**	-12.1 ‰	0.0‰	-91.3‰	0.0‰	-14.9‰	0.0‰
	Maximum	-0.2‰	1.7‰	-8.9‰	20.0	15.6‰	9.5
	Average	-7.1‰	0.3‰	-50.7‰	2.4‰	5.9‰	1.0‰
	Range	11.9‰		82.4‰		30.5‰	
	SD	2.5‰		19.6‰		5.4‰	
Atlantic	**Minimum**	-10.4‰	0.0‰	-72.7‰	0.0‰	2.4‰	0.1‰
	Maximum	-1.4‰	0.4‰	-8.9‰	2.1‰	15.6‰	2.7‰
	Average	-5.9‰	0.1‰	-38.1‰	0.8‰	8.9‰	0.5‰
	Range	9.0‰		63.8‰		13.2‰	
	SD	2.6‰		21.3‰		3.0‰	
Pacific	**Minimum**	-12.1‰	0.0‰	-91.3‰	0.1‰	-14.9‰	0.0‰
	Maximum	-0.2‰	1.7‰	-16.0‰	20.0‰	15.3‰	9.5‰
	Average	-7.5‰	0.4‰	-55.6‰	3.1‰	4.7‰	1.2‰
	Range	11.9‰		75.3‰		30.2	
	SD	2.3‰		16.6‰		5.7‰	

Inter-Element Correlation

The Pearson's correlation analysis between oxygen and hydrogen yielded a very strong relationship between the two elements ($r = 0.96$, $p < 0.0001$, $n = 158$). However, the relationships between oxygen and hydrogen versus deuterium excess were weak ($r = -0.24$, $p < 0.003$, $n = 158$) and non-existent, respectively. Furthermore, the correlation between the measured $\delta^{18}O$ values and the predicted $\delta^{18}O$ from IsoMAP was explored (Bowen *et al.* 2019; Ammer 2019). It yielded a weak negative correlation ($r = -0.10$, $p < 0.2$).

Inter-City Variance

The Kruskal-Wallis test was employed to explore whether the isotope ratios of $\delta^{18}O$, $\delta^{2}H$, and d-excess differed significantly between the sampling locations (significance set at $\alpha = 0.05$). The test yielded p-values less than the significance level 0.05 and it can be concluded that there are significant differences between the locations.

Standard Deviation Correlations

Table 5.2.2 shows the stable isotope variability for the sampled locations. Notably, the average and maximum standard deviations (SD) for the $\delta^{18}O$ and $\delta^{2}H$ values are significantly larger than the long-time analytical precision ($1\sigma = 0.06$ and 0.22‰). The average standard deviations by location are significantly higher in the Pacific basin than in the Atlantic basin. The

standard deviations correlated moderately with longitude, latitude, and only minimally with elevation (Figure 5.2.4). Two locations in Baja California are responsible for the highest intra-location standard deviations: Tecate for δ^2H and d-excess, and Tijuana for δ^{18}O. Population size did not show a relationship between the SDs of δ^{18}O, δ^2H and d-excess.

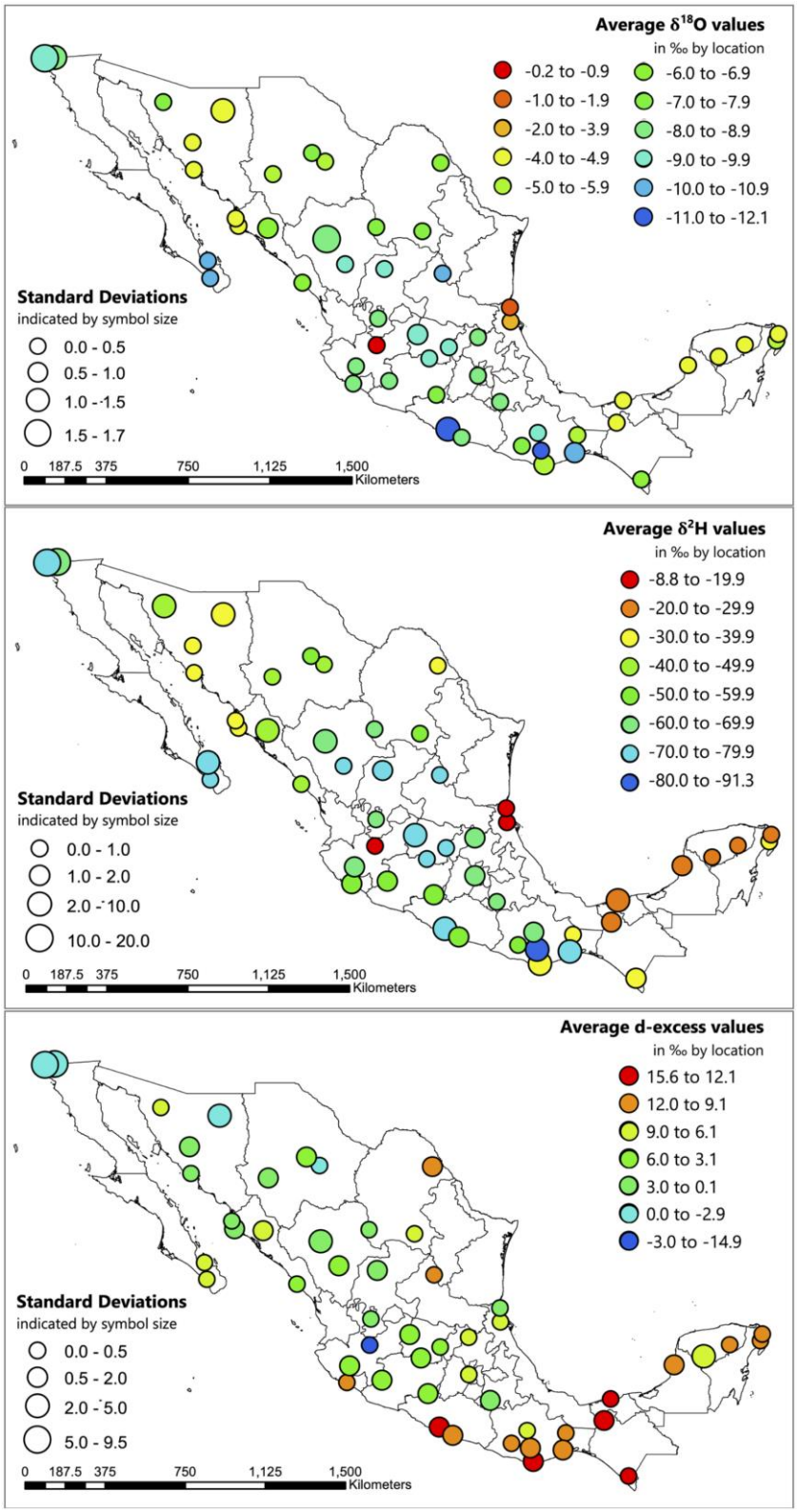

Figure 5.2.4. Map of Mexico showing the average δ^{18}O, δ^2H, and d-excess isotope ratios as well as standard deviations (indicated by the size of the colored point) for the sampling locations.

Environmental Covariates

All environmental covariates were analyzed as a whole dataset, and later split into an Atlantic and a Pacific drainage basin dataset. The Pearson's correlation coefficients clearly show that the assignment of a drainage basin has a significant influence on the relationship between the isotopic values and the environmental covariates (Table 5.2.3).

Table 5.2.3. Correlation coefficients with p-values for environmental covariates (all data, Atlantic basin, Pacific basin).

		$\delta^{18}O$		$\delta^{2}H$		d-excess	
		r	**p**	**r**	**p**	**r**	**p**
Longitude	All	0.18	0.02	0.34	< 0.001	0.55	< 0.001
	Atlantic	0.55	< 0.001	0.60	< 0.001	0.44	0.003
	Pacific	-0.19	0.04	-0.06	0.55	0.47	< 0.001
Latitude	All	0.13	0.10	-0.004	0.96	-0.51	< 0.001
	Atlantic	-0.18	0.25	-0.20	0.19	-0.20	0.19
	Pacific	0.27	0.003	0.13	0.18	-0.53	< 0.001
Elevation	All	-0.36	< 0.001	-0.46	< 0.001	-0.33	< 0.001
	Atlantic	-0.90	< 0.001	-0.93	< 0.001	-0.41	0.005
	Pacific	-0.11	0.23	-0.24	0.01	-0.33	< 0.001
Distance to Ocean	All	0.01	0.86	-0.10	0.21	-0.42	< 0.001
	Atlantic	-0.76	< 0.001	-0.78	< 0.001	-0.22	0.15
	Pacific	0.31	< 0.001	0.19	0.04	-0.45	< 0.001
Precipitation 2017-2018	All	0.18	0.02	0.33	< 0.001	0.51	< 0.001
	Atlantic	0.55	< 0.001	0.61	< 0.001	0.49	< 0.001
	Pacific	-0.09	0.35	0.06	0.53	0.46	< 0.001
Precipitation 2015-2018	All	0.19	0.017	0.34	1.8^{-5}	0.52	< 0.001
	Atlantic	0.55	< 0.001	0.60	< 0.001	0.49	< 0.001
	Pacific	-0.05	0.63	0.12	0.23	0.49	< 0.001
Mean Annual Temperature	All	0.27	< 0.001	0.39	< 0.001	0.40	< 0.001
	Atlantic	0.83	< 0.001	0.88	< 0.001	0.46	0.002
	Pacific	0.07	0.49	0.22	0.02	0.42	< 0.001

When using the dataset in its entirety, the relationships between oxygen and environmental covariates are consistently weak and not useful for predictive analyses. Hydrogen performs somewhat better and shows moderate correlations to longitude, elevation, and both precipitation covariates. Deuterium excess correlates strongest to environmental covariates. All shows moderate to strong relationships except for mean annual temperature. The strength of the correlations between environmental and isotope values vastly shifted when the dataset was split into an Atlantic and a Pacific drainage basin.

Various variables show opposing correlations (*e.g.*, latitude and longitude), a phenomenon that will be discussed later. For oxygen and hydrogen, isotopic values are more strongly correlated with the environmental variables in the Atlantic basin compared to the Pacific basin (Figure 5.2.5).

The most striking difference can be seen in the elevation and distance to the ocean correlation for oxygen and hydrogen. While the precipitation data mostly failed as a determining factor in the Pacific, the correlations with the isotopic values of oxygen and hydrogen in the Atlantic were strong. While the Pacific dataset weakly correlated to mean annual temperature, the Atlantic dataset showed strong correlations.

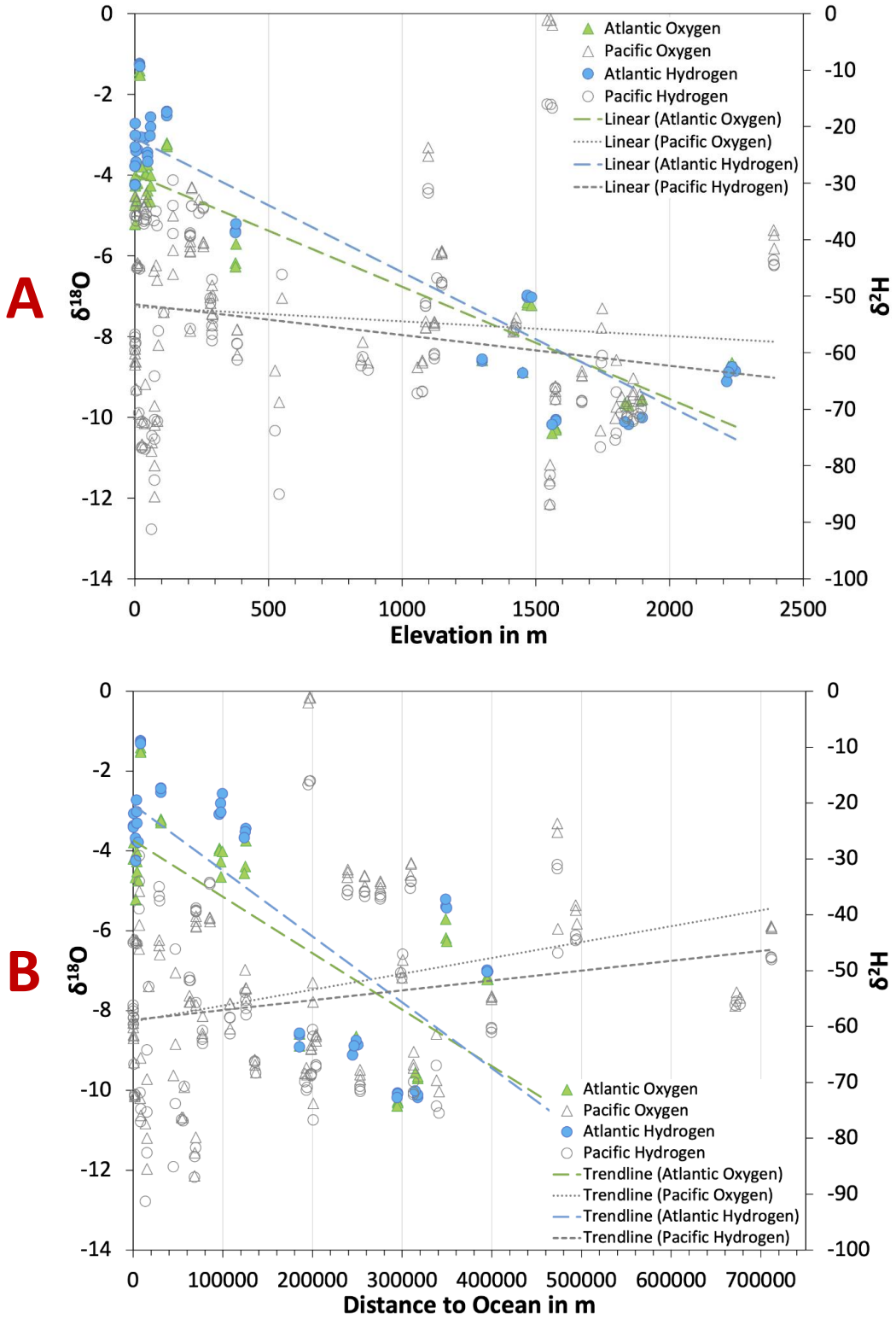

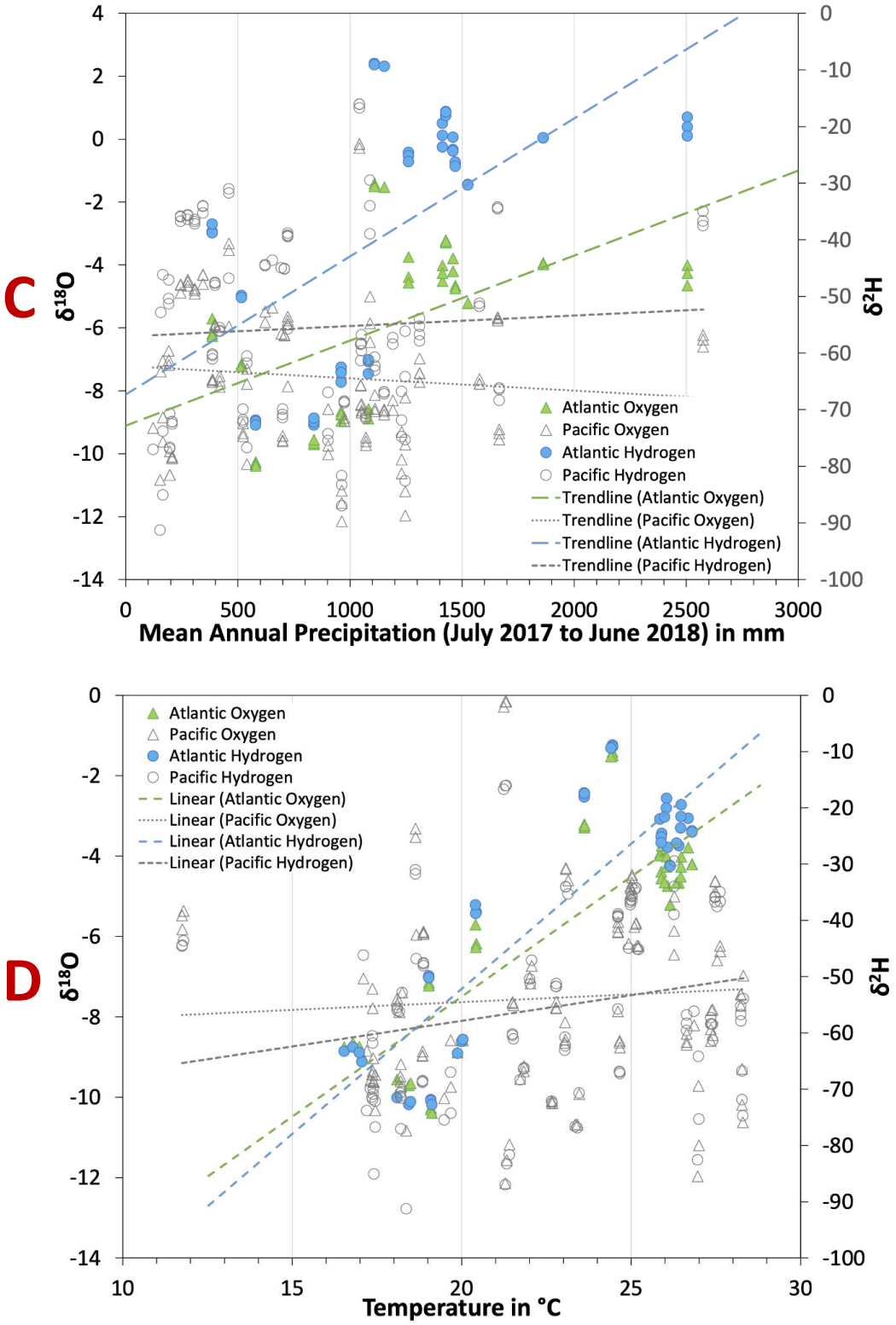

Figure 5.2.5. The relationship of $\delta^{18}O$ (primary y-axis) and $\delta^{2}H$ (secondary y-axis) with A) Elevation (in m) B) Distance to Ocean (in m) C) Mean Annual Precipitation (in mm) and D) Temperature (in °C) classified by the Atlantic (east) and Pacific (west) drainage basin divides.

Socioeconomic Covariates

Since the access to clean tap water and running water, in general, is largely dependent on the prosperity of the household, various socioeconomic covariates were analyzed. The results of the Pearson's correlation analyses can be found in Table 5.2.4. The overall strongest correlation was found between HDI and $\delta^{18}O$; it was, however, weak. All other correlations between social covariates and $\delta^{18}O$ and $\delta^{2}H$ were also weak or non-existent. The correlations for deuterium excess, however, were observed to be rather strong (except for population size). While HDI was negatively correlated, the percentages of the population living in poverty by states, speaking an indigenous language, and being of indigenous ancestry were positively correlated to d-excess.

Table 5.2.4. Correlation coefficients with p-values for socioeconomic covariates.

	Population Size		**HDI**		**% Poverty**		**% Indigenous Speaking**		**% Indigenous Ancestry**	
	r	**p**	**r**	**p**	**r**	**p**	**r**	**p**	**r**	**p**
$\delta^{18}O$	-0.10	0.21	0.19	0.02	-0.15	0.06	-0.03	0.73	0.004	0.96
$\delta^{18}O$ Atlantic	-0.37	0.01	-0.30	0.05	0.34	0.02	0.28	0.07	0.27	0.08
$\delta^{18}O$ Pacific	0.10	0.29	0.33	< 0.001	-0.33	< 0.001	-0.16	0.08	-0.18	0.06
$\delta^{2}H$	-0.13	0.12	0.06	0.44	-0.01	0.88	0.14	0.07	0.12	0.15
$\delta^{2}H$ Atlantic	-0.40	0.007	-0.37	0.01	0.40	0.007	0.32	0.03	0.33	0.03
$\delta^{2}H$ Pacific	-0.02	0.84	0.18	0.05	-0.17	0.08	-0.01	0.88	-0.00	0.97
d-excess	-0.09	0.24	-0.47	< 0.001	0.52	< 0.001	0.51	< 0.001	0.53	< 0.001
d-excess Atlantic	-0.27	0.08	-0.56	< 0.001	0.47	0.001	0.37	0.01	0.46	0.002
d-excess Pacific	-0.39	< 0.001	-0.54	< 0.001	0.60	< 0.001	0.53	< 0.001	0.55	< 0.001

Large-scale spatial patterns

For $\delta^{2}H$, $\delta^{18}O$, and d-excess, statistical analysis showed that the data distribution was non-random, and that spatial structure is present. Moran's I was used to quantify spatial autocorrelation (Spatial Statistics Toolbox, ArcGIS 10.6). The tap water ratio data are defined by Moran's Indices of 0.843, 0.856, and 0.689; z-scores of 7.5, 7.6, and 6.2; and $p < 0.000001$ for $\delta^{18}O$, $\delta^{2}H$, and d-excess, respectively. Furthermore, the outcome of the cross validation using ordinary kriging with a standard semivariogram shows strong relationships for $\delta^{2}H$, $\delta^{18}O$ and d-excess (Figure 5.2.6). The Root Mean Square Error, determining the prediction accuracy, for $\delta^{2}H$, $\delta^{18}O$, and d-excess were 5.9768, 0.6738, and 2.2709, respectively.

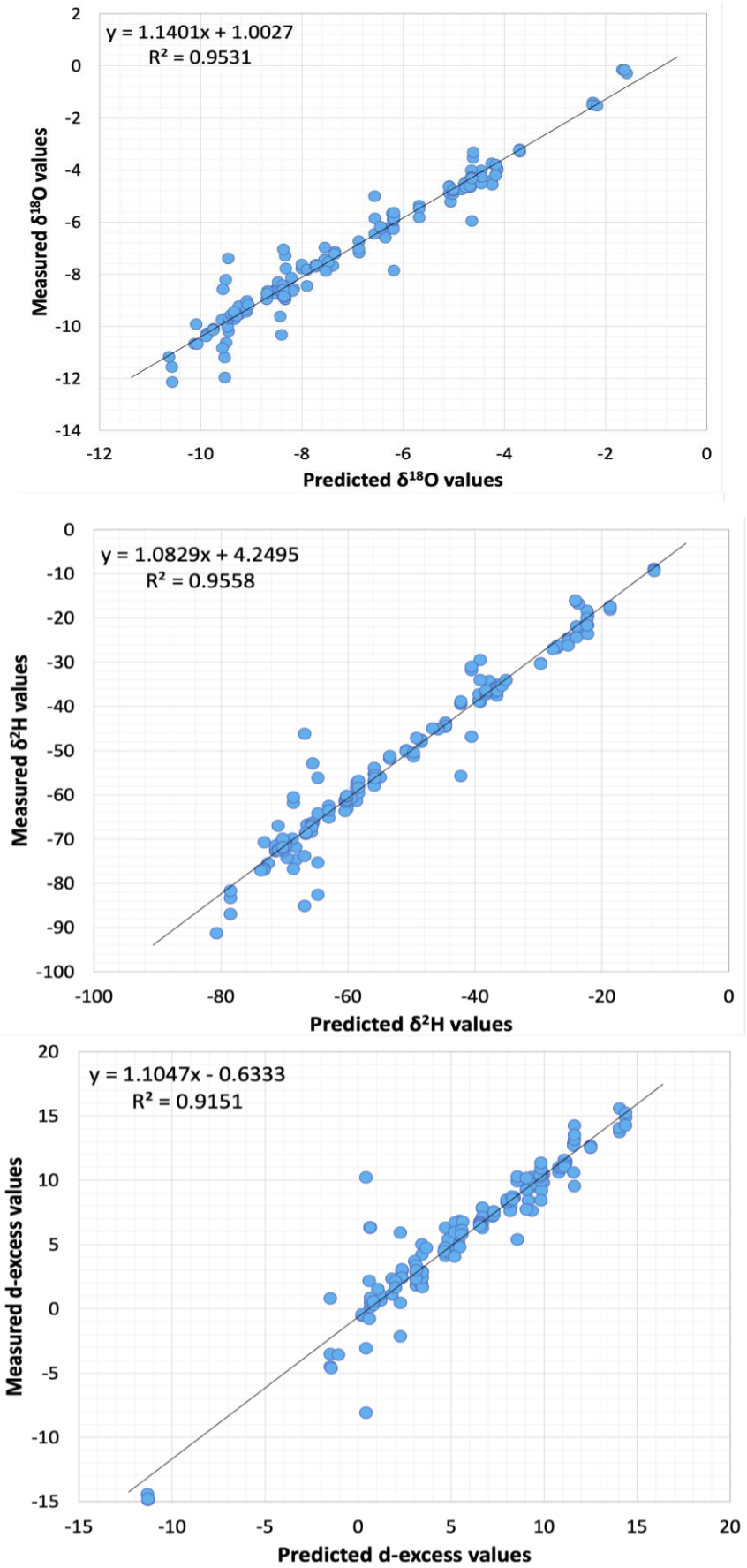

Figure 5.2.6. Relationship between predicted and measured isotopic values (δ^2H, δ^{18}O and d-excess) for Mexico.

The large-scale spatial distribution and patterns of δ^2H, δ^{18}O, and d-excess in Mexican tap water are depicted in Figure 5.2.7. The close relationship of the δ^2H and δ^{18}O values is visualized by nearly identical looking isoscapes (Figure 5.2.7). Generally, the highest isotopic values for both elements were found in the regions of lowest elevation, primarily the Yucatan peninsula and stretching north along the Caribbean and the coast of the Gulf of Mexico (Figure 5.2.7 red to yellow points and areas of interpolation). The lowest values are primarily found in areas defined by higher elevations and generally more inland. Geographically, these areas are dominated by the southern part of the Central Mexican Plateau (also known as the Mexican Altiplano-Mesa Central) and the Sierra Madre del Sur range, reaching towards the southwest of the country. The intermediate values are predominantly found in arid to semiarid areas in the northern parts of the country and Mexican Plateau as well as the Baja peninsula. Overall, only one location falls far outside of the normal regional ranges: Guadalajara, Jalisco. This deviation from the surrounding values can clearly be seen in Figures 4 and 7, the implications are discussed below.

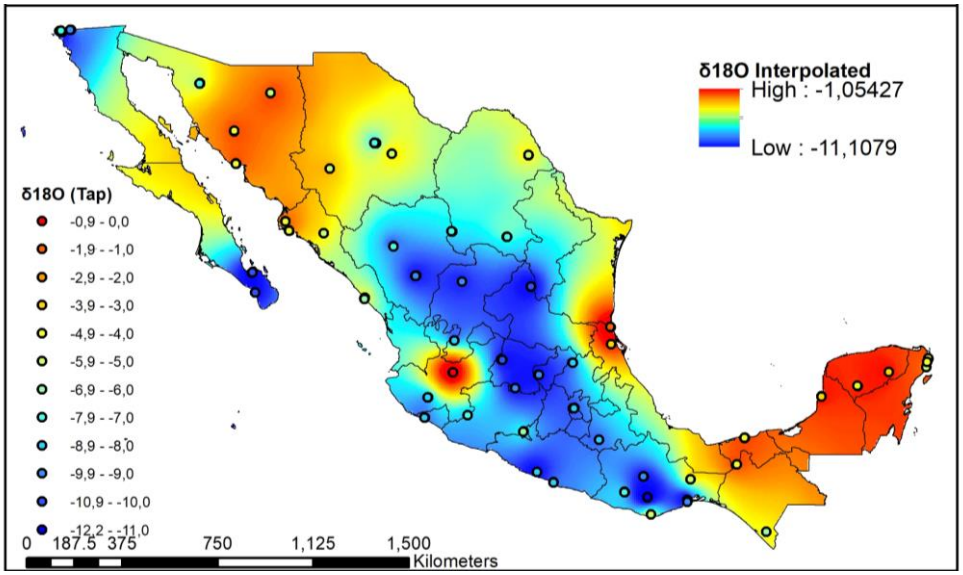

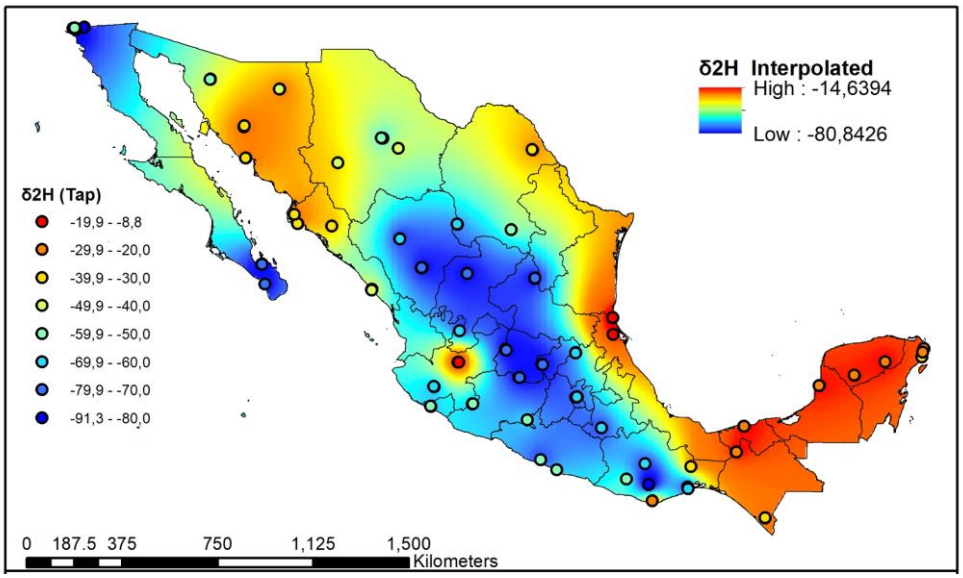

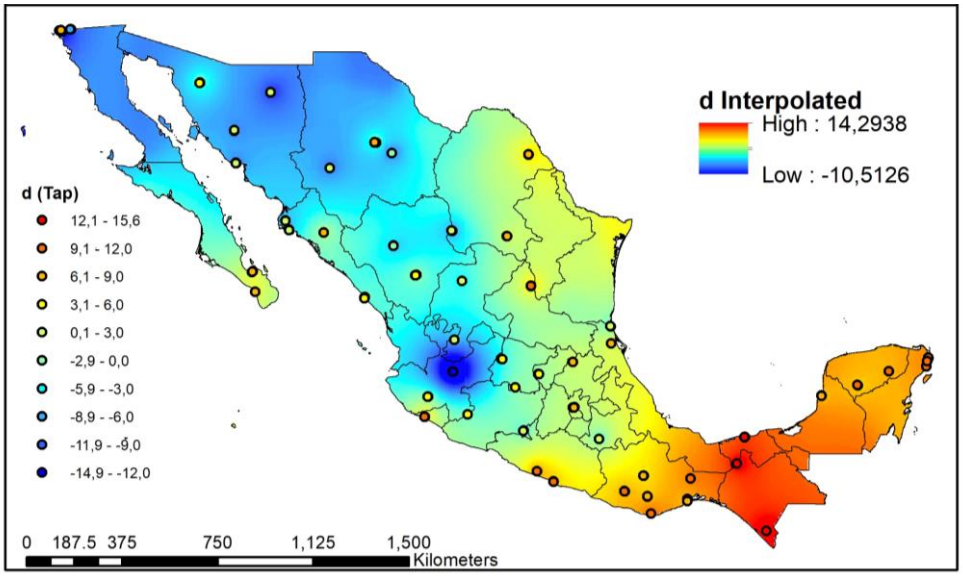

Figure 5.2.7. Prediction maps showing estimated isotope ratios for δ^2H, δ^{18}O, and deuterium excess for tap water in Mexico. The values are reported in ‰ and relative to the VSMOW standard.

5.2.4. Discussion

As can be seen from the results, the Mexican tap water isotopic values show spatially coherent variability. Cross validation of the measured values for δ^2H, δ^{18}O, and deuterium excess generated by ordinary kriging of the raw isotope data yields substantive results. Nonetheless, the prediction standard error output (Figure 5.2.8) shows that there are still certain areas of the country that need further sampling in order to obtain an improved isoscape. The highest values for both, δ^{18}O and δ^2H are observed in the data from Guadalajara, Jalisco. As shown in Figures 4 and 7, the isotope values fall entirely out of the typical regional range. This is mainly due to the fact that Guadalajara's main water source is Lake Chapala, Mexico's largest freshwater lake (von Bertrab 2003). Lakes are very sensitive to precipitation and prone to the associated evaporation, explaining the deviation from the values surrounding the area. Nonetheless, it is rather remarkable that not more local-scale variability is found among the samples. One could expect to see more variability in the tap water isotopic values due to the fact that the water supply and storage within a town or city can be highly variable and can also differ from household to household.

From the results, it was apparent that there are significant differences between the isotopic values obtained from the Atlantic versus the Pacific side of the country (Table 5.2.2, Figure 5.2.9). Both, the oxygen and hydrogen isotopic values are found to be enriched in the Atlantic dataset when compared to the Pacific dataset (Table 5.2.5). Nonetheless, the δ^{18}O values in the Pacific represent the highest as well as the lowest values in the entire dataset.

Table 5.2.5. Minimum, maximum and average values for the Atlantic and the Pacific data.

	Atlantic		Pacific	
	$\delta^{18}O$	$\delta^{2}H$	$\delta^{18}O$	$\delta^{2}H$
Minimum	-10.4	-72.2	-12.1	-91.3
Maximum	-1.4	-8.9	-0.2	-16.0
Average	-5.9	-38.1	-7.5	-55.6

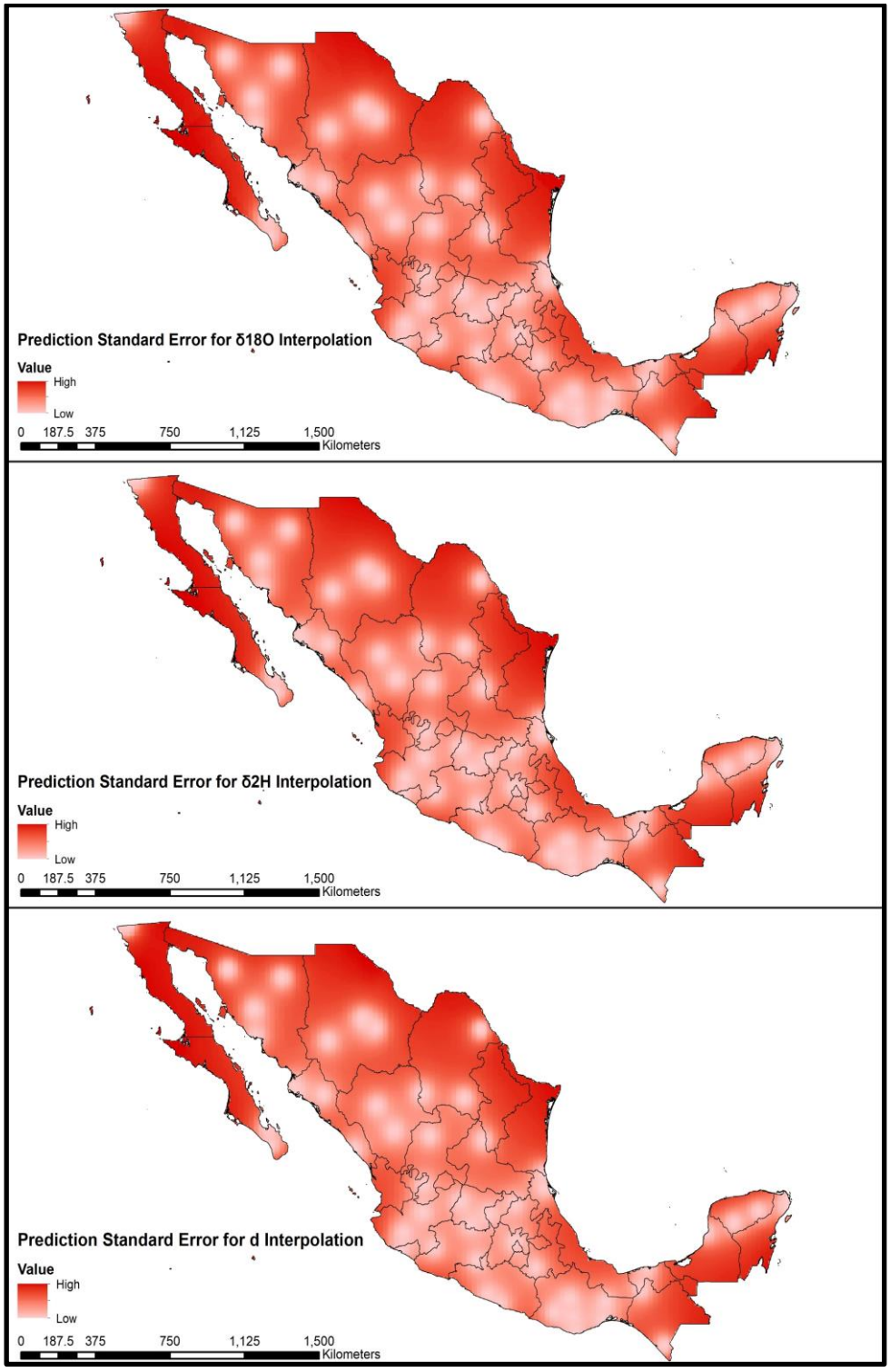

Figure 5.2.8. Prediction standard error outputs for the δ^2H, δ^{18}O, and deuterium excess isoscapes for tap water in Mexico (Figure 5.2.7).

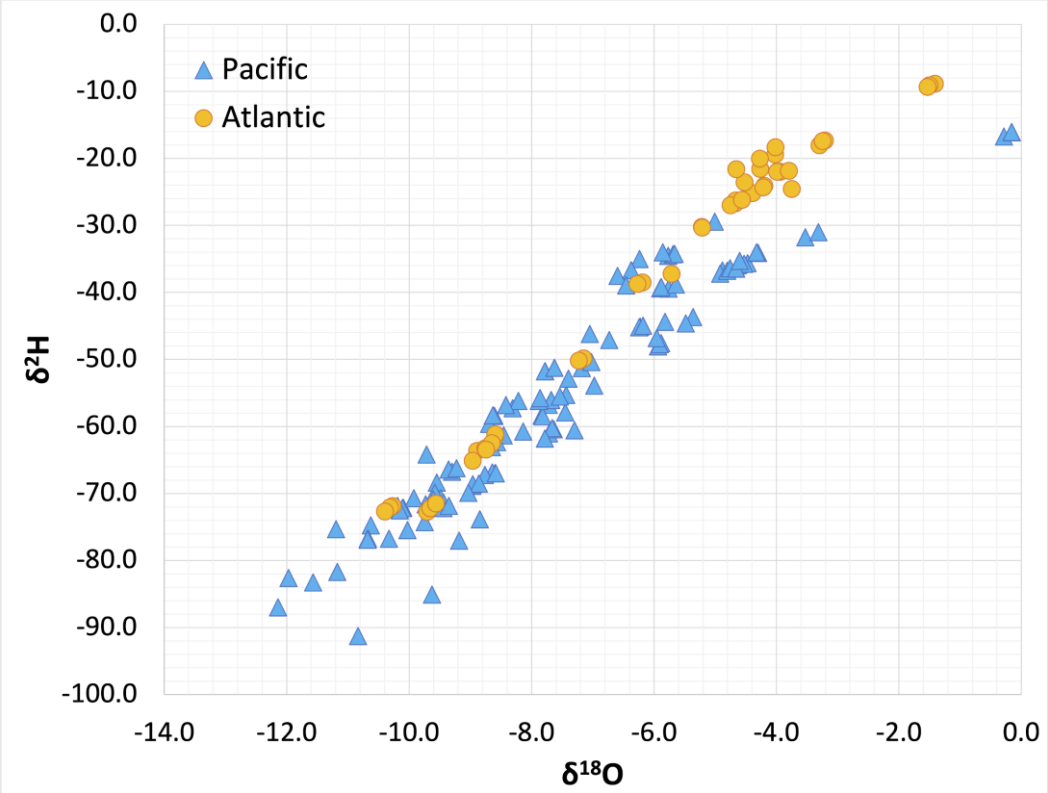

Figure 5.2.9. Oxygen versus hydrogen isotopic values found in the Atlantic and Pacific datasets.

Environmental Covariates

Furthermore, differences in the relationship between isotopic values and various covariates are apparent. While the Atlantic side shows strong correlations for all environmental covariates explored in this study, the Pacific only shows weak correlations. This is also observed in the standard deviations for the locations. The standard deviations are much larger in the Pacific than they are in the Atlantic. This difference needs to be further explored, but one factor could be the mountainous ranges of the Central Mexican Plateau (also known as the Mexican Altiplano-Mesa Central) and the Sierra Madre del Sur range dividing the country into two main drainage basins.

Through this divide, Mexico shows mainly two different climate and moisture sources. In the northwest of the country, the moisture is sourced primarily from the Gulf of California and the subtropical Pacific during the monsoon season. Across the rest of the country, the circulation comes mainly from the east/northeast towards the west/southwest, thus transporting the moisture off the Atlantic. The Atlantic is therefore on the windward side of the rainout gradient while the Pacific side is in the rain shadow. This phenomenon is therefore expected to provide a strong and systematic gradient in the isotopic values on the Atlantic side, and less of a systematic gradient on the Pacific side. These higher elevation areas practically divide Mexico into an eastern and a western side. Rozanski, Araguás-Araguás and Gonfiantini (1993) had shown that isotopic values

mimic the topography of the sampled continent and that mountainous chains manifest more negative $\delta^{18}O$ isotopic values. The isotope data collected throughout Mexico show a similar effect of the abovementioned mountainous ranges on the isotopic values. Similarly to the phenomenon Wassenaar *et al.* (2009) observed in Mexican ground water and what has been observed in Panama and Costa Rica (Lachniet *et al.* 2007; Lachniet and Patterson 2002), the Atlantic side showed a strong correlation with elevation while the Pacific side lacked such correlation. Most likely, the large gradient in amount of precipitation from north to south (Figure 5.2.2) complicates the elevation correlation on the Pacific side. This also explains the opposing correlations found for latitude and longitude in the Atlantic versus Pacific dataset.

It would be beneficial to create a model that includes not only the classic longitude/latitude variables into its prediction but also the other covariates explored here, and potentially divides the country into an eastern and a western side when predicting isotopic values. In this study, the dataset was divided into an Atlantic and a Pacific dataset based on the shortest distance to the respective ocean. While the mountainous ranges of Mexico are close to dividing the country along its mean longitudinal gradient, the assignment presented here does not reflect the true geology of Mexico. In the future, raster maps showing the exact Atlantic and Pacific drainage basins could be used to improve the divide of the data into the two regions and develop a model that automatically takes into account these various geographic and environmental covariates.

Socioeconomic variables

To evaluate whether the correlations found between isotopic values and socioeconomic covariates are merely a function of autocorrelation between socioeconomic and geographic/environmental variables, Pearson's correlations were performed among the socioeconomic variables as well as the socioeconomic variables and the geographic/environmental ones. As can be seen in Table 5.2.6, the correlations among the socioeconomic covariates were all strong (except for Population Size). These correlations were expected because the covariates (except for Population Size) are known to be intertwined (*e.g.* the indigenous population makes for a large percentage of the poor population) (Freire *et al.* 2015). Nonetheless, it was important to explore various socioeconomic covariates because each one takes into account a different socioeconomic angle as well as well the fact that the covariates have not been explored as factors related to isotopic values.

Furthermore, the socioeconomic variables correlate to varying degrees with geographic and environmental variables. Longitude, latitude, and the two precipitation factors showed the strongest correlations. The results are skewed because all socioeconomic variables, expect for

Population Size, are measured on a statewide level. Furthermore, some states are, due to their location and geography, more heavily sampled as other, which in turn influence the correlations in a more significant manner.

Table 5.2.6. Pearson's Correlations among socioeconomic covariates and correlations between socioeconomic and geographic covariates.

	% of pop. living in poverty		% of state pop. w/ indigenous ancestry		% of state pop. speaking ind. language		Population Size		HDI	
	r	p	r	p	r	p	r	p	r	p
% of pop. living in poverty			0.68	< 0.001	0.74	< 0.001	-0.18	= 0.03	-0.93	< 0.001
% of state pop. w/ indigenous ancestry	0.68	< 0.001			0.95	< 0.001	-0.14	= 0.08	-0.70	< 0.001
% of state pop. speaking ind. language	0.74	< 0.001	0.95	< 0.001			-0.15	= 0.06	-0.77	< 0.001
Population Size	-0.18	= 0.03	-0.14	= 0.08	-0.15	= 0.06			0.31	< 0.001
HDI	-0.93	< 0.001	-0.70	< 0.001	-0.77	< 0.001	0.31	< 0.001		
Longitude	0.54	< 0.001	0.68	< 0.001	0.65	< 0.001	0.00	= 0.98	-0.58	< 0.001
Latitude	-0.77	< 0.001	-0.66	< 0.001	-0.63	< 0.001	-0.04	= 0.62	0.76	< 0.001
Elevation	-0.13	= 0.27	-0.26	= 0.001	-0.18	= 0.02	0.34	< 0.001	0.07	= 0.40
Temperature	0.43	< 0.001	0.48	< 0.001	0.38	< 0.001	-0.29	< 0.001	-0.38	< 0.001
Distance to ocean	-0.30	< 0.001	-0.37	< 0.001	-0.30	< 0.001	0.18	= 0.03	0.20	= 0.01
Distance to ocean w/o gulf	-0.43	< 0.001	-0.43	< 0.001	-0.37	< 0.001	0.09	= 0.27	0.37	< 0.001
Three-year precipitation	0.74	< 0.001	0.61	< 0.001	0.67	< 0.001	-0.06	= 0.49	-0.72	< 0.001
One-year precipitation	0.73	< 0.001	0.63	< 0.001	0.66	< 0.001	-0.04	= 0.60	-0.73	< 0.001

Population size did not correlate with the standard deviations suggesting that the tap water does not show greater variation in larger populations compared to smaller ones. This is very useful for future studies as it was suspected that larger cities could introduce a higher error to the predictions. Indigenous language correlates slightly better to deuterium excess than the percentage of the population being of indigenous ancestry. The correlations with deuterium are particularly interesting. Deuterium excess appears to increase with higher rates of poverty and the percentage of people being of indigenous ancestry or speaking an indigenous language. Due to the fact that a higher HDI indicates higher wealth, the correlation is inverse. A potential reason for this observation is that high evaporation may occur where poorer people live as well as and how poorer people live. Generally speaking, higher evaporation is expected in more arid areas and poorer individuals often live in more arid and marginal regions. This could lead to a climatic effect and the correlations of poverty indicators to deuterium excess. However, this observation could also result from a social effect, for instance because poorer individuals have less access to ground water and therefore make use of the available surface water.

Comparison to Groundwater and IAEA GNIP Station data

The results were plotted on a $\delta^{18}O$ versus $\delta^{2}H$ diagram (Figure 5.2.10), which also compares the values to the data collected by IAEA/WMO (2018) GNIP Stations in Veracruz and Chihuahua as well as Groundwater data collected by Wassenaar *et al.* (2009). The ground and tap water data were used without removing any outliers.

Wassenaar *et al.* 2009 defined the Mexican Meteoric Water Line by combining the two IAEA GNIP Stations in Veracruz and Chihuahua (IAEA/WMO 2018) with a site near Mexico City (Cortés *et al.* 1997). These geographically very limited values resulted in a regression line of $\delta^{2}H = 7.5\ \delta^{18}O + 6.1‰$ ($r^2 = 0.96$) (Figure 5.2.10 blue line). The tap water data falls close to the Mexican Meteoric Water Line, which suggests that little evaporation occurs in the drinking water sources. If evaporation would have a significant effect, it would result in significant isotopic excursions to the right of the meteoric water line as well as shallower slopes. This is rather remarkable since the samples were collected during the summer (high evaporation and high precipitation). Nonetheless, several tap water sampling sites fall below the ground water array. For $\delta^{18}O$, the range of values found in the ground water samples is significantly smaller than in the tap water (GW: min.: -10.8‰, max.: -2.3‰ vs. TW: min.: -12.1‰, max.: -0.2‰) while maintaining the same averages (GW and TW: -7.1‰). The same observation was made for the $\delta^{2}H$ values (GW: min.: -77.5‰, max.: -13.0‰, avg.: -49.4‰ vs. TW: min.: -91.3‰, max.: -8.9‰, avg.: -50.7‰). While the values of $\delta^{18}O$ and $\delta^{2}H$ are overall similar, the deuterium excess values show some greater differences. While the Mexican ground water only showed a minimum value of -4.8‰, the tap water was significantly lower at -14.9‰. The maximum values, however, are higher for the ground water than they are for the tap water (GW: 37.1‰ and TW: -15.6‰). The average d-excess value of ground water was slightly higher than for the tap water (GW: 7.3‰ and TW: 5.9‰). Overall, the values are consistent with another but sugggest that some locations are using more evaporated surface water. Overall, the spatial distribution of the tap water ratios is similar to the stable isotope ratios in groundwater reported by Wassenaar and colleagues (2009).

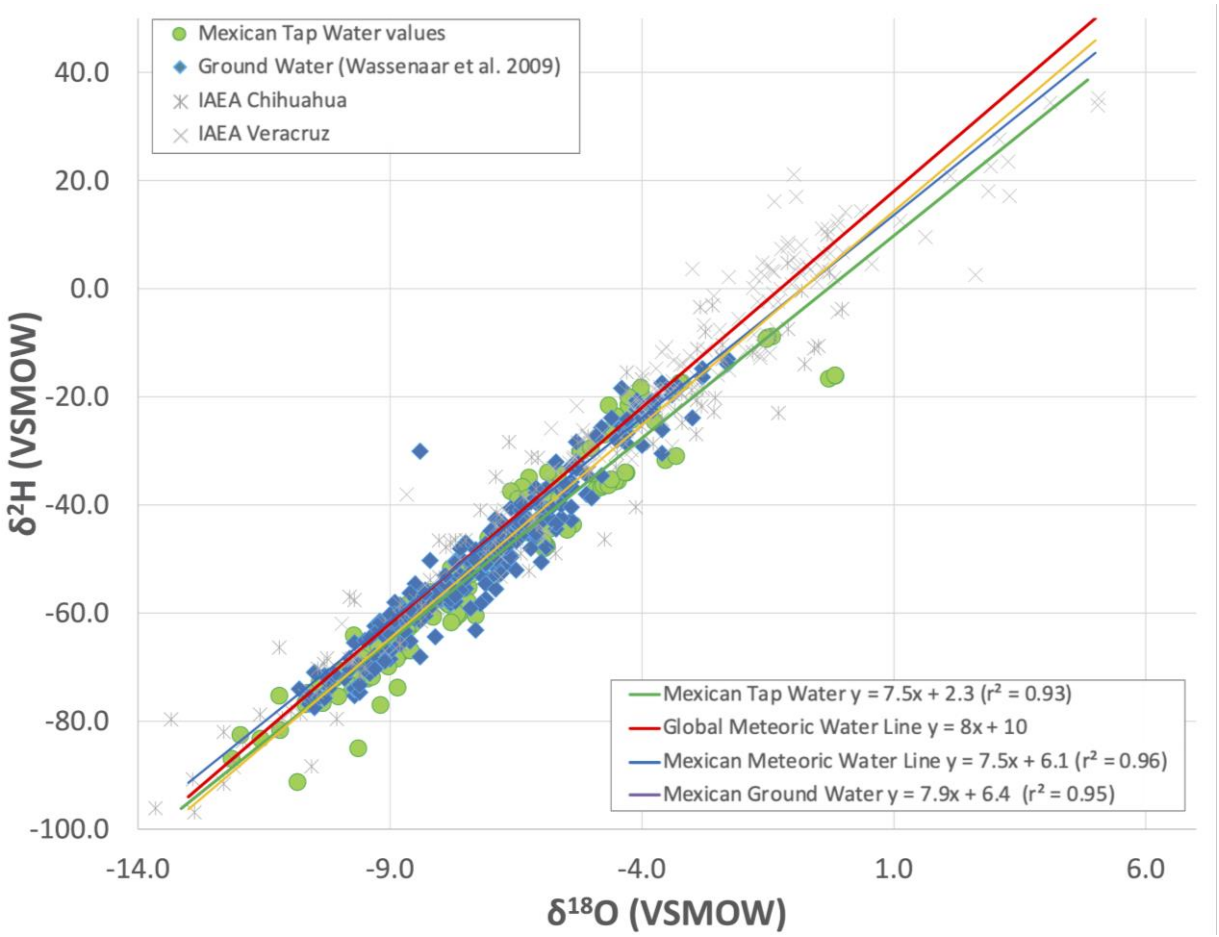

Figure 5.2.10. $\delta^{18}O$ versus $\delta^{2}H$ in Mexican tap water, groundwater and IAEA GNIP stations.

As outlined in the methods section, the tap water and ground water values/isoscapes were compared by extracting isotope values from the isoscapes to the sampling locations of the other water system. The recorded differences were, on average and in the statistical ranges, smaller when using the tap water isoscapes to extract values to ground water sampling locations. It was apparent that the average differences were very similar for all comparisons (Table 5.2.7, Figure 5.2.11). However, the ranges of differences were significantly smaller when using the tap water isoscape to extract values to ground water sampling locations (Table 5.2.7). The most significant differences in measured versus predicted/extracted values were found in areas that were somewhat under sampled, such as Tamaulipas and the Baja peninsula (Figure 5.2.12).

The $\delta^{18}O$ Tap Water isoscape (Figure 5.2.12 B) produced a smaller error range than the Ground Water isoscape (Figure 5.2.12 A) when comparing the interpolated values to the measured values. For $\delta^{2}H$, the error range was very similar but shifted. The ground water isoscape (Figure 5.2.12 C) predicted higher values compared to the measured tap water values while the tap water isoscape (Figure 5.2.12 D) predicted lower values compared to the measured ground water values.

Table 5.2.7. Differences in $\delta^{18}O$ and $\delta^{2}H$ from the recorded values of the isoscapes to the extracted values at the sampling locations. (TW= tap water, GW= ground water)

	$\delta^{18}O$		$\delta^{2}H$	
	TW Isoscape to GW Sampling Locations	**GW Isoscape to TW Sampling Locations**	**TW Isoscape to GW Sampling Locations**	**GW Isoscape to TW Sampling Locations**
Minimum Difference	-3.8‰	-4.3‰	-29.5‰	-50.1‰
Maximum Difference	4.1‰	8.5‰	31.6‰	46.9‰
Average Difference	-0.1‰	0.3‰	0.8‰	0.8‰

One interesting difference between the groundwater isotopic values reported by Wassenaar *et al.* 2009 are the values in the Tijuana (Baja California) area. While their research reports very high values, the tap water samples from this area are particularly low. Potentially, this can be explained by the city's almost 90% reliance on water from the Colorado River (Rodríguez 2005; Navarro Chaparro *et al.* 2016). Even though this may be an explanation for the deviation from the groundwater values, it is also important to note that there was a relatively large variability within the three collected samples from this city (Table 5.2.1).

Comparing the least-square regression lines, the tap water [$\delta^{2}H = 7.5\ \delta^{18}O + 2.3$ ($r^2 = 0.93$)] was nearly identical to the Mexican meteoric water line, the IAEA GNIP stations, and the groundwater. The slopes of all regression lines fall between 7 and 8 and therefore close to the slope of the global meteoric water line's slope of 8 ($\delta^{2}H = 8.0 \times \delta^{18}O + 10$ (Craig 1961)). The intercepts of the regression lines vary, however. While the Veracruz IAEA GNIP station is similar to the groundwater and Mexican meteoric water line, the tap water is closer to the IAEA GNIP station in Chihuahua (Figure 5.2.1). All values lay below the 10‰ value of the global meteoric water line.

As visualized in Figure 5.2.10, the tap water isotope data correspond closely to the available precipitation data even though the IAEA GNIP data are geographically very limited and also temporarily restricted to the 1960s to 1980s. The precipitation stations show a larger range of isotope values compared to the recorded tap water values. The smaller variability of isotopic values in the tap water compared to the precipitation stations can be explained by the seasonality of the sampling and therefore, the seasonal isotopic variability of precipitation.

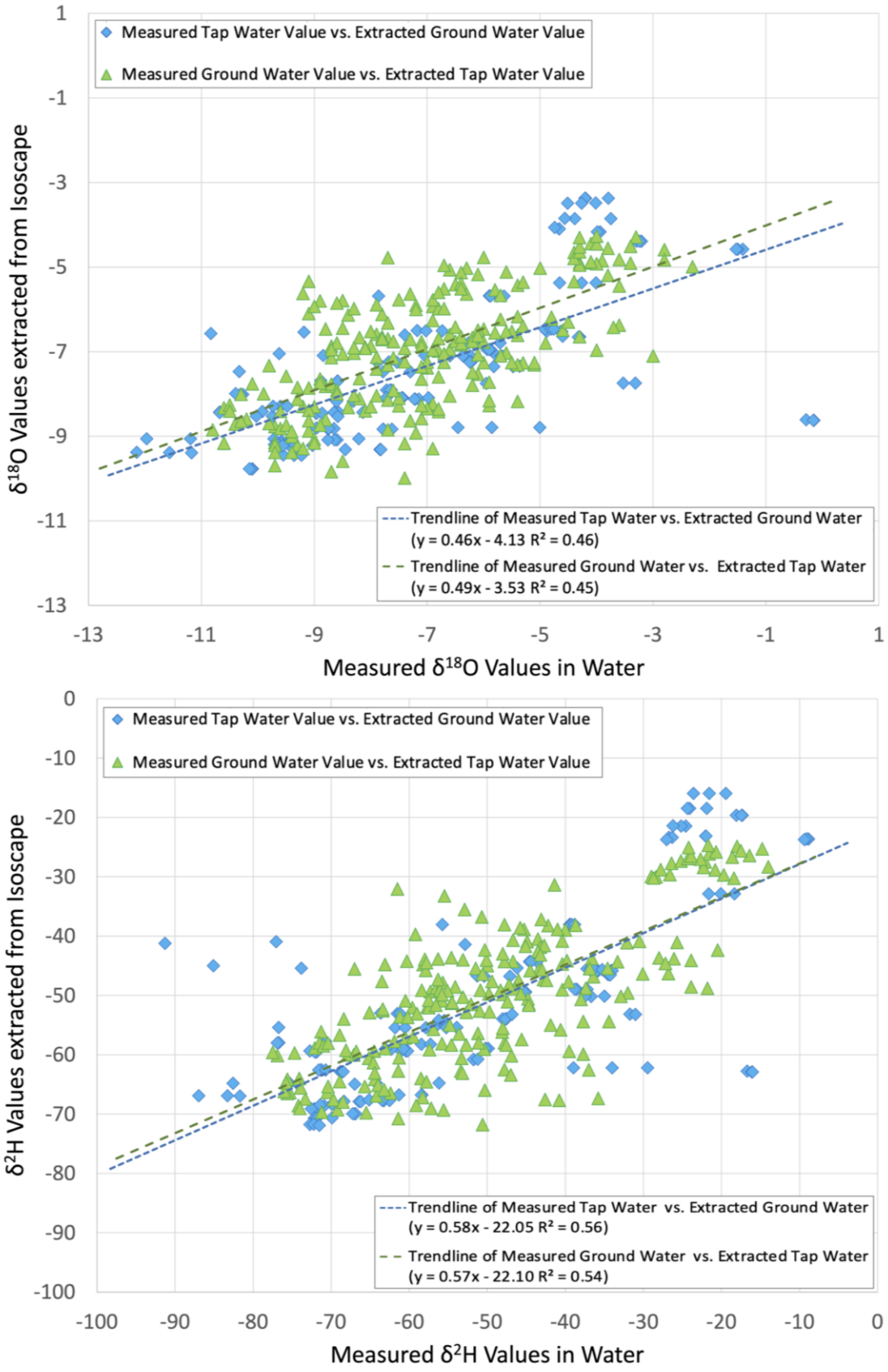

Figure 5.2.11. Measured Isotope Values versus Extracted Isotope Values from previously generated isoscapes.

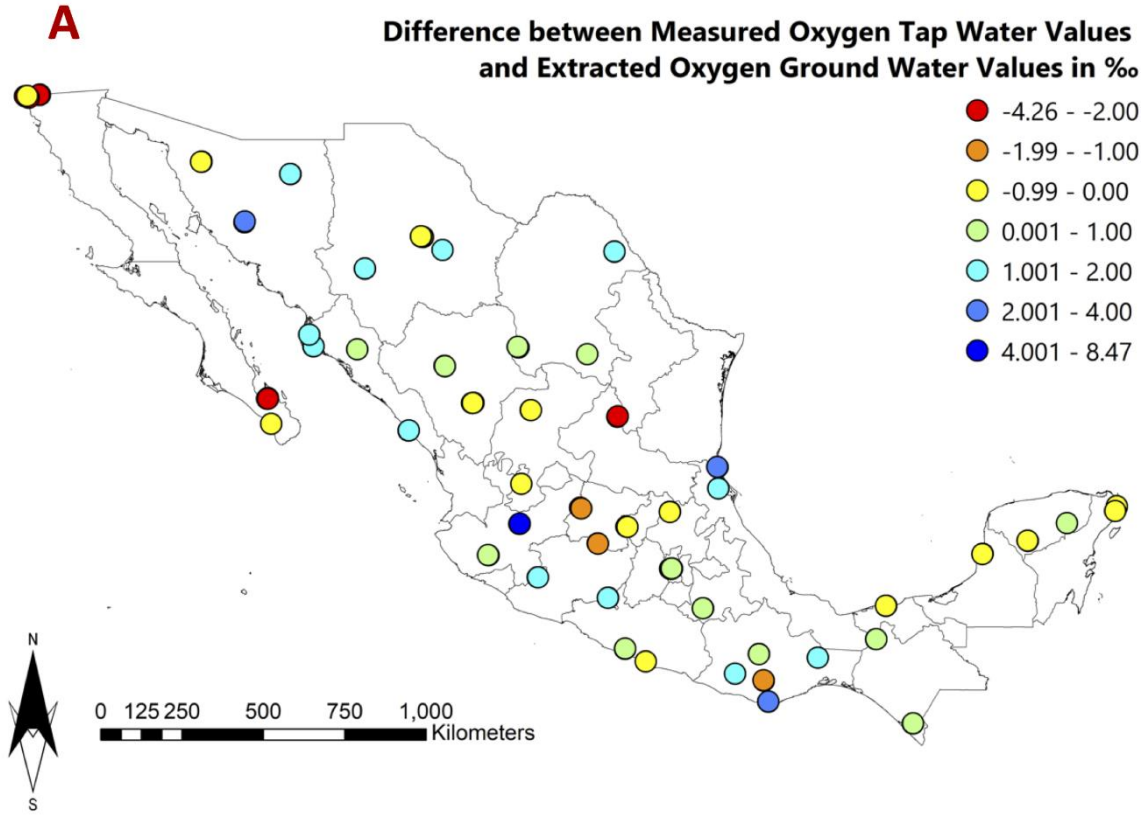
A
Difference between Measured Oxygen Tap Water Values
and Extracted Oxygen Ground Water Values in ‰
-4.26 - -2.00
-1.99 - -1.00
-0.99 - 0.00
0.001 - 1.00
1.001 - 2.00
2.001 - 4.00
4.001 - 8.47
N
S
0 125 250 500 750 1,000
Kilometers

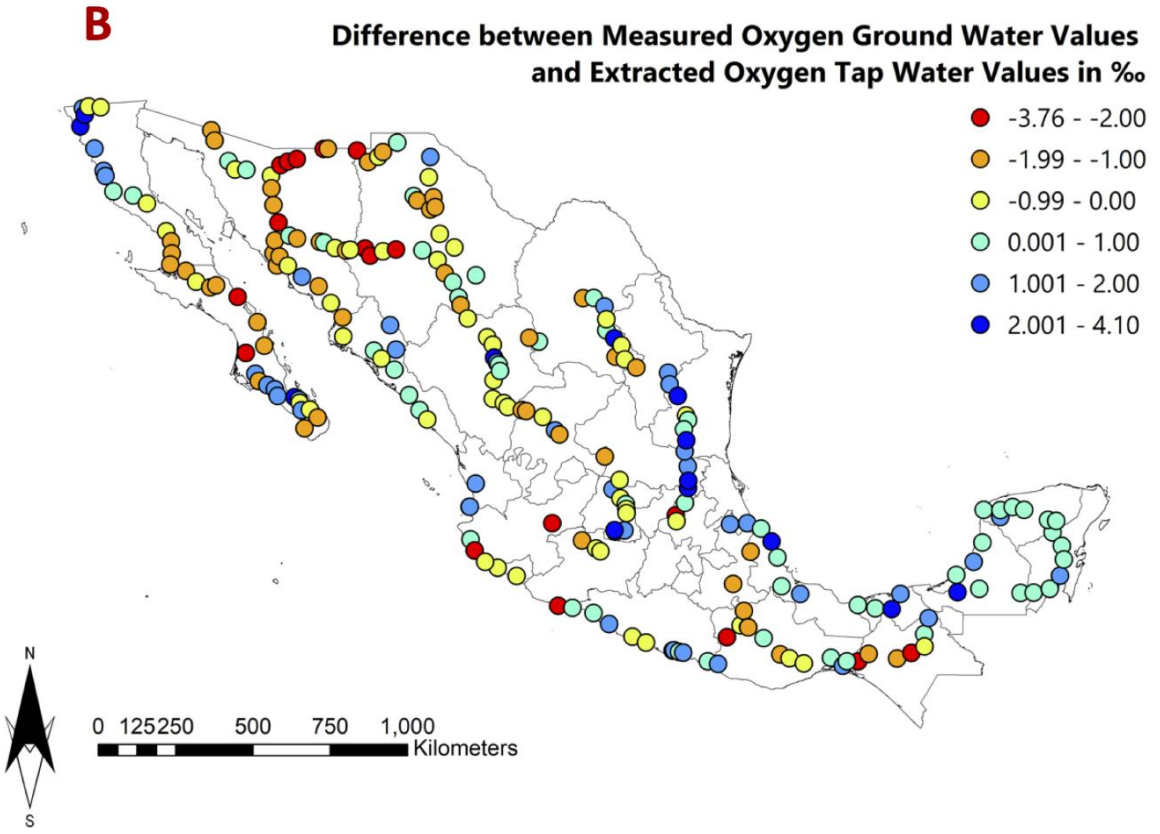
B
Difference between Measured Oxygen Ground Water Values
and Extracted Oxygen Tap Water Values in ‰
-3.76 - -2.00
-1.99 - -1.00
-0.99 - 0.00
0.001 - 1.00
1.001 - 2.00
2.001 - 4.10
N
S
0 125250 500 750 1,000
Kilometers

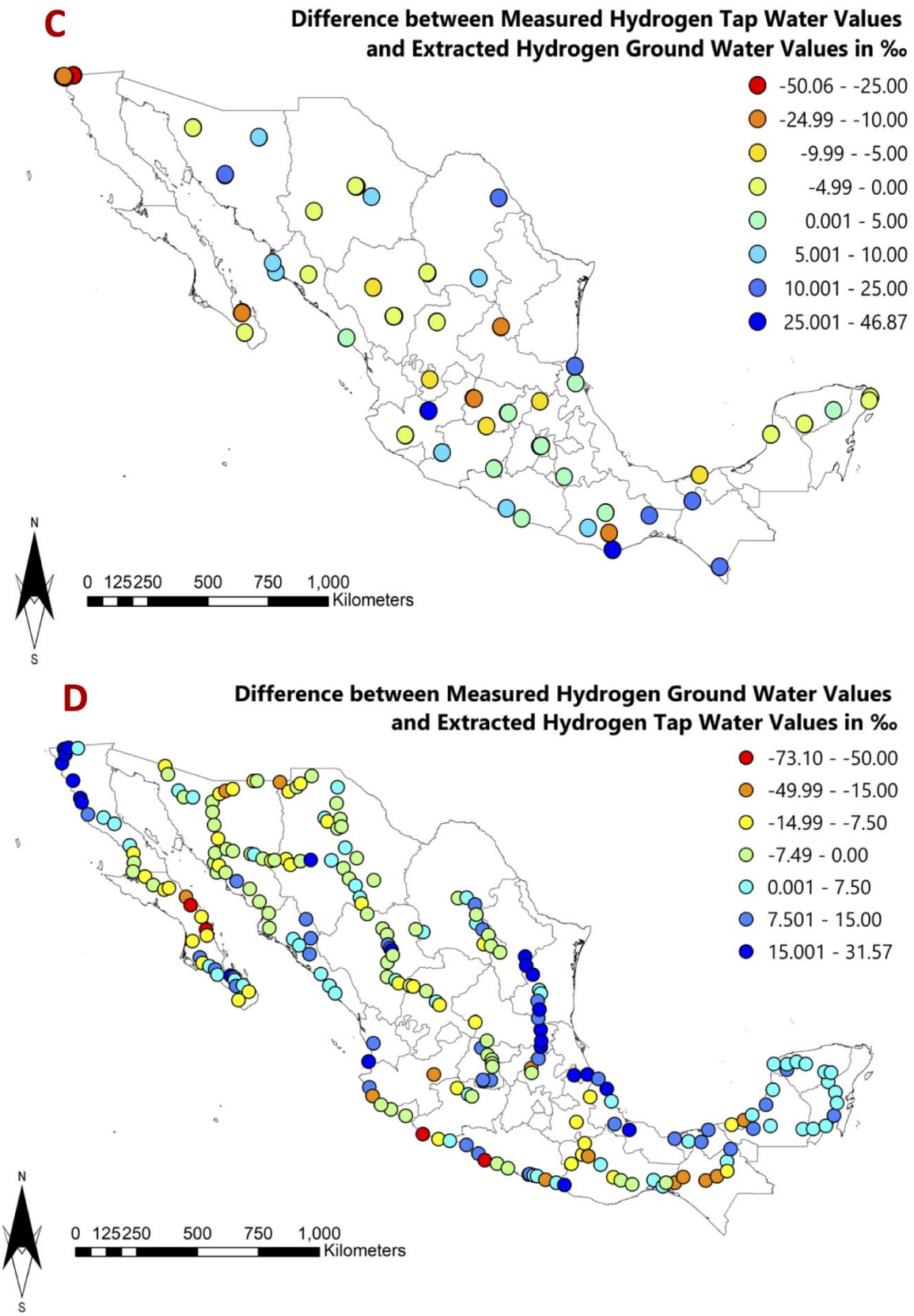

Figure 5.2.12. Differences between Measured Isotope Values versus Extracted Isotope Values from previously generated isoscapes.

Comparison to IsoMAP Prediction

The Mexican $\delta^{18}O$ tap water values were further compared to the IsoMAP predictive model of precipitation $\delta^{18}O$ (Bowen *et al.* 2019, Ammer 2019). While the isoscapes show similarity (Figure 5.2.7 and 13), the predicted versus measured graph (Figure 5.2.14) shows the limitations in comparing the two datasets.

There are several reasons why the predictive map from IsoMAP may not reflect the measured tap water values. One reason may be that the predictive map, in fact, predicts precipitation values and not tap water values. The data comparison (Figures 10 and 11) showed that the measured tap water data are very similar to the Mexican groundwater as well as the IAEA GNIP stations (Chihuahua region $\delta^{18}O$- tap water: -6.4±1.0‰, ground water: -7.34±1.0‰, GNIP: -6.53±3.4‰; the Veracruz region was not comparable due to the lack of sampling locations in close proximity to the GNIP station). Furthermore, the resolution also presents a possible reason for discrepancy as point measurements are compared with a coarsely gridded map product in this study. Another possible reason is the lack of reported values that can be used for predicting precipitation $\delta^{18}O$ in Mexico and the surrounding areas. Lastly, the comparison of tap water to precipitation values itself can present analytical issues as there are significant hydrological dissimilarities; such as the transport, evaporation, the usage of older ground water, among other factors. This reiterates the dire need for more sampling in these areas to be able to predict isotopic values accurately as well as use these for, for example, region of origin assignments of unidentified individuals.

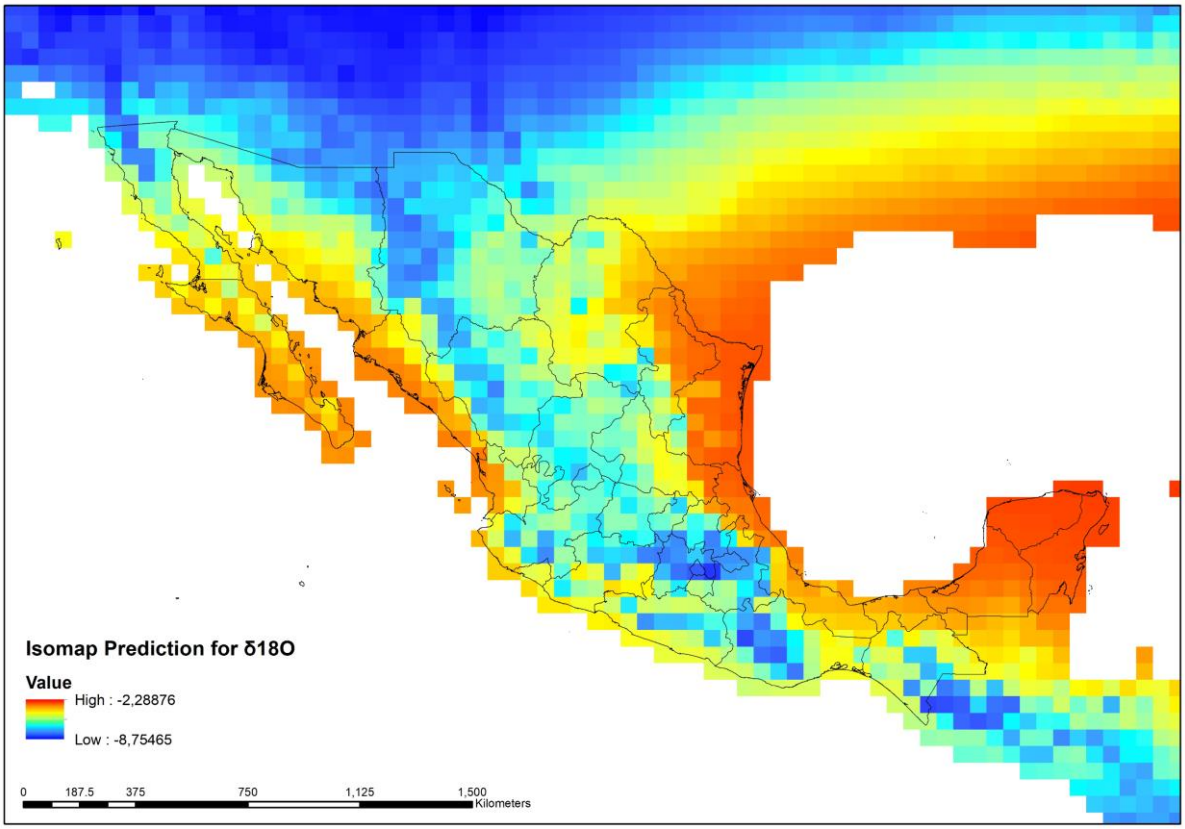

Figure 5.2.13. IsoMAP prediction map for $\delta^{18}O$ precipitation values in Mexico and surrounding areas.

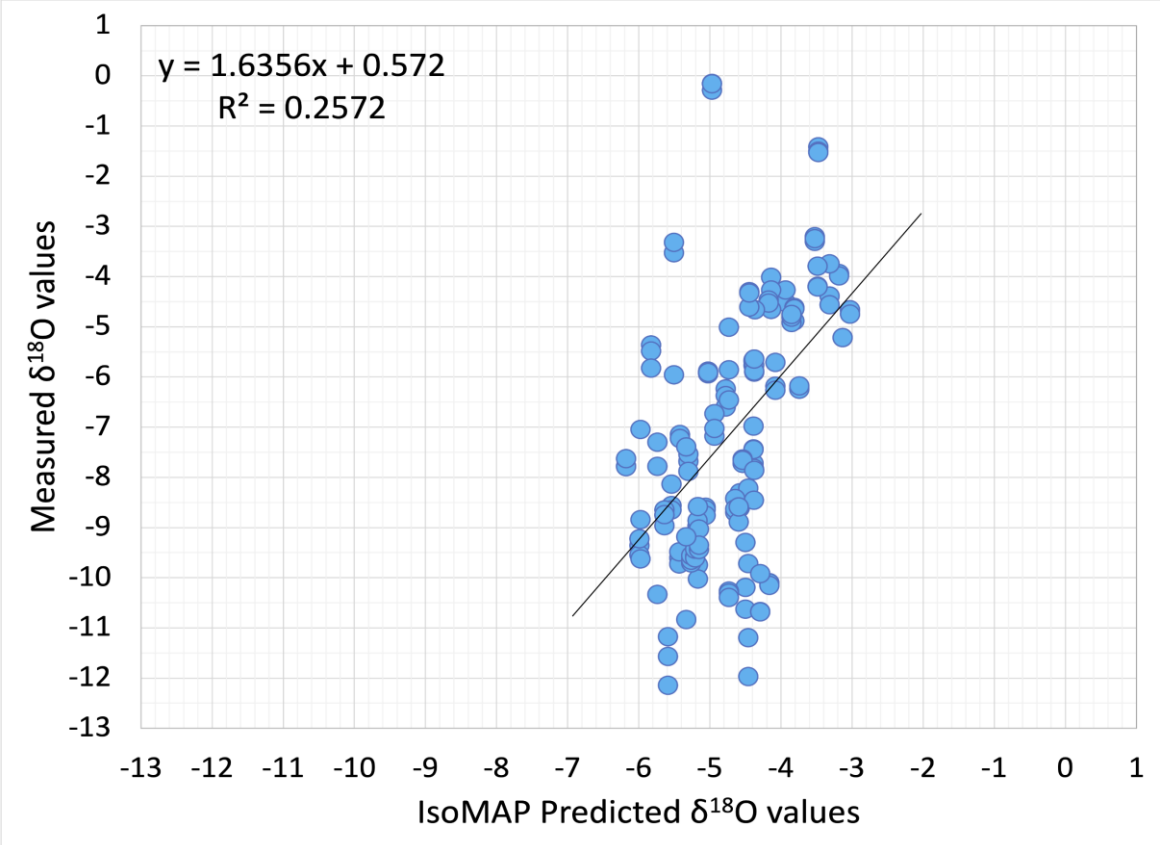

Figure 5.2.14. IsoMAP predicted $\delta^{18}O$ precipitation values for sampling locations versus measured tap water values.

5.2.5. Conclusion

The results demonstrate that there is significant spatial variability for $\delta^{18}O$ and $\delta^{2}H$ isotope values in Mexican tap water. The findings show that the tap water values measured in this sample are within the range of the previously reported values and that they can be used for predictive isoscape modeling. Further sampling will be beneficial to the resolution of the tap water isoscapes of Mexico. Nonetheless, the collected dataset provided important baseline data for extrapolation of values for Mexico, and the associated isoscapes show great potential for usage in hydrological contexts. It is advisable to use caution when using this dataset as a baseline for further studies as they are, as they do not capture the full dynamics of isotopic variation within Mexican tap water. Further exploration of tap water hydrology in general but Mexican tap water hydrogeology is needed to investigate the recharging processes of tap water. Not only will it be important to investigate the lakes, rivers, and reservoirs but also the actual recharging processes (anthropogenic versus natural) of the tap water sources. Furthermore, an investigation into the social background of Mexican tap water is needed to describe what tap water is used for in everyday life as well as the specific sources of drinking water in different regions. In the future, a model should be created that goes beyond the scope of ordinary kriging. Ideally, an R model (*e.g.*, random forest) would be able to include the other covariates explored here to provide a more detailed overview of the isotopic values found in Mexican tap water.

Overall, this study highlights that there is a dire need for more water sampling in Mexico (as well as in Central and South America), to provide a tool for understanding hydrological patterning and for predicting region of origin for animals, including unidentified deceased humans. A large-scale baseline database is needed for many hydrological projects but also to help solve humanitarian issues, such as aiding the identification of undocumented border crossers found at the Mexico-United States border. Isotope analysis has demonstrated its value in identifying travel histories of individuals as well as regions of origin for unidentified remains (Bartelink *et al.* 2018; Chesson *et al.* 2018; Bartelink *et al.* 2014a). Therefore, this study is an important milestone to create a spatially extensive overview of the isotopic values of water in North America.

Acknowledgements

I offer my sincere thanks to all the individuals that let me sample their tap waters throughout Mexico. Furthermore, I want to thank Sagarika Banerjee and the SIRFER Lab at the University of Utah for analyzing the ridiculous number of samples in such a short period of time. Thank you also to the American Academy of Forensic Sciences (AAFS) Humanitarian and Human Rights Resource Center (HHRRC) grant, financed by the AAFS and National Institute of Justice (U.S. Department of Justice) for supporting my research endeavors.

Table 5.2.1. Isotopic composition of tap water in Mexico.

Location	$\delta^{18}O$	$\delta^{2}H$	Latitude	Longitude
Acapulco, Guerrero	-8.6	-58.4	16.85662037	-99.86120573
Acapulco, Guerrero	-8.3	-57.3	16.85528544	-99.86018672
Acapulco, Guerrero	-8.2	-56.2	17.21363076	-100.4289369
Atoyac de Álvarez, Guerrero	-12.0	-82.6	17.21110834	-100.4323238
Atoyac de Álvarez, Guerrero	-11.2	-75.3	17.21085532	-100.4340383
Atoyac de Álvarez, Guerrero	-9.7	-64.2	17.21176526	-100.4338576
Campeche, Campeche	-4.2	-24.4	19.84535561	-90.53723326
Campeche, Campeche	-4.2	-24.1	19.84616019	-90.5375653
Campeche, Campeche	-3.8	-21.9	19.83437196	-90.54422607
Cancún, Quintana Roo	-4.7	-27.0	21.03219115	-86.86863717
Cancún, Quintana Roo	-4.7	-26.7	21.14313436	-86.82493771
Cancún, Quintana Roo	-4.7	-26.3	21.16368257	-86.82850309
Chihuahua, Chihuahua	-7.9	-56.2	28.64607196	-106.0804909
Chihuahua, Chihuahua	-7.7	-56.0	28.62735671	-106.0255696
Chihuahua, Chihuahua	-7.5	-55.5	28.63274252	-106.073369
Creel, Chihuahua	-5.5	-44.6	27.75332902	-107.6348494
Creel, Chihuahua	-5.8	-44.4	27.75217274	-107.6344445
Creel, Chihuahua	-5.4	-43.7	27.74753518	-107.6339282
Durango, Durango	-9.4	-71.4	24.02763271	-104.648994
Durango, Durango	-9.6	-70.9	24.03080708	-104.6217408
Durango, Durango	-9.6	-69.9	24.02497814	-104.6634502
El Grullo, Jalisco	-8.6	-63.1	19.80499101	-104.2158897
El Grullo, Jalisco	-8.6	-62.3	19.80043202	-104.2114479
El Grullo, Jalisco	-8.1	-60.8	19.80739435	-104.2266648
El Salto, Sinaloa	-7.9	-55.7	25.51183792	-107.8451687
El Salto, Sinaloa	-5.8	-39.5	25.5113653	-107.8452367
El Salto, Sinaloa	-5.9	-39.4	25.51371039	-107.8451465
El Salto, Sinaloa	-5.9	-39.2	25.51270462	-107.8445431
El Salto, Sinaloa	-5.6	-38.8	25.51117482	-107.8444021
General Capeda, Coahuila	-7.2	-50.2	25.37893224	-101.4788728
General Capeda, Coahuila	-7.2	-50.2	25.37754972	-101.4749006
General Capeda, Coahuila	-7.1	-49.9	25.37933394	-101.477069
Guadalajara, Jalisco	-0.3	-16.7	20.67465823	-103.3597438
Guadalajara, Jalisco	-0.2	-16.1	20.67053772	-103.3461779
Guadalajara, Jalisco	-0.2	-16.0	20.6769747	-103.3432922
Guaymas, Sonora	-4.7	-36.4	27.92352242	-110.9001258
Guaymas, Sonora	-4.5	-35.7	27.92256214	-110.8880772
Guaymas, Sonora	-4.5	-35.6	27.92560837	-110.8956171
Hermosillo, Sonora	-4.6	-35.3	29.03148741	-110.9601386
Hermosillo, Sonora	-4.3	-34.1	29.06200737	-110.9548842
Hermosillo, Sonora	-4.3	-34.0	29.06397331	-110.9541726
Heroica Caborca, Sonora	-7.2	-51.3	30.71168596	-112.1509689
Heroica Caborca, Sonora	-7.0	-50.4	30.71213209	-112.1615848

Heroica Caborca, Sonora	-6.7	-47.1	30.72267433	-112.1510654
Huetamo de Núñez, Michoacán	-7.4	-57.9	18.62317935	-100.9003365
Huetamo de Núñez, Michoacán	-7.7	-56.8	18.62670008	-100.9012997
Huetamo de Núñez, Michoacán	-7.4	-55.3	18.62613315	-100.9019349
Huetamo de Núñez, Michoacán	-7.0	-53.9	18.61809157	-100.9062351
Huixtla, Chiapas	-6.6	-37.5	15.14090296	-92.46037834
Huixtla, Chiapas	-6.4	-36.7	15.13752163	-92.46576562
Huixtla, Chiapas	-6.2	-35.0	15.13499293	-92.46242344
Jacala, Hidalgo	-8.9	-63.6	21.00905659	-99.18929595
Jacala, Hidalgo	-8.6	-61.5	21.0072641	-99.19012198
Jacala, Hidalgo	-8.6	-61.2	21.0060399	-99.18999471
La Paz, Baja California Sur	-10.7	-76.9	24.14550413	-110.3173719
La Paz, Baja California Sur	-10.7	-76.7	24.14094078	-110.33541
La Paz, Baja California Sur	-9.9	-70.7	24.16378456	-110.3134876
León, Guanajuato	-10.0	-75.5	21.10331892	-101.6425654
León, Guanajuato	-9.7	-74.3	21.11978246	-101.6750055
León, Guanajuato	-8.6	-67.0	21.1226318	-101.6739098
Lindavista, Chiapas	-4.7	-21.7	17.47391514	-93.47851396
Manzanillo, Colima	-8.7	-59.6	19.10367666	-104.3278092
Manzanillo, Colima	-8.6	-58.3	19.10845764	-104.3355666
Manzanillo, Colima	-8.4	-56.8	19.09841756	-104.3246771
Matehuala, San Luis Potosi	-10.4	-72.7	23.65811323	-100.6364345
Matehuala, San Luis Potosi	-10.3	-72.1	23.64285916	-100.6443153
Matehuala, San Luis Potosi	-10.3	-71.9	23.64384027	-100.6442706
Mazatlán, Sinaloa	-6.2	-45.2	23.26668883	-106.4170429
Mazatlán, Sinaloa	-6.2	-45.1	23.25724513	-106.4245749
Mazatlán, Sinaloa	-6.2	-45.0	23.22513395	-106.4263271
Mexico City, Mexico	-9.0	-65.1	19.43683513	-99.1303126
Mexico City, Mexico	-8.7	-63.5	19.4341711	-99.144544
Mexico City, Mexico	-8.8	-63.3	19.42634249	-99.18673368
Mexico City, Mexico	-8.6	-62.5	19.42067391	-99.16557001
Miahuatlán de Porfirio Díaz, Oaxaca	-12.1	-87.0	16.32533872	-96.59337016
Miahuatlán de Porfirio Díaz, Oaxaca	-11.6	-83.3	16.32849844	-96.59299059
Miahuatlán de Porfirio Díaz, Oaxaca	-11.2	-81.7	16.33991477	-96.59979229
Moroleón, Guanajuato	-9.7	-71.6	20.13184908	-101.1889844
Moroleón, Guanajuato	-9.6	-71.3	20.1299541	-101.1901155
Moroleón, Guanajuato	-9.5	-70.7	20.12796804	-101.1827869
Nacozari de García, Sonora	-6.0	-46.8	30.37697297	-109.6974512
Nacozari de García, Sonora	-3.5	-31.8	30.37198458	-109.6896482
Nacozari de García, Sonora	-3.3	-31.0	30.37367993	-109.687868
Oaxaca, Oaxaca	-9.5	-68.4	17.06522288	-96.72369042
Oaxaca, Oaxaca	-9.4	-66.4	17.05797749	-96.72738841
Oaxaca, Oaxaca	-9.2	-66.2	17.05794239	-96.7286993
Ozuluama de Mascareñas, Veracruz	-3.3	-18.1	21.66028677	-97.85035254

Ozuluama de Mascareñas, Veracruz	-3.2	-17.4	21.65798716	-97.8498047
Ozuluama de Mascareñas, Veracruz	-3.2	-17.3	21.65941866	-97.85047861
Paraíso, Tabasco	-4.5	-23.6	18.39554957	-93.21427496
Paraíso, Tabasco	-4.3	-21.6	18.39991428	-93.21112948
Paraíso, Tabasco	-4.0	-19.5	18.40081619	-93.20867087
Pedro Meoqui, Chihuahua	-5.9	-48.0	28.26968285	-105.4814373
Pedro Meoqui, Chihuahua	-5.9	-47.7	28.26780764	-105.4814317
Pedro Meoqui, Chihuahua	-5.9	-47.6	28.26769163	-105.4805257
Plan de Ayala, Chiapas	-4.3	-20.1	17.47378116	-93.48635766
Plan de Ayala, Chiapas	-4.0	-18.3	17.47451202	-93.48712946
Puerto Morelos, Quintana Roo	-5.2	-30.3	20.85731102	-86.90149248
Puerto Morelos, Quintana Roo	-5.2	-30.3	20.85629645	-86.90160179
Río Grande, Zacatecas	-9.4	-72.2	23.82898015	-103.0410154
Río Grande, Zacatecas	-9.4	-71.8	23.82414684	-103.0343507
Río Grande, Zacatecas	-9.0	-69.9	23.82565563	-103.0344594
Salina Cruz, Oaxaca	-10.6	-74.8	16.24207517	-95.21369857
Salina Cruz, Oaxaca	-10.2	-71.9	16.23413048	-95.21180031
Salina Cruz, Oaxaca	-9.3	-66.8	16.1726963	-95.2005281
San Jacinto Tlacotepec, Oaxaca	-7.8	-51.8	16.52038347	-97.38612235
San Jacinto Tlacotepec, Oaxaca	-7.8	-51.8	16.51978001	-97.38550594
San Jacinto Tlacotepec, Oaxaca	-7.6	-51.2	16.51954227	-97.38692549
San Juan Guichicovi, Oaxaca	-5.8	-34.5	16.96355204	-95.0953177
San Juan Guichicovi, Oaxaca	-5.7	-34.3	16.96129769	-95.09406536
San Juan Guichicovi, Oaxaca	-5.7	-34.3	16.96033101	-95.09437934
San Pedro Pochutla, Oaxaca	-6.5	-39.0	15.74321161	-96.46584583
San Pedro Pochutla, Oaxaca	-5.9	-34.0	15.74572948	-96.46664838
San Pedro Pochutla, Oaxaca	-5.0	-29.5	15.74599957	-96.46486652
Santiago de Querétaro, Querétaro	-9.7	-72.7	20.59277316	-100.3896554
Santiago de Querétaro, Querétaro	-9.7	-72.2	20.5925566	-100.394883
Santiago de Querétaro, Querétaro	-9.6	-71.5	20.59025415	-100.3661751
Santiago Papasquiaro, Durango	-10.3	-76.7	25.05911027	-105.4260955
Santiago Papasquiaro, Durango	-7.8	-61.8	25.04638336	-105.4198078
Santiago Papasquiaro, Durango	-7.3	-60.5	25.04835005	-105.4207351
Tampico, Tamaulipas	-1.5	-9.4	22.25661057	-97.87647877
Tampico, Tamaulipas	-1.5	-9.1	22.24684176	-97.8731706
Tampico, Tamaulipas	-1.4	-8.9	22.2473159	-97.8735128
Tecate, Baja California	-9.6	-85.1	32.56534583	-116.6500504
Tecate, Baja California	-8.8	-73.8	32.5725987	-116.6255893
Tecate, Baja California	-7.0	-46.2	32.56546646	-116.6248733
Tehuitzingo, Puebla	-8.8	-67.2	18.33272712	-98.27642986
Tehuitzingo, Puebla	-8.6	-66.9	18.3322784	-98.27532006
Tehuitzingo, Puebla	-8.6	-66.9	18.33140609	-98.27517187
Tekax de Álvaro Obregón, Yucatan	-4.6	-26.2	20.2078044	-89.29432566
Tekax de Álvaro Obregón, Yucatan	-4.4	-25.2	20.20340555	-89.28747023

Tekax de Álvaro Obregón, Yucatan	-3.7	-24.6	20.20120534	-89.28569726
Tepalcatepec, Michoacán	-8.5	-61.3	19.19239397	-102.8448005
Tepalcatepec, Michoacán	-7.8	-58.5	19.191637	-102.8431749
Tepalcatepec, Michoacán	-7.8	-58.4	19.18880027	-102.845742
Tijuana, Baja California	-10.8	-91.3	32.49248989	-116.93513
Tijuana, Baja California	-9.2	-77.1	32.5320066	-117.0367819
Tijuana, Baja California	-7.4	-52.9	32.5427587	-116.9785219
Tlaltenango de Sánchez Román, Zacatecas	-9.0	-68.8	21.78197047	-103.3054219
Tlaltenango de Sánchez Román, Zacatecas	-9.0	-68.6	21.78306745	-103.3039239
Tlaltenango de Sánchez Román, Zacatecas	-8.9	-68.5	21.78282933	-103.3027044
Todos Los Santos, Baja California Sur	-10.2	-72.5	23.44905243	-110.2258597
Todos Los Santos, Baja California Sur	-10.1	-72.2	23.44554666	-110.2254055
Todos Los Santos, Baja California Sur	-10.1	-72.1	23.44932136	-110.2229936
Topolobampo, Sinaloa	-4.9	-36.7	25.59974997	-109.0524669
Topolobampo, Sinaloa	-4.6	-36.0	25.59677577	-109.0541026
Topolobampo, Sinaloa	-4.6	-35.8	25.59631223	-109.055251
Torreón, Coahuila	-7.7	-61.1	25.55998229	-103.3799816
Torreón, Coahuila	-7.6	-60.4	25.56670866	-103.3837421
Torreón, Coahuila	-7.7	-60.2	25.58162045	-103.3986472
Valladolid, Yucatan	-4.0	-22.0	20.69020344	-88.2024172
Valladolid, Yucatan	-3.9	-22.0	20.69057627	-88.20029181
Villa de Ahome, Sinaloa	-4.9	-37.2	25.9204777	-109.1719661
Villa de Ahome, Sinaloa	-4.8	-36.8	25.9210369	-109.1740906
Villa de Ahome, Sinaloa	-4.8	-36.4	25.91925004	-109.1731003
Villa Unión, Coahuila	-6.3	-38.8	28.22653048	-100.7258758
Villa Unión, Coahuila	-6.2	-38.5	28.21817791	-100.7245366
Villa Unión, Coahuila	-5.7	-37.2	28.22848279	-100.7277947

5. 3. Oxygen isotopes in human hair from Mexico: Interpretations and Data Challenges

Abstract:

This chapter discusses the issues encountered with analysis and results of the $\delta^{18}O$ isotopic values found in the human hair samples from Mexico. Due to technical issues, the samples had to be reanalyzed which lead to interesting questions regarding quality control and data interpretation. Here, the data from two datasets, the one from September 2019 and the one from March 2020, are presented and discussed. While there is no knowledge of potential issues during the second sample run, the data raise concerns. Both datasets passed the quality control checks and could have theoretically been used as representation for the Mexican population. However, it is of concern concerning that all statistical and geostatistical tools employed performed poorer in the newer dataset than in the older dataset. Therefore, it is suggested that the samples must be re-run again in order to draw definite conclusions which dataset may be most accurate.

KEYWORDS: Mexico, human hair, isotopes, oxygen

5.3.1. Introduction

Human hair is formed of keratin, which is a tough structural fibrous protein that comprises of 50% carbon, 21% nitrogen, 17.5% hydrogen, 6.5% oxygen, and 5% sulfur, but also includes trace contents of metals such as strontium and lead. The elements are integrated into the hair structure through diet and exposure to outside sources such as air and water. Once hair is long enough to exit the protection of the skin, it dies. Human scalp hair grows at an average of 1 cm per month, and since the elemental exchange between hair and blood ceases when it "dies off", it retains the biogenic and dietary information (Font *et al.* 2012; Krause and Foitzik 2006).

Through the easily accessibility and its makeup, hair has become a more prominent human tissue in isotope analysis and the forensic sciences over the last decade. Human hair has been used to document periods of nutritional deprivation, for example due to malnutrition and starvation (Mekota *et al.* 2006; Neuberger *et al.* 2013). These nutritional studies use predominantly δ^{15}N and δ^{13}C as unbiased biomarkers to document these cases. Furthermore, several authors have recorded baseline data for countries around the world, giving indications which δ^{15}N, δ^{13}C, and δ^{34}S values can be expected in the respective regions (Lehn *et al.* 2015; Bender *et al.* 2015; Valenzuela *et al.* 2011; Thompson *et al.* 2010).

The available data for δ^{18}O isotopic values is unfortunately scarcer. Most prominently, Ehleringer *et al.* (2008) developed isoscapes based on the δ^{18}O and δ^{2}H values of human hair samples from 65 cities across the United States. The δ^{18}O values of human hair are thought to be influenced by several factors, such as atmospheric oxygen and dietary inputs. Those dietary inputs include food as well as drinking water. Through those influences, previous research demonstrated a predictable relationship between δ^{18}O values of human hair and tap water.

Therefore, the research aim for this study was to establish a reference database of δ^{18}O values in Mexican human hair and to determine which geological and socioeconomic factors may influence the isotopic composition of the samples. Furthermore, it was proposed to determine if the δ^{18}O values in human hair correlate to the collected δ^{18}O tap water samples and if they do correlate, how predictable they are.

5.3.2. Materials and methods

Sample Acquisition

A total of 101 hair samples from all over Mexico were collected from barbershops and hairdressers during a six-week period in June and July 2018. The samples originated from thirty-two towns and cities (Figure 5.3.1). A total of twenty-one states were sampled: Baja California, Sonora, Baja California Sur, Sinaloa, Zacatecas, Durango, Chihuahua, Coahuila, San Luis Potosi,

Veracruz, Hidalgo, Guanajuato, Jalisco, Michoacán, Guerrero, Puebla, Oaxaca, Chiapas, Tabasco, Yucatan, Quintana Roo. At least three samples were collected from each location, with two exceptions. Only one sample was collected in La Paz, Baja California Sur and Saltillo, Coahuila.

The samples were collected from the floors of the shops and without the recording of any personal information. Since the samples were collected anonymously, the research was conducted under the assumption that the customers were locals and that their dietary differences were not large enough to affect the results. The samples were stored in individual paper envelopes in airtight zip-log bags at room temperature.

A detailed description for the sample acquisition of the tap water samples can be found in Chapter 5.2. As can be seen in Figure 5.3.1, water samples were collected from more locations than hair samples. Therefore, only a subset of the water samples will be compared to the hair samples, namely the ones from locations from where hair and water samples were collected.

The sampling locations were chosen by geographic aspects to obtain a somewhat complete coverage of Mexico. Nonetheless, a main factor was accessibility because, for example, some municipalities turn off the water source during the day to preserve water or other locations could not be sampled due to roadblocks and safety concerns.

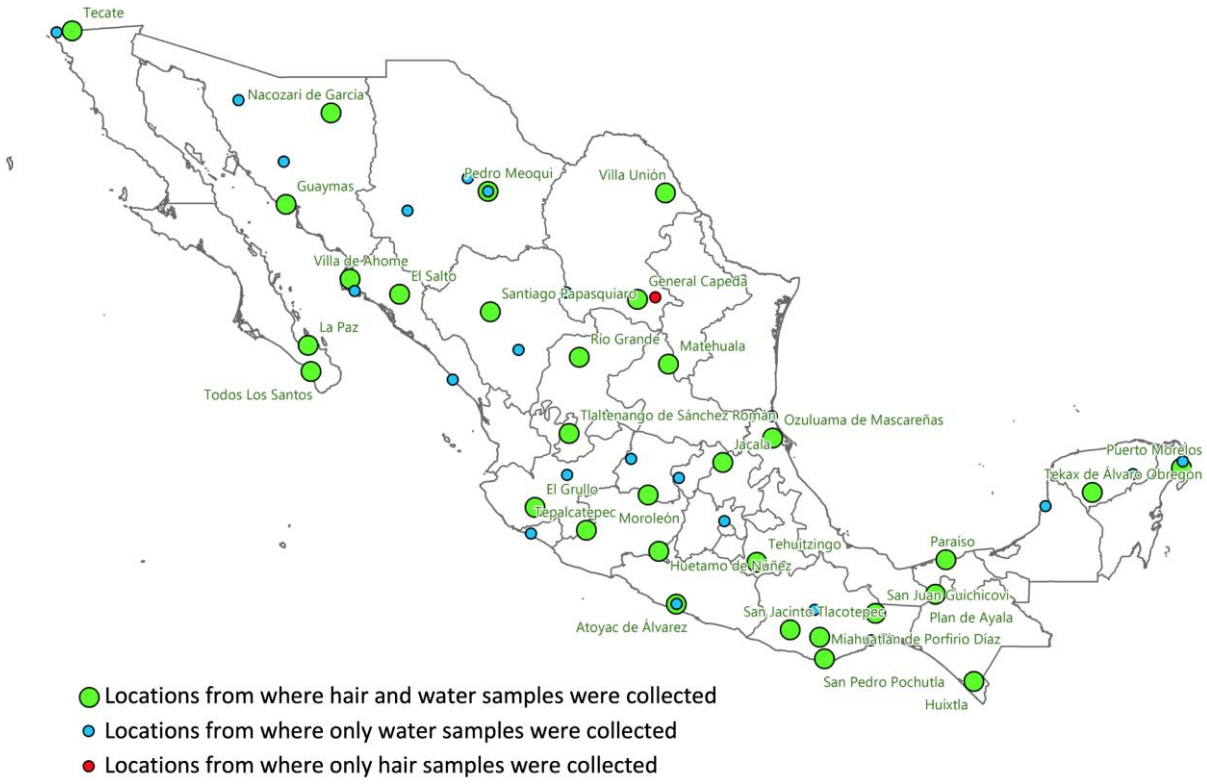

Figure 5.3.1. Hair and tap water sampling locations. (green = hair and water locations, blue = water only locations, red = hair only locations).

Sample Preparation and Analysis

A vacuum funnel in combination with an extractor hood was used to clean the collected hair samples. To remove any surface contaminants and lipids, the samples were placed on filter paper within the funnel and a 2:1 chloroform/methanol mixture was poured over the samples. After the samples were soaked for ~20 seconds, the funnel was evacuated using the vacuum pump. This step was followed by a ~20 second MilliQ soak. The two steps were repeated five times. Whenever a filter paper appeared to be soiled, it was replaced by a new one. Once the soaking steps were completed, the samples were placed between two clean filter papers and wrapped in aluminum foil to be transported to the laminar flow hood where they were partially unwrapped to be air-dried. In between the samples, the working space, glassware, and utensils were cleaned using acetone, ethanol, and MilliQ to avoid contamination. The samples were cut into small pieces using surgical grade scissors. For the $\delta^{18}O$ analyses, 400µg ±10% of hair was loaded into silver capsules.

All samples were analyzed at the University of California Davis Stable Isotope Facility, using an elementar PyroCube (Elementar Analysensysteme GmbH, Hanau, Germany) interfaced to an Isoprime VisION (Isoprime Ltd., Stockport, UK, a unit of Elementar Analysensysteme GmbH, Hanau, Germany). The samples were thermally decomposed to CO in a reactor filled with glassy carbon, graphite felt, and lamp black at 1400°C. An adsorption trap isolates CO from any interfering N_2.

Several reference materials were measured alongside the samples. Nylon, lab reference material used for order correction; Alanine, lab reference material used for size correlation and elemental totals, IAEA-600 (caffeine); USGS-35 (sodium nitrate), international reference materials used for normalization; and Cellulose, used as an internal check. The results for $\delta^{18}O$ values are presented on the Vienna Standard Mean Ocean Water (VSMOW) scale.

The sample's provisional isotope ratio was measured relative to the reference gas peak that was analyzed with the respective sample. These values of the entire batch were corrected based on the known values of the included internal laboratory reference materials. In order to capture the minor differences in stable isotope abundance ratios (R), they were expressed as δ values against an internationally defined standard in units 'per mil' (‰): $\delta = (R_{Samp} / R_{RM} - 1)$, where R_{Samp} is the ratio of the sample and R_{RM} is the ratio of the internationally agreed scale zero-point (Dunn and Carter 2018).

Statistical and geostatistical analyses

The statistical analyses were conducted with the programming language R (R Core Team 2020). The Pearson's product-moment correlation was used to explore the relationship between the isotopic values found in Mexican hair and metric variables, such as geographic/environmental and socioeconomic covariates. Strength of the correlations was categorized as follows: significant > 0.5, moderate 0.5 > 0.3, weak 0.3 > 0.1, non-existent- arrow).

The following geographic and environmental variables were investigated.

- Longitude
- Latitude
- Elevation (United States Department of the Interior- U.S. Geological Survey 2007)
- Mean annual temperature (Fick and Hijmans 2017)
- Precipitation (Tropical Rainfall Measuring Mission (TRMM) satellite product 3B43 version 7- Acker and Leptoukh 2007)
- Distance to the nearest ocean
- Distance to the nearest ocean excluding the Gulf of California

Correlations between the following socioeconomic variables were explored:

- Population size (Instituto Nacional de Estadística y Geografía 2015a; 2010)- number of inhabitants at the sampling locations.
- Percent of population living in poverty per state (Consejo Nacional de Evaluación de la Política de Desarrollo Social 2018)
- Number of people living in poverty by state (Consejo Nacional de Evaluación de la Política de Desarrollo Social 2018)
- Human Development Index by state (HDI) ((Smits and Permanyer 2019), Table 5.3.1)
- Percent Indigenous Ancestry (of total state population) (Instituto Nacional de Estadística y Geografía 2015b)
- Percent Indigenous Speaking (of total state population) (Instituto Nacional de Estadística y Geografía 2015a)

More detailed and elaborate explanations for each variable can be found in Ammer *et al.* (2020). All covariates were correlated to the entire sample set and the location averages. Furthermore, the dataset was split into the Atlantic and the Pacific drainage basin to explore potential differences between the drainage basins.

A One-Sample Kolmogorov-Smirnov Test was employed to determine whether a sample comes from a population which is normally distributed. A QQ plot was used to visually check the normality of the data. A Kruskal-Wallis test was employed to compare the isotopic data independently for each location in order to evaluate potential differences (R Core Team 2020). This test establishes whether there are significant differences between a continuous dependent variable (*i.e.*, the isotopic value) and a categorical independent variable (*i.e.*, the location). All tests were completed using the R programming language (R Core Team 2020).

The geostatistical analyses were done using the ArcGIS Geostatistical Analyst toolbox and Geostatistical Wizard (Environmental Systems Research Institute (ESRI) 2018). The Global Moran's I Spatial Autocorrelation tool was used to evaluate the spatial autocorrelation of the locations of the data points (sample locations) and the corresponding isotopic values. The resulting index provides information as to whether the isotopic data is spatially clustered, dispersed, or random (Environmental Systems Research Institute (ESRI) 2018).The isoscapes were generated using ArcGIS ordinary kriging with a semivariogram function (Environmental Systems Research Institute (ESRI) 2018).

Table 5.3.1. Human Development Indexes (HDI) for Mexican states that hair samples were collected from. The color indicates the strength of the index (green- high HDI, red- low HDI). Grayed out states were not sampled for this study. For a visual representation, please refer to Ammer *et al.* (2020).

State	HDI	State	HDI
Aguascalientes		México	
Baja California	0.803	Nayarit	
Baja California Sur	0.811	Nuevo León	
Campeche		Oaxaca	0.710
Chiapas	0.700	Puebla	0.742
Chihuahua	0.793	Querétaro	
Coahuila	0.799	Quintana Roo	0.781
Colima		San Luis Potosí	0.757
Distrito Federal		Sinaloa	0.804
Durango	0.775	Sonora	0.806
Guanajuato	0.757	Tabasco	0.773
Guerrero	0.717	Tamaulipas	
Hidalgo	0.761	Tlaxcala	
Jalisco	0.788	Veracruz	0.744
Michoacán	0.745	Yucatán	0.773
Morelos		Zacatecas	0.760

5.3.3. Results

Unfortunately, during the $\delta^{18}O$ analysis of these Mexican hair samples, a technical malfunction occurred during the initial sample run, which lead to the decision to reanalyze the entire dataset. The furnace failed after sample 011-002, written in red in Supporting Information 1. A total of 101 Mexican hair samples were analyzed for their $\delta^{18}O$ isotope values. The results for all $\delta^{18}O$ values of human hair measurements for the September and the March dataset can be found in Supporting Information 1 and the basic descriptive statistics can be found in Table 5.3.2. The samples of the first dataset (here referred to as "September") were prepared and made ready for the analyses at the Vrije Universiteit in Amsterdam. Because the samples had to be reanalyzed, the samples of the second dataset (here referred to as "March") were prepared at the laboratory of UC Davis.

The $\delta^{18}O$ isotopic values in the human hair samples ranged from +9.8 ‰ to + 14. 0‰ ($\Delta\delta^{18}O$ = 4.2 ‰) in the September data set and from +9.1 ‰ to + 14. 0‰ ($\Delta\delta^{18}O$ = 4.9 ‰) in the March data set. While the range of isotopic values is the same in the March dataset for both the Atlantic and the Pacific drainage basin ($\Delta\delta^{18}O$ = 4.3 ‰), the earlier September analyses resulted in a slightly smaller range in the Atlantic drainage basin ($\Delta\delta^{18}O$ = 3.4 ‰ vs. $\Delta\delta^{18}O$ = 3.6 ‰). Overall, the range of values is clearly much smaller in the September dataset than in the March dataset.

Table 5.3.2. Basic descriptive statistics of the $\delta^{18}O$ human hair results from September and March.

		September 2019 $\delta^{18}O$ Hair in ‰	**September 2019 Location Variability (Stand. Dev.)**	**March 2020 $\delta^{18}O$ Hair in ‰**	**March 2020 Location Variability (Stand. Dev.)**
All data	**Minimum**	9.8	0.2	9.1	0.2
	Maximum	14.0	0.9	14.0	1.1
	Mean	11.8	0.5	11.5	0.7
	Standard Deviation	1.0		1.1	
	Range	4.2		4.9	
Atlantic data	**Minimum**	10.6	0.3	9.7	0.4
	Maximum	14.0	0.9	14.0	1.1
	Mean	12.4	0.6	12.0	0.7
	Standard Deviation	1.0		1.0	
	Range	3.4		4.3	
Pacific data	**Minimum**	9.8	0.2	9.1	0.2
	Maximum	13.4	0.9	13.4	1.1
	Mean	11.5	0.5	11.3	0.6
	Standard Deviation	0.8		1.0	
	Range	3.6		4.3	

Table 5.3.2. also shows the stable isotope variability for the sampled locations. Notably, the average standard deviations (SD) for the $\delta^{18}O$ values in human hair are very similar for the entire set, the Atlantic drainage basin and the Pacific drainage basin. The minimum and maximum standard deviations by location are also very similar but the minimum SD is slightly elevated in the Atlantic drainage basin. The mean of the SD values is lower and the range smaller in the September 2019 dataset when compared to the March 2020 dataset.

A visual representation of the distribution of the $\delta^{18}O$ values in human hair from the isotopic analyses of September 2019 and March 2020 can be found in Figure 5.3.2. The violin plot shows the numeric data as well as the kernel density plot on each side, highlighting the probability density of the data at different the various $\delta^{18}O$ values. The September 2019 data is slightly elevated over the March 2020 data. The March 2020 data shows more variability over the September data. These findings were previously quantified in Table 5.3.1.

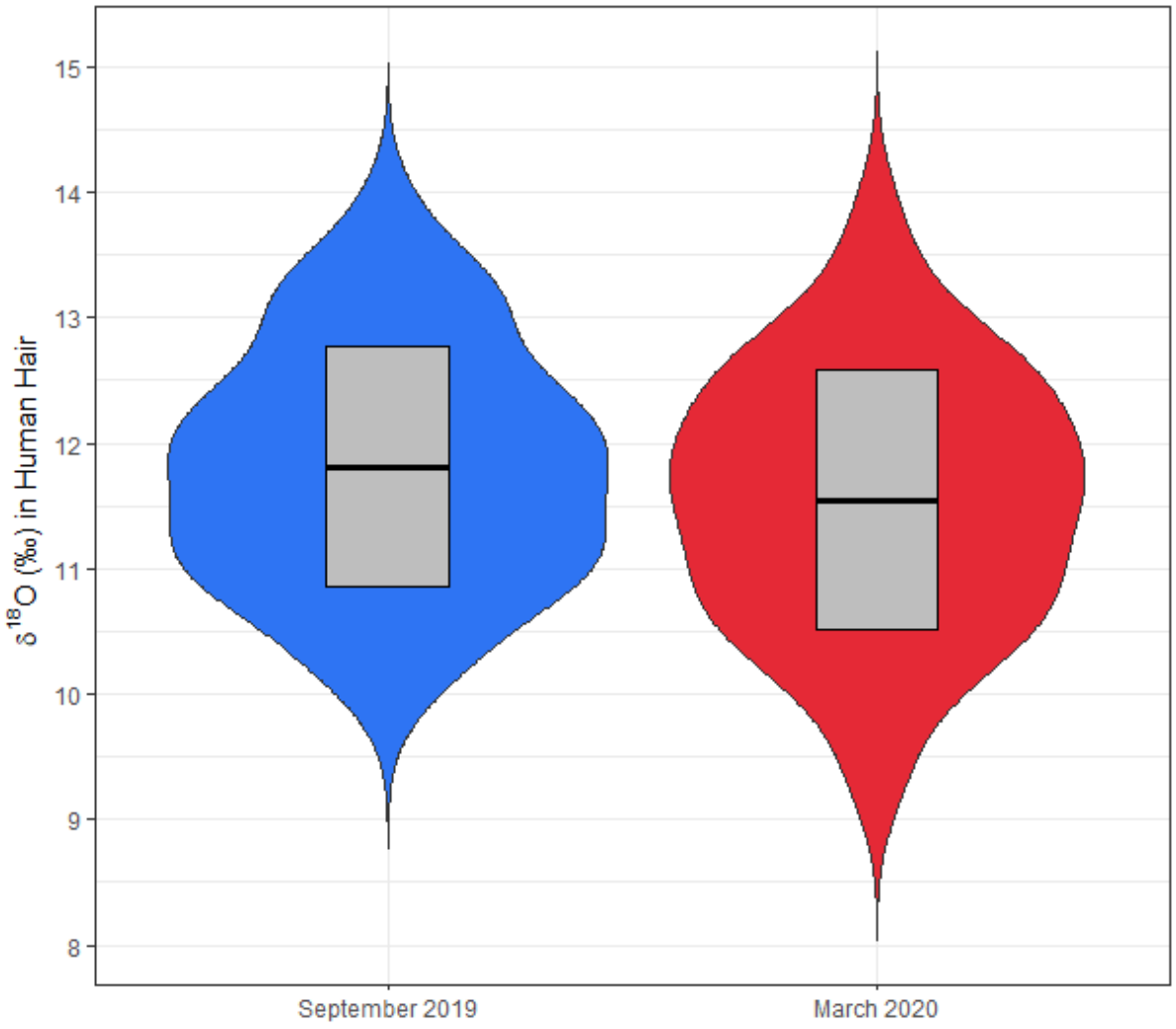

Figure 5.3.2. Violin plot showing $\delta^{18}O$ values in human hair from Mexico, comparing the two datasets: September 2019 and March 2020. The mean ± standard deviation was added as a crossbar.

The one-sample Kolmogorov-Smirnov Test concluded that the data of both datasets are normally distributed. A visualization, in form of a QQ plot with 45-degree reference lines can be found in Figure 5.3.3. The Kruskal-Wallis rank-sum test was used to compare the isotopic data independently for each location to evaluate the differences between them (significance set at $\alpha = 0.05$). It showed that it could be concluded that there are significant differences in the isotopic values from the different locations.

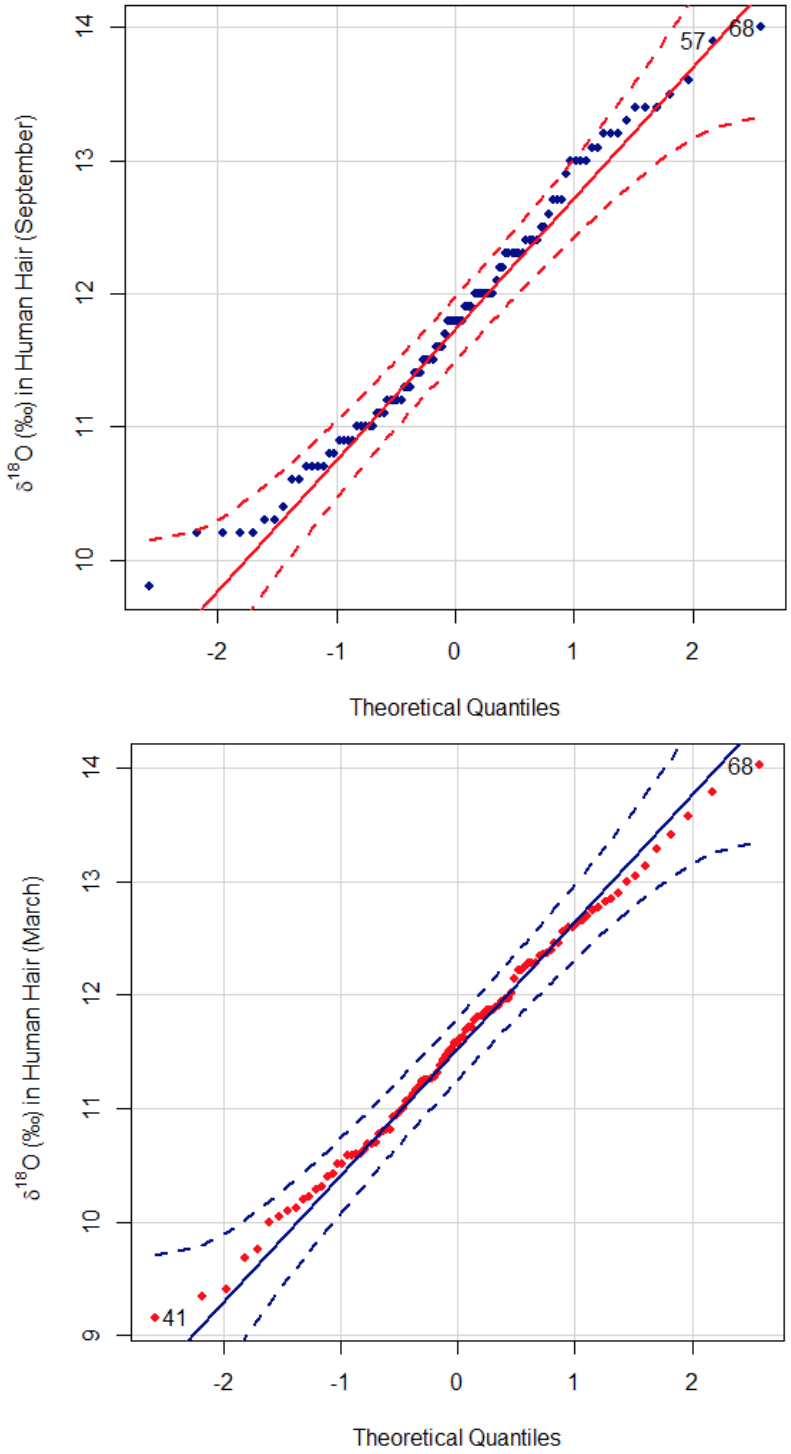

Figure 5.3.3. Quantile-quantile plot (QQ plot) showing the correlation between the given samples and the normal distribution. A 45-degree reference line is also plotted.

A total of 23 samples from the March 2020 dataset showed lower isotopic values than the previously analyses from September 2019 (marked in blue in Supporting Information 1). Three samples reported higher isotopic values (marked in orange in Supporting Information 1). The furnace failed after sample 011-002 in the September 2019 dataset. Therefore, 14 of the 23 samples that showed lower isotopic values in the re-run were reported before sample 011-002. Only nine samples showed lower isotopic values in the re-run post 011-002. All three samples that reported higher isotopic values in March than in September appeared post 011-002. Overall, 14 of the 26 samples showing higher errors than ±0.5 ‰ appeared in the first third of the samples, while 12 of the 26 samples appeared in the other two thirds.

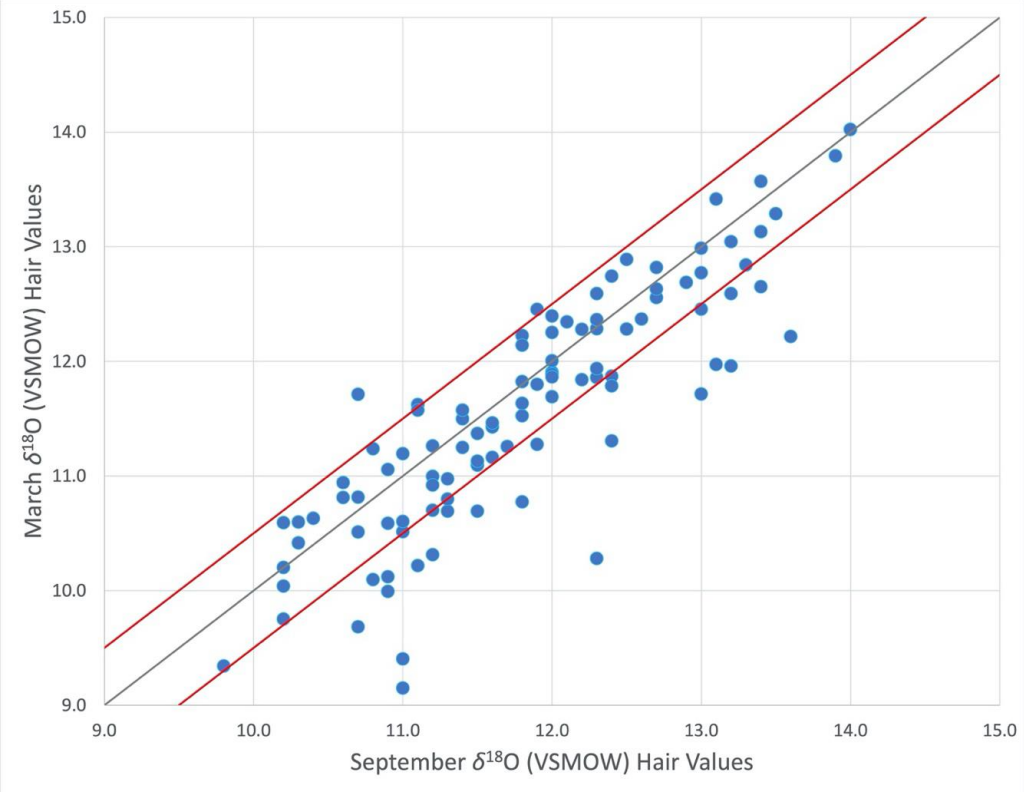

Figure 5.3.4. Comparison of measured δ^{18}O values in human hair from September 2019 and March 2020. The grey line represents the 1:1 line while the red lines represent the ±0.5 ‰ errors.

The δ^{18}O values of the September and the March datasets showed very different strength of correlations to the geographic/environmental and socioeconomic covariates explored in this study. Overall, the correlations were much stronger in the September 2019 dataset, with the exceptions of the two distance to the water covariates, which were stronger in the March 2020 dataset. Interestingly, the September δ^{18}O values showed a moderate correlation ($r = 0.35$, $p < 0.001$) to the respective longitude values while the March δ^{18}O values showed the same moderate correlation with latitude. Elevation and the September δ^{18}O values showed a strong correlation in the Atlantic drainage basin and a weaker one in the Pacific drainage basin. To some extent, this

observation was also made in the March 2020 dataset. While the March dataset did not show any correlation to the precipitation covariates, the September dataset showed moderate correlations. The standard deviation values showed stronger correlations to the geographic/environmental covariates in the March 2020 dataset than in the September 2019 dataset.

Table 5.3.3. Pearson's Correlations between $\delta^{18}O$ isotopic values and geographic/environmental covariates for the March 2020 dataset.

	Longitude September 2019		**Longitude March 2020**	
	r	**p**	**r**	**p**
Oxygen	0.35	< 0.001	0.02	0.87
Oxygen Location Average	0.35	0.05	0.03	0.86
Oxygen Location SD	0.01	0.95	0.27	0.15
Oxygen Atlantic	0.36	0.05	-0.03	0.87
Oxygen Pacific	0.09	0.46	-0.19	0.11
	Latitude September 2019		**Latitude March 2020**	
	r	**p**	**r**	**p**
Oxygen	0.04	0.71	0.35	< 0.001
Oxygen Location Average	0.09	0.63	0.37	0.05
Oxygen Location SD	0.08	0.67	-0.04	0.84
Oxygen Atlantic	-0.16	0.05	0.14	0.44
Oxygen Pacific	0.13	0.29	0.39	< 0.001
	Elevation September 2019		**Elevation March 2020**	
	r	**p**	**r**	**p**
Oxygen	-0.34	< 0.001	-0.28	0.006
Oxygen Location Average	-0.47	0.008	-0.18	0.33
Oxygen Location SD	0.14	0.44	0.52	0.003
Oxygen Atlantic	-0.75	< 0.001	-0.45	0.01
Oxygen Pacific	-0.14	0.26	-0.18	0.15
	Temperature September 2019		**Temperature March 2020**	
	r	**p**	**r**	**p**
Oxygen	0.22	0.03	0.00	0.96
Oxygen Location Average	0.26	0.17	-0.10	0.58
Oxygen Location SD	-0.04	0.84	-0.31	0.10
Oxygen Atlantic	0.09	0.48	0.20	0.28
Oxygen Pacific	-0.14	0.26	-0.07	0.58
	Three-year precipitation September 2019		**Three-year precipitation March 2020**	
	r	**p**	**r**	**p**
Oxygen	0.32	0.001	0.01	0.91
Oxygen Location Average	0.32	0.09	-0.002	0.99
Oxygen Location SD	-0.09	0.64	-0.06	0.74
Oxygen Atlantic	0.39	0.03	0.07	0.69
Oxygen Pacific	0.21	0.09	-0.10	0.39

	One-year precipitation September 2019		One-year precipitation March 2020	
	r	**p**	**r**	**p**
Oxygen	0.29	0.003	0.08	0.45
Oxygen Location Average	0.29	0.12	0.06	0.75
Oxygen Location SD	-0.07	0.71	-0.16	0.39
Oxygen Atlantic	0.34	0.06	0.17	0.36
Oxygen Pacific	0.16	0.20	-0.02	0.84
	Distance to ocean September 2019		**Distance to ocean March 2020**	
	r	**p**	**r**	**p**
Oxygen	-0.02	0.86	0.09	0.36
Oxygen Location Average	-0.07	0.71	0.22	0.25
Oxygen Location SD	0.51	0.004	0.40	0.03
Oxygen Atlantic	-0.45	0.01	-0.08	0.66
Oxygen Pacific	0.11	0.39	0.12	0.34
	Distance to ocean excluding gulf September 2019		**Distance to ocean excluding gulf March 2020**	
	r	**p**	**r**	**p**
Oxygen	0.10	0.32	0.24	0.02
Oxygen Location Average	0.08	0.68	0.36	0.05
Oxygen Location SD	0.40	0.03	0.27	0.14
Oxygen Atlantic	-0.45	0.01	-0.08	0.66
Oxygen Pacific	0.34	0.005	0.38	0.001

The socioeconomic covariates explored in this study did not perform strongly for both datasets. The strongest correlation was produced by HDI ($r = 0.25$, $p = 0.01$) in the March dataset. Interestingly, the September $\delta^{18}O$ data set values did not correlate to the same covariate ($r = 0.03$, $p = 0.79$). The percentage of the population living in poverty showed opposing correlations in the Atlantic and the Pacific drainage basin. The percentage of the population living in poverty covariate showed opposing correlations for the two drainage basins. This observation was made for both datasets, although somewhat shifted.

Table 5.3.4. Pearson's Correlations between $\delta^{18}O$ isotopic values and socioeconomic covariates.

	Population Size September 2019		**Population Size March 2020**	
	r	**p**	**r**	**p**
Oxygen	-0.15	0.14	-0.15	0.14
Oxygen Location Average	-0.23	0.22	-0.12	0.55
Oxygen Location SD	-0.17	0.37	-0.21	0.26
Oxygen Atlantic	-0.13	0.50	-0.22	0.24
Oxygen Pacific	-0.15	0.22	-0.11	0.38
	% of population living in poverty September 2019		**% of population living in poverty March 2020**	
	r	**p**	**r**	**p**
Oxygen	-0.01	0.88	-0.19	0.06
Oxygen Location Average	-0.02	0.90	-0.21	0.28
Oxygen Location SD	-0.27	0.15	-0.27	0.14
Oxygen Atlantic	0.24	0.19	0.12	0.53
Oxygen Pacific	-0.10	0.40	-0.30	0.01
	# of people living in poverty September 2019		**# of people living in poverty March 2020**	
	r	**p**	**r**	**p**
Oxygen	0.19	0.05	0.04	0.69
Oxygen Location Average	0.18	0.33	-0.004	0.98
Oxygen Location SD	-0.04	0.82	-0.15	0.43
Oxygen Atlantic	0.36	0.05	0.35	0.06
Oxygen Pacific	0.12	0.32	-0.13	0.29
	HDI September 2019		**HDI March 2020**	
	r	**p**	**r**	**p**
Oxygen	0.03	0.79	0.25	0.01
Oxygen Location Average	0.09	0.65	0.30	0.11
Oxygen Location SD	0.21	0.27	0.12	0.54
Oxygen Atlantic	-0.07	0.72	0.01	0.96
Oxygen Pacific	0.04	0.73	0.32	0.01
	% of population being of indigenous ancestry September 2019		**% of population being of indigenous ancestry March 2020**	
	r	**p**	**r**	**p**
Oxygen	0.13	0.19	-0.13	0.19
Oxygen Location Average	0.12	0.52	-0.21	0.27
Oxygen Location SD	-0.34	0.06	-0.04	0.84
Oxygen Atlantic	0.07	0.69	-0.18	0.34
Oxygen Pacific	0.11	0.38	-0.16	0.20
	% of population speaking an indigenous language September 2019		**% of population speaking an indigenous language March 2020**	
	r	**p**	**r**	**p**
Oxygen	0.15	0.14	-0.07	0.48
Oxygen Location Average	0.15	0.42	-0.12	0.53
Oxygen Location SD	-0.36	0.05	-0.08	0.67
Oxygen Atlantic	-0.02	0.93	-0.17	0.35
Oxygen Pacific	0.18	0.15	-0.07	0.57

Spatial Autocorrelation

September 2019

The Moran's Index was 0.537 (Z-score= 1.9, p = 0.06) for $\delta^{18}O$ in human hair from Mexico. When plotting the predicted versus measured values for all sample values, the root-mean-square error was: RMSE = 0.99.

March 2020

The Moran's Index was 0.332 (Z-score= 1.2, p = 0.24) for $\delta^{18}O$ in human hair from Mexico. When plotting the predicted versus measured values for all sample values, the root-mean-square error was: RMSE = 0.77.

Isoscape September 2019

The large-scale spatial distribution and patterns of $\delta^{18}O$ in Mexican human hair from the September 2019 analyses are depicted in Figure 5.3.5. The highest values were found along the coast of the Gulf of Mexico, the Yucatan peninsula and Chiapas in the south, and Coahuila in the north of the country. The lowest respective values were found in the areas of higher elevation, specifically along Central Mexican Plateau (also known as the Mexican Altiplano-Mesa Central) and the Sierra Madre del Sur range.

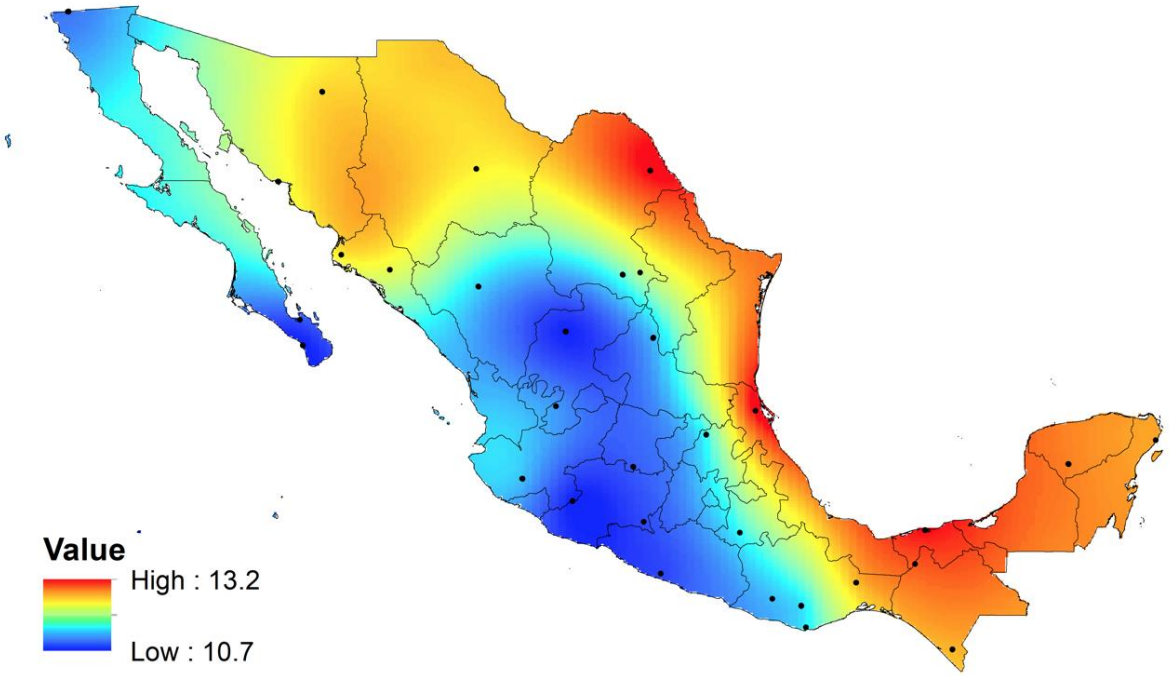

Figure 5.3.5. Prediction map showing estimated isotope ratios for $\delta^{18}O$ for Mexican human hair from the September 2019 analysis. The values are reported in ‰ and relative to the VSMOW standard.

Isoscape March 2020

The large-scale spatial distribution and patterns of $\delta^{18}O$ in Mexican human hair from the March 2020 analyses are depicted in Figure 5.3.6. The highest isotopic values were found in the regions of lowest elevation, primarily the north of Mexico (states of Coahuila and Chihuahua), along the Caribbean and the coast of the Gulf of Mexico, and the Yucatan peninsula (Figure 5.3.6 red to yellow areas of interpolation). The lower and intermediate values are primarily found in the southwest of the country and areas defined by higher elevations that are generally more inland. Geographically, these areas are dominated by the Pacific Ocean coast, the southern part of the Central Mexican Plateau (also known as the Mexican Altiplano-Mesa Central), and the Sierra Madre del Sur range. Baja California also showed low $\delta^{18}O$ values.

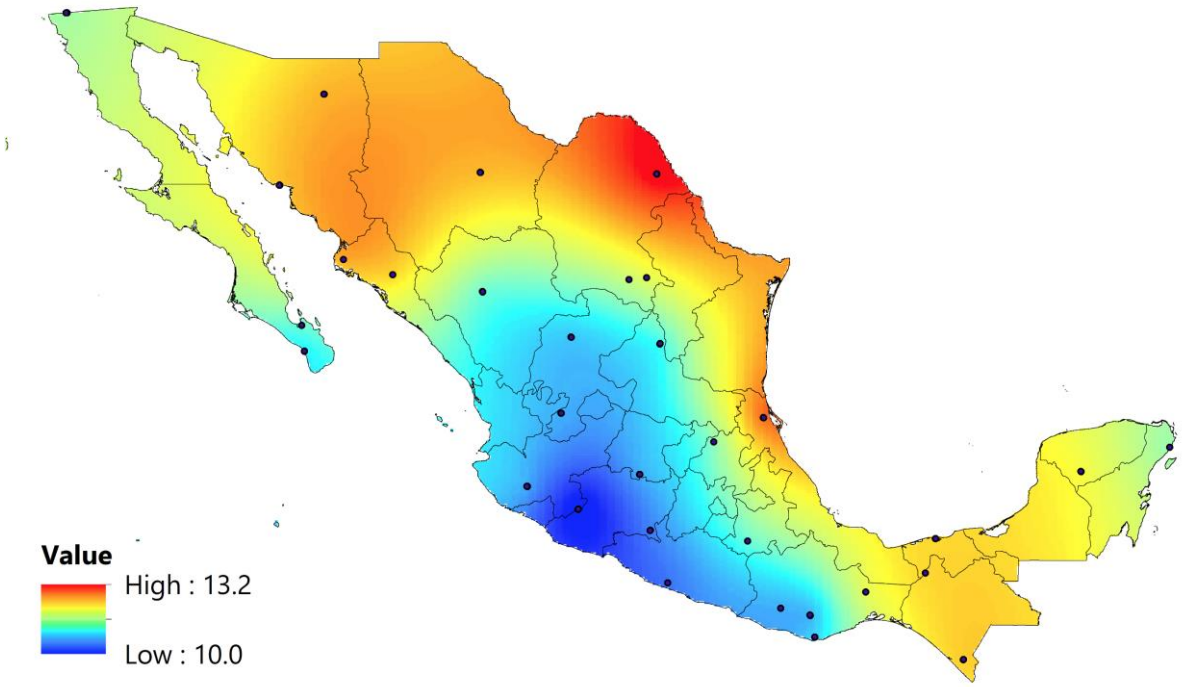

Figure 5.3.6. Prediction map showing estimated isotope ratios for $\delta^{18}O$ for Mexican human hair from the March 2020 analysis. The values are reported in ‰ and relative to the VSMOW standard.

5.3.4. Discussion

As explained in greater detail earlier in the chapter, two datasets were presented due to a hardware malfunction during the first run. Both datasets were normally distributed and passed quality control checks. However, the values of the initial dataset recorded after the technical issue appeared to be slightly elevated when compared to the values of the second run. Another issue that arose during the analyses of the second dataset was the fact that the laboratory protocol does not include analysis of international hair standards alongside the Mexican human hair samples to allow for quality control checks.

Because the only indication to choose the March 2020 dataset over the September 2019 dataset is the fact that there is knowledge of a furnace failure, it was decided to present the results of both datasets here in this chapter. While some aspects of the datasets will be discussed here, third run is compulsory to ensure the values are valid and representative of the Mexican population.

Figures 5.3.7 and 5.3.8 depict the prediction error maps of the previously presented isoscapes (Figures 5.3.5 and 5.3.6). The errors ranged from the 0.2 to 1.2‰ in the September 2019 dataset while the March 2019 showed a much larger range of prediction errors. The errors were as high as 3.5‰, which are especially very large considering the range of recorded human hair $\delta^{18}O$ values was only 4.9 ‰ in this dataset (Table 5.3.2). Here, the prediction errors are high across the entire nation and predictions are only reliable in the sampling areas and close by. The areas of the highest errors are the areas which are under-sampled, such as the states of Tamaulipas, Baja California, and Baja California Sur. The same areas are also seen to have higher errors in the September 2019 dataset.

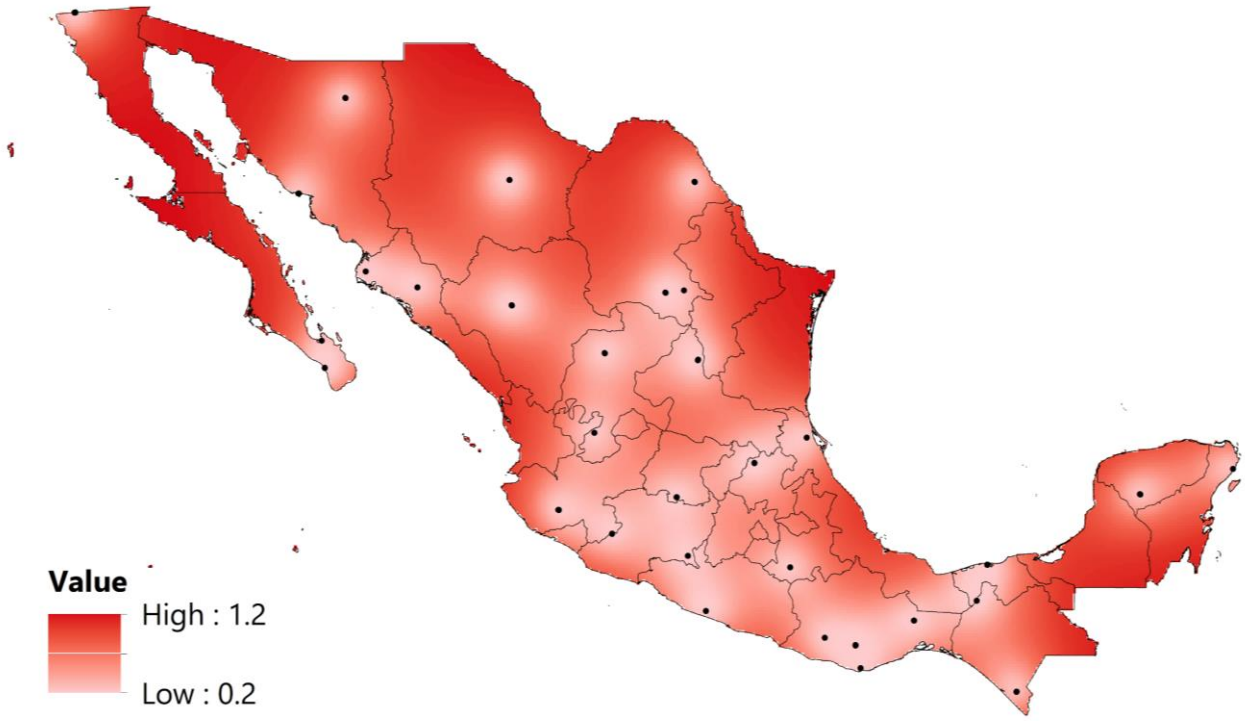

Figure 5.3.7. Prediction standard error output for the September 2019 $\delta^{18}O$ human hair isoscape (Figure 5.3.5).

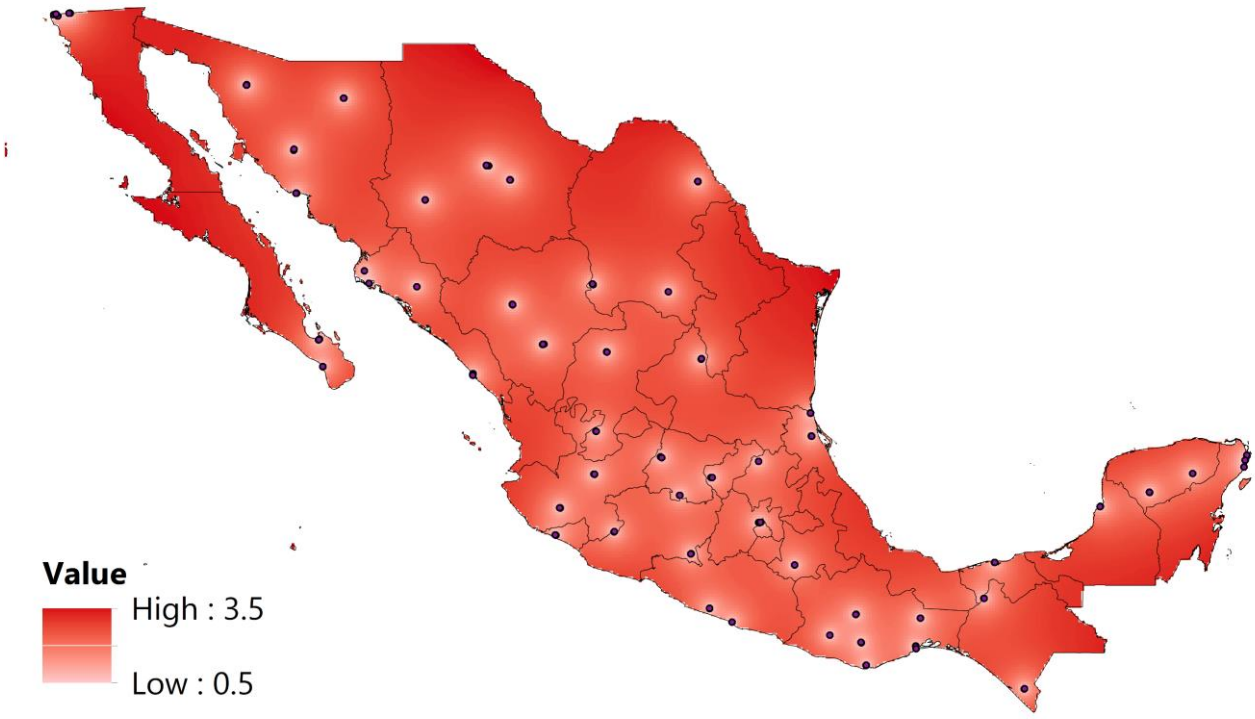

Figure 5.3.8. Prediction standard error output for the March 2020 δ^{18}O human hair isoscape (Figure 5.3.6).

As mentioned above the Moran's Index was 0.537 (Z-score= 1.9, p = 0.06) for September 2019 δ^{18}O in human hair from Mexico. Given the z-score of 1.9, there is a less than 10% likelihood that this clustered pattern could be the result of random chance. When plotting the predicted versus measured values for all sample values, the root-mean-square error was: RMSE = 0.99. The values of the RMSE should be close to one if the prediction standard errors are valid. Here, it can be concluded that the prediction errors are indeed valid and that the δ^{18}O values are clustered without a high likelihood of random chance.

For the March 2020 dataset, the Moran's Index was 0.332 (Z-score= 1.2, p = 0.24) for the δ^{18}O values. Given the z-score of 1.2, the pattern does not appear to be significantly different than random. The Moran's I correlation coefficient analysis supports above observation as it showed no spatial autocorrelation for the δ^{18}O in Mexican human hair. When plotting the predicted versus measured values for all sample values, the root-mean-square error was: RMSE = 0.77. Because the RMSE is less than one, it can be concluded that the variability in the predictions is overestimated.

Overall, these observations are very concerning regarding the validity of the data. While it is, in theory, plausible that the March 2020 data is indeed the "true" data, it is unlikely that all spatial autocorrelation analyses perform significantly worse in the later dataset than in the former due to the fact that δ^{18}O values are known to present spatial variability in Mexico's tap water

(Chapter 5.2) as well as in human hair in the neighboring country United States (Ehleringer *et al.* 2008).

Comparison to Mexican Tap Water

The basic descriptive statistics of the $\delta^{18}O$ tap water values can be found in Table 5.3.5. Unsurprisingly, the samples from the locations from where also hair samples were collected showed a smaller range than the entire sample set, which was presented in Chapter 5.2).

Table 5.3.5. Basic descriptive statistics of the $\delta^{18}O$ Tap Water results from the location that hair was collected from.

	$\delta^{18}O$ Tap Water	**$\delta^{18}O$ Tap Water Location Averages**
Minimum	-12.1 ‰	-11.6 ‰
Maximum	-3.2 ‰	-3.2 ‰
Mean	-7.2 ‰	-7.1 ‰
Standard Deviation	2.3 ‰	2.3 ‰
Range	8.9 ‰	8.4 ‰

There are significant differences in correlation between the Mexican human hair $\delta^{18}O$ values and the respective $\delta^{18}O$ tap data values from the same locations for the September 2019 and March 2020 datasets. Figure 5.3.9 and 5.3.10 show the correlations between all data points as well as the correlations for the location averages.

For the March 2020 dataset, the Mexican human hair $\delta^{18}O$ values did not show strong correlations to the respective $\delta^{18}O$ tap data values from the same locations. For all data points, the correlation was the following: $\delta^{18}O$ Tap Water = 1.34 * $\delta^{18}O$ Human Hair -22.6; R^2 = 0.39. Using the location averages, the correlation slightly improved to: $\delta^{18}O$ Tap Water = 1.85 * $\delta^{18}O$ Human Hair -28.6; R^2 = 0.45 (Figure 5.3.10). The correlation of human hair and tap water was significantly better in the earlier (September 2019) dataset. For all data, the correlation was represented by the following equation: $\delta^{18}O$ Tap Water = 1.68 * $\delta^{18}O$ Human Hair -27.1 (R^2 = 0.51). When using the location averages for both sets of values the relationship improved: $\delta^{18}O$ Tap Water = 2.33 * $\delta^{18}O$ Human Hair -34.7 (R^2 = 0.70).

A multitude of $\delta^{18}O$ sources could potentially be incorporated into human hair. An individual hair "dies" once it exits the scalp, thus halting elemental exchange between hair and blood. On average, human hair grows ~1 cm per month and undergoes a life-long cycle of growth, regression, and a resting period. This leads to the biogenic dietary information, which was initially inherited from the blood, being retained in the hair strand. Therefore, hair retains a longitudinal record of isotope signatures (Chau *et al.* 2017; Font *et al.* 2012; Krause and Foitzik 2006).

Furthermore, keratin tissues (*e.g.* hair) are thought to potentially incorporate environmental signatures, such as bathing water or dust (Tipple et al 2018; Chau *et al.* 2017). Since the data from the two datasets both passed the quality insurance test and are normally distributed, it is perplexing how different the strengths of correlation are between the two datasets.

Ehleringer *et al.* (2008) showed that, in the United States, the drinking water explained over 85% of the isotopic variation seen in the human hair samples. While it could be argued that the Mexican population may not drink as much locally sourced water due to contamination issues, this argument is not supported by the analysis of $^{87}Sr/^{86}Sr$ ratios of human hair and tap water from the same locations. As presented in Ammer *et al.* (2020) as well as Chapter 5.4, the $^{87}Sr/^{86}Sr$ ratios of human hair and tap water correlated strongly ($R^2 = 0.87$ for location averages and $R^2 = 0.80$ when using individual data points).

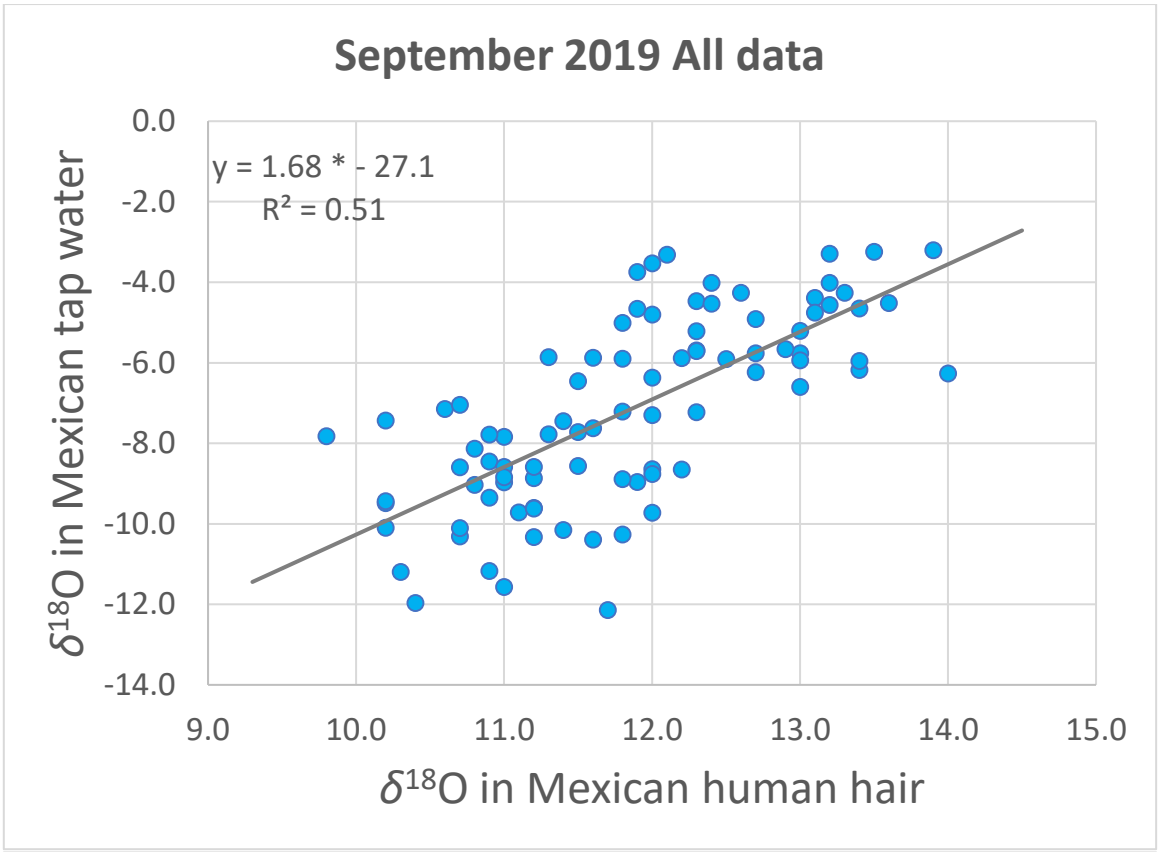

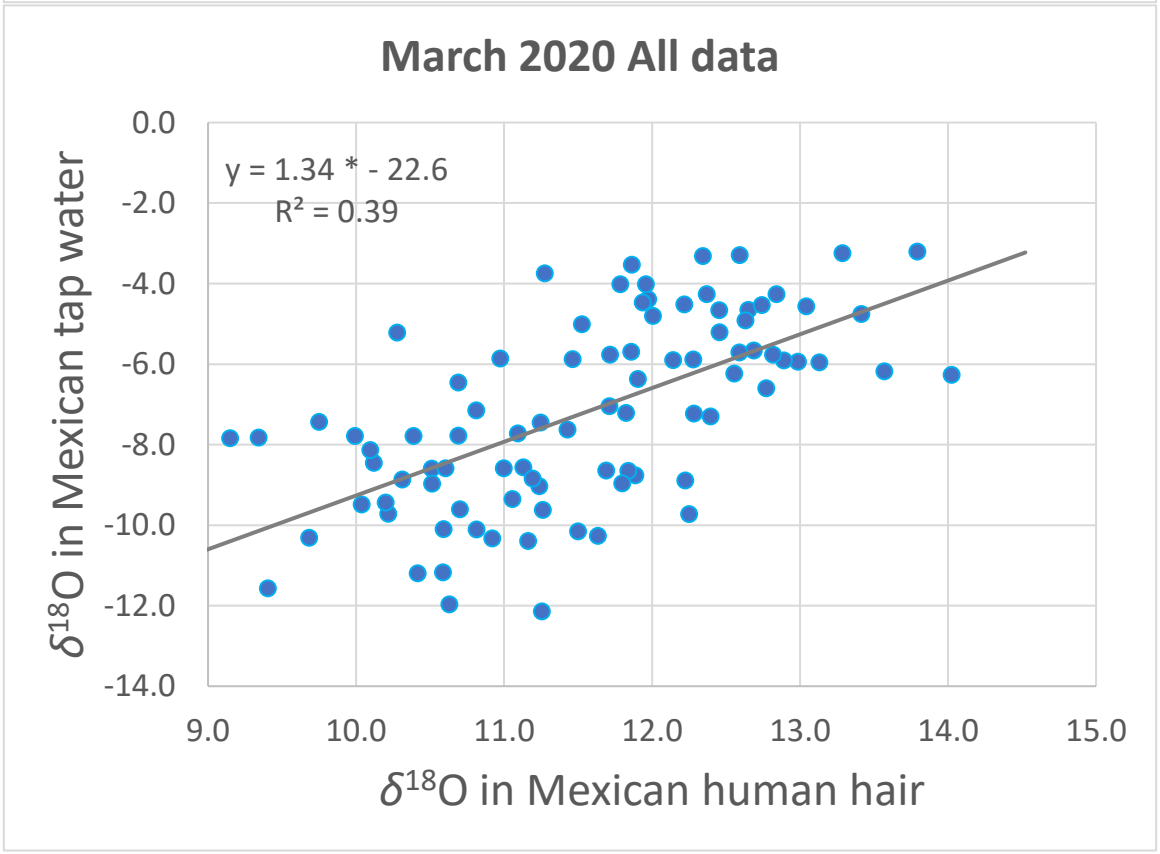

Figure 5.3.9. Relationship of $\delta^{18}O$ values in human hair and tap water for all data collected from the sample locations.
September 2019: all data ($\delta^{18}O$ Tap Water = 1.68 * $\delta^{18}O$ Human Hair -27.1; R^2 = 0.51)
March 2020: all data ($\delta^{18}O$ Tap Water = 1.34 * $\delta^{18}O$ Human Hair -22.6; R^2 = 0.39)

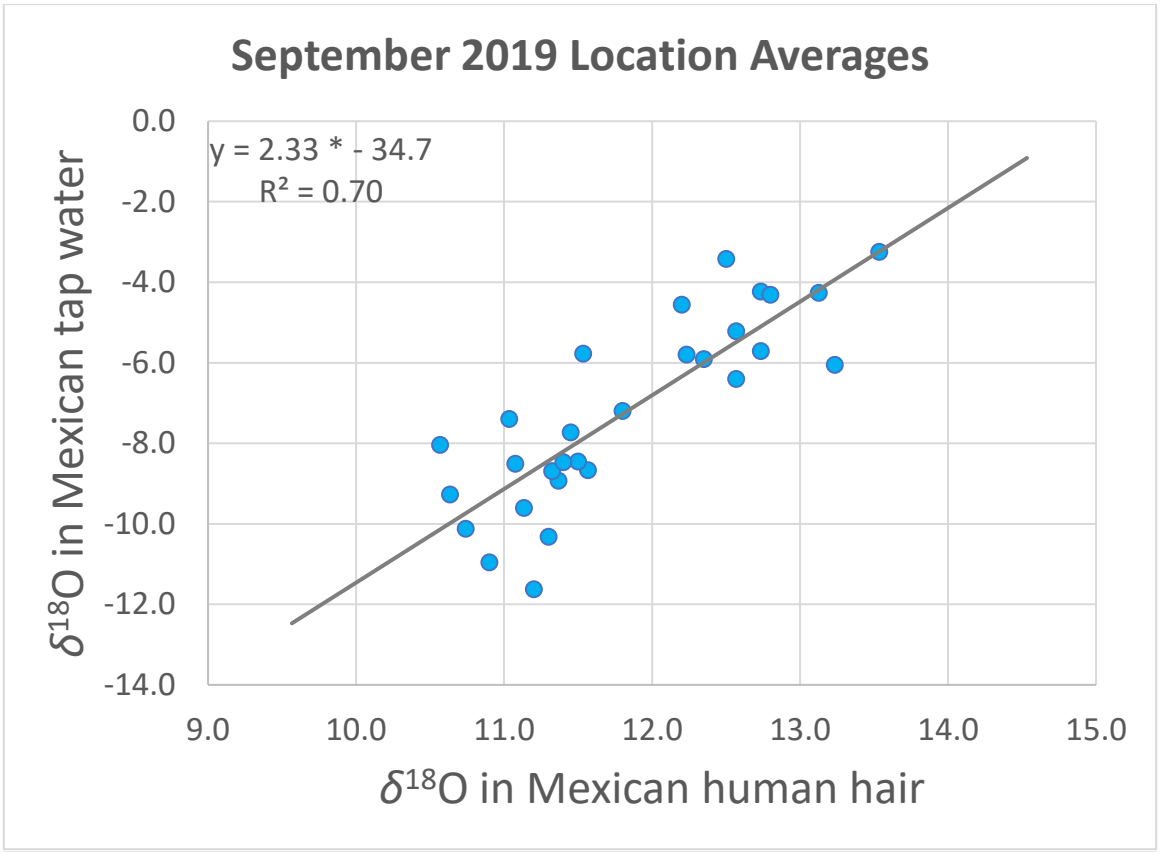

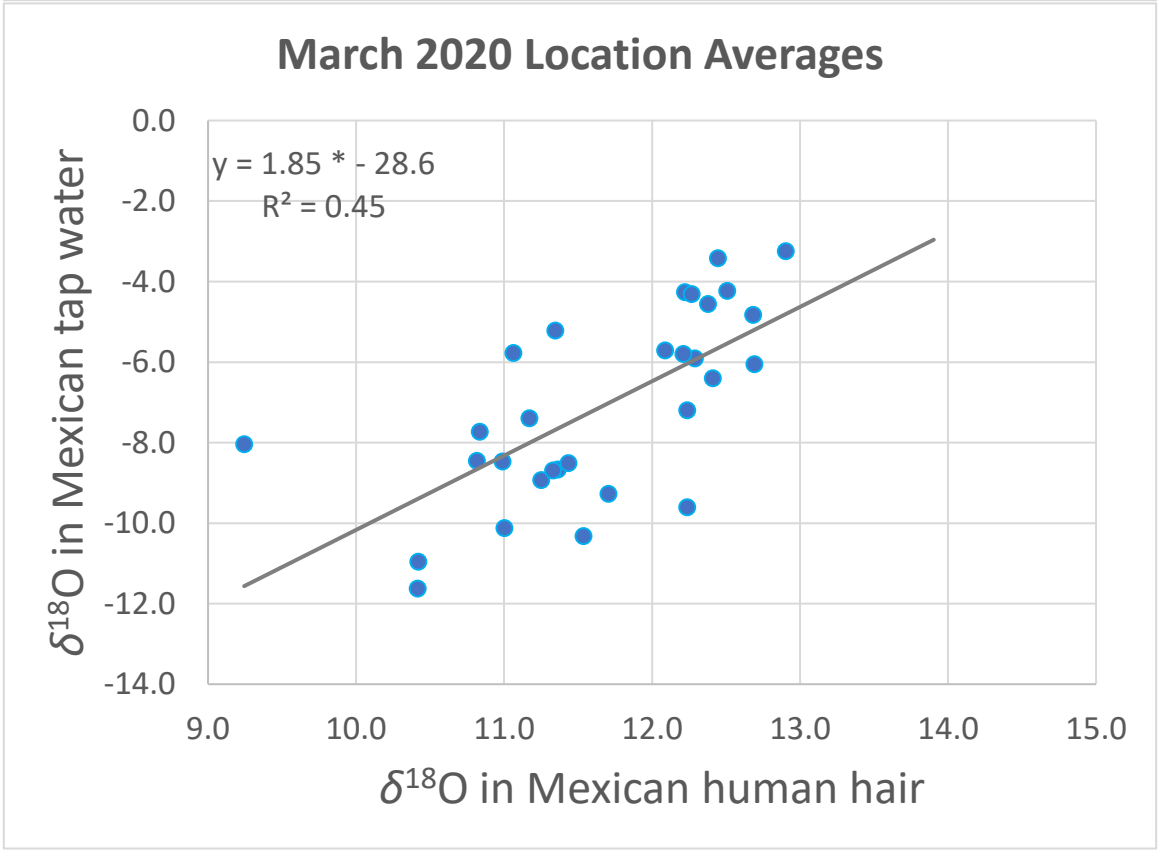

Figure 5.3.10. Relationship of all $\delta^{18}O$ values in human hair and tap water for the location averages collected from the sample locations.
September 2019: location averages ($\delta^{18}O$ Tap Water = 2.33 * $\delta^{18}O$ Human Hair -34.7; R^2 = 0.70)
March 2020: location averages ($\delta^{18}O$ Tap Water = 1.85 * $\delta^{18}O$ Human Hair -28.6; R^2 = 0.45)

The correlations of the tap water to the geographic/environmental as well as socioeconomic covariates were also compared to the correlations of the human hair datasets to the covariates. Here some of the most striking observations are discussed. The correlations of the $\delta^{18}O$ tap water values to the various covariates can be found in Chapter 5.2.

While the tap water correlations showed inverse coefficients from the Atlantic and Pacific drainage basin to longitude and latitude, only the September 2019 latitude correlations showed the same effect. Overall, the Atlantic drainage basin showed a much stronger correlation of the isotopic values with latitude and longitude in the tap water data. This effect was also seen in the September 2019 dataset. The March 2020 dataset, however, showed the Pacific drainage basin to have a stronger relationship.

For the precipitation covariates, both the tap water and the March 2020 data show inverse correlations in the Atlantic and the Pacific drainage basin. This is not the case for the September 2019 dataset. This dataset, however, shows the greater influence of the Atlantic drainage basin, which is also visible in the tap water data. The March 2020 did not show this effect.

The distance to the ocean correlations of the September 2019 dataset are in agreement with the tap water data, which shows significant inverse correlations in the Atlantic and the Pacific drainage basin with the Atlantic drainage basin having a greater effect. The March 2020 dataset showed the Pacific drainage basin to have a greater influence on the overall correlation.

Overall, the September 2019 showed more similarities to the correlation coefficients of the tap water than the March 2020 dataset, which adds to the concerns that there may be further issues with the dataset that need investigating.

While the correlations of the human hair and the tap water $\delta^{18}O$ values are overall not very strong) and the statistics showed a relatively poor performance of the Mexican human hair data in a spatial context (especially for the March 2020 dataset, the similarities in the developed isoscapes are striking (Figure 5.3.11). This observation does not have any statistical significance but shows overall spatial pattern that can observed in Mexico.

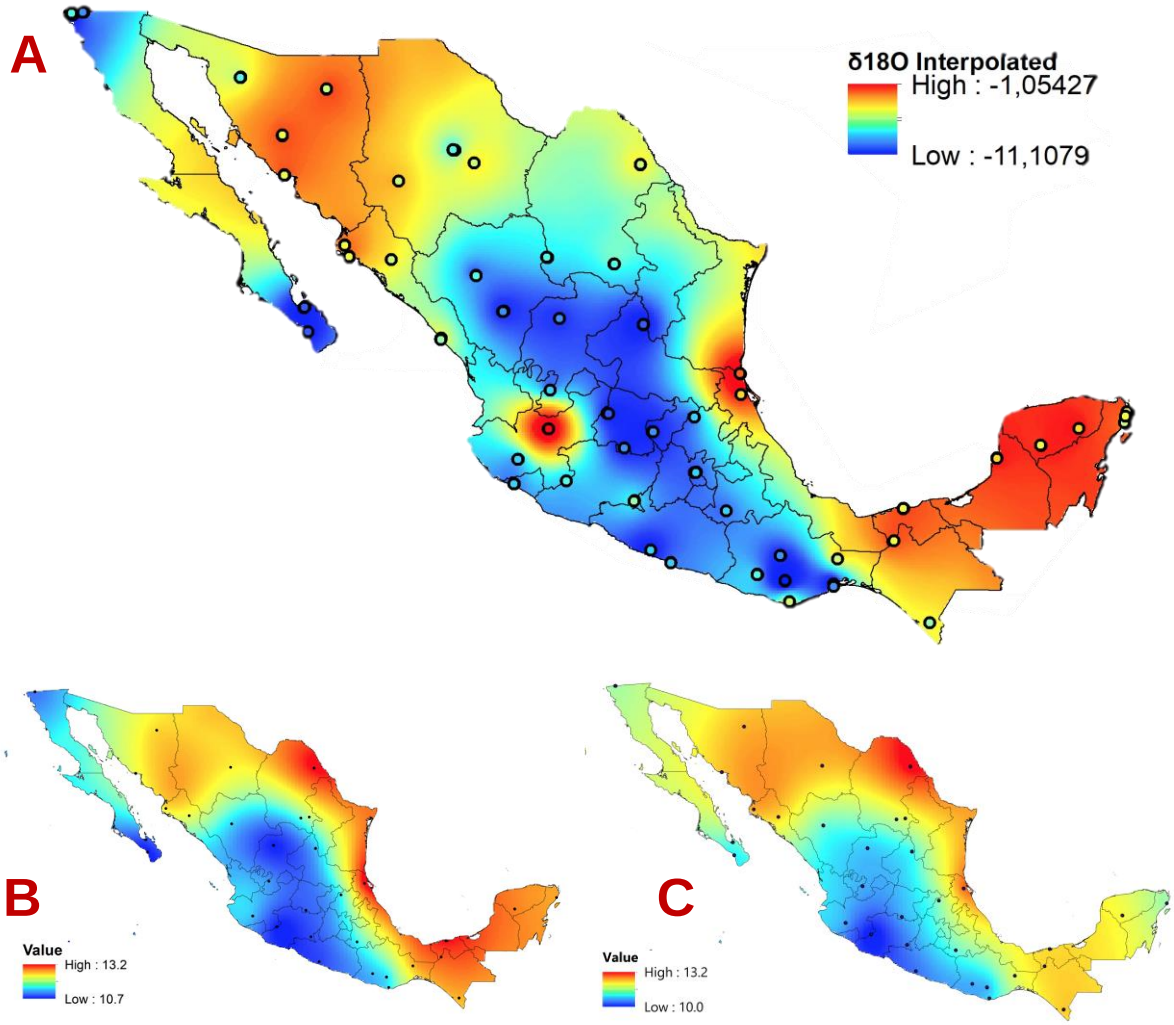

Figure 5.3.11. Tap water and human hair $\delta^{18}O$ isoscapes for comparison of spatial patterns (reproduced from Figure 5.3.7 of Chapter 5.2 and Figures 5.3.5/5.3.6 of this chapter).
A: Tap water $\delta^{18}O$ isoscape
B: Human hair $\delta^{18}O$ isoscape September 2019
C: Human hair $\delta^{18}O$ isoscape March 2020

It is very concerning that both datasets have passed the quality control checks and seem relatively similar yet result in very different values and correlations with the chosen geographic/environmental and socioeconomic covariates. The issue that arose during these analyses shows that all scientific analyses and isotopic values need to be analyzed and interpreted with extreme caution to avoid incorrect conclusions. As isotopic analyses in forensic sciences and especially on forensic human remains, which includes human hair, is still relatively new, it is unavoidable to further investigate this issue and draw conclusions as to where the sample preparation, analyses, and interpretation needs advancing.

5.3.5. Conclusion

In this chapter, the results of the $\delta^{18}O$ isotopic analyses in Mexican human hair were presented and the arising issues were discussed. It is only known that there was a furnace issue during the first run, yet it is unknown if there may have been other issues during the second sample run. For this reason, the second sample run should be used and taken as the true representative of the $\delta^{18}O$ values in Mexican human hair. However, it is very concerning that all statistical and geostatistical tools employed here (and employed for all other isotope systems) performed poorer in the newer March 2020 dataset than in the September 2019 dataset.

Unfortunately, it is not possible to draw definitive conclusions for the $\delta^{18}O$ analyses of Mexican human hair now. Ideally, the analyses will be repeated at an independent laboratory to validate which dataset shows validity and is representative of the Mexican population. Furthermore, it needs to be ensured that all possible and sensible standards are used to ensure that the values hold up the international standards and quality insurance.

Supporting Information 1. Results of the $\delta^{18}O$ (VSMOW) analyses of Mexican human hair from September 2019 and March 2020.

Sample ID	Location	September δ18O (VSMOW) Hair	March δ18O (VSMOW) Hair	Difference
001-001	Puerto Morelos, Quintana Roo	12.30	10.28	2.02
001-002	Puerto Morelos, Quintana Roo	13.00	12.45	0.55
001-003	Puerto Morelos, Quintana Roo	12.40	11.31	1.09
002-001	Tekax de Álvaro Obregón, Yucatan	11.90	11.27	0.63
002-002	Tekax de Álvaro Obregón, Yucatan	13.10	11.97	1.13
002-003	Tekax de Álvaro Obregón, Yucatan	13.20	13.04	0.16
003-001	Paraíso, Tabasco	13.60	12.22	1.38
003-002	Paraíso, Tabasco	13.20	11.96	1.24
003-003	Paraíso, Tabasco	13.30	12.84	0.46
003-004	Paraíso, Tabasco	12.40	11.87	0.53
004-001	Plan de Ayala, Chiapas	12.40	11.78	0.62
004-002	Plan de Ayala, Chiapas	12.60	12.37	0.23
004-003	Plan de Ayala, Chiapas	13.40	12.65	0.75
005-001	Huixtla, Chiapas	12.70	12.55	0.15
005-002	Huixtla, Chiapas	12.00	11.90	0.10
005-003	Huixtla, Chiapas	13.00	12.77	0.23
006-001	San Juan Guichicovi, Oaxaca	13.00	11.71	1.29
006-002	San Juan Guichicovi, Oaxaca	12.30	11.86	0.44
006-003	San Juan Guichicovi, Oaxaca	12.90	12.69	0.21
007-001	San Pedro Pochutla, Oaxaca	11.30	10.97	0.33
007-002	San Pedro Pochutla, Oaxaca	11.50	10.69	0.81
007-003	San Pedro Pochutla, Oaxaca	11.80	11.52	0.28
008-001	Miahuatlán de Porfirio Díaz, Oaxaca	11.70	11.25	0.45
008-002	Miahuatlán de Porfirio Díaz, Oaxaca	11.00	9.40	1.60
008-003	Miahuatlán de Porfirio Díaz, Oaxaca	10.90	10.59	0.31
009-001	San Jacinto Tlacotepec, Oaxaca	11.30	10.69	0.61
009-002	San Jacinto Tlacotepec, Oaxaca		10.39	
009-003	San Jacinto Tlacotepec, Oaxaca	11.60	11.43	0.17
010-001	Tehuitzingo, Puebla	10.70	10.51	0.19
010-002	Tehuitzingo, Puebla	12.00	11.69	0.31
010-003	Tehuitzingo, Puebla	12.00	11.89	0.11
011-001	Atoyac de Álvarez, Guerrero	10.30	10.42	-0.12
011-002	Atoyac de Álvarez, Guerrero	10.40	10.63	-0.23
011-003	Atoyac de Álvarez, Guerrero	11.10	10.22	0.88
011-004	Atoyac de Álvarez, Guerrero	11.80	10.77	1.03
012-001	Huetamo de Núñez, Michoacán	11.50	11.09	0.41
012-002	Huetamo de Núñez, Michoacán	10.20	9.75	0.45
012-003	Huetamo de Núñez, Michoacán	11.40	11.25	0.15
013-001	Tepalcatepec, Michoacán	10.90	10.12	0.78
013-002	Tepalcatepec, Michoacán	11.00	9.15	1.85
013-003	Tepalcatepec, Michoacán	9.80	9.34	0.46

014-001	El Grullo, Jalisco	11.50	11.13	0.37
014-002	El Grullo, Jalisco	12.20	11.84	0.36
014-003	El Grullo, Jalisco	10.80	10.09	0.71
015-001	Tlaltenango de Sánchez Román, Zacatecas	11.00	10.51	0.49
015-002	Tlaltenango de Sánchez Román, Zacatecas	11.90	11.80	0.10
015-003	Tlaltenango de Sánchez Román, Zacatecas	11.20	10.31	0.89
016-001	Moroleón, Guanajuato	11.20	10.70	0.50
016-002	Moroleón, Guanajuato	12.00	12.25	-0.25
016-003	Moroleón, Guanajuato	10.20	10.04	0.16
017-001	Jacala, Hidalgo	11.80	12.22	-0.42
017-002	Jacala, Hidalgo	11.20	11.00	0.20
017-003	Jacala, Hidalgo	11.00	10.60	0.40
017-004	Jacala, Hidalgo	11.30	10.80	0.50
018-001	Ozuluama de Mascareñas, Veracruz	13.20	12.59	0.61
018-002	Ozuluama de Mascareñas, Veracruz	13.90	13.79	0.11
018-003	Ozuluama de Mascareñas, Veracruz	13.50	13.29	0.21
019-001	Matehuala, San Luis Potosi	11.80	11.63	0.17
019-002	Matehuala, San Luis Potosi	10.70	9.68	1.02
019-003	Matehuala, San Luis Potosi	11.60	11.16	0.44
019-004	Matehuala, San Luis Potosi	11.10	11.62	-0.52
020-001	General Capeda, Coahuila	11.80	11.82	-0.02
020-002	General Capeda, Coahuila	10.60	10.81	-0.21
020-003	General Capeda, Coahuila	12.30	12.28	0.02
020-004	Saltillo, Coahuila	12.50	12.28	0.22
021-001	Villa Unión, Coahuila	13.40	13.57	-0.17
021-002	Villa Unión, Coahuila	14.00	14.02	-0.02
021-003	Villa Unión, Coahuila	12.30	12.59	-0.29
022-001	Pedro Meoqui, Chihuahua	11.60	11.46	0.14
022-002	Pedro Meoqui, Chihuahua	13.00	12.99	0.01
022-003	Pedro Meoqui, Chihuahua	12.50	12.89	-0.39
022-004	Pedro Meoqui, Chihuahua	12.30	12.36	-0.06
023-001	Santiago Papasquiaro, Durango	11.20	10.92	0.28
023-002	Santiago Papasquiaro, Durango	10.90	9.99	0.91
023-003	Santiago Papasquiaro, Durango	12.00	12.39	-0.39
023-004	Santiago Papasquiaro, Durango	11.50	11.37	0.13
024-001	Río Grande, Zacatecas	10.20	10.20	0.00
024-002	Río Grande, Zacatecas	10.80	11.24	-0.44
024-003	Río Grande, Zacatecas	10.90	11.06	-0.16
025-001	El Salto, Sinaloa	12.70	12.82	-0.12
025-002	El Salto, Sinaloa	11.80	12.14	-0.34
025-003	El Salto, Sinaloa	12.20	12.28	-0.08
026-001	Villa de Ahome, Sinaloa	12.70	12.63	0.07
026-002	Villa de Ahome, Sinaloa	12.00	12.01	-0.01

026-003	Villa de Ahome, Sinaloa	13.10	13.41	-0.31
027-001	Todos Los Santos, Baja California Sur	10.20	10.59	-0.39
027-002	Todos Los Santos, Baja California Sur	10.70	10.81	-0.11
027-003	Todos Los Santos, Baja California Sur	11.40	11.50	-0.10
027-004	Todos Los Santos, Baja California Sur	11.10	11.57	-0.47
027-005	Todos Los Santos, Baja California Sur	10.30	10.60	-0.30
027-006	La Paz, Baja California Sur	10.60	10.94	-0.34
028-001	Guaymas, Sonora	12.30	11.94	0.36
028-002	Guaymas, Sonora	12.40	12.74	-0.34
028-003	Guaymas, Sonora	11.90	12.45	-0.55
029-001	Nacozari de García, Sonora	12.00	11.86	0.14
029-002	Nacozari de García, Sonora	12.10	12.34	-0.24
029-003	Nacozari de García, Sonora	13.40	13.13	0.27
030-001	Tecate, Baja California	10.70	11.71	-1.01
030-002	Tecate, Baja California	11.00	11.19	-0.19
030-003	Tecate, Baja California	11.20	11.26	-0.06
030-004	Tecate, Baja California	11.40	11.57	-0.17

5. 4. Comparison of strontium isotope ratios in Mexican human hair and tap water as provenance indicators

Paper published in Forensic Science International
Digital Object Identifier:
doi: 10.1016/j.forsciint.2020.110422

Authors:
Saskia T. M. Ammer,[1] M.Sc.; Lisette Kootker, Ph.D. [2]; Eric J. Bartelink,[3] Ph.D.; Bruce E. Anderson,[4] Ph.D.; Eugénia M. Cunha,[1] Ph.D.; Gareth Davies, Ph.D. [2]

Affiliations:
[1] University of Coimbra, Laboratory of Forensic Anthropology, Department of Life Sciences Calçada Martim de Freitas, Coimbra, PT 3000-456
[2] Vrije Universiteit Amsterdam, Faculty of Science, Geology & Geochemistry cluster, de Boelelaan 1085, 1081 HV Amsterdam, the Netherlands
[3] Department of Anthropology, California State University, Chico, Chico, CA.
[4] Pima County Office of the Medical Examiner, 2825 E District St, Tucson, AZ 85714.

Highlights:

- $^{87}Sr/^{86}Sr$ of 101 human hair and 151 tap water samples are reported from across Mexico
- $^{87}Sr/^{86}Sr$ ratios range between 0.70424 and 0.71613 ($\Delta Sr_{max–min}$ = 0.01189) in Mexican human hair samples
- $^{87}Sr/^{86}Sr$ ratios range between 0.70404 and 0.71385 ($\Delta Sr_{max–min}$ = 0.00981) in Mexican tap water samples
- A strong correlation (R^2= 0.80) is observed between $^{87}Sr/^{86}Sr$ of human hair and tap water data and location averages have a stronger correlation (R^2= 0.87)
- These data provide the basis for provenance studies in forensic anthropology

Abstract:

Deceased undocumented border crossers are some of the most difficult individuals to identify due to the inability to narrow down the region of origin and therefore to obtain family reference samples for DNA comparison. The isotopic compositions of various body tissues have been demonstrated to be useful biomarkers for tracking locations and movements to aid in the identification of human remains. This study closes the large spatial gap of available $^{87}Sr/^{86}Sr$ ratios from North America in tap water and presents the first $^{87}Sr/^{86}Sr$ human tissue-based ratios from Mexico. The 101 hair samples from 32 locations in Mexico range in $^{87}Sr/^{86}Sr$ ratios from 0.70424 to 0.71613 ($\Delta Sr_{max–min}$ =0.01189). Furthermore, 151 tap water samples from 51 locations range between 0.70404 to 0.71385 ($\Delta Sr_{max–min}$ = 0.00981). Overall, small variations in the hair and tap water samples collected from individual locations were recorded ($\Delta Sr_{max–min}$ = 0.00041 and 0.00034 respectively). Despite the fact that Mexico is one of the largest bottled water consumers in the world, the $^{87}Sr/^{86}Sr$ ratios of human hair and tap water correlated strongly (R^2 = 0.87 for location averages and R^2 = 0.80 when using individual data points). These data represent a valuable resource for identifying the provenance of human remains.

KEYWORDS: $^{87}Sr/^{86}Sr$, isotope ratio analysis, forensic provenancing, tap water, modern human hair, Mexico

5.4.1. Introduction

Migratory and refugee movements have become major humanitarian crises around the world. Over 7000 individuals have perished along the Mexico - United States border since 1998 and the numbers continue to rise (Colibrí Center for Human Rights 2018; Humane Borders Inc. 2020). Many of the undocumented border crosser remains found, especially those recovered in Arizona, originated from Mexico (Martinez *et al.* 2015; Anderson and Parks 2008; Massey, Durand, and Malone 2002). Undocumented border crossers are difficult to identify and many remain unidentified forever. One of the issues associated with the lack of identification is the inability to narrow down the region of origin and therefore identify family members in order to obtain reference samples for DNA comparison.

Due to the fact that human tissues reflect the intake of biologically available strontium (Sr) during the time of formation, strontium isotopes can be used for migration studies and region of origin predictions (Bartelink and Chesson 2019; Rauch *et al.* 2007). Strontium isotopes have been used for studies in archaeology, past conflicts and animal migration in various regions of the world, including Africa (Sillen, Hall, and Armstrong 1995; Sealy *et al.* 1991), Asia (Regan 2006), the Americas (Wright 2012; Price *et al.* 2015; Laffoon *et al.* 2017; Knudson *et al.* 2005; Ezzo, Johnson, and Price 1997), and Europe (Kootker *et al.* 2016; Bentley and Knipper 2005; Schweissing and Grupe 2003). More recently, the field of forensic anthropology has discovered the usefulness of strontium isotope ratios to provenance unidentified individuals from various contexts, such as forensic casework and undocumented border crossers found along the United States border (Bartelink *et al.* 2018; Lehn and Graw 2016; Font *et al.* 2015). Isotope analysis cannot be used to identify an individual's exact location of origin, but can add critical information to the identification process. Isotope analysis to narrow down geographic origins of unknown individuals is most useful when combining several isotope systems, such as the use of oxygen and strontium in combination (Font *et al.* 2015).

To date, limited isotopic research has been conducted into bioavailable elements in modern Mexican environments, large scale efforts thus far only focused on the oxygen, hydrogen and deuterium excess in ground and tap water (Wassenaar *et al.* 2009, Ammer in prep). Some spatially limited archaeological studies have explored lead and strontium isotopes for monitoring ancient human migration (Sharpe *et al.* 2016; Hodell *et al.* 2004). The limited available data is a major concern when trying to answer research questions from various fields, such as forensic anthropology, archaeology, hydrology and food forensics. As an initial contribution to addressing this deficiency, this study reports $^{87}Sr/^{86}Sr$ ratio in the environment as determined in human hair and tap water from Mexico.

As Mexico is known to be one of the highest bottled water consumer in the world (Contreras 2019; Inter-American Development Bank 2011), this study will also aim to examine the impact on $^{87}Sr/^{86}Sr$ ratios of high tap water intake into the human body. Bottled water in the United States is often of local origin and hence has oxygen (O) and hydrogen (H) isotope signatures very similar to the local waters (Bowen *et al.* 2005). A similar relationship is expected for Mexican bottled waters but is not yet validated. This work assesses if tap water is a good proxy for the local bioavailable Sr and hence mimics the $^{87}Sr/^{86}Sr$ ratio found in the human body, in this case hair.

Due to the fact that the modern human's diet is becoming increasingly globalized, researchers have argued that isotopic signatures are becoming more and more homogenized (Ehleringer *et al.* 2008; Nardoto *et al.* 2006) and may therefore inhibit scientists from distinguishing populations. This was most recently been demonstrated in the Netherlands, where there is no correlation between human enamel samples and tap water and that water could not be used as a proxy in a mobility contexts (Kootker *et al.* 2020). For Mexico, over half of the food product imports originate from the United States (World Bank- World Integrated Trade Solution 2018). Based on the fact that food intake is a major contributor to $^{87}Sr/^{86}Sr$ ratios found in human hair, this study will examine whether or not the "supermarket" diet influences the Mexican human hair ratios significantly.

Researchers have argued that the $^{87}Sr/^{86}Sr$ ratios in human hair may be skewed due to exogenous signatures embedded in human hair, such as bathing water and dust (Tipple *et al.* 2019; Vautour *et al.* 2015; Tipple *et al.* 2013; Font *et al.* 2012). Any "contamination" is in fact local and therefore will not significantly influence the goal of characterizing the bioavailable Sr of a region. It is important to note, however, that human hair from forensic cases are most often contaminated by the burial contexts and are not suitable to be used for region of origin predictions. This phenomenon has also been observed in cases of undocumented border crossers found in the Arizona desert (Ammer in preparation).

This study presents and contrasts the $^{87}Sr/^{86}Sr$ ratios found in human hair and tap water from Mexico and compares the data to the United States. The objective is to provide the first large scale tap water and human tissue-based Sr isotope reference dataset for Mexico as a complementary dataset to the rest of North America.

Strontium Isotopes ($^{87}Sr/^{86}Sr$)

Strontium has four naturally occurring stable isotopes with ^{87}Sr being the decay product of ^{87}Rb (rubidium, Faure and Powell 1972). The isotopic composition of Sr is reported as the

$^{87}Sr/^{86}Sr$ ratio because of their similar relative abundances. Strontium isotopes in the environment largely represent the underlying bedrock and predominantly vary based on the age of the rock and the initial amount of rubidium present, *e.g.*, higher Sr isotope ratios are associated with older and Rb-rich rocks/sediments (Faure 1986). Strontium is removed from the bedrock through (differential) weathering and is transferred to our food chain though soil, flora and fauna. Strontium substitutes in biological systems for calcium and retains local geological information from the primary consumer to high-level consumers (such as humans) (Åberg 1995). Not only is mass dependent fractionation negligible in strontium isotopic analyses due to its high atomic mass, it is also corrected for through the routine normalization procedures during the mass spectrometry measurements (Faure 1986). Therefore, in contrast to light isotopic systems such as oxygen and hydrogen, measured $^{87}Sr/^{86}Sr$ record no isotopic fractionation due to biological processes. Furthermore, as explained in detail by Bataille *et al.* (2018), the regional Sr isotope signatures are predictable because they are controlled by geological variations, *i.e.* age and rock composition. The isotopic signature is passed from the underlying bedrock to the soil and consequently the bioavailable Sr is taken up by the food chain. The $^{87}Sr/^{86}Sr$ ratio of tissues reflect the intake of bioavailable $^{87}Sr/^{86}Sr$ ratios during the time of tissue formation so that strontium isotopes are commonly used for migration studies and region of origin predictions (Bartelink *et al.* 2016; Chesson *et al.* 2018; Rauch *et al.* 2007).

Keratin as a record of bioavailable Sr

The human head typically has between 80,000 to 150,000 hair follicles. These small pockets in the skin and the blood vessels around them create more cells, which then grow hair (Krause and Foitzik 2006). Once the hair exits the scalp, it dies off and elemental exchange between hair and blood stops. The biogenetic dietary information initially inherited from the blood is retained. While the organ undergoes a life-long cycle of growth, regression and a resting period before it falls out, it has been determined that, on average, human hair grows ~1 cm per month. Therefore, hair retains a longitudinal record of isotope signatures and is thought to be useful to examine the recent geographic movement of an individual prior to their death (Chau *et al.* 2017; Font *et al.* 2012; Krause and Foitzik 2006). Keratin tissues, such as hair, are, however, thought to potentially incorporate environmental contamination, such as bathing water or dust (Tipple et al 2018; Chau *et al.* 2017).For this study, however, even if there is significant environmental contamination it would be of local origin. Nonetheless, it is important to note that it is always preferable to compare the same body tissues (*e.g.* develop a baseline database of Mexican human

teeth to compare with teeth of undocumented border crossers). However, due to issues of practicality and the time constraints, hair was chosen as the human proxy.

Water as a record of bioavailable Sr

Like many nations around the globe, Mexico faces a constant challenge to provide sufficient drinkable tap water resources to its citizens. The Mexican authorities and other institutions like the Inter-American Development Bank have attempted to resolve the issue of contamination in the Mexican river and lake system and improve the sanitation system (Inter-American Development Bank 2013; 2011; United Nations 2008). However, there is still a lack of clean tap water throughout the country. Over 30 million Mexican citizens lack high quality water services or have limited access to water and Mexico is one of the largest bottled water consumers in the world (Inter-American Development Bank 2013; 2011; World Bank 2018; Contreras 2019). Strontium isotope ratios of water have commonly been used to examine ecosystem processes and answer various hydrological and geological questions, such as surface and ground water interactions, source mixing, contaminations, provenancing of water and mineral weathering (Nigro *et al.* 2017; Hogan *et al.* 2000; Capo *et al.* 1998; Négrel and Petelet-Giraud 2005; Frei and Frei 2011). It is commonly assumed that the $^{87}Sr/^{86}Sr$ signature is directly reflective of the Sr found in the local ecosystem and local bedrock. However, this is not the case for water as water will mimic the $^{87}Sr/^{86}Sr$ of bedrock that is more soluble through weathering (such as limestone) (Stewart, Capo, and Chadwick 1998; Shand *et al.* 2009). Therefore, bedrock more susceptible to weathering will have a greater influence on the $^{87}Sr/^{86}Sr$ ratios of water than less soluble bedrocks (Chesson *et al.* 2012). Overall, ground water and therefore tap water is expected to reflect a wide range of Sr isotope ratios as it will reflect a mixture of recent rainwater and weathered bedrock (Kootker *et al.* 2020). This study is designed to assess how well drinking water reflects the bioavailable Sr taken up by hair of local individuals.

5.4.2. Methods

Sample Acquisition and Preparation

During a six-week period between June and July 2018, a total of 101 discarded human hair and 151 tap water samples were collected throughout Mexico by the lead author. The chosen sample locations were selected to cover Mexico's major geographic variation. The population sizes for the sampled hair locations ranged from approximately 1500 to 200,000 inhabitants. For tap water, the population sizes ranged from approximately 1500 to 21 million. The hair collection occurred in 32 locations across 22 states and was completely anonymous (red and green dots in

Figure 1). Hair samples, but no water samples, were collected from Puerto Morelos, Quintana Roo (n = 3) and Saltillo, Coahuila (n = 1) (green dots in Figure 1). No information was collected regarding the sex, age, dietary preferences or travel history. Therefore, this study works under the assumption that the hair samples belonged to local individuals. At least three samples per location were gathered except for La Paz, Baja California Sur and Saltillo, Coahuila, from where one sample was collected. Since the hair samples were collected from the floors of barber shops, only bunches of hair were collected to ensure that the samples were not cross-contaminated. Each individual hair sample was examined to ensure that texture and color was homogenous. The samples were stored in separate paper envelopes in airtight zip-log bags at room temperature. The cleaning procedure adopted to remove dust and grease from the human hair samples is outlined in the Supporting Information 1.

Tap water samples were obtained from 30 of the 32 hair sample locations (for the remainder of the study named "hair locations"). Tap water samples were collected from 21 further locations and 5 additional states (blue dots in Figure 1). Samples were collected from local tap water sources by running cold water for approximately 10 seconds before filling a clean 30 mL low-density polyethylene (LDPE) vial (Ammer *et al.* 2020). The cleaning procedure for the vials can be found in the Supporting Information 2.

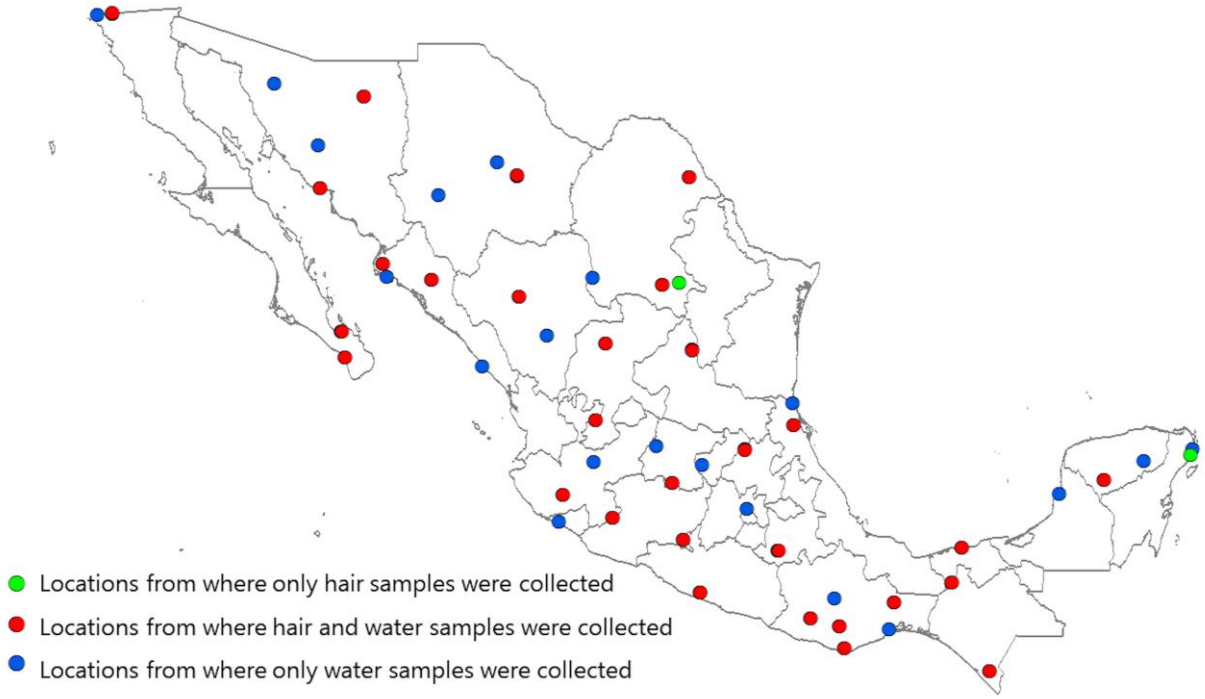

Figure 5.4.1. Map of Mexico showing the sampling locations (green: n=2, red: n=30, blue: n=21). Color figure available online.

Sample Analysis

All samples were analyzed for their strontium isotope composition at the Vrije Universiteit Amsterdam, using a ThermoFinnigan Triton Plus thermal ionization mass spectrometer (TIMS). The protocols for Sr extraction and loading can be found in the Supporting Information 3. Procedural blanks were prepared with the human hair and tap water samples and analyzed alongside reference material. The reference material included the Standard Reference Material® 987 and an internal tooth standard from the Vrije Universiteit Amsterdam. Isotope ratios were corrected for mass-fractionation to $^{86}Sr/^{88}Sr = 0.1194$. The NBS987 standard gave an $^{87}Sr/^{86}Sr$ mean of 0.710256 ± 0.000009 (n=45). The procedural blanks contained on average 37 pg strontium (n=26).

Statistical and Geospatial Methods

Spatial representation of the data was carried out using ArcGIS 10.6 (Environmental Systems Research Institute (ESRI) 2018). The geostatistical analyses for this study were performed using the ArcGIS Geostatistical Analyst toolbox and Geostatistical Wizard (Environmental Systems Research Institute (ESRI) 2018). The tool "Global Moran's I Spatial Autocorrelation" was used to determine the spatial autocorrelation based on the locations of the data points (hair and tap water sampling locations) and their corresponding isotopic ratios. The weight matrix was determined using inverse distance. The resultant Moran's Index provided information as to whether the isotopic data is random, dispersed, or clustered in a spatial context (Environmental Systems Research Institute (ESRI) 2018). Normality was tested using the D'Agostino-Pearson omnibus normality test. P-values were considered significant at the $\alpha = 0.05$ level. The nonparametric Mann-Whitney U Test was employed to compare the different datasets.

5.4.3. Results

A total of 101 hair and 151 tap water samples were analyzed for their $^{87}Sr/^{86}Sr$ ratios. The basic descriptive statistics can be found in Table 1 and the results for all $^{87}Sr/^{86}Sr$ ratios of human hair and tap water measurements in Supporting Information 4 and 5, respectively. Sr isotope ratios for the human hair samples ranged from 0.70424 to 0.71613, with a range ($\Delta^{87}Sr/^{86}Sr$) of 0.01189. The tap water samples varied from 0.70404 to 0.71385 ($\Delta^{87}Sr/^{86}Sr = 0.00981$). The mean ratio for the hair samples was higher (0.70706) than for the tap water samples (0.70665 for all 51 locations and 0.70663 for the 30 hair locations) but all averages are within 1 SD (0.0018). Averaging the ratios recorded for each sampling location, calculating a so-called location average, reduces the range of the hair ratios 0.70429 to 0.71239, with an average of 0.70698. The tap water average

location minimum and maximum ratios were the same for the 51 locations as for the 30 hair locations, ranging from 0.70408 to 0.71347. The mean $^{87}Sr/^{86}Sr$ of tap water from the hair locations (0.70673) is within error of the mean $^{87}Sr/^{86}Sr$ of tap water from all locations (0.70670).

Table 5.4.1. Basic descriptive statistics for human hair and tap water samples.

	Human hair- all data	**Human hair- location averages**	**Tap water- all data**	**Tap water- location averages**	**Tap water from hair locations- all data**	**Tap water from hair locations- location averages**
N	101	30	151	51	88	30
Min	0.70424	0.70429	0.70404	0.70408	0.70404	0.70408
Max	0.71613	0.71239	0.71385	0.71347	0.71385	0.71347
Mean*	0.70706	0.70698	0.70665	0.70670	0.70663	0.70673
SD	0.00180	0.00178	0.00185	0.00183	0.00205	0.00212
Range	0.01189	0.00810	0.00981	0.00939	0.00981	0.00939

*all are within error

The distribution of $^{87}Sr/^{86}Sr$ ratios is reported in Figure 2. The $^{87}Sr/^{86}Sr$ ratios for both human hair and tap water samples are not normally distributed. Normality was tested using the D'Agostino-Pearson omnibus normality test (human hair: $K^2 = 52.5$, p-value < 0.001; tap water: $K^2 = 44.0$, p-value < 0.001).

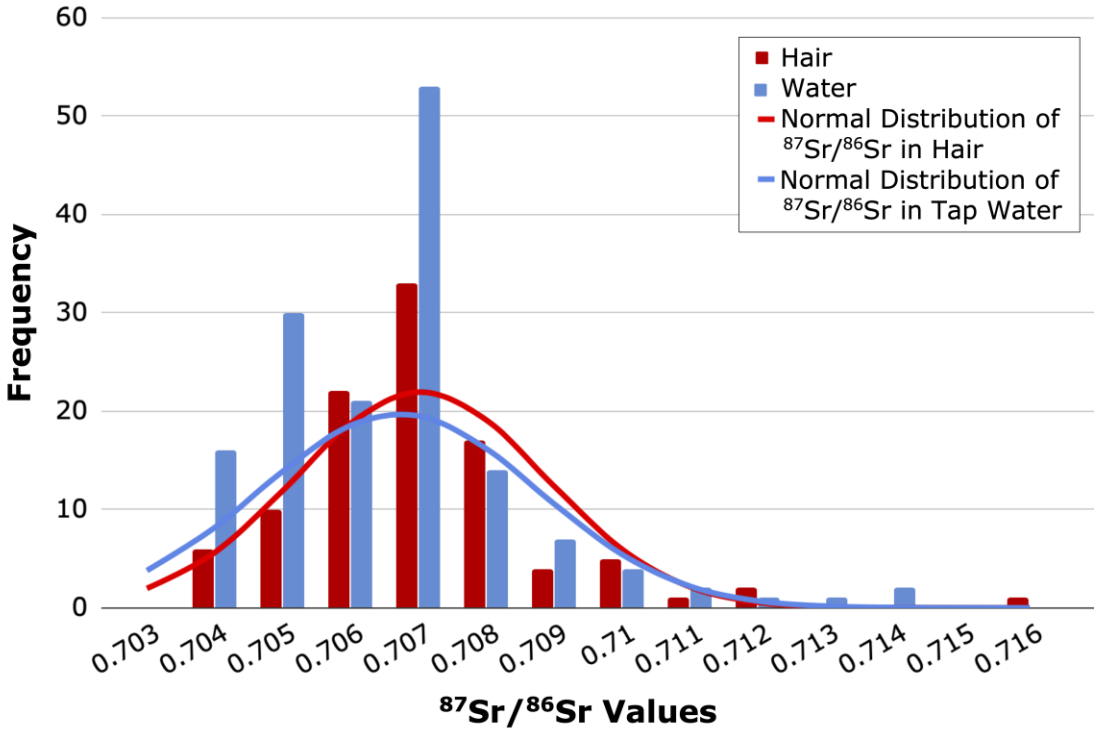

Figure 5.4.2. Distribution of human hair and tap water $^{87}Sr/^{86}Sr$ ratios in Mexico. Color figure available online.

A visualization of the spatial distribution of $^{87}Sr/^{86}Sr$ ratios of the hair and tap water samples can be found in Figure 3. The Moran's Index for the hair samples yielded 0.344, with a p-value of 0.186. Given the z-score of 1.323, the pattern does not appear to be significantly different from random. In contrast, the tap water samples yielded an index of 0.768 with a p-value of 0.000. Given the z-score of 6.467, there is a less than 1% likelihood that this clustered pattern could be a result of random chance.

For both hair and tap water samples, the lowest Sr isotope ratios appear along the west coast and Sierra Madre mountainous range, mainly in the states of Guanajuato, Jalisco and Michoacán. The highest $^{87}Sr/^{86}Sr$ ratios were found in the states of Oaxaca and the north-west of Mexico, specifically Tijuana (Baja California) (Figures 3a and 3b). The lowest $^{87}Sr/^{86}Sr$ ratios recorded in human hair was documented in Moroleón, Guanajuato (0.70424), and the highest in Miahuatlán de Porfirio Díaz, Oaxaca (0.71613) (Table 1, Figure 3a). The lowest $^{87}Sr/^{86}Sr$ ratios of tap water was found in El Grullo, Jalisco (0.70404), and the highest in Miahuatlán de Porfirio Díaz, Oaxaca (0.71385) (Table 1).

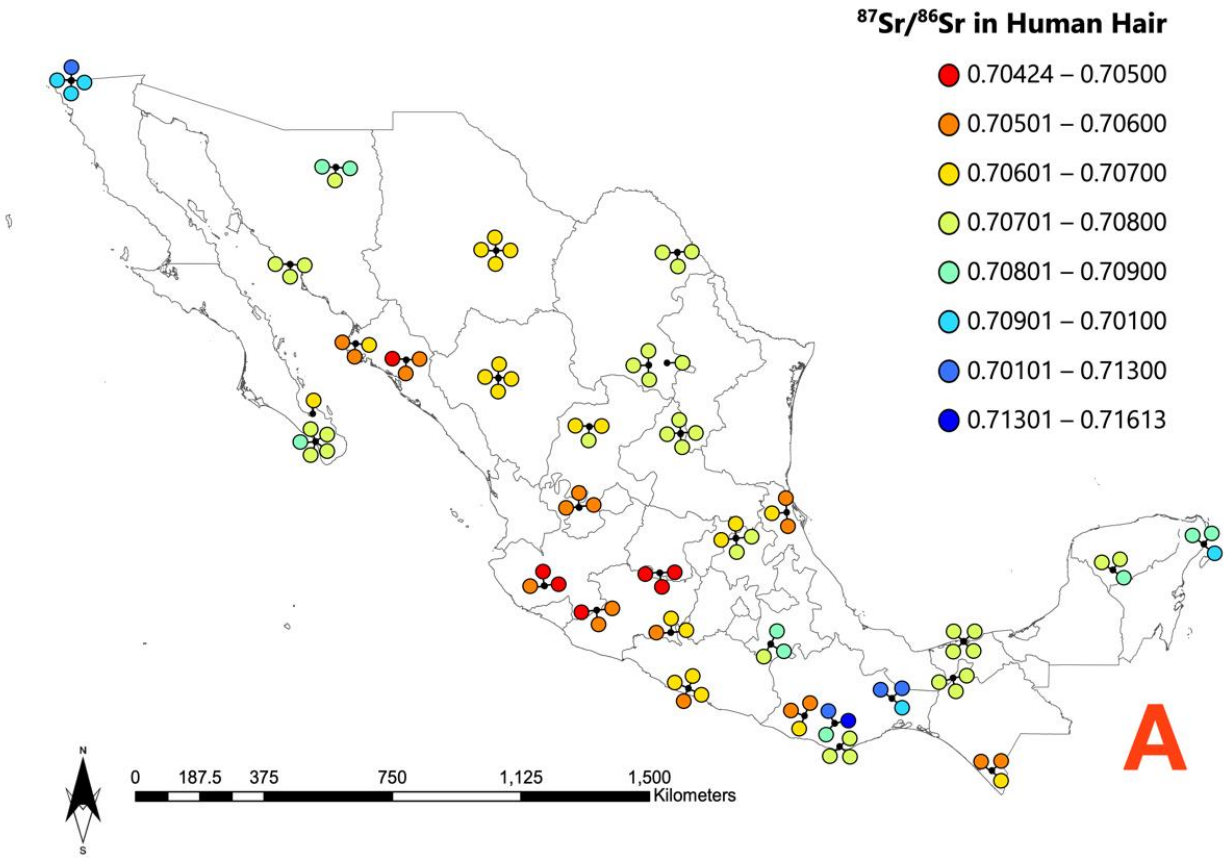

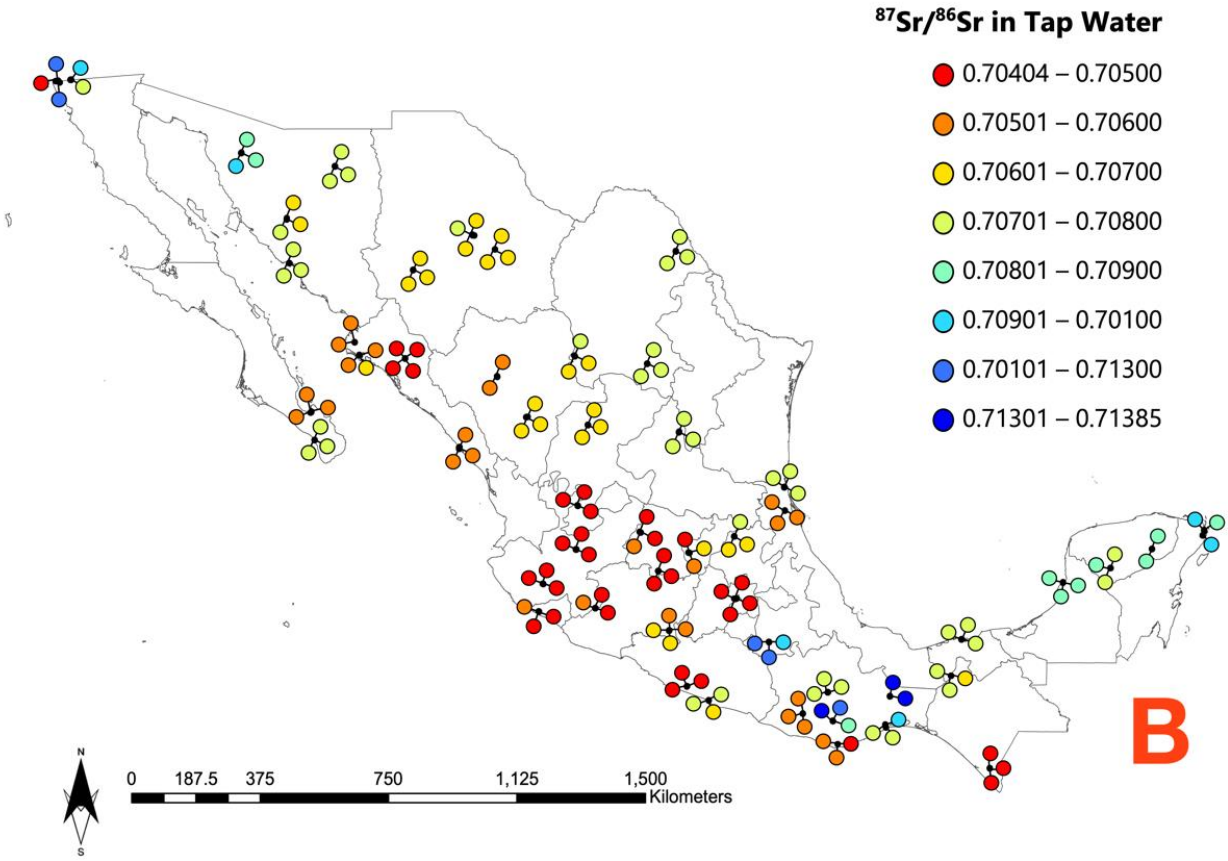

Figure 5.4.3. Graphical distribution of modern human hair (A) and tap water (B) $^{87}Sr/^{86}Sr$ ratios in Mexico. Color figure available online.

Standard deviations were calculated for each location. The results for the human hair samples, tap water samples and the tap water samples from hair locations can be found in Table 2. A spatial visualization of the standard deviations for the human hair and tap water sample locations can be found in Figures 4. The smallest standard deviation (0.000009) in the human hair samples was recorded in Villa Unión, Coahuila (n =3) and the highest in Miahuatlán de Porfirio Díaz, Oaxaca (0.00372, n = 3). When removing the latter location from the dataset, the maximum standard deviation drops to 0.00130 (Paraíso, Tabasco, n = 4). On average, the locations showed a standard deviation of 0.00041 (0.00029 when excluding Miahuatlán de Porfirio Díaz).

Tap water samples were analytically indistinguishable at Tampico, Tamaulipas (n = 3). The highest standard deviation was 0.00335 in Tijuana, Baja California (n = 3). Excluding Tijuana, the standard deviation maximum was 0.00286, recorded in Miahuatlán de Porfirio Díaz, Oaxaca (n = 3). The average standard deviation for tap water samples was 0.00034, 0.00028 when removing Tijuana from the dataset. The highest standard deviation at the hair sample locations was at Miahuatlán de Porfirio Díaz, Oaxaca. The average standard deviation was 0.00027. A

justification for removing the two abovementioned locations (Tijuana and Miahuatlán) will be presented in the discussion. Furthermore, as can be seen in Figure 3, 4 and 6, both locations are clear outliers for the hair and the tap water samples, respectively.

Table 5.4.2. Standard deviation values for human hair and tap water.

	Human Hair	**Tap Water from Hair Locations**	**Tap Water**
Min	0.000009	0.000005	0.000002
Max	0.00372 / 0.00130*	0.00286	0.00335 / 0.00286#
Mean	0.00041 / 0.00029*	0.00027	0.00034 / 0.00028#

* These values exclude the location (Miahuatlán de Porfirio Díaz, Oaxaca) with the highest standard deviation within the collected samples.
# These values exclude the location (Tijuana, Baja California) with the highest standard deviation within the collected sample

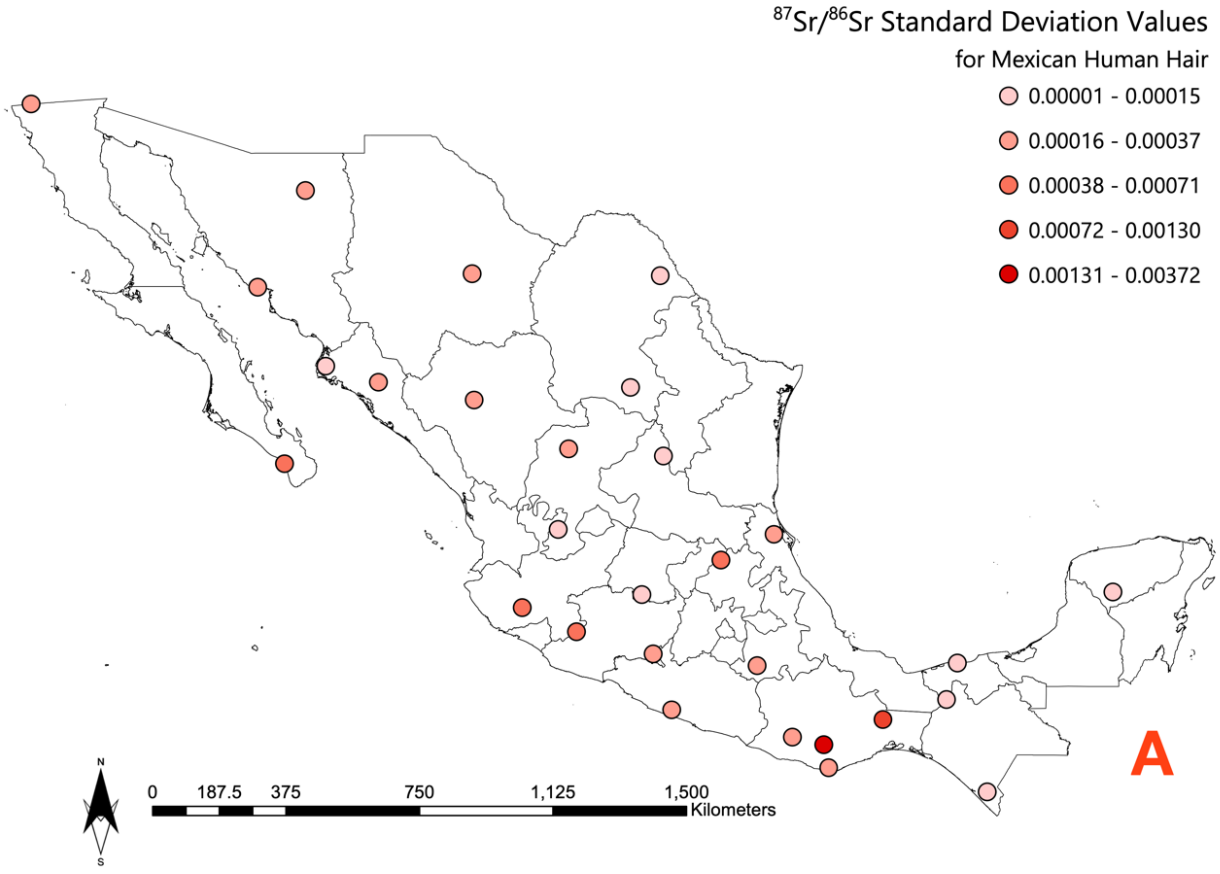

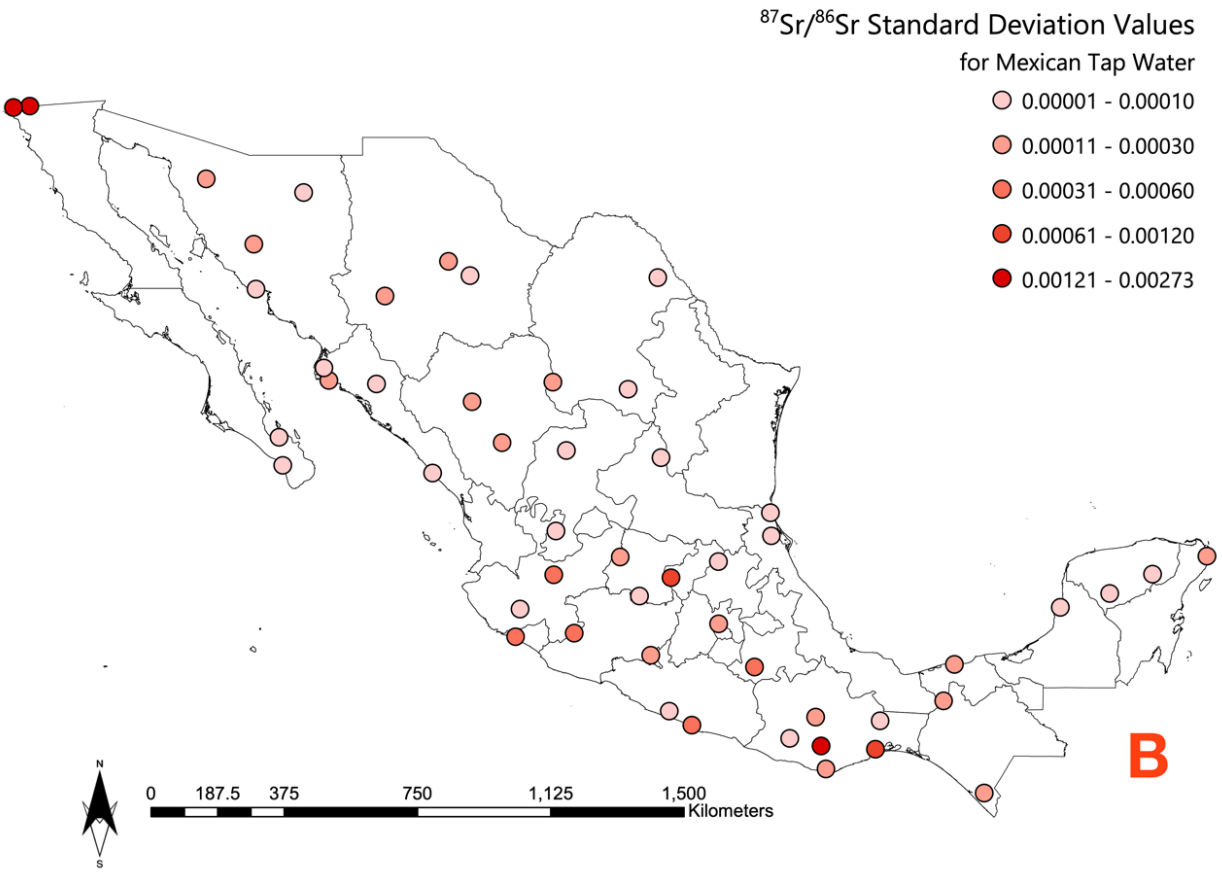

Figure 5.4.4. Variation in $^{87}Sr/^{86}Sr$ ratios at sampling locations of modern human hair (A) and tap water (B) in Mexico. Color figure available online.

5.4.4. Discussion

The $^{87}Sr/^{86}Sr$ ratios in Mexican human hair and tap water have a relatively large absolute range ($\Delta Sr_{max-min}$ = 0.01189 and $\Delta Sr_{max-min}$ = 0.00981, respectively) while, at the same time, showing limited variation within the samples collected from one location, typically $\Delta^{87}Sr/^{86}Sr$ = <0.0003. The Mann-Whitney U Test showed that there was a significant difference (W = 8867, p-value = 0.029 for all data, W = 5004, p-value = 0.024 for the 30 locations with combined tap water – hair data) between the $^{87}Sr/^{86}Sr$ ratios of human hair and the $^{87}Sr/^{86}Sr$ ratios of tap water. However, when using the location averages for the 30 hair locations, the Mann-Whitney U Test showed no significant difference between the two datasets (W = 478, p-value = 0.378). The $^{87}Sr/^{86}Sr$ ratios in human hair and tap water correlated strongly to one another (Figure 5a and 5b), but did not yield a 1:1 relationship. The correlation between the $^{87}Sr/^{86}Sr$ ratios of tap water and human hair yields an R^2 of 0.80. When using the averages calculated for each sampled location the correlation increases R^2 to 0.87.

Three main sources are considered to contribute to the $^{87}Sr/^{86}Sr$ ratios in human hair: exogenous, drinking water and diet. Despite the fact that several studies have reported potential

exogenous signatures embedded in human hair, most likely influenced by bathing in local tap water and from local dust (Tipple *et al.* 2019; Vautour *et al.* 2015; Tipple *et al.* 2013; Font *et al.* 2012), it is argued in this study, that the "contamination" would be of local origin and therefore not significantly offset the results in terms of potential provenance information. As previously mentioned, Mexico is known to be one of the highest bottled water consumers in the world. In many industrialized countries, such as the United States, bottled water is regionally sourced and therefore almost indistinguishable from the local tap water (Chesson *et al.* 2010). It is unknown if this is also the case for Mexico but from anecdotal evidence that the bottled water used for drinking and cooking is mostly produced by large regional companies and transported to local communities. Future study of Mexican bottled water could potentially indicate the proportion of Sr in human body tissues derived from bottled and tap water. Even though the low Sr content in drinking water means that the bulk of Sr ingested by humans is from food (Kootker *et al.* 2020), it is a significant finding of this work that the $^{87}Sr/^{86}Sr$ ratios of human hair and tap water are strongly correlated.

While more rural communities grow most of their own produce there will, nonetheless, be an influence of the so called "supermarket diet". Certain foods will be transported to the communities and therefore could, potentially, lead to homogenization of isotopic signatures recorded in human tissue. This effect has been demonstrated most recently by Kootker *et al.* (2020) examining the relationship of $^{87}Sr/^{86}Sr$ ratios in Dutch tap water and human tooth samples. While a direct comparison with the Netherlands is invalid, due to the significant socio-economic differences between the countries, this study clearly establishes that regional geology has a major influence and hence it can be concluded that the supermarket diet does not significantly skew the data in Mexico.

Overall, the human hair samples are more radiogenic than the tap water counterparts in the same locations up to Sr isotope ratios of circa 0.708. Above 0.708, the Sr isotope composition of tap water is more radiogenic than that of the hair samples. This phenomenon could be explained by ambient dust contamination of hair coupled with the fact that low ^{87}Sr originates from volcanic rocks that contain Sr-rich plagioclase with low Rb and hence low $^{87}Sr/^{86}Sr$. Breakdown of plagioclase will release Sr with lower $^{87}Sr/^{86}Sr$ than the bulk rock that will more readily enter the ground water, leaving soil with higher $^{87}Sr/^{86}Sr$ (Bain and Bacon 1994; Jung et al 2004). In contrast, silica rich crustal rocks preferentially break down potassium feldspar and micas with higher $^{87}Sr/^{86}Sr$ into the water leaving soils with lower $^{87}Sr/^{86}Sr$. The presence of Cretaceous carbonates in parts of Mexico is another contributing factor. Sr-rich marine carbonates have $^{87}Sr/^{86}Sr$ derived from seawater and have fluctuated between 0.707 and 0.709 over the last 500

Myr, with Cretaceous rocks close to 0.708. Redistribution of marine derived Sr in rainwater and as dust from the carbonate rocks will drive bioavailable Sr towards $^{87}Sr/^{86}Sr$ ratios of 0.708 to 0.709. A more systematic evaluation of the causes of the isotopic offset between water and human tissues is warranted, taking the role of the local climate and hence weathering processes into account. Further research is also required into uptake of Sr into other human tissues, such as bones and dental enamel, in order to evaluate the predictive strength of human hair as well as tap water into different tissue types.

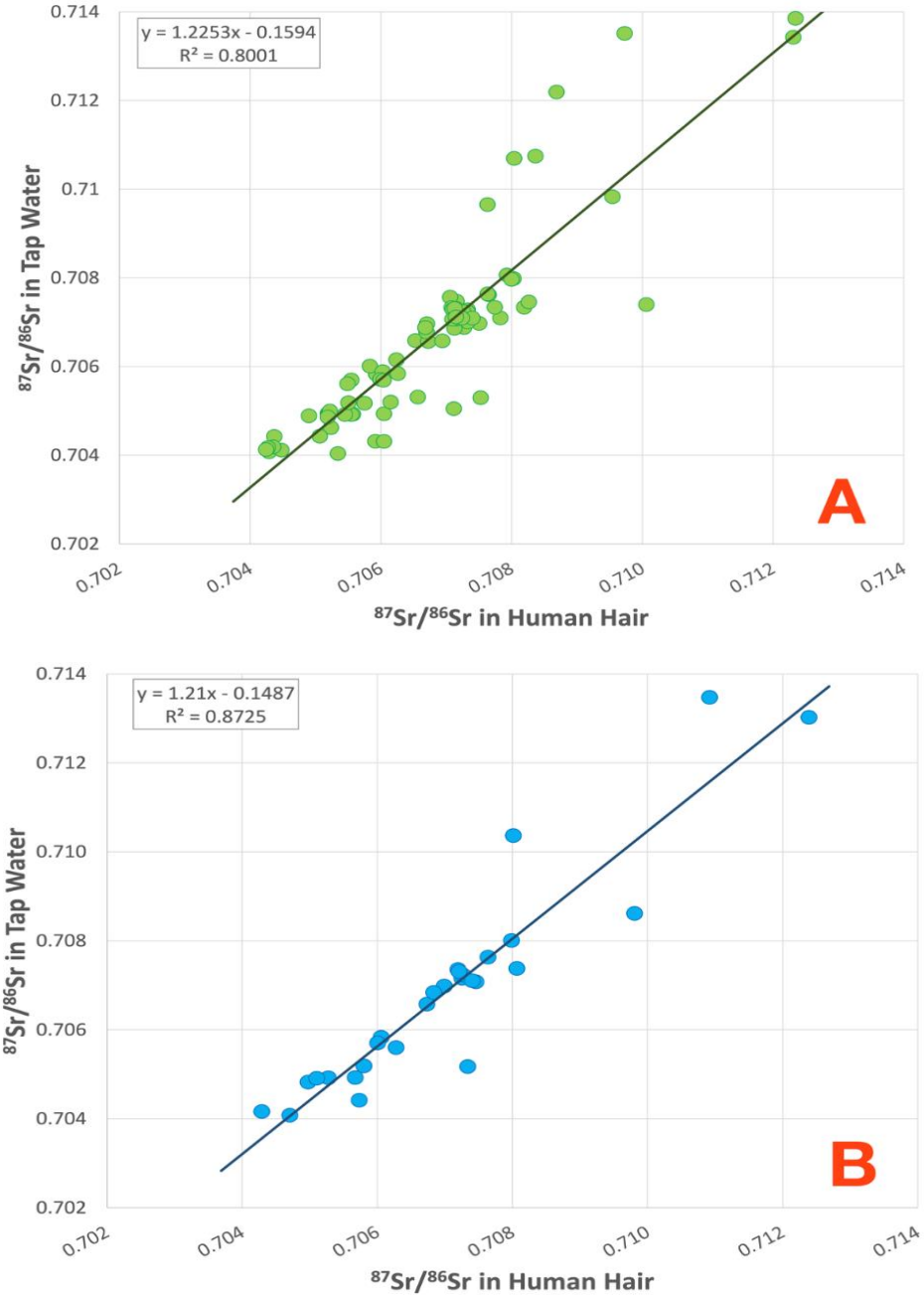

Figure 5.4.5. Relationship of $^{87}Sr/^{86}Sr$ ratios in human hair and tap water collected from the sample locations (n=30).
A: all data ($^{87}Sr/^{86}Sr$ Tap Water = 1.23 * $^{87}Sr/^{86}Sr$ Human Hair -0.16; R^2 = 0.80)
B: location averages ($^{87}Sr/^{86}Sr$ Tap Water = 1.21 * $^{87}Sr/^{86}Sr$ Human Hair -0.15; R^2 = 0.87)

Geospatial Patterns

The Moran's Index established that the hair samples appear to be randomly spatially dispersed while the tap water samples appear to be clustered. There are two main reasons why the results of the Moran's Index may be contradictory. Prior to the sample collecting trip, a geological map of Mexico was used to choose sampling locations. A total of 30 locations were chosen by geological variation in order to obtain a relatively complete coverage of Mexico. These were the locations from where hair samples were collected. It is unexpected that the Moran's Index recognizes spatial patterns from merely 30 locations that are primarily based on geology (and are therefore not necessarily spatially clustered). Since the samples were collected on a road trip, more tap water samples were collected from locations that lay geographically between the 30 hair locations. Therefore, more spatial clustering can be expected since more locations were sampled, which are also in closer proximity to one another. The spatial patterns and the relationships of the $^{87}Sr/^{86}Sr$ ratios to the underlying bedrock will be examined in the future. Overall, the standard deviations of both human hair and tap water were relatively small for individual locations, giving confidence in the sampling strategy and emphasizing that these locations are supplied with water from similar sources. Specifically, the $\Delta^{87}Sr/^{86}Sr_{total}$ is 0.0018 for the datasets (Table 1) while the average $\Delta^{87}Sr/^{86}Sr_{locations}$ is <0.0003.

Variance in $^{87}Sr/^{86}Sr$

There was no correlation between the size of the local human population and the recorded SD in the Sr isotope data (for human hair, $R^2 = 0.0006$, or tap water, $R^2 = 0.0002$). The population sizes for the sampled hair locations ranged from approximately 1500 to 200,000 inhabitants (Instituto Nacional de Estadística y Geografía 2010; 2015). For tap water, the population sizes ranged from approximately 1500 to 21 million (Instituto Nacional de Estadística y Geografía 2010; 2015). The fact that population size did not influence the isotopic variation shows that the sampling strategy was successful, especially as it was designed to aid predict the region of origin of undocumented border crossers, who have traditionally originated from smaller and more rural locations. Nonetheless, it would be advisable to further investigate larger municipalities as a recent shift has been documented towards migration from more urban areas (Unger 2005). Furthermore, analyzing megacities such as Mexico City would provide greater detail of the isotopic ranges in human hair within the entire Mexican population.

Miahuatlán de Porfirio Díaz (Oaxaca) recorded the highest $^{87}Sr/^{86}Sr$ ratios and variance for human hair and the second highest in tap water. The highest SD value in the tap water data was documented in Tijuana (Baja California), which also showed the highest SD values for

oxygen and hydrogen in a previous study examining the same tap water samples (Ammer forthcoming). This variation is probably due to the city's reliance on multiple water sources (*e.g.* the Colorado River) (Rodríguez 2005; Navarro Chaparro *et al.* 2016). Despite limited number of samples per location (n = 2-5) the Sr isotope variance in water and hair samples show a general correlation (Figure 4a and 4b) with R^2 of 0.52 when the location of Tecate (Baja California) was disregarded.

Comparison with the United States

This research aims to provide a comparative baseline for the provenance of human remains found along the Mexico-United States border, hence it is pertinent to compare the Mexican data to data reported from the United States (Chesson *et al.* 2012; Tipple *et al.* 2019). By comparing data, it will potentially be possible to determine whether an individual originated from Mexico or the United States or may have moved between the two countries.

Mann-Whitney U Test showed that there is a significant difference between the available hair and tap water data from the United States and the hair data and tap water data from Mexico ($W= 9185$, $p < 0.001$ for hair; $W= 12534$, $p <0.001$ for tap water). Furthermore, the Mexican Sr isotope ratios for human hair and tap water, are, on average, lower compared to the United States (Figure 6). For the hair samples, approximately 75% percent of the data fall below the lowest recorded ratios in the United States human hair dataset (Tipple *et al.* 2019, Figure 6). Therefore, based on the current dataset, $^{87}Sr/^{86}Sr$ ratios below 0.707 are indicative for individuals of Mexican decent. Ratios above cannot be distinguished. In contrast, there is a complete overlap of the Mexican tap water and the United States tap water. The lowest ratios recorded for tap water in Mexico are comparable to the lowest ratios found in the United States (Figure 6). Furthermore, the fourth quantile of the Mexican data reaches the median of the United States ratios.

This observation can be explained by the younger underlying bedrock in Mexico (Barton *et al.* 2003). As explained in the introduction, lower $^{87}Sr/^{86}Sr$ ratios are associated with younger volcanic bedrock (Beard and Johnson 2000; Faure and Powell 1972; Åberg 1995; Capo *et al.* 1998). While these isotopic differences are certainly meaningful, it is important to note that the data from the United States includes few samples from either of the coasts, which may somewhat bias the data. Based on the absence of sample locations in the western United States, where lower Sr isotope ratios are predicted in underlying bedrock (Bataille and Bowen 2012; Beard and Johnson 2000), the observation of an isotopic difference in hair samples could be subject to change in the future. This illustrates the importance of using a multi-isotope approach when provenancing (*e.g.* combine Sr and O isotopes). Nonetheless, considering that undocumented border crossers

are usually found in burial contexts inconsistent with United States citizens, this research will be able to serve as a basis for provenancing unidentified individuals.

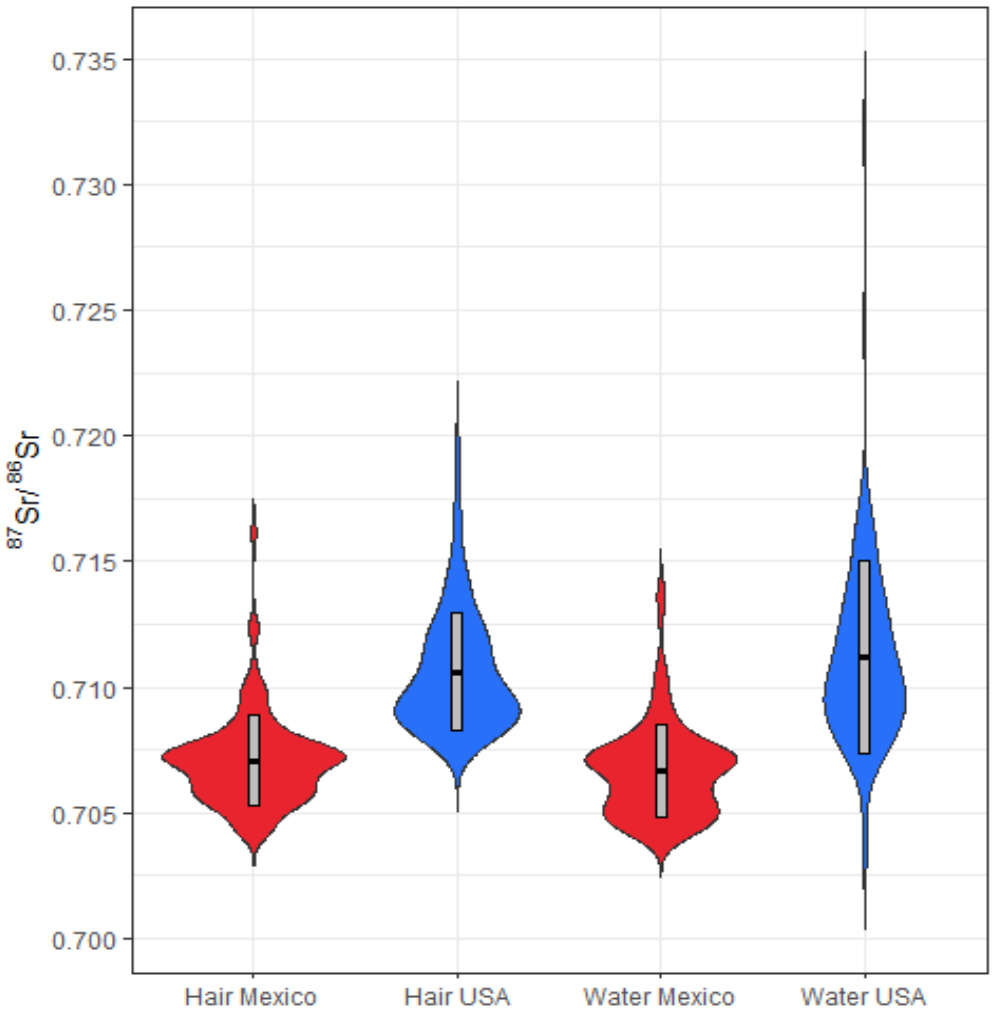

Figure 5.4.6. Violin plot showing $^{87}Sr/^{86}Sr$ ratios in human hair and tap water from Mexico and the United States (Tipple *et al.* 2019; Chesson *et al.* 2012). The mean ± standard deviation was added as a crossbar.

Additional isotope datasets

Limited isotopic research has been conducted into bioavailable elements in modern Mexican environments, with large scale studies limited to oxygen, hydrogen and deuterium excess. There have been, however, some spatially limited Sr isotope studies. The $^{87}Sr/^{86}Sr$ ratios previously recorded for modern Mexican teeth range from ~0.7053 to 0.7080, falling within the ranges recorded in this study (Kamenov and Curtis 2017; Juarez 2011). Hodell and colleagues (Hodell *et al.* 2004) presented data of water, bedrock, soils and plants for the Yucatan Peninsula, with $^{87}Sr/^{86}Sr$ ratios (0.7071 to 0.7099) covering the same range as reported here for human hair and tap water in the region (Figure 3). Archaeological human bone and tooth enamel from southern Mexico showed that the $^{87}Sr/^{86}Sr$ range of the samples (approximately 0.704 to 0.708) is

the same as this study (Price *et al.* 2000). Overall, the limited available Sr isotope data from modern and archaeological human tissues as well as environmental samples validate the spatial variation recorded in this study.

5.4.5. Conclusion

This study presents the first large scale modern human tissue based $^{87}Sr/^{86}Sr$ ratios from Mexico and has closed a large spatial gap in $^{87}Sr/^{86}Sr$ tap water ratios available in North America. The hair samples from 32 locations in Mexico define a range in $^{87}Sr/^{86}Sr$ ratios from 0.70424 to 0.71613 ($\Delta Sr_{max–min}$ = 0.01189). The tap water samples from 51 locations ranged from 0.70404 to 0.71385 ($\Delta Sr_{max–min}$ = 0.00981). A strong correlation (R^2= 0.80) is observed between $^{87}Sr/^{86}Sr$ of human hair and tap water data and location averages correlated more strongly (R^2= 0.87).

This study has shown that the $^{87}Sr/^{86}Sr$ ratios in human hair and tap water from Mexico have great potential to be used for provenancing studies, such as determining potential regions of origin of undocumented border crossers found along the Mexico- United States border. Nonetheless, it is pertinent to expand the research to other known body tissue samples in order to establish potential relationships of human hair to body tissues more frequently consulted in forensic anthropology. Following the example of Kootker *et al.* (2020), dental enamel samples could be collected in order to determine the predictive strength of human hair as well as examine the question whether tap water serve as an indicator for tissues that are not potentially exposed to external contamination.

Since Mexico is one of the highest bottled water consumers per capita in the world, the examination of Mexican bottled water could potentially yield indicators as to what degree the human body tissues are influenced by diet, bottled water and tap water. Lastly, this research will serve as a basis for various machine learning regression approaches, which will include multivariate models, to determine regional Sr isoscape for Mexico (Ammer forthcoming). Following the approach of Bataille *et al.* (2018), the resulting isoscapes will take into consideration various geological covariates, such as the underlying bedrock and weathering regime in order to enable future provenancing studies.

Acknowledgements

The authors would like to sincerely thank the 101 anonymous hair donors throughout Mexico for enabling this research. Dr. Janne Koornneef, Richard Smeets and Anna Pals from the Vrije Universiteit Amsterdam, the Netherlands, are thanked for training the first author and for their guidance. The first author's research project is financially supported by the American Academy of Forensic Sciences (AAFS) Humanitarian and Human Rights Resource Center (HHRRC) grant, supported by the AAFS and National Institute of Justice (U.S. Department of Justice).

SUPPORTING INFORMATION

Supporting Information 1. Cleaning and sample preparation procedures for human hair samples All samples were cleaned according to the standard protocol at the Vrije Universiteit Amsterdam using a vacuum funnel and extractor hood. A 2:1 chloroform-methanol mixture was used to remove any surface contaminants and lipids from the hair samples.

1. The hair samples were placed on filter paper and the mixture left to soak for about 20 seconds.
2. The mixture was then removed through the vacuum and replaced with Milli-Q distilled water.
3. After another 20 seconds, the procedure was repeated four more times. (Whenever the filter paper got visibly soiled during these steps, it was replaced by a clean one.)
4. After the fifth round of cleaning, the hair sample was placed between two new filter papers and wrapped with aluminum foil.
5. The foil was opened up on its ends under the laminar flow hood for the samples to dry.
6. Once dry, the samples were cut with surgical grade scissors.

Supporting Information 2. Cleaning procedure of 30mL vials for tap water samples in the class 100 clean laboratory

1. All vials were rinsed with Milli-Q water to get rid of any coarse contamination
2. The vials were then filled with 1-2M HNO_3 to the top, so a bulge at the neck of the vial formed (in order to make sure the inside of the lid was also cleaned)
3. The vials were stored laying down for one week, after the first week they were rotated and stored to clean for another week
4. The vials were emptied, and the acid discarded.
5. The vials and caps were then rinsed once with Milli-Q water and then left to dry on a hotplate (in a flow hood) at 50˚C.
6. The vials were then stored in clean re-sealable zipper storage bags before usage.

Supporting Information 3. Sample Dissolution and Sr Extraction protocol, Loading procedure for analysis on TIMS Triton

- The hair samples were dissolved in pre-cleaned Teflon beakers using concentrated HNO_3, HCl 6.5M and HF. Following a drying down step, the samples were re-dissolved in 0.7N HBr and concentrated HNO_3.
- The tap water samples were dried down in pre-cleaned Teflon beakers and re-dissolved with 0.7N HBr and concentrated HNO_3.
- Column extraction:
    - 130µL of Eichrom® Sr resin were used for all columns
    - The columns were washed three times alternating between HNO_3 3M and MilliQ
    - The columns were conditioned with 0.5mL of HNO_3 3M
    - The samples were added to the columns and washed with 2x 500 µL of HNO_3 3M and 1x 1mL of HNO_3 3M (beaker with pre-fraction was discarded)
    - For Sr fraction, 1 mL MilliQ was pipetted onto column
    - Sr fraction was dried down overnight
    - The Sr fraction was nitrated using 4-5 drops of concentrated HNO_3 for two hours on a hotplate at 120 °C
    - Fraction was dried down and stored until TIMS Triton Analysis
- Loading procedure
    - The samples were dissolved in 4µL 10% HNO_3
    - 1.5µL TaCl were loaded onto Annealed rhenium filaments, followed by 2µL of the dissolved sample
    - Filament was loaded onto turret

Supporting Information 4. Location and $^{87}Sr^{86}Sr$ in Human Hair from Mexico.

Location	$^{87}Sr^{86}Sr$ Human Hair	± 2SE
Puerto Morelos, Quintana Roo	0.709003	9.62E-06
Puerto Morelos, Quintana Roo	0.708449	9.64E-06
Puerto Morelos, Quintana Roo	0.708981	9.50E-06
Tekax de Álvaro Obregón, Yucatan	0.708031	9.37E-06
Tekax de Álvaro Obregón, Yucatan	0.707928	9.19E-06
Tekax de Álvaro Obregón, Yucatan	0.707998	9.55E-06
Paraíso, Tabasco	0.707158	9.62E-06
Paraíso, Tabasco	0.707183	9.83E-06
Paraíso, Tabasco	0.707059	9.25E-06
Paraíso, Tabasco	0.707371	9.93E-06
Plan de Ayala, Chiapas	0.707153	9.35E-06
Plan de Ayala, Chiapas	0.707276	9.77E-06
Plan de Ayala, Chiapas	0.707329	9.39E-06
Huixtla, Chiapas	0.705234	9.65E-06
Huixtla, Chiapas	0.705917	9.78E-06
Huixtla, Chiapas	0.706048	9.84E-06
San Juan Guichicovi, Oaxaca	0.712310	9.81E-06
San Juan Guichicovi, Oaxaca	0.710714	9.79E-06
San Juan Guichicovi, Oaxaca	0.709729	9.76E-06
San Pedro Pochutla, Oaxaca	0.707372	9.63E-06
San Pedro Pochutla, Oaxaca	0.707525	8.66E-06
San Pedro Pochutla, Oaxaca	0.707114	9.07E-06
Miahuatlán de Porfirio Díaz, Oaxaca	0.716131	9.38E-06
Miahuatlán de Porfirio Díaz, Oaxaca	0.712344	9.16E-06
Miahuatlán de Porfirio Díaz, Oaxaca	0.708688	9.65E-06
San Jacinto Tlacotepec, Oaxaca	0.706259	9.03E-06
San Jacinto Tlacotepec, Oaxaca	0.705981	9.48E-06
San Jacinto Tlacotepec, Oaxaca	0.705928	9.36E-06
Tehuitzingo, Puebla	0.708365	9.40E-06
Tehuitzingo, Puebla	0.708039	9.43E-06
Tehuitzingo, Puebla	0.707631	9.58E-06
Atoyac de Álvarez, Guerrero	0.705575	9.68E-06
Atoyac de Álvarez, Guerrero	0.705547	8.82E-06
Atoyac de Álvarez, Guerrero	0.706048	9.16E-06
Atoyac de Álvarez, Guerrero	0.705523	1.19E-05
Huetamo de Núñez, Michoacán	0.705831	9.13E-06
Huetamo de Núñez, Michoacán	0.706238	1.04E-05
Huetamo de Núñez, Michoacán	0.705547	8.75E-06
Tepalcatepec, Michoacán	0.705489	9.41E-06
Tepalcatepec, Michoacán	0.705065	9.10E-06

Tepalcatepec, Michoacán	0.704369	1.48E-05
El Grullo, Jalisco	0.704290	9.45E-06
El Grullo, Jalisco	0.705342	9.59E-06
El Grullo, Jalisco	0.704478	9.31E-06
Tlaltenango de Sánchez Román, Zacatecas	0.705186	9.28E-06
Tlaltenango de Sánchez Román, Zacatecas	0.705450	9.59E-06
Tlaltenango de Sánchez Román, Zacatecas	0.705191	9.17E-06
Moroleón, Guanajuato	0.704353	9.55E-06
Moroleón, Guanajuato	0.704272	9.72E-06
Moroleón, Guanajuato	0.704243	9.65E-06
Jacala, Hidalgo	0.706429	9.40E-06
Jacala, Hidalgo	0.706705	9.78E-06
Jacala, Hidalgo	0.707504	9.75E-06
Jacala, Hidalgo	0.707330	9.35E-06
Ozuluama de Mascareñas, Veracruz	0.705752	9.80E-06
Ozuluama de Mascareñas, Veracruz	0.705504	9.31E-06
Ozuluama de Mascareñas, Veracruz	0.706151	9.73E-06
Matehuala, San Luis Potosi	0.707273	9.93E-06
Matehuala, San Luis Potosi	0.707328	9.66E-06
Matehuala, San Luis Potosi	0.707206	9.82E-06
Matehuala, San Luis Potosi	0.707258	9.51E-06
General Capeda, Coahuila	0.707083	9.90E-06
General Capeda, Coahuila	0.707098	9.50E-06
General Capeda, Coahuila	0.707129	9.25E-06
Saltillo, Coahuila	0.707527	9.21E-06
Villa Unión, Coahuila	0.707649	9.53E-06
Villa Unión, Coahuila	0.707635	9.34E-06
Villa Unión, Coahuila	0.707633	9.64E-06
Pedro Meoqui, Chihuahua	0.706528	9.56E-06
Pedro Meoqui, Chihuahua	0.706724	9.72E-06
Pedro Meoqui, Chihuahua	0.706941	9.76E-06
Pedro Meoqui, Chihuahua	0.706740	9.62E-06
Santiago Papasquiaro, Durango	0.706309	9.66E-06
Santiago Papasquiaro, Durango	0.706566	9.98E-06
Santiago Papasquiaro, Durango	0.706029	9.15E-06
Santiago Papasquiaro, Durango	0.706208	9.78E-06
Río Grande, Zacatecas	0.707124	9.33E-06
Río Grande, Zacatecas	0.706699	9.50E-06
Río Grande, Zacatecas	0.706681	9.30E-06
El Salto, Sinaloa	0.704899	9.50E-06
El Salto, Sinaloa	0.705220	9.35E-06
El Salto, Sinaloa	0.705187	9.64E-06
Villa de Ahome, Sinaloa	0.705979	9.58E-06

Villa de Ahome, Sinaloa	0.705991	9.78E-06
Villa de Ahome, Sinaloa	0.706041	9.67E-06
Todos Los Santos, Baja California Sur	0.707160	9.74E-06
Todos Los Santos, Baja California Sur	0.707400	8.58E-06
Todos Los Santos, Baja California Sur	0.707096	9.31E-06
Todos Los Santos, Baja California Sur	0.708841	9.37E-06
Todos Los Santos, Baja California Sur	0.707492	9.26E-06
La Paz, Baja California Sur	0.706768	9.45E-06
Guaymas, Sonora	0.707241	8.88E-06
Guaymas, Sonora	0.707150	8.25E-06
Guaymas, Sonora	0.707826	9.43E-06
Nacozari de García, Sonora	0.707743	9.52E-06
Nacozari de García, Sonora	0.708191	9.86E-06
Nacozari de García, Sonora	0.708263	9.76E-06
Tecate, Baja California	0.710061	9.26E-06
Tecate, Baja California	0.709545	9.58E-06
Tecate, Baja California	0.709919	9.40E-06
Tecate, Baja California	0.709708	9.61E-06

Supporting Information 5. Location and $^{87}Sr/^{86}Sr$ in Tap Water from Mexico

Location	87Sr/86Sr Tap Water	± 2SE
Cancún, Quintana Roo	0.708551	8.00E-06
Cancún, Quintana Roo	0.709016	7.00E-06
Cancún, Quintana Roo	0.709047	6.00E-06
Valladolid, Yucatan	0.708214	6.00E-06
Valladolid, Yucatan	0.708199	6.00E-06
Tekax de Álvaro Obregón, Yucatan	0.707987	7.00E-06
Tekax de Álvaro Obregón, Yucatan	0.708066	7.00E-06
Tekax de Álvaro Obregón, Yucatan	0.707970	8.00E-06
Campeche, Campeche	0.708069	9.00E-06
Campeche, Campeche	0.708067	7.00E-06
Campeche, Campeche	0.708170	7.00E-06
Paraíso, Tabasco	0.707475	5.00E-06
Paraíso, Tabasco	0.707025	1.00E-05
Paraíso, Tabasco	0.707567	9.02E-06
Plan de Ayala, Chiapas	0.707312	7.68E-06
Plan de Ayala, Chiapas	0.706883	7.52E-06
Lindavista, Chiapas	0.707282	7.46E-06
Huixtla, Chiapas	0.704625	8.50E-06
Huixtla, Chiapas	0.704315	9.00E-06
Huixtla, Chiapas	0.704312	8.00E-06
San Juan Guichicovi, Oaxaca	0.713429	8.54E-06
San Juan Guichicovi, Oaxaca	0.713516	7.00E-06
Salina Cruz, Oaxaca	0.709186	1.30E-05
Salina Cruz, Oaxaca	0.707399	1.00E-05
Salina Cruz, Oaxaca	0.707115	7.00E-06
San Pedro Pochutla, Oaxaca	0.704845	1.30E-05
San Pedro Pochutla, Oaxaca	0.705299	1.10E-05
San Pedro Pochutla, Oaxaca	0.705051	8.68E-06
Miahuatlán de Porfirio Díaz, Oaxaca	0.708287	1.40E-05
Miahuatlán de Porfirio Díaz, Oaxaca	0.713853	8.00E-06
Miahuatlán de Porfirio Díaz, Oaxaca	0.712193	8.00E-06
San Jacinto Tlacotepec, Oaxaca	0.705842	8.00E-06
San Jacinto Tlacotepec, Oaxaca	0.705823	1.54E-05
San Jacinto Tlacotepec, Oaxaca	0.705831	1.10E-05
Oaxaca, Oaxaca	0.707100	9.32E-06
Oaxaca, Oaxaca	0.707018	4.50E-06
Oaxaca, Oaxaca	0.707369	8.86E-06
Tehuitzingo, Puebla	0.710748	8.48E-06
Tehuitzingo, Puebla	0.710696	1.11E-05
Tehuitzingo, Puebla	0.709656	7.00E-06

Atoyac de Álvarez, Guerrero	0.704928	1.00E-05
Atoyac de Álvarez, Guerrero	0.704921	6.00E-06
Atoyac de Álvarez, Guerrero	0.704936	7.27E-06
Acapulco, Guerrero	0.707505	8.00E-06
Acapulco, Guerrero	0.707340	7.00E-06
Acapulco, Guerrero	0.706680	4.93E-06
Huetamo de Núñez, Michoacán	0.705994	7.96E-06
Huetamo de Núñez, Michoacán	0.706013	9.00E-06
Huetamo de Núñez, Michoacán	0.706156	8.00E-06
Huetamo de Núñez, Michoacán	0.705699	9.00E-06
Tepalcatepec, Michoacán	0.705613	8.00E-06
Tepalcatepec, Michoacán	0.704432	9.00E-06
Tepalcatepec, Michoacán	0.704426	9.00E-06
Manzanillo, Colima	0.705019	6.18E-06
Manzanillo, Colima	0.704612	9.24E-06
Manzanillo, Colima	0.704125	6.00E-06
El Grullo, Jalisco	0.704079	4.29E-06
El Grullo, Jalisco	0.704041	4.16E-06
El Grullo, Jalisco	0.704117	7.97E-06
Guadalajara, Jalisco	0.704939	8.00E-06
Guadalajara, Jalisco	0.704921	7.00E-06
Guadalajara, Jalisco	0.704279	9.38E-06
Tlaltenango de Sánchez Román, Zacatecas	0.704939	8.00E-06
Tlaltenango de Sánchez Román, Zacatecas	0.704921	7.00E-06
Tlaltenango de Sánchez Román, Zacatecas	0.704909	1.00E-05
León, Guanajuato	0.705398	7.94E-06
León, Guanajuato	0.704861	9.09E-06
León, Guanajuato	0.704739	8.74E-06
Moroleón, Guanajuato	0.704189	4.55E-06
Moroleón, Guanajuato	0.704171	3.87E-06
Moroleón, Guanajuato	0.704128	1.13E-05
Santiago de Querétaro, Querétaro	0.704605	7.92E-06
Santiago de Querétaro, Querétaro	0.705628	7.32E-06
Santiago de Querétaro, Querétaro	0.706684	7.26E-06
Jacala, Hidalgo	0.706969	9.00E-06
Jacala, Hidalgo	0.706975	8.00E-06
Jacala, Hidalgo	0.707009	8.00E-06
Ozuluama de Mascareñas, Veracruz	0.705174	9.00E-06
Ozuluama de Mascareñas, Veracruz	0.705188	8.00E-06
Ozuluama de Mascareñas, Veracruz	0.705202	9.00E-06
Tampico, Tamaulipas	0.707459	8.95E-06
Tampico, Tamaulipas	0.707462	8.30E-06
Tampico, Tamaulipas	0.707462	6.74E-06

Matehuala, San Luis Potosi	0.707231	8.00E-06
Matehuala, San Luis Potosi	0.707239	8.70E-06
Matehuala, San Luis Potosi	0.707240	9.52E-06
General Capeda, Coahuila	0.707330	8.74E-06
General Capeda, Coahuila	0.707288	7.94E-06
General Capeda, Coahuila	0.707312	7.62E-06
Villa Unión, Coahuila	0.707620	9.18E-06
Villa Unión, Coahuila	0.707640	9.06E-06
Villa Unión, Coahuila	0.707639	8.52E-06
Torreón, Coahuila	0.707149	8.83E-06
Torreón, Coahuila	0.706986	8.58E-06
Torreón, Coahuila	0.706771	9.99E-06
Pedro Meoqui, Chihuahua	0.706586	7.65E-06
Pedro Meoqui, Chihuahua	0.706567	7.71E-06
Pedro Meoqui, Chihuahua	0.706580	6.54E-06
Chihuahua, Chihuahua	0.706739	8.74E-06
Chihuahua, Chihuahua	0.706648	1.02E-05
Chihuahua, Chihuahua	0.707112	7.65E-06
Creel, Chihuahua	0.706060	8.44E-06
Creel, Chihuahua	0.706268	7.57E-06
Creel, Chihuahua	0.706034	9.18E-06
Topolobampo, Sinaloa	0.706014	7.42E-06
Topolobampo, Sinaloa	0.705773	8.21E-06
Topolobampo, Sinaloa	0.705776	7.64E-06
Villa de Ahome, Sinaloa	0.705713	7.20E-06
Villa de Ahome, Sinaloa	0.705694	6.72E-06
Todos Los Santos, Baja California Sur	0.707071	8.11E-06
Todos Los Santos, Baja California Sur	0.707094	6.88E-06
Todos Los Santos, Baja California Sur	0.707068	6.04E-06
Santiago Papasquiaro, Durango	0.705313	7.80E-06
Santiago Papasquiaro, Durango	0.705888	8.58E-06
Durango, Durango	0.706907	7.46E-06
Durango, Durango	0.706554	7.01E-06
Durango, Durango	0.706773	7.14E-06
Mazatlán, Sinaloa	0.705305	7.85E-06
Mazatlán, Sinaloa	0.705291	7.62E-06
Mazatlán, Sinaloa	0.705291	8.61E-06
Río Grande, Zacatecas	0.706862	7.22E-06
Río Grande, Zacatecas	0.706783	7.50E-06
Río Grande, Zacatecas	0.706879	6.77E-06
El Salto, Sinaloa	0.704891	7.03E-06
El Salto, Sinaloa	0.704998	7.11E-06
El Salto, Sinaloa	0.704865	6.48E-06

El Salto, Sinaloa	0.704884	6.43E-06
Guaymas, Sonora	0.707095	7.16E-06
Guaymas, Sonora	0.707120	7.52E-06
Guaymas, Sonora	0.707098	5.60E-06
Hermosillo, Sonora	0.706760	7.60E-06
Hermosillo, Sonora	0.707195	8.22E-06
Hermosillo, Sonora	0.706777	8.01E-06
Nacozari de García, Sonora	0.707339	6.00E-06
Nacozari de García, Sonora	0.707338	6.52E-06
Nacozari de García, Sonora	0.707456	6.81E-06
Heroica Caborca, Sonora	0.709199	8.89E-06
Heroica Caborca, Sonora	0.708540	7.43E-06
Heroica Caborca, Sonora	0.708818	6.28E-06
Tecate, Baja California	0.707400	6.42E-06
Tecate, Baja California	0.709831	6.69E-06
La Paz, Baja California Sur	0.705751	7.00E-06
La Paz, Baja California Sur	0.705887	1.00E-05
La Paz, Baja California Sur	0.705885	8.00E-06
Tijuana, Baja California	0.710196	9.00E-06
Tijuana, Baja California	0.710319	8.17E-06
Tijuana, Baja California	0.704462	7.67E-06
Mexico City, Mexico	0.704462	7.67E-06
Mexico City, Mexico	0.704473	8.66E-06
Mexico City, Mexico	0.704996	8.20E-06
Mexico City, Mexico	0.704490	8.12E-06

5. 5. Results and Discussion of the Isotopic Analyses of the Undocumented Border Crossers

Throughout the following four sections, the results of the isotopic analyses of the 55 samples from the 16 undocumented border crossers are presented, interpreted, and discussed.

Section 5.5.1 *Results and Discussion of the Carbon, Nitrogen and Sulfur Isotope Analyses of Body Tissues of Undocumented Border Crossers* outlines the isotopic values recorded for the 16 undocumented border crossers cases. Furthermore, the correlations of the collagen and carbonate values to the hair keratin values are discussed. The interpretation of the values proved to be difficult due to the lack of modern reference values of human bones and teeth.

Section 5.5.2 *Results and Discussion of the Oxygen Isotope Analyses of Body Tissues of Undocumented Border Crossers* presents the results of the oxygen isotope analyses but also outlines the challenges associated with these analyses. The section shows how the methodology of preparation and analyses can greatly alter the isotopic values recovered from a skeletal tissue and thus, how pertinent it is to establish an internally uniform methodology for the isotopic analyses of human tissues. Nonetheless, the region-of-origin predictions for the teeth of eight of the 16 undocumented border crossers are presented.

In section 5.5.3, two successful case studies are presented. The $\delta^{18}O$ isotopic values of two tooth enamel samples collected from two undocumented border crossers whose remains were being examined at the PCOME were analyzed and compared to the isotopic values recorded in Mexican tap water. The Mexican tap water values were visualized in an isoscape using a Spine with Barriers interpolation method. The individuals were plotted on the developed isoscape using conditional correlations. The methodology was successful in assigning the correct regions-of-origin for the two individuals, which shows the tremendous potential of the developed isoscape.

- Ammer, S.; Bartelink, E.; Vollner, J.; Anderson, B. and E. Cunha. *Spatial Distributions of Oxygen Stable Isotope Ratios in Tap Water From Mexico for Region of Origin Predictions of Unidentified Border Crossers*. Journal of Forensic Sciences 2020. doi: 10.1111/1556-4029.14283

Lastly, in section 5.5.4. *Results and Discussion of the Strontium Isotope Analyses of Body Tissues of Undocumented Border Crossers*, the 55 samples from the UBCs are presented, including the region-of-origin prediction maps for each of the 16 individuals. Furthermore, the isoscape, on which the prediction is based is briefly introduced. Lastly, the elevated $^{87}Sr/^{86}Sr$ ratios seen in the hair samples of the undocumented border crossers are discussed.

5. 5. 1. Results and Discussion of the Carbon, Nitrogen, and Sulfur Isotope Analyses of Body Tissues of Undocumented Border Crossers

In following section, the results of the dietary isotopes carbon, nitrogen and sulfur found in the body tissues of undocumented border crossers are presented and discussed.

Carbon (δ^{13}C) isotope values are especially informative regarding the source of dietary nutrients for an individual and vary according to the three following photosynthetic pathways used by the plant (C3, C4, and CAM). A discussion of the various photosynthetic pathways can be found in Chapter II. Nitrogen (δ^{15}N) values inform about the types of animal proteins a person consumes. Moving up the food chain, δ^{15}N become higher by 2-4 ‰ due to the fractionation during nitrogen metabolism, a trophic level effect (Meier-Augenstein 2018; Reitsema 2015; Steele and Daniel 1978; O'Connell *et al.* 2012). δ^{15}N values give an indication over a person's dietary habits and also about the nutritional status (*e.g.* stress, health or pregnancy) (Fuller *et al.* 2004; Petzke at al. 2010; Meier-Augenstein 2018). Sulfur (δ^{34}S) isotope values provide insight regarding the consumption of marine protein resources (*e.g.*, marine fish), proximity to seawater, and foods consumed from different geological regions. Higher δ^{34}S values reflect consumption of marine ecosystems, intermediate δ^{34}S values are terrestrial ecosystems, and low δ^{34}S values are seen in freshwater ecosystems (Reitsema 2015).

Further discussion of the isotopes and their usefulness can be found in Chapter 2 and 5.1.

In section 5. 1., the carbon (C), nitrogen (N) and sulfur (S) isotope ratios measured in human hair collected throughout Mexico were presented. The recorded values ranged from −18.3 ‰ to −12.8 ‰ for δ^{13}C, 6.8 ‰ to 10.8 ‰ for δ^{15}N, and from 2.7 ‰ to 8.0 ‰ for δ^{34}S. For all three isotope systems, the socioeconomic covariates explored showed some strong correlations to the recorded isotopic values. Furthermore, the results provided records of the dietary preferences and practices throughout Mexico and showed some spatial variation. Here, these results are compared to the values recorded for the various tissues of the undocumented border crossers.

Carbon ($\delta^{13}C$)

The results of the $\delta^{13}C$ analyses in the bones and teeth of sixteen undocumented border crossers can be found in Table 5.5.1.1. Both the carbonate in bioapatite and the collagen were analyzed for the tooth and bone samples. For the teeth, the enamel was used for the carbonate analysis and the root dentin was used for the collagen analysis. The carbonate of bioapatite reflects the whole diet while the collagen is heavily biased toward dietary protein (Ambrose 1993; J. A. Lee-Thorp 2008; Tieszen and Fagre 1993). The results of $\delta^{13}C$ analyses in bones, teeth, and hair of the samples are shown in Figure 5.5.1.1. Comparing the $\delta^{13}C$ values recorded for the various body tissues to the $^{87}Sr/^{86}Sr$ ratios of same tissues (Chapter 5.5.4), it becomes apparent that several cases show the same offset. For example, the $^{87}Sr/^{86}Sr$ ratios of the cases 17-1466 and 17-1944 both indicate that the person did not move during their lifetime. While $\delta^{13}C$ values primarily reflect diet, the $\delta^{13}C$ values in Mexican human hair showed spatial variation, suggesting regional differences in diet (Chapter 5.1). Therefore, this could, on the one hand reflect that this individual did not change his diet during his lifetime, but also that he did not move to a different place with a different diet during his lifetime. Other cases show a similar pattern but show the tooth value to be lower in comparison to the bone values (*e.g.* 17-1314, 16-2326 and 16-3187). This could indicate that the diet of this individual changed from childhood to adulthood.

The visual comparison of $\delta^{13}C$ carbonate and collagen values found in Mexican long bones, ribs, and teeth of UBCs can be found in Figure 5.5.1.2. As mentioned above, collagen and carbonate represent different parts of the diet, with the collagen primarily being representative of the dietary protein intake. The Pearson's product-moment correlation between the collagen and carbonate values found in the skeletal tissues of the 16 undocumented border crossers revealed the tooth values to be most closely related ($r = 0.92$ ($p < 0.001$)), followed by the long bone values ($r = 0.81$ ($p < 0.001$)), and lastly the rib values ($r = 0.87$ ($p < 0.001$)). These correlations were established using the programming language R (R Core Team 2020). It has been shown that the carbon isotopic values of hair keratin and bone collagen correlated to the whole diet of the individual, with the keratin values enriched by +1 to +3‰ and collagen values enriched by approximately +5‰ relative to the diet (Ambrose and Norr 1993; Katzenberg and Krouse 1989; Tieszen and Fagre 1993). This explains why some of the human hair $\delta^{13}C$ values in Figure 5.5.1.1. are lower in comparison to the other tissue values (*e.g.* 17-1742, 16-01822, 16-01616, 17-1466). This is, however, not the case for all the UBC values. For cases 17-1314 and 17-1682, the keratin values appear elevated compared to the values recorded for the long bone and tooth, respectively.

Krueger and Sullivan (1984) as well as Lee-Thorp *et al.* (1989) reported average $\Delta^{13}C_{carbonate\text{-}collagen}$ values of +7 ‰ for herbivores while reporting +3 ‰ and +4 ‰ for carnivores,

respectively. In the samples of UBCs, the $\Delta^{13}C_{carbonate\text{-}collagen}$ values ranged from 5.0 to 7.6 (mean = 6.8, standard deviation 0.8) for the teeth, 3.1 to 6.3 (mean = 4.8, standard deviation 0.9) for the long bones, and 2.2 to 6.0 (mean = 4.2, standard deviation 0.9) for the ribs. Krueger and Sullivan (1984) showed that human populations on a high protein, high fat diet are closer to the carnivore pattern while low-protein, low-fat populations are closer to the herbivore pattern. Here, we see that the ranges from carnivore to herbivore, with the tooth $\Delta^{13}C$ being significantly closer to the herbivore diet defined above. The mean values for the bones lie between the herbivore and the carnivore diet, with some outliers being present (*e.g.* 16-01616).

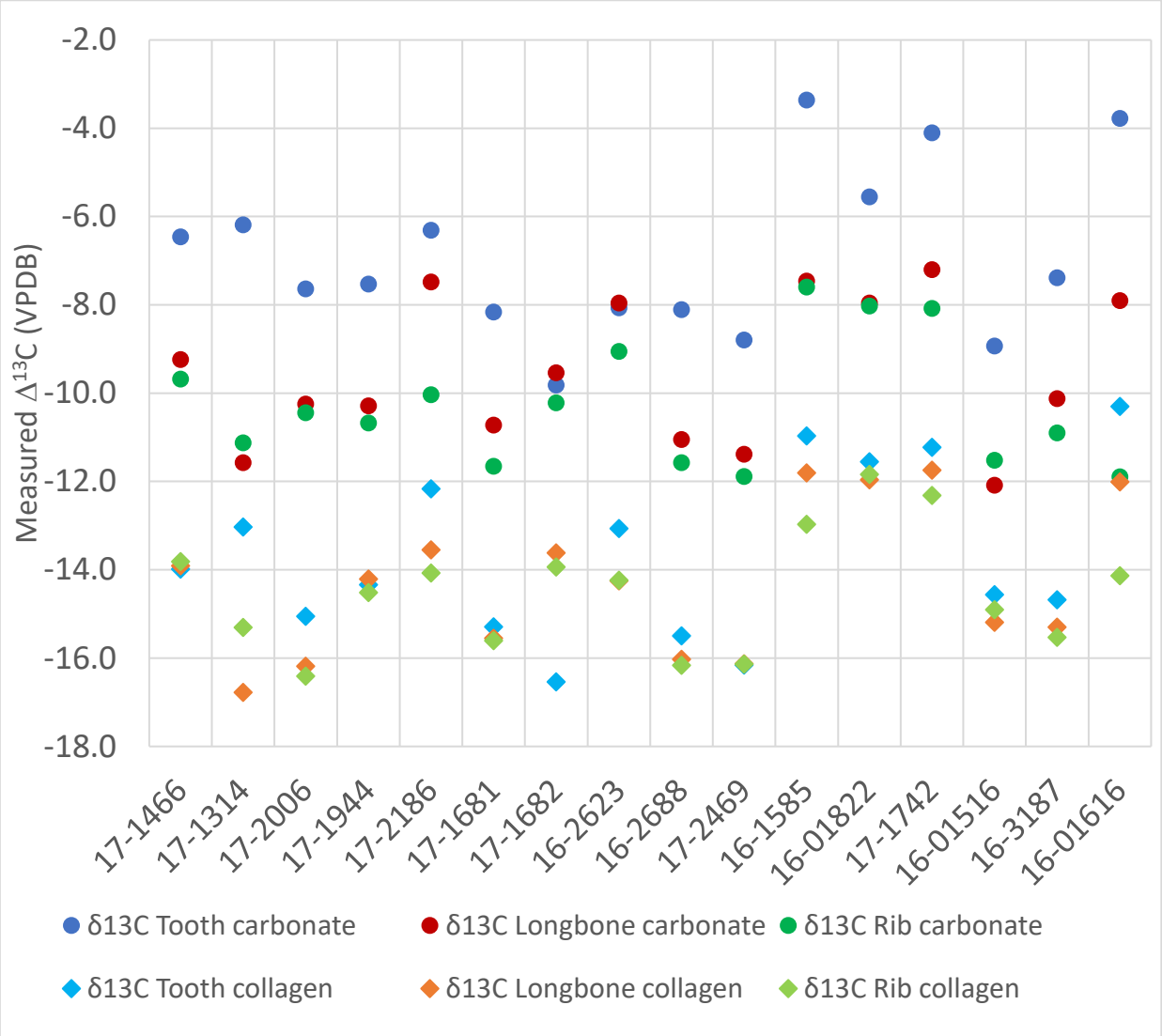

Figure 5.5.1.2. Comparison of $\delta^{13}C$ carbonate and collagen values found in Mexican long bones, ribs, and teeth of UBCs. All values in ‰.

A comparison of Mexican Reference hair δ^{13}C values to δ^{13}C values found in hair, long bones, ribs, and teeth of UBCs using a violin plot can be found in Figure 5.5.1.3. The violin plot shows the probability density of the data at different values. Overall, the δ^{13}C carbonate values are elevated relative to the δ^{13}C hair keratin values. For the tooth values, the values are between 5.5‰ and 11.4‰ higher, with a mean difference of 8.5‰ (standard deviation 2.1‰). The long bones are on average, elevated by 5.6‰ with a standard deviation of 1.3‰ (min.: 3.1‰, max.: 7.3‰). The rib bones are least elevated compared to the keratin values with an average difference of 4.8‰ and a standard deviation of 0.9‰ (min.: 3.3‰, max.: 5.6‰).

The δ^{13}C collagen values of the teeth, long bones, and ribs are overall elevated over the δ^{13}C of the hair keratin of the respective samples. The tooth δ^{13}C values are the most elevated compared to the bone values. The mean difference of the tooth values is 1.9‰ with a standard deviation of 2.0‰. One of the seven samples has a lower value relative to their respective hair keratin value. Therefore, the minimum difference spans from -1.2‰ to 4.9‰. For the long bone δ^{13}C collagen values, a different individual showed lower values, with a mean difference of 1.3‰ (minimum = -0.4‰; maximum = 3.2‰; standard deviation of 1.2‰). The rib values are, with an average value of 1.2‰ (standard deviation of 0.4‰), the least enriched values relative to keratin. The difference spans from 0.3‰ to 1.8‰.

Thus far, it has not been established if and how the δ^{13}C values in human hair keratin are related to the δ^{13}C values in collagen and/or carbonate. Therefore, the relationships between those values were next analyzed. Table 5.5.1.2 outlines the results of the Pearson's product-moment correlation analysis between the δ^{13}C values in hair keratin and the δ^{13}C values of the other human tissues (rib, long bone, tooth) sampled. The correlations were established using the programming language R (R Core Team 2020). The strength of the correlations was primarily defined by the strength of association (r-value): large/strong > 0.5, medium/moderate 0.5 > 0.3, small/weak 0.3 > 0.1, 0.1 > 0 non-existent. Like collagen, hair keratin represents more of the dietary protein than the whole diet. This is evident in the closer relationship of the collagen to the keratin compared to the carbonate. Gordon *et al.* (2019) showed that the δ^{13}C values of human hair are not significantly altered through environmental exposure one-year postmortem. This fact would indicate that the hair samples of UBCs reflect the diet of the individual during the last couple of months prior to their death. Overall, collagen δ^{13}C values correlate stronger than the carbonate δ^{13}C values to the δ^{13}C keratin values. Furthermore, an increased correlation with tissues that represent the time closer to death can be seen. The stronger correlation to the ribs and weaker correlation to the teeth could potentially be explained by the closer temporal relationship of the tissues. Furthermore, the bone collagen and tooth dentin most likely differ because the tooth dentin stores information about

the childhood diet while the bone collagen stores information about the adult diet. Because of the obvious movement of the individuals, the relationship may not be identical (r = 1.0) but the correlation of r = 0.95 ($p < 0.001$) is very strong. While a relationship is clearly visible, it is not possible to quantify the relationship yet. It is important to note that the number of available samples for comparison is very small. Therefore, it is pertinent to further study the correlation of the keratin $\delta^{13}C$ values to the $\delta^{13}C$ values of collagen und carbonate in human bones and teeth.

Overall, the values recorded here for the undocumented border crossers fall within the range of values found for undocumented border crossers recovered in Arizona, as previously presented by Dr. Bartelink at the American Academy of Forensic Sciences 2020 presentation in Anaheim, California (Ammer and Bartelink 2020).

Table 5.5.1.2. Pearson's product-moment correlation results for hair keratin $\delta^{13}C$ and the $\delta^{13}C$ values of carbonate and collagen in bones and teeth found in the undocumented border crossers (n=16).

	Tooth $\delta^{13}C$		Long bone $\delta^{13}C$		Rib $\delta^{13}C$	
	Carbonate	Collagen	Carbonate	Collagen	Carbonate	Collagen
Hair $\delta^{13}C$ Keratin	r = 0.39 p = 0.38	r = 0.43 p = 0.33	r = 0.75 p = 0.05	r = 0.83 p = 0.02	r = 0.83 p = 0.02	r = 0.95 p < 0.001

Table 5.5.1.1. Results of $\delta^{13}C$ analyses in bones, teeth, and hair of sixteen undocumented border crossers housed at the PCOME. All values in ‰.

	$\delta^{13}C$ Tooth carb.	stdev	$\delta^{13}C$ LB carb.	stdev	$\delta^{13}C$ Rib carb.	stdev	$\delta^{13}C$ Tooth collagen	Total C (µg)	$\delta^{13}C$ LB collagen	Total C (µg)	$\delta^{13}C$ Rib collagen	Total C (µg)	$\delta^{13}C$ Hair a	Total C (µg)	$\delta^{13}C$ Hair b	Total C (µg)	$\delta^{13}C$ Hair c	Total C (µg)	$\delta^{13}C$ Hair mean	Total C (µg)
17-1466	-6.5	0.2	-9.2	0.3	-9.7	0.1	-13.99	415.76	-13.91	530.61	-13.82	549.50	-14.98	225.76	-15.16	198.88	-14.98	192.35	-15.04	205.67
17-1314	-6.2	0.1	-11.6	0.1	-11.1	0.1	-13.03	450.03	-16.77	490.76	-15.30	487.70	-16.40	240.17	-16.45	214.71	-16.21	224.15	-16.35	226.35
17-2006	-7.6	0.2	-10.2	0.1	-10.4	0.3	-15.05	437.62	-16.19	507.98	-16.41	467.06								
17-1944	-7.5	0.2	-10.3	0.2	-10.7	0.2	-14.34	429.19	-14.21	441.96	-14.52	541.10								
17-2186	-6.3	0.2	-7.5	0.2	-10.0	0.1	-12.17	454.90	-13.55	475.13	-14.07	448.14								
17-1681	-8.2	0.1	-10.7	0.1	-11.7	0.1	-15.29	464.38	-15.55	437.70	-15.60	544.40								
17-1682	-9.8	0.2	-9.5	0.0	-10.2	0.1	-16.54	441.88	-13.62	445.49	-13.94	531.97	-15.30	236.29	-15.33	191.93	-15.35	191.44	-15.33	206.56
16-2623	-8.1	0.2	-8.0	*	-9.1	0.1	-13.07	470.41	-14.25	482.34	-14.24	502.79								
16-2688	-8.1	0.1	-11.0	0.1	-11.6	0.1	-15.49	409.12	-16.03	530.43	-16.17	540.88								
17-2469	-8.8	0.3	-11.4	0.1	-11.9	0.2	-16.16	481.90	-16.13	541.72	-16.14	548.28								
16-1585	-3.4	0.2	-7.5	0.1	-7.6	0.2	-10.97	434.27	-11.80	460.07	-12.97	478.63								
16-01822	-5.6	0.1	-8.0	0.1	-8.0	0.2	-11.56	478.32	-11.96	446.87	-11.84	493.37	-13.80	216.22	-13.63	230.29	-13.42	213.18	-13.62	219.89
17-1742	-4.1	0.2	-7.2	0.2	-8.1	0.1	-11.23	489.44	-11.75	540.60	-12.32	504.55	-13.48	217.09	-13.50	207.75	-13.80	208.34	-13.60	211.06
16-01516	-8.9	0.2	-12.1	0.1	-11.5	0.1	-14.57	443.91	-15.19	460.68	-14.91	450.61	-15.36	234.63	-15.18	190.11	-15.15	233.92	-15.23	219.55
16-3187	-7.4	0.1	-10.1	0.1	-10.9	0.1	-14.68	428.94	-15.30	482.32	-15.53	467.34								
16-01616	-3.8	0.2	-7.9	0.1	-11.9	0.1	-10.30	431.71	-12.01	451.34	-14.13	458.20	-15.21	234.55	-15.10	202.24	-15.30	135.94	-15.20	190.91

carb. = carbonate
LB = Long bone
stdev = standard deviation
* only one peak was produced during the analysis
Green writing: Sample analysis completed at the Stable Isotope Ratio Facility for Environmental Research University of Utah
Red writing: Sample analysis completed at UC Davis Stable Isotope Facility

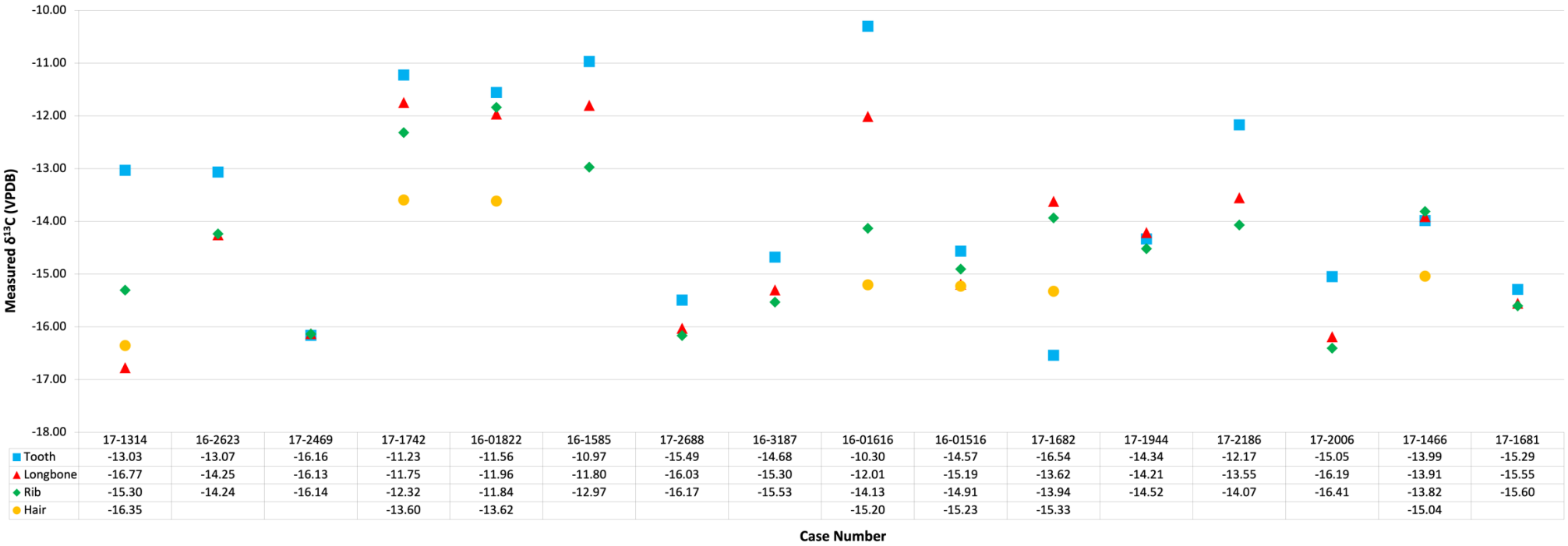

	17-1314	16-2623	17-2469	17-1742	16-01822	16-1585	17-2688	16-3187	16-01616	16-01516	17-1682	17-1944	17-2186	17-2006	17-1466	17-1681
Tooth	-13.03	-13.07	-16.16	-11.23	-11.56	-10.97	-15.49	-14.68	-10.30	-14.57	-16.54	-14.34	-12.17	-15.05	-13.99	-15.29
Longbone	-16.77	-14.25	-16.13	-11.75	-11.96	-11.80	-16.03	-15.30	-12.01	-15.19	-13.62	-14.21	-13.55	-16.19	-13.91	-15.55
Rib	-15.30	-14.24	-16.14	-12.32	-11.84	-12.97	-16.17	-15.53	-14.13	-14.91	-13.94	-14.52	-14.07	-16.41	-13.82	-15.60
Hair	-16.35			-13.60	-13.62				-15.20	-15.23	-15.33				-15.04	

Figure 5.5.1.1. Visualization of the results of δ^{13}C collagen analyses in bones, teeth, and hair of sixteen undocumented border crossers housed at the PCOME. All values in ‰.

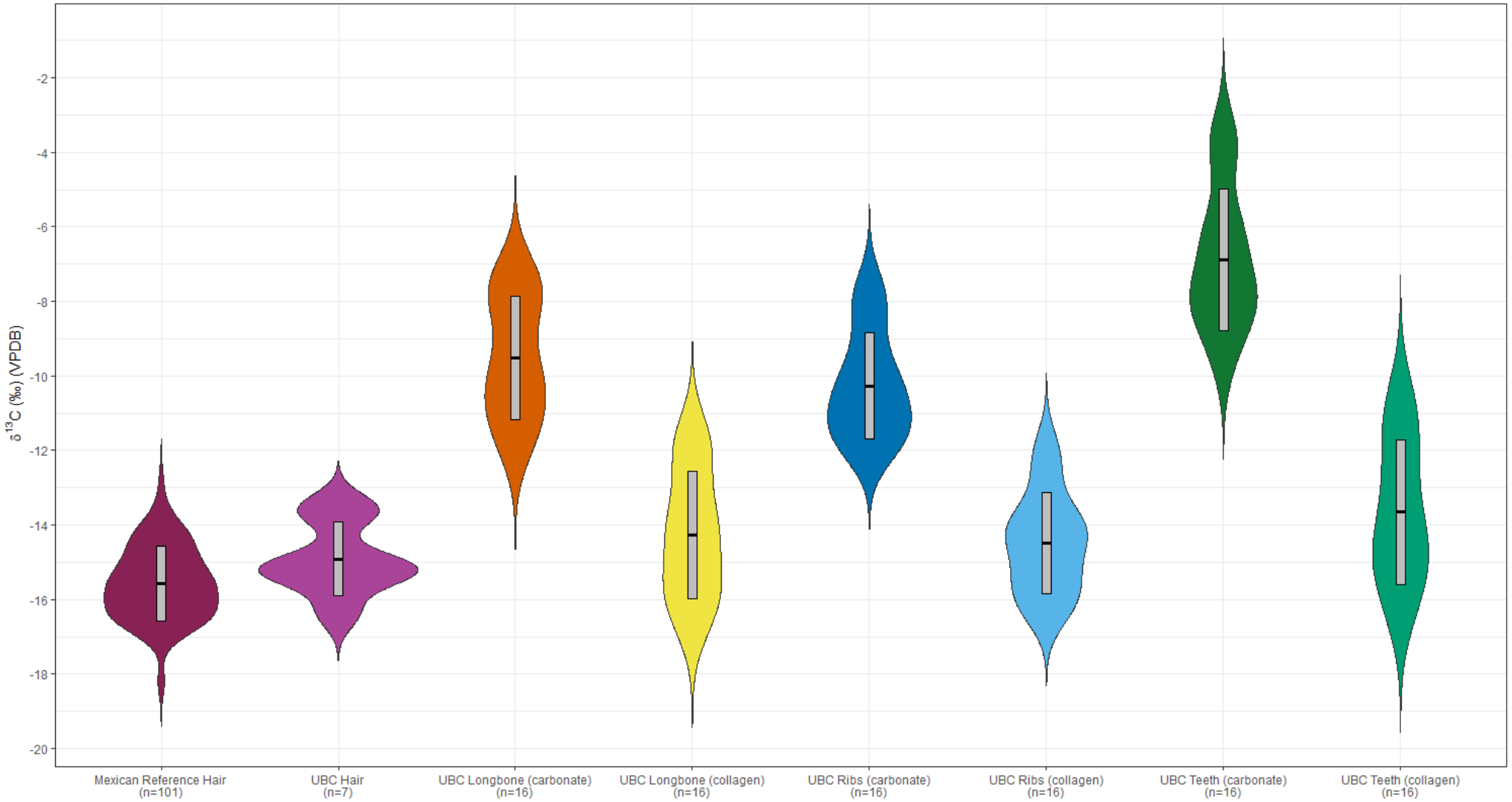

Figure 5.5.1.3. Comparison of Mexican reference hair $\delta^{13}C$ values to $\delta^{13}C$ values found in hair, long bones, ribs, and teeth of UBCs. All values in ‰.

Nitrogen (δ^{15}N)

The results of the δ^{15}N analyses in bones and teeth and of the sixteen UBCs can be found in Table 5.5.1.3. The data are presented in Figure 5.5.1.4 and the probability density of the data at different values is shown in the violin plots in Figure 5.5.1.5. The data show that the δ^{15}N collagen values were, on average, elevated relative to the hair keratin values.

For the teeth, δ^{15}N values are elevated 0.8‰, with a standard deviation of 0.8‰. Two individuals (16-01822 and 17-1742) showed lower δ^{15}N collagen values compared to their respective hair samples. Therefore, the difference in values ranged from -0.2‰ to 1.6‰. The same two individuals also showed lower long bone δ^{15}N values relative to their keratin value. The mean difference was significantly lower than in the tooth values (0.3‰ with a standard deviation of 0.8‰). The values ranged from -1.3‰ to 1.0‰.

Lastly, the rib δ^{15}N values were elevated 0.3‰. One of the individuals (16-01822) that showed lower values for the δ^{15}N tooth and long bone collagen also showed a low δ^{15}N rib value relative to their hair keratin. This individual is the one that showed the lowest δ^{15}N values in the other skeletal elements. Overall, the mean difference between the rib δ^{15}N values compared to the hair keratin was 0.9‰ (standard deviation of 0.7‰), ranging from -0.4‰ to 1.4‰.

Comparing these results to the findings of O'Connell *et al.* (2001), the mean differences were similar for the tooth and rib δ^{15}N collagen values but higher relative to the long bone values (0.3‰ vs. 0.86‰ in O'Connell *et al.* (2001)). O'Connell *et al.* (2001) found a much lower standard deviation in their samples (0.17‰) as well as no cases of hair keratin showing higher δ^{15}N values than their bone collagen counterparts.

Overall, the correlations of δ^{15}N collagen values with their respective δ^{15}N hair keratin values were strong. The strongest correlation was found between the teeth dentinal collagen and the hair ($r = 0.70$, $p = 0.08$). The correlation between the bones (long bones and ribs) and the respective hair were similar, with correlations of $r = 0.64$ ($p = 0.12$) and $r = 0.65$ ($p = 0.11$), respectively. While these correlations are significant, they do no not allow for the establishment of conversion equations.

Gordon *et al.* (2019) not only showed that the δ^{13}C values of human hair are not significantly altered through environmental exposure one-year postmortem but also showed the same for the δ^{15}N. This fact would indicate that the hair samples of UBCs in fact reflect the diet of the individual during the last couple of weeks prior to their death. According to Meier-Augenstein (2018), the δ^{15}N in hair range from slightly below +8 ‰ in vegans to approximately +11 ‰ in omnivores (bordering on carnivores). This would indicate that UBCs ate less meat than the average Mexican population during their last weeks prior to death. Research by Mekota *et al.*

(2006) also showed increased δ^{15}N in human hair during periods of malnutrition and starvation. Potentially, it cannot be excluded that the undocumented border crossers who died in the dessert had suffered malnutrition and starvation prior to their death because a single hair strand takes approximately 6-12 days to exit the scalp and that a geographic location change takes a minimum of 6-12 days to show in the δ^{15}N values of male facial hair (Nakamura *et al.* 1982; Valkovic *et al.* 1975). Here, the hair strands were not cut at the scalp but pulled with the root and should therefore reflect the time closer to death than the studies mentioned above. Nonetheless, the hair values will not be representative of the immediate time before passing. Furthermore, because the hair samples were analyzed in bulk, it is not possible to tell if and how the eating habits of the traveling undocumented border crossers may have changed during their journey.

Generally, the bone collagen δ^{15}N values recorded for these 16 undocumented border crossers fall into the reported range of values for undocumented border crossers previously recovered from Arizona (Ammer and Bartelink 2020).

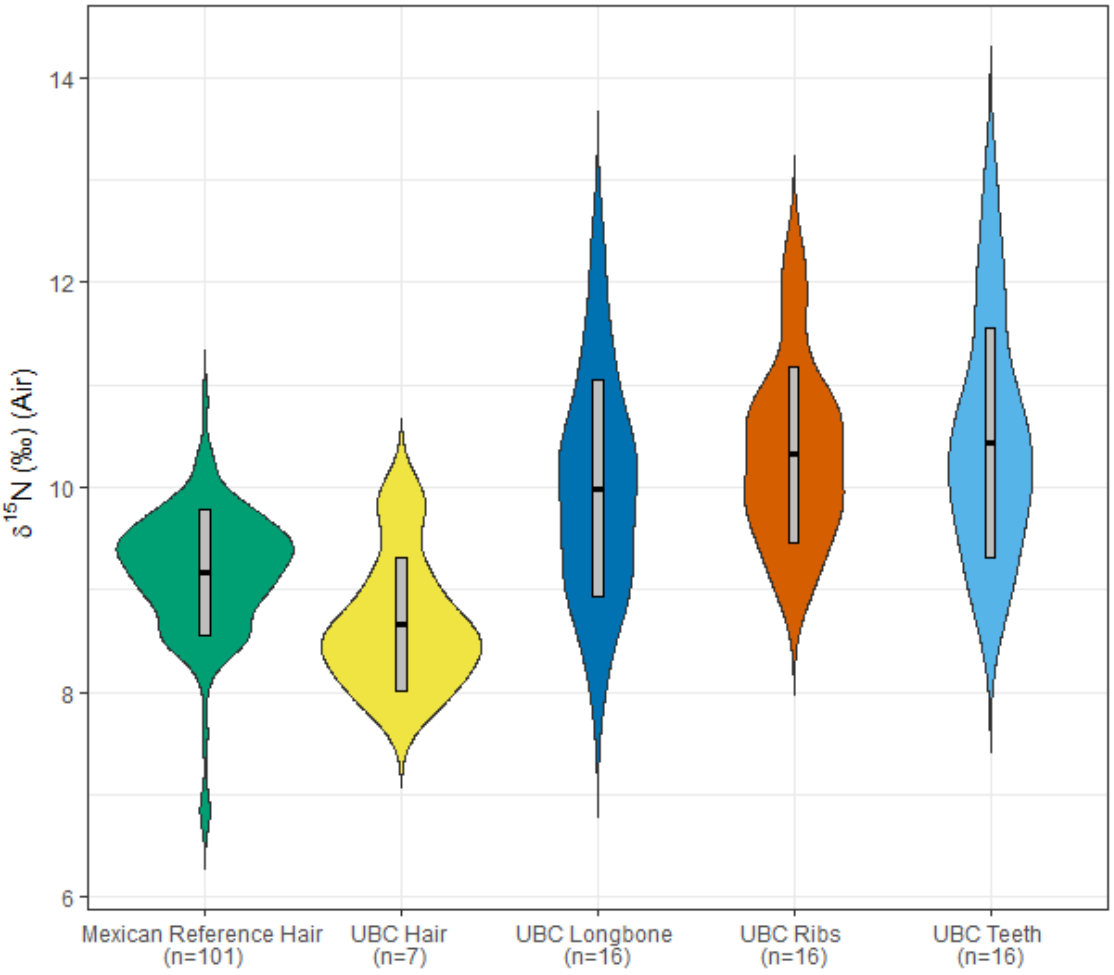

Figure 5.5.1.5. Comparison of Mexican reference hair δ^{15}N values to δ^{15}N values found in hair, long bones, ribs, and teeth of UBCs. All values in ‰.

Table 5.5.1.3. Results of δ^{15}N analyses in bones, teeth, and hair of sixteen undocumented border crossers housed at the PCOME. All values in ‰.

	δ^{15}N Tooth	Total N (µg)	δ^{15}N LB	Total N (µg)	δ^{15}N Rib	Total N (µg)	δ^{15}N *Hair a*	Total N (µg)	δ^{15}N *Hair b*	Total N (µg)	δ^{15}N *Hair c*	Total N (µg)	δ^{15}N *Hair mean*	Total N (µg)
17-1466	11.08	150.28	10.26	190.38	10.76	196.02	9.84	77.04	9.85	64.75	9.84	62.72	9.84	68.17
17-1314	10.08	163.47	9.09	174.28	9.83	174.28	8.55	80.98	8.53	69.72	8.54	75.66	8.54	75.45
17-2006	10.21	152.68	10.57	173.87	10.55	154.88								
17-1944	10.39	155.31	9.66	159.88	9.85	194.18								
17-2186	9.89	164.00	9.26	165.76	9.25	153.25								
17-1681	11.92	166.11	11.20	156.17	10.94	187.29								
17-1682	9.73	159.73	10.23	161.73	10.69	190.57	9.48	77.10	9.12	65.93	9.16	62.59	9.25	68.54
16-2623	10.58	170.28	10.39	170.27	10.73	174.84								
16-2688	12.88	148.97	12.26	183.69	12.19	186.86								
17-2469	10.54	174.80	9.96	192.54	9.87	195.49								
16-1585	8.83	157.47	8.96	163.42	10.10	168.85								
16-01822	9.26	173.85	8.19	161.30	9.01	176.84	9.32	72.54	9.52	78.39	9.54	72.85	9.46	74.59
17-1742	9.03	176.98	8.85	193.97	9.42	179.00	9.01	68.99	9.20	69.05	9.13	65.80	9.12	67.94
16-01516	11.97	162.07	11.35	167.82	11.70	159.05	10.35	76.82	10.51	62.45	10.27	80.64	10.37	73.30
16-3187	10.90	154.18	10.25	169.73	10.38	157.78								
16-01616	9.68	154.13	9.29	163.49	9.83	162.04	8.51	78.71	8.49	68.44	8.55	44.16	8.52	63.77

LB = Long bone
Sample analysis completed at UC Davis Stable Isotope Facility

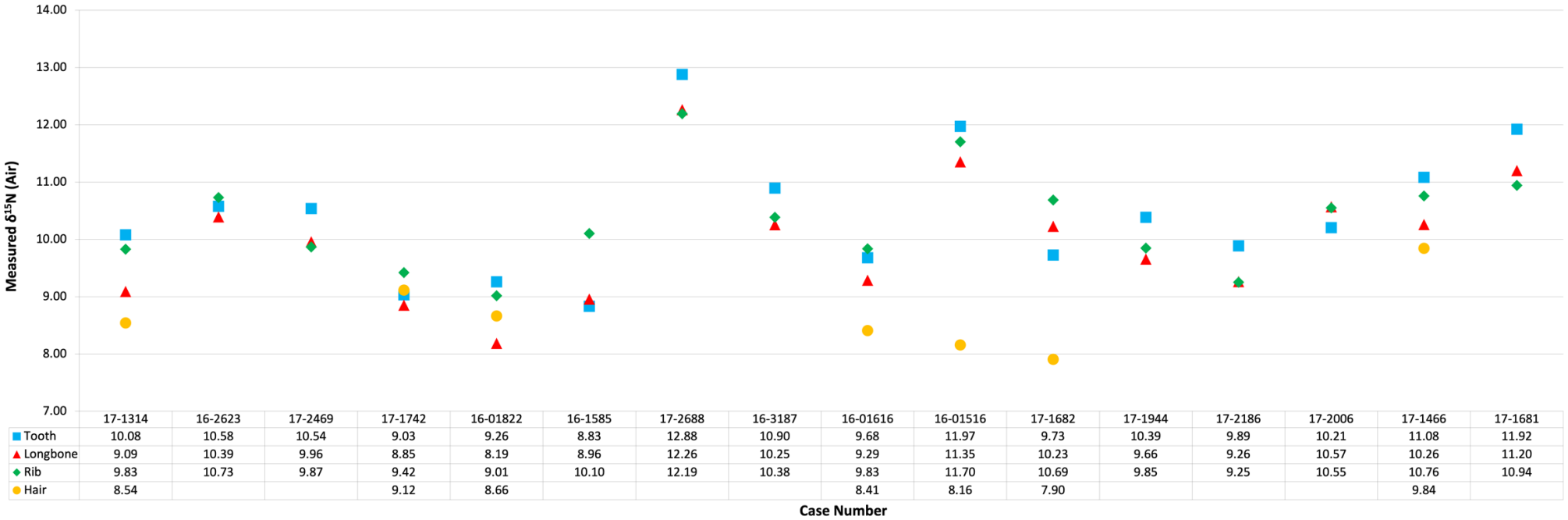

	17-1314	16-2623	17-2469	17-1742	16-01822	16-1585	17-2688	16-3187	16-01616	16-01516	17-1682	17-1944	17-2186	17-2006	17-1466	17-1681
Tooth	10.08	10.58	10.54	9.03	9.26	8.83	12.88	10.90	9.68	11.97	9.73	10.39	9.89	10.21	11.08	11.92
Longbone	9.09	10.39	9.96	8.85	8.19	8.96	12.26	10.25	9.29	11.35	10.23	9.66	9.26	10.57	10.26	11.20
Rib	9.83	10.73	9.87	9.42	9.01	10.10	12.19	10.38	9.83	11.70	10.69	9.85	9.25	10.55	10.76	10.94
Hair	8.54			9.12	8.66				8.41	8.16	7.90				9.84	

Figure 5.5.1.4. Visualization of the results of δ^{15}N analyses in bones, teeth, and hair of sixteen undocumented border crossers housed at the PCOME. All values in ‰.

Sulfur ($\delta^{34}S$)

An overview of the results of the $\delta^{34}S$ analyses in bones and teeth of the sixteen UBCs can be found in Table 5.5.1.4. The values presented in Figure 5.5.1.6 and the probability density of the data at the different isotopic values is shown in the violin plots in Figure 5.5.1.7. These figures show that $\delta^{34}S$ collagen values were overall slightly elevated relative to their hair keratin values.

The teeth collagen values are elevated between 0.1‰ and 4.3‰, with an average difference of 1.9‰ (standard deviation of 1.3‰). The long bones $\delta^{34}S$ values are, on average, much lower while maintaining a similar standard deviation, with an average difference of 0.8‰ and a standard deviation of 1.5‰. Two individuals showed low $\delta^{34}S$ collagen values relative to their hair keratin. The values ranged from -1.2‰ to 3.3‰.

The ribs show a narrower window of values. The same two individuals that showed low $\delta^{34}S$ values in their long bones as well as an additional third individual showed lower $\delta^{34}S$ bone collagen values than their keratin values. The lowest value was -1.3‰ and the highest value was 1.6‰. The average value was -0.1‰ with a standard deviation of 1.0‰, which means that overall, the rib collagen $\delta^{34}S$ values were slightly smaller relative to hair keratin values.

This could indicate that human hair keratin $\delta^{34}S$ values reflect collagen values in other human tissues, such as bones and tooth dentin. While researchers have found spatial variation in the $\delta^{34}S$ keratin values in the United States and Canada (Valenzuela *et al.* 2011; Clement P. Bataille *et al.* 2020), this relationship was not found in Mexican hair samples (Chapter 5.1). Therefore, this finding could be of use for region-of-origin predictions north of Mexico while it may not be useful (yet) to this ongoing research.

The correlations of the $\delta^{34}S$ collagen values in bones and teeth to their respective hair keratin values varied substantially between different tissues. While the teeth and long bones did not show strong correlations to the hair keratin values ($r = 0.38$, $p = 0.40$ and $r = 0.28$, $p = 0.54$, respectively), the rib $\delta^{34}S$ collagen values correlated strongly to their respective hair samples, with a correlation of 0.70 ($p = 0.08$). Nonetheless, this correlation was not strong enough to draw further conclusions.

Thus far, the $\delta^{34}S$ isotopic values have been underutilized due to the lack of research into which factors influence the variation observed in the $\delta^{34}S$ values of human tissues. $\delta^{34}S$ isotopic values are largely influenced by direct or indirect marine consumption, either through the direct ingestion of marine sourced foods or through the aerosols of the so-called “sea spray effect”. In the human hair references, there was little evidence showing that the proximity to the water influenced the $\delta^{34}S$ isotopic values, which further complicates the interpretation. While currently

understudied and the Mexican reference hair values showing promising results, there are certainly great opportunities to use δ^{34}S isotopic values for region-of-origin predictions in the future.

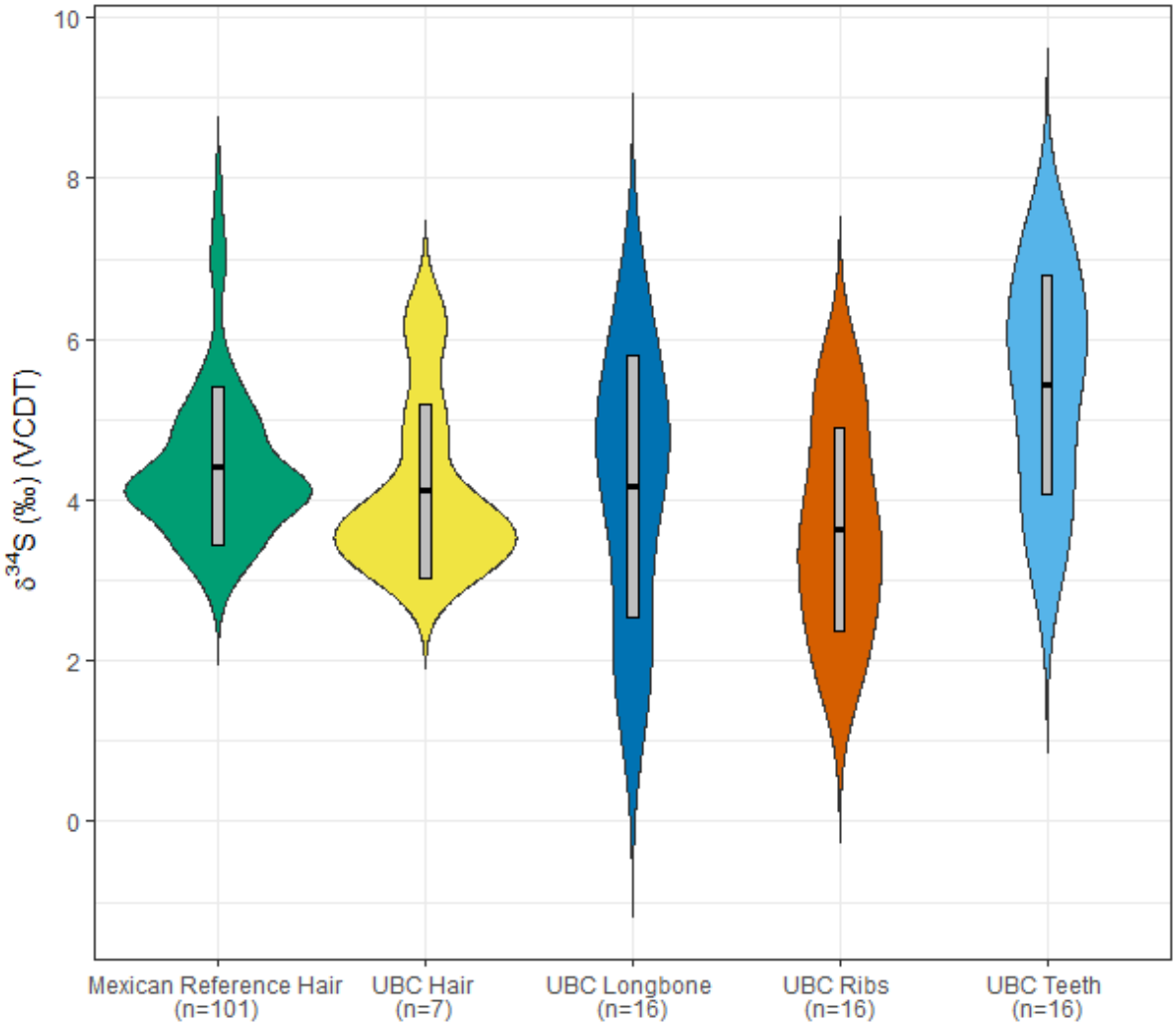

Figure 5.5.1.7. Comparison of Mexican reference hair δ^{34}S values to δ^{34}S values found in hair, long bones, ribs, and teeth of UBCs. All values in ‰.

Table 5.5.1.4. Results of δ^{34}S analyses in bones, teeth. and hair of sixteen undocumented border crossers housed at the PCOME. All values in ‰.

	$\delta^{34}S$ Tooth	Total S (µg)	$\delta^{34}S$ LB	Total S (µg)	$\delta^{34}S$ Rib	Total S (µg)	$\delta^{34}S$ *Hair a*	Total S (µg)	$\delta^{34}S$ *Hair b*	Total S (µg)	$\delta^{34}S$ *Hair c*	Total S (µg)	$\delta^{34}S$ *Hair mean*	Total S (µg)
17-1466	3.7	29	2.4	23	2.3	24	3.6	70	3.6	78	3.7	77	3.6	75
17-1314	5.8	26	4.4	25	3.9	23	3.9	75	3.8	72	3.9	75	3.9	74
17-2006	6.1	26	5.5	24	5.4	23								
17-1944	4.5	29	3.1	24	3.3	22								
17-2186	6.1	27	4.3	22	3.9	24								
17-1681	5.0	25	4.1	26	3.6	25								
17-1682	5.0	29	5.0	25	2.9	24	3.0	76	3.4	75	3.6	79	3.3	77
16-2623	4.0	28	2.2	24	2.5	26								
16-2688	5.8	27	5.3	26	4.6	23								
17-2469	3.6	28	1.3	22	1.7	23								
16-1585	7.0	28	4.7	22	3.5	24								
16-01822	6.9	29	6.5	26	5.5	26	5.0	75	5.0	81	5.0	75	5.0	77
17-1742	7.5	29	6.5	25	4.8	26	3.2	69	3.2	70	3.2	71	3.2	70
16-01516	6.9	27	5.5	22	5.5	24	6.0	79	6.2	79	6.4	77	6.2	78
16-3187	3.0	27	1.6	25	1.9	23								
16-01616	6.0	29	4.2	25	2.9	24	3.6	76	3.6	69	3.6	72	3.6	72

LB = Long bone

Sample analysis completed at UC Davis Stable Isotope Facility

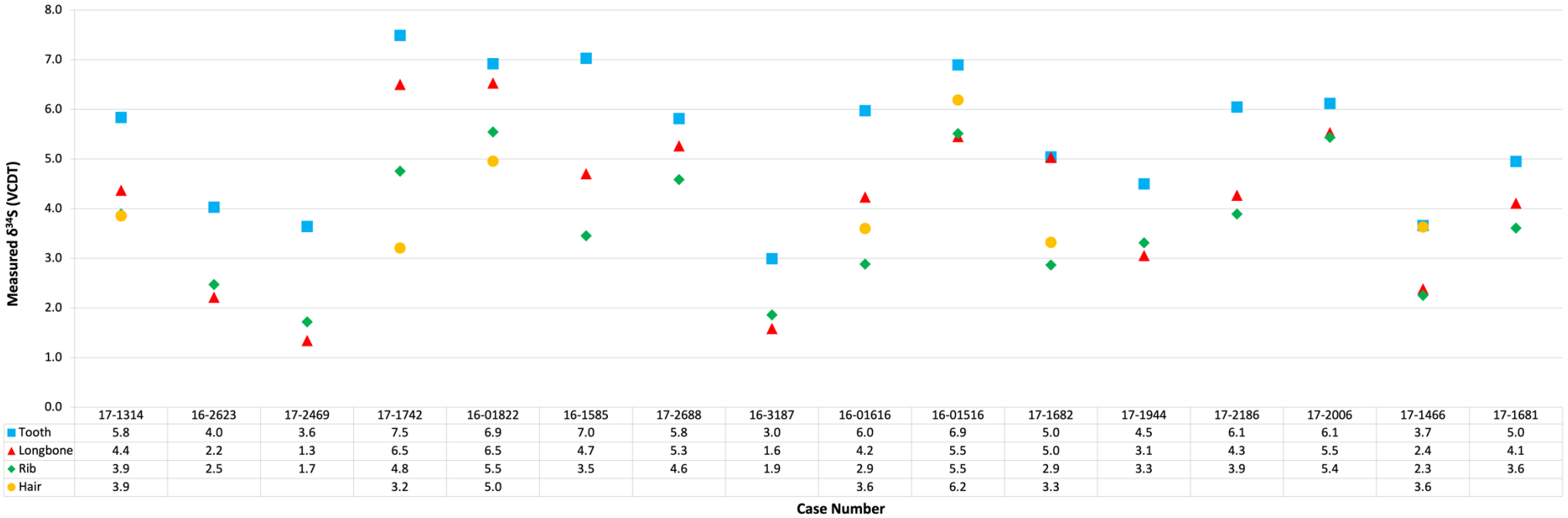

	17-1314	16-2623	17-2469	17-1742	16-01822	16-1585	17-2688	16-3187	16-01616	16-01516	17-1682	17-1944	17-2186	17-2006	17-1466	17-1681
Tooth	5.8	4.0	3.6	7.5	6.9	7.0	5.8	3.0	6.0	6.9	5.0	4.5	6.1	6.1	3.7	5.0
Longbone	4.4	2.2	1.3	6.5	6.5	4.7	5.3	1.6	4.2	5.5	5.0	3.1	4.3	5.5	2.4	4.1
Rib	3.9	2.5	1.7	4.8	5.5	3.5	4.6	1.9	2.9	5.5	2.9	3.3	3.9	5.4	2.3	3.6
Hair	3.9			3.2	5.0				3.6	6.2	3.3				3.6	

Figure 5.5.1.6. Visualization of the results of δ^{34}S analyses in bones, teeth, and hair of sixteen undocumented border crossers housed at the PCOME. All values in ‰.

Conclusion

Overall, the interpretation of carbon, nitrogen, and sulfur isotopic values demonstrate difficulties due to the significant lack of reference data, especially for the collagen and carbonate values of human tissues, such as bones and teeth. While archaeological research may be used for broader interpretation, such as that the variation of $\delta^{13}C$ is explained by the consumption of different relative amounts of C_3 vs. C_4 plants, and that the $\delta^{15}N$ variation is correlated to the amount of proteins consumed by a person, there are no controlled values available for direct interpretation other than hair data. The foremost issues with the available hair data is that the correlations of hair keratin to other skeletal tissues is understudied, and while the existing studies give indication of the direction of the correlation, no conversion equations could be established thus far. Similarly, some significant correlations were discovered in this study but due to the small sample size, no further conclusions could be drawn. It can be assumed that many variables play into the isotopic values of body tissues and before any equations for conversions (from *e.g.* hair keratin to bone collagen) can be established, these variables need to be thoroughly studies. Thus far, many questions remain unanswered regarding the interpretation of the carbon, nitrogen and sulfur isotopic values obtained from the undocumented border crossers.

5. 5. 2. Results and Discussion of the Oxygen Isotope Analyses of Body Tissues of Undocumented Border Crossers

Oxygen isotope ($\delta^{18}O$) values are thought to be an indicator of climate and diet because approximately 60% percent of the human body is composed of oxygen and hydrogen (Emsley 2011). $\delta^{18}O$ values reflect the water that an individual imbibes during life. The geological signal that is taken up in liquid form through the water is transferred to various tissues, internally and externally (Ehleringer *et al.* 2010). This means that probable regions of origin can be predicted for individuals based on their measured isotope ratios. While the theory of predicting regions of origins is rather straight forward, this research has shown that many issues can arise and make the process much more difficult than originally anticipated.

The significant issues which arose during the analyses of the Mexican reference hair samples were outlined in detail in Chapter 5.3. Unfortunately, at this point, no reference database for comparison could be built. However, a reference database of $\delta^{18}O$ in tap water was established and corresponding isoscapes were developed (Chapter 5.2).

The results of the $\delta^{18}O$ analyses in bones, teeth, and hair of sixteen UBCs from the PCOME are reported in Table 5.5.2.1. The $\delta^{18}O$ values are plotted using the (VPDB) scale in Figure 5.5.2.1. As can be seen in table, there are significant differences between the $\delta^{18}O$ values recorded from the teeth analyzed at the Stable Isotope Ratio Facility for Environmental Research of the University of Utah and the $\delta^{18}O$ values recorded from the teeth analyzed at IsoForensics (green and blue writing). Recent research showed that the methodology of the analysis (*e.g.* the temperature at which the samples are run) influence the resulting $\delta^{18}O$ values (L. A. Chesson *et al.* 2019). Unfortunately, this fact further inhibits the ability to establish region of origin predictions. It is, however, important to note that two cases, recently identified by the Pima County Office of the Medical Examiner, were successfully used for region of origin predictions. These two successful case studies are presented in Chapter 5.5.5. Therefore, here the cases analyzed by Isoforensics (blue writing in Table 5.5.2.1) will be presented.

The isoscape used for the following region of origin assignments was previously presented and discussed in Chapter 5.2. The assignments were created using a conditional correlation approach, which is further discussed in Chapter 5.5.3. In order to use the $\delta^{18}O$ (VPDB) values for region of origin assignments, the values had to be converted onto the VSMOW scale (Coplen 1988; Iacumin *et al.* 1996; Daux *et al.* 2008).

1. *Tooth apatite $\delta^{18}O$ (VPDBcarbonate) --> Tooth apatite $\delta^{18}O$ (VSMOWcarbonate)*

   1.03091 * $\delta^{18}O$ (VPDBcarbonate) + 30.91 = $\delta^{18}O$ (VSMOWcarbonate)

2. *Tooth apatite $\delta^{18}O$ (VSMOWcarbonate)--> Tooth apatite $\delta^{18}O$ (VSMOWphosphate)*

   0.998 * $\delta^{18}O$ (VSMOWcarbonate) - 8.5 = $\delta^{18}O$ (VSMOWphosphate)

3. *Tooth apatite (VSMOWphosphate)-->Predicted water (VSMOWphosphate)*

   1.54 * $\delta^{18}O$ (VSMOWphosphate) - 33.72 = $\delta^{18}O$ (VSMOWphosphate)

The equation used for this conversion is also presented in Chapter 5.5.3 and discussed in greater detail.

Table 5.5.2.1. Results of $\delta^{18}O$ analyses in bones, teeth, and hair of sixteen undocumented border crossers housed at the PCOME. All values in ‰.

	$\delta^{18}O$ (VPDB) Tooth	StDev	$\delta^{18}O$ (VPDB) Long bone	StDev	$\delta^{18}O$ (VPDB) Rib	StDev	$\delta^{18}O$ (VPDB) Hair
17-1466	-5.9	0.4	-2.4	0.3	-6.3	0.2	11.7
17-1314	-7.0	0.1	-4.7	0.1	-3.3	0.1	10.5
	-3.4						
17-2006	-4.1	0.2	-2.9	0.2	-2.3	0.3	
17-1944	-5.0	0.3	-5.3	0.1	-4.8	0.3	
17-2186	-6.0	0.2	-4.5	0.1	-7.2	0.1	
17-1681	-4.6	0.2	-3.0	0.1	-1.1	0.2	
17-1682	-3.9	0.2	-5.0	0.2	-7.9	0.1	10.1
	-5.6						
16-2623	-4.8	0.1	-2.1	*	-2.5	0.1	
	-3.0						
16-2688	-5.4	0.1	-3.8	0.1	-4.4	0.1	
	-4.5						
17-2469	-2.8	0.5	-5.9	0.1	-5.7	0.1	
16-1585	-5.7	0.3	-3.7	0.1	-1.8	0.2	
16-01822	-5.5	0.2	-3.4	0.2	-5.5	0.1	11.1
	-5.4						
17-1742	-6.4	0.2	-5.3	0.2	-5.1	0.2	12.5
	-5.4						
16-01516	-5.2	0.2	-1.6	0.2	-3.7	0.1	11.0
	-6.2						
16-3187	-5.6	0.2	-5.6	0.1	-4.0	0.2	
16-01616	-4.7	0.2	-3.2	0.2	-6.4	0.3	12.7
	-5.6						

* only one peak was produced during the analysis

Green writing: Sample analysis completed at the Stable Isotope Ratio Facility for Environmental Research University of Utah

Blue writing: Sample analysis completed at IsoForensics for Prof. Bartelink

Red writing: Sample analysis completed at UC Davis Stable Isotope Facility

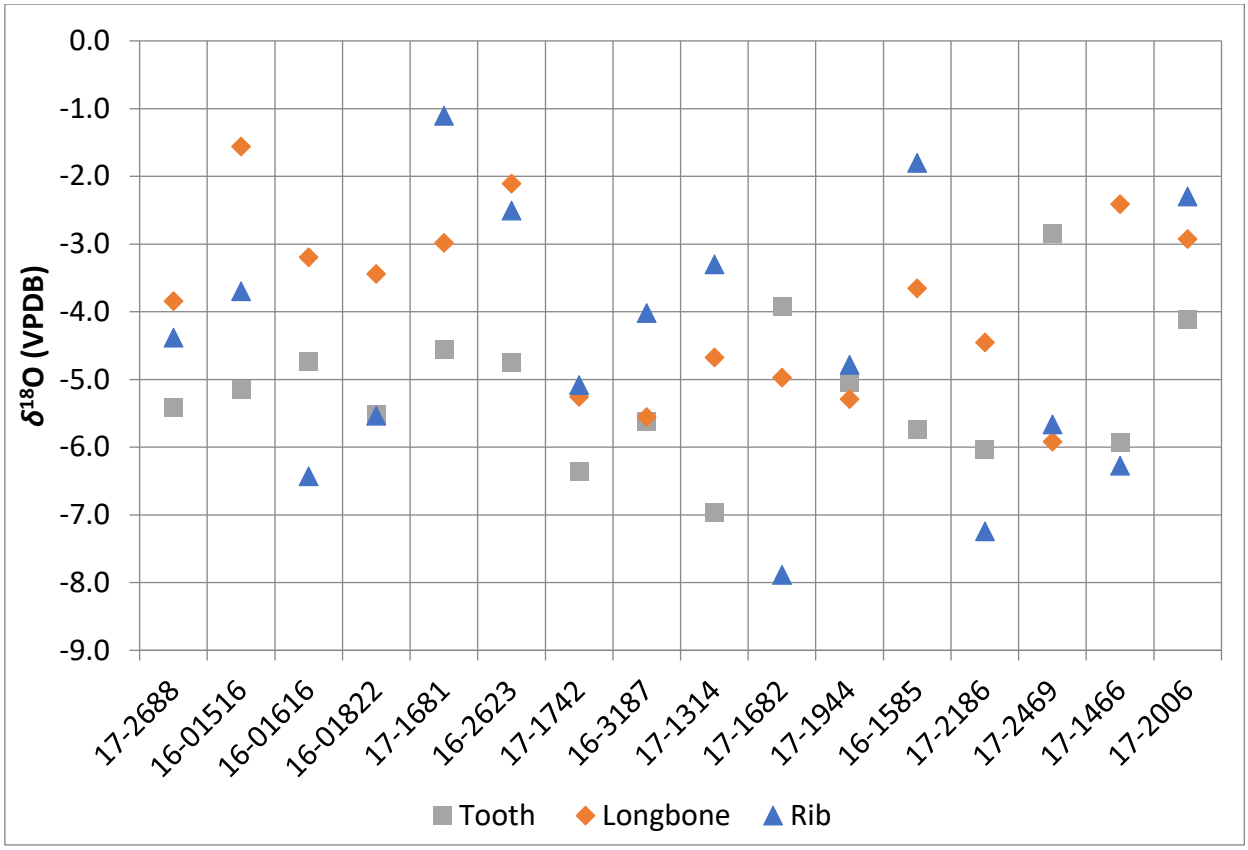

Figure 5.5.2.1. $\delta^{18}O$ (VPDB) values of the 16 undocumented border crossers teeth, long bones, and ribs (analyzed at the University of Utah). All values in ‰.

17-1742

The $\delta^{18}O$ value of -5.4‰ was reported for the right second maxillary premolar. The conversion and subsequent conditional correlation approach yielded potential areas of origin in Baja California as well as lower elevation areas of the Sierra Madre mountainous range. Furthermore, parts of the states Oaxaca and Guerrero are marked as potential regions of origin based on the $\delta^{18}O$ value.

Figure 5.5.2.2. $\delta^{18}O$ region of origin predictions for individual 17-1742 based on the right second maxillary premolar.

17-1682

For individual 17-1682, the left second maxillary premolar yielded a $\delta^{18}O$ value of -5.6‰. The predicted regions of origin lay in the medium altitude regions of Mexico as well as the northern part of Baja California. Overall, the predicted regions of origin concentrate on the south west of Mexico.

Figure 5.5.2.3. $\delta^{18}O$ region of origin predictions for individual 17-1682 for the left second maxillary premolar.

17-1314

The recorded $\delta^{18}O$ value for Individual 17-1314 was -3.4‰ based on the left second maxillary premolar. The predicted regions of origin focus on the Yucatan peninsula as well as a large region in the states of Sonora and Chihuahua. A smaller area of prediction lays in the east of the country, inland from the coastline of the Gulf of Mexico.

Figure 5.5.2.4. $\delta^{18}O$ region of origin predictions for individual 17-1314 based on the left second maxillary premolar.

16-2688

The $\delta^{18}O$ value of -4.5‰ was reported for the left first maxillary premolar. The conversion and subsequent conditional correlation approach yielded potential areas of origin in the north of the country, along the coastline of Sinaloa as well as the states of Chihuahua, Coahuila, and Nuevo Leon. The predicted areas also include the midsection of the Baja Peninsula and the most southern part of Mexico in the state of Chiapas.

Figure 5.5.2.5. $\delta^{18}O$ region of origin predictions for individual 16-2688 based on the left first maxillary premolar.

16-2623

The recorded $\delta^{18}O$ value for Individual 16-2623 was -3.0‰ based on for the left first maxillary premolar. The predicted regions of origin focus on the south east of the state of Sonora as well as the states of the Yucatan peninsula (Yucatan, Quintana Roo, Campeche, parts of Chiapas). The predicted areas also include areas along the inland coast stretch of the Gulf of Mexico.

Figure 5.5.2.6. $\delta^{18}O$ region of origin predictions for individual 16-2623 based on the left first maxillary premolar.

16-01822

The recorded $\delta^{18}O$ value for Individual 16-01822 was -5.4‰ based on the right first maxillary premolar. This individual is subject of the following chapter (5.5.3) as well as the associated publication (Ammer *et al.* 2020b).

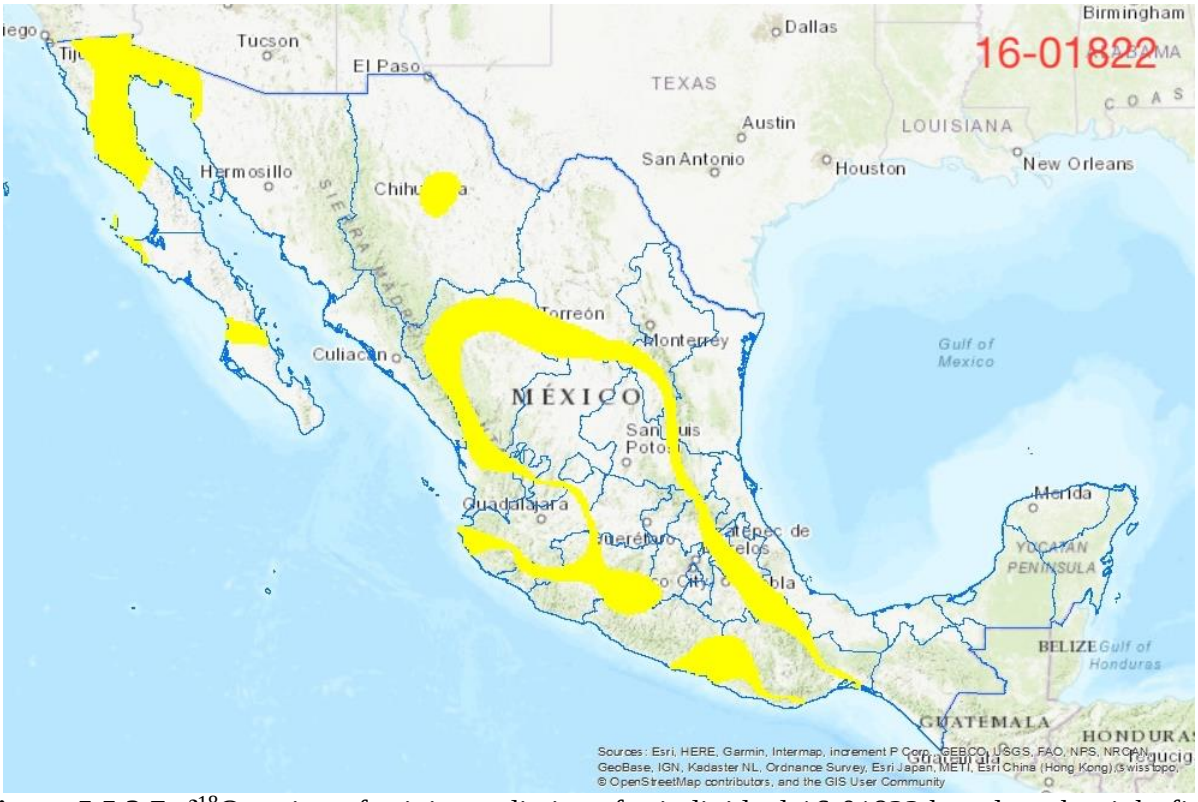

Figure 5.5.2.7. $\delta^{18}O$ region of origin predictions for individual 16-01822 based on the right first maxillary premolar.

16-01616

The recorded $\delta^{18}O$ value for Individual 16-01616 was -5.6‰ based on the right first maxillary premolar. This individual is subject of the following chapter (5.5.3) as well as the associated publication (Ammer *et al.* 2020b).

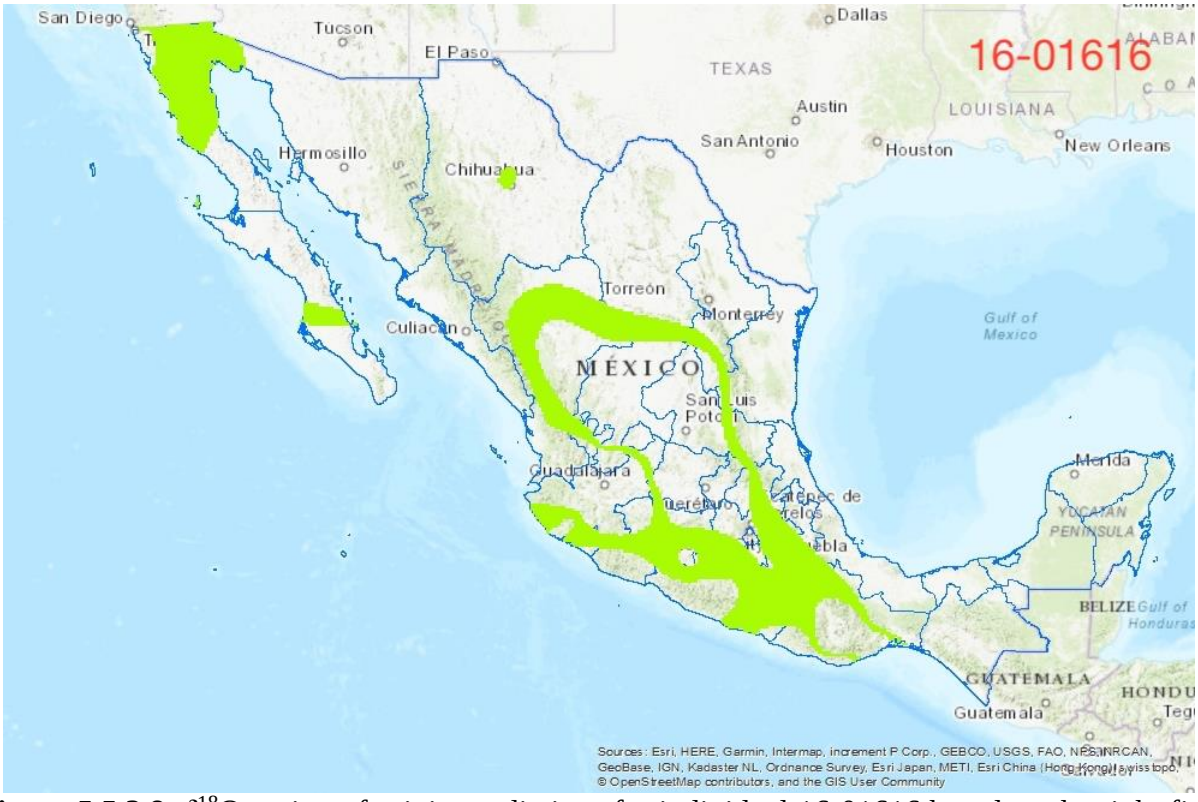

Figure 5.5.2.8. $\delta^{18}O$ region of origin predictions for individual 16-01616 based on the right first maxillary premolar.

16-01516

The $\delta^{18}O$ value of -6.2‰ was reported for the left first maxillary premolar. The conversion and subsequent conditional correlation approach yielded potential areas of origin in the states of Guanajuato, Oaxaca, Guerrero, Puebla, Michoacán and surrounding areas.

Figure 5.5.2.9. $\delta^{18}O$ region of origin predictions for individual 16-01516 based on the left first maxillary premolar.

Two of the above presented cases are also presented in the following Chapter (5.5.3), which have previously been published in the *Journal of Forensic Sciences* (Ammer *et al.* 2020b). While those two case studies can be counted as successes, there are still various issues that need to be addressed. As mentioned before, the methodology for the preparation and analysis of human tissues for $\delta^{18}O$ needs to be addressed and further developed. Several issues arose during the analyses of the tissues and made it impossible to use the hair samples as well as other tissues for further analysis. Going forward, international methodological standards need to be established to make the values and results comparable and useable across the different entities.

Furthermore, while the conditional correlation approach can be successful, as demonstrated in Chapter 5.5.3 (Ammer *et al.* 2020), it is pertinent to start implementing approaches that include maps showing the underlying error and also making predictions based on the available reference values as well as the probability that the interpolated values are accurate and are representative of the region. Ideally, it will also consider further underlying factors such as environmental, geological, and geographic variables. Lastly, since the predictions are relatively coarse, the $\delta^{18}O$ predictions should be combined with other isotope systems, such as strontium, hydrogen, or dietary isotopes (*e.g.*, carbon, nitrogen, sulfur) as applicable.

5. 5. 3. Spatial Distribution of Oxygen Stable Isotope Ratios in Tap Water from Mexico for Region of Origin Prediction of Unidentified Border Crossers

Paper published in the Journal of Forensic Sciences Anthropology section
Digital Object Identifier:
doi: 10.1111/1556-4029.14283

Authors:
Saskia T. M. Ammer,[1] M.Sc.; Eric J. Bartelink,[2] Ph.D.; Jennifer M. Vollner,[3] Ph.D.; Bruce E. Anderson,[3] Ph.D.; and Eugénia M. Cunha,[1] Ph.D.

Affiliations:
[1]Laboratory of Forensic Anthropology, Department of Life Sciences Cal"cada Martim de Freitas, University of Coimbra, Coimbra, PT 3000-456.
[2]Department of Anthropology, California State University, Chico, Chico, CA.
[3]Pima County Office of the Medical Examiner, 2825 E District St, Tucson, AZ 85714.

Presented at the 71st Annual Scientific Meeting of the American Academy of Forensic Sciences, February 18-23, in Baltimore, MD.

Abstract:
One of the many difficulties associated with identifying undocumented border crossers stems from an inability to narrow down the search area for the region of origin and family members to obtain family reference samples for DNA comparison. While the geography of regions of origins is wide, the biological profiles of the undocumented border crossers often show strong similarities, young and male. The iso- topic composition of human bones, teeth, and hair has been demonstrated to be useful biomarkers for tracing locations and movements of individuals and for aiding in the identification of human remains. Data obtained from human remains can be compared to and aligned with various reference sources, such as soils and bedrock, archaeological remains, or cultural data. Here, the spatial deficiency in isotopic reference data for Mexico, specifically for oxygen ($\delta^{18}O$) isotopes in tap water, is being addressed through the collection and analysis of over 150 water samples and explored with tooth enamel isotopic values from recently identified Mexican nationals. The isoscape was developed using a Spine with Barriers interpolation method and shows sufficient detail to narrow down the regions where specific isotopic values are represented. The individuals were plotted on the developed isoscape using conditional correlations. The methodology was successful in assigning the correct regions of origin for the two individuals, which shows the tremendous potential of the developed isoscape. Nonetheless, there is more research needed to further improve upon this geolocation method, including analysis of multiple isotopes in different tissues, and the development of new iso- topic methods.

KEYWORDS: Forensic science, forensic anthropology, stable isotopes, tap water, Mexico, undocumented border crossers, region of origin prediction

5.5.3.1. Introduction

Usually, distinctive features (*e.g.*, birthmarks, surgical scars, etc.), DNA profiles, fingerprints, and medical and dental records are used for forensic human identification. However, despite using this wide range of methods, many human remains stay unidentified for long periods of time or still have yet to be identified. This is especially the case with undocumented border crossers. Thus, it is important to determine whether the stable isotope ratios of oxygen ($\delta^{18}O$) can provide valuable information about the places of origin and residence as well as travel history during the lifetimes of unidentified remains.

Since 1998, over 7000 individuals died while attempting to cross the border from Mexico into the United States (Colibrí Center for Human Rights 2018; Humane Borders 2020). Over 1000 individuals are unidentified, 1125 individuals since 2000 at the Pima County Office of the Medical Examiner alone, and Colibrí currently has over 3000 open missing person cases (Colibrí Center for Human Rights 2018; Anderson and Spradley 2016). Previous research has shown that most of the positively identified undocumented border crossers crossing in Arizona originated from Mexico (Martinez *et al.* 2013; Anderson and Parks 2008; Massey 2002). The number of deaths increased significantly after the implementation so of the policy known now as "prevention through deterrence". The hope was that after increased enforcement and militarization of the border communities and ports of entry, potential unauthorized migrants would be deterred from entering the United States as the borderlands are known to be an incredibly harsh environment to survive in. However, due to the ongoing violence and economic hardships (among many other person reasons), people did not cease crossing but merely moved to more dangerous and deadly terrain. Through this policy, the number of migrant deaths in Arizona rose from an annual average of 12 to 170 (Illingworth 2015).

Accurate numbers for deaths and missing persons can only be estimated as many decedents are likely to never be found (based on the isolated and difficult terrain where individuals cross) and many individuals are not reported missing to the authorities. The ability to narrow down the potential regions of origin would be a tremendous help to all parties involved in the identification process of these individuals (*e.g.* medical examiner's offices, law enforcement agencies, foreign consulates, non-governmental organizations, universities).

Isotopic composition of human bone, teeth, and hair has been demonstrated to be useful biomarkers for archaeological and forensic researchers to trace locations and movements of individuals, and aid in the identification of remains (Bartelink *et al.* 2018; Chesson *et al.* 2018; Bartelink *et al.* 2014). While it will not be possible to identify an individual by the means of isotope analysis, it can certainly give valuable investigative leads to the entities involved in the

identification process.

While the Global Network for Isotopes in Precipitation (GNIP) dataset provides a key foundation for establishing global precipitation controlled isotopic landscapes (isoscapes), this dataset has insufficient spatial coverage in Mexico. GNIP is a combined initative of the IAEA's Water Resources Programme and the World Meteorological Organization (WMO) that have been surveying the stable hydrogen and oxygen isotope precipitation around the globe for almost 60 years. The data repository allows for temporal and spatial analysis of the isotopic variations found in precipitation by providing basic data for the use of isotopes in disciplines such as hydrology, climatology, oceanography but also for food forensics and traceability (including human mobility).

There are 39 recording stations in the United States but merely two in Mexico (located in Veracruz and Chihuahua) (International Atomic Energy Agency World Meteorological Organization 2018). This spatial deficiency is a major concern when attempting to answer research questions on how hydrological processes influence large-scale oxygen isotope patterns throughout Mexico, and how forensic scientists can use this information to predict potential region of origin of deceased undocumented border crossers. Fortunately, water is relatively easy and affordable to analyze for their $\delta^{18}O$ and $\delta^{2}H$ isotopic values, which makes these isotopes an ideal baseline for future comparisons and analyses. Moreover, tap water is not always derived directly from local rainwater sources. This current research reports a first attempt to overcome the major limitation in the oxygen isotope data for Mexico using isoscape methods.

Isoscapes represent spatially explicit predictions of elemental isotope ratios by providing global-scale patterning in natural spatial isotopic distributions. These isoscapes are produced by executing process-level models of elemental isotope fractions or distribution in a Geographic Information System (GIS) (Bowen 2010b; West *et al.* 2010). This newly created Mexican tap water isoscape is further tested to establish conditional correlations and assign the isotopic data gathered from human remains to regions in Mexico. These established conditional correlations serve the purpose of narrowing down the regions of origins for unidentified undocumented border crossers.

5.5.3.2. Materials and Methods

As part of a larger project, 158 tap water samples from 51 towns and cities were collected throughout Mexico during a six-week period from June to July 2018. At least three samples were collected from each location in order to evaluate local variation as well as inter-regional variation within Mexico. The locations were chosen by geology as well as accessibility. Some locations

that were on the list prior to the collection journey could not be sampled due to inaccessibility and/or security concerns. The data obtained from these tap water samples will be presented in greater details in an upcoming publication. Nonetheless, the raw data are available on waterisotopes.org (Project ID 198- MEX Water). The samples were analyzed for their $\delta^{18}O$ and $\delta^{2}H$ values at the SIRFER/SPATIAL lab at the University of Utah.

Several tissue samples were collected by the Pima County Office of the Medical Examiner and provided for isotope analysis to Dr. Bartelink at the California State University, Chico, and its Stable Isotope Preparation Laboratory. The samples used here for region of origin predictions consist of one tooth enamel sample for each individual. Tooth enamel is composed of ~97% inorganic minerals (hydroxyapatite), ~1% organic protein (amelogenin) and ~2% water (Hillson 1996; He 2007; Lafoon 2017). Because of its high mineral content, enamel is the hardest tissue found in the human body. Furthermore, unlike bone and dentine, enamel does not turn over and once it is deposited, it permanently locks in isotope signatures (Ortner 2003). This makes teeth very elementally stable and therefore, ideal for isotope analysis.

IsoForensics, a commercial stable isotope laboratory in Salt Lake City (Utah), conducted the analysis on the two enamel samples according to their certified standard operating procedures. All stable isotope contents are presented as $\delta = [(R_{sample} - R_{standard}) / R_{standard}] \bullet 1000$ (‰) to better capture the minor differences in isotopic abundance ratios (R), and are expressed as δ values against an internationally defined standard. The following two individuals were sampled after all traditional investigative leads were initially exhausted. However, they have recently been identified through DNA family reference samples and can now be used to test the isotopic database and methodology. Both individuals, here named Individual 1 and Individual 2 for clarity, were found in the Sonoran Desert in Pima County, Arizona, in 2016. For both individuals, a premolar was retained for isotopic analysis.

The tap water isoscape of the $\delta^{18}O$ values was created using ArcGIS 10.6 (Environmental Systems Research Institute (ESRI) 2018) with a Spline with Barrier interpolation. A Spline with Barrier interpolation is beneficial for country shapes like Mexico because it honors any discontinuities by constraining newly estimated values using the input barrier features (country polygon) and input point data. It includes all data by associating it with any near land pixel and passing through the exact data point locations. This issue appears with changes in scaling and can lead to datapoint that are closely located to the country borders to be offshore. This issue is avoiding by using a Spline with Barrier interpolation.

Through several calculations, it is possible to convert the $\delta^{18}O$ values obtained from a tooth sample into a tap water $\delta^{18}O$ value (Sample calculations for Individual 1 and Individual 2 are provided below in the Results section):

1. Tooth apatite $\delta^{18}O$ (VPDBcarbonate) --> Tooth apatite $\delta^{18}O$ (VSMOWcarbonate)
   1.03091 * $\delta^{18}O$ (VPDBcarbonate) + 30.91 = $\delta^{18}O$ (VSMOWcarbonate)
   (Coplen 1988)
2. Tooth apatite $\delta^{18}O$ (VSMOWcarbonate)--> Tooth apatite $\delta^{18}O$ (VSMOWphosphate)
   0.998 * $\delta^{18}O$ (VSMOWcarbonate) - 8.5 = $\delta^{18}O$ (VSMOWphosphate)
   (Iacumin *et al.* 1996)
3. Tooth apatite (VSMOWphosphate)-->Predicted water (VSMOWphosphate)
   1.54 * $\delta^{18}O$ (VSMOWphosphate) - 33.72 = $\delta^{18}O$ (VSMOWphosphate)
   (Daux *et al.* 2008)

In order to fully grasp how and why the above conversions are needed, additional explanations are warranted:

Daux *et al.* (2008) established the conversion from tooth and bone $\delta^{18}O$ values to tap water $\delta^{18}O$ values (3rd equation). While this discovery is a tremendous scientific step, the measurement of VSMOWphosphate values in bones and teeth involves the production of silver phosphate, which is not only a labor intensive but also a dangerous procedure (Chesson *et al.* 2018b). Contrary, carbonates in teeth and bones are easily measured through acidification and the collection of CO_2. Therefore, most laboratories choose the second option.

Furthermore, the VPDB scale is traditionally used to report $\delta^{18}O$ values of carbonates. (PDB stands for Peedee Belemnite, which represents the isotopic composition found in shells from the South Carolina's Peedee geological formation- the original PDB sample was made up of calcium carbonate.) Therefore, a conversion is needed from the VPDBcarbonate scale to the VSMOWcarbonate scale (1st equation; Coplen 1988).

Because the first equation presents the result on the VSMOWcarbonate scale and the third equation works on the VSMOWphosphate scale, a further conversion from VSMOWcarbonate to VSMOWphosphate is needed (2nd equation; Iacumin *et al.* 1996).

Using the interpolated tap water $\delta^{18}O$ isoscape, maps highlighting the predicted regions of origin for the individual are developed. As a first order approximation of uncertainties, an error window of ±0.5‰ is used for the visualization for the region of origin predictions (Chesson *et al.*

2018b). The prediction isoscapes are produced using the raster calculator of ArcGIS using a conditional correlation calculation. Here, the values of the cells are determined to be either true or false within the specified conditional statement. In this case, true means that the $\delta^{18}O$ value obtained from the individual ±0.5‰ can be found in the marked areas. Furthermore, existing oxygen and hydrogen proxy data was gathered from the literature and compared to the collected Mexican tap water data as well as the created isoscape shown in the results (Cortés *et al.* 1997; International Atomic Energy Agency World Meteorological Organization 2018; Wassenaar 2009).

5.5.3.3. Results

The $\delta^{18}O$ values of tap water ranged from −12.1‰ to −0.2‰, while $\delta^{2}H$ ranged from −91.3‰ to −8.9‰. Those values fall within the reported ranges for other water data from Mexico (Cortés *et al.* 1997; International Atomic Energy Agency World Meteorological Organization 2018; Wassenaar 2009). The obtained tap water values were compared to existing data, specifically to precipitation values from the GNIP Stations (International Atomic Energy Agency World Meteorological Organization 2018) and ground water data (Wassenaar 2009). Wassenaar and colleagues (2009) determined a Mexican meteoric water line, using data from the limited number of precipitation International Atomic Energy Agency (IAEA) stations located in Chihuahua and Veracruz (International Atomic Energy Agency World Meteorological Organization 2018) as well as one site near Mexico City (Cortés *et al.* 1997). It is reported to be $\delta^{2}H = 7.5 * (\delta^{18}O) + 6.1‰$ ($r^2 = 0.96$). The Global Meteoric Water Line (GMWL) is internationally defined as $\delta^{2}H = 8 * (\delta^{18}O) + 10‰$ (Craig 1961). The regression line reported for the Mexican ground water samples was also added to the visualization of the data: $\delta^{2}H = 7.5 * (\delta^{18}O) + 2.3‰$ ($r^2 = 0.93$) (Wassenaar 2009, Figure 2). The equation that describes the isotopic $\delta^{18}O$ values collected for the Mexican tap water is defined as $\delta^{2}H = 7.5 * (\delta^{18}O) + 2.3‰$ ($r^2 = 0.93$) (Figure 2). All $\delta^{18}O$ tap water values were plotted against their respective $\delta^{2}H$ values, also depicting the various water lines (Figure 2). Most tap water data falls slightly below the Global Meteoric Water Line and the Mexican meteoric water line. Some of the higher values observed in the Mexican tap water are elevated above the defined water lines.

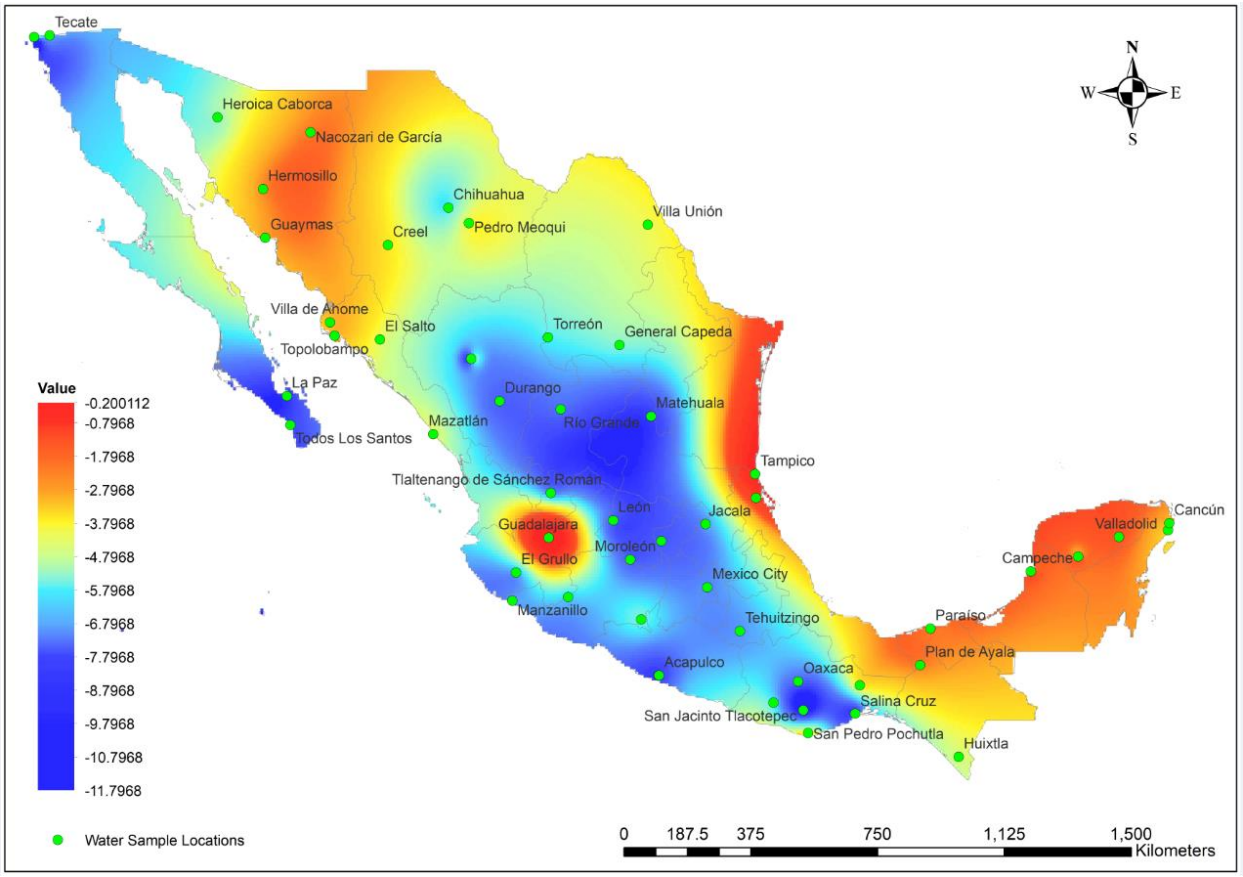

Figure 5.5.3.1. $\delta^{18}O$ interpolated isoscape of Mexican tap water with the sampling locations marked in green. Some sampling locations are labeled for spatial reference.

The final tap water $\delta^{18}O$ isoscape shows clear geographic patterns (Figure 2). The tap water isoscape shows particularly low isotopic values in the area of the Central Mexican Plateau and the Sierra Madre del Sur mountain range. The highest values are recorded on the Yucatan peninsula and along the Gulf of Mexico coast.

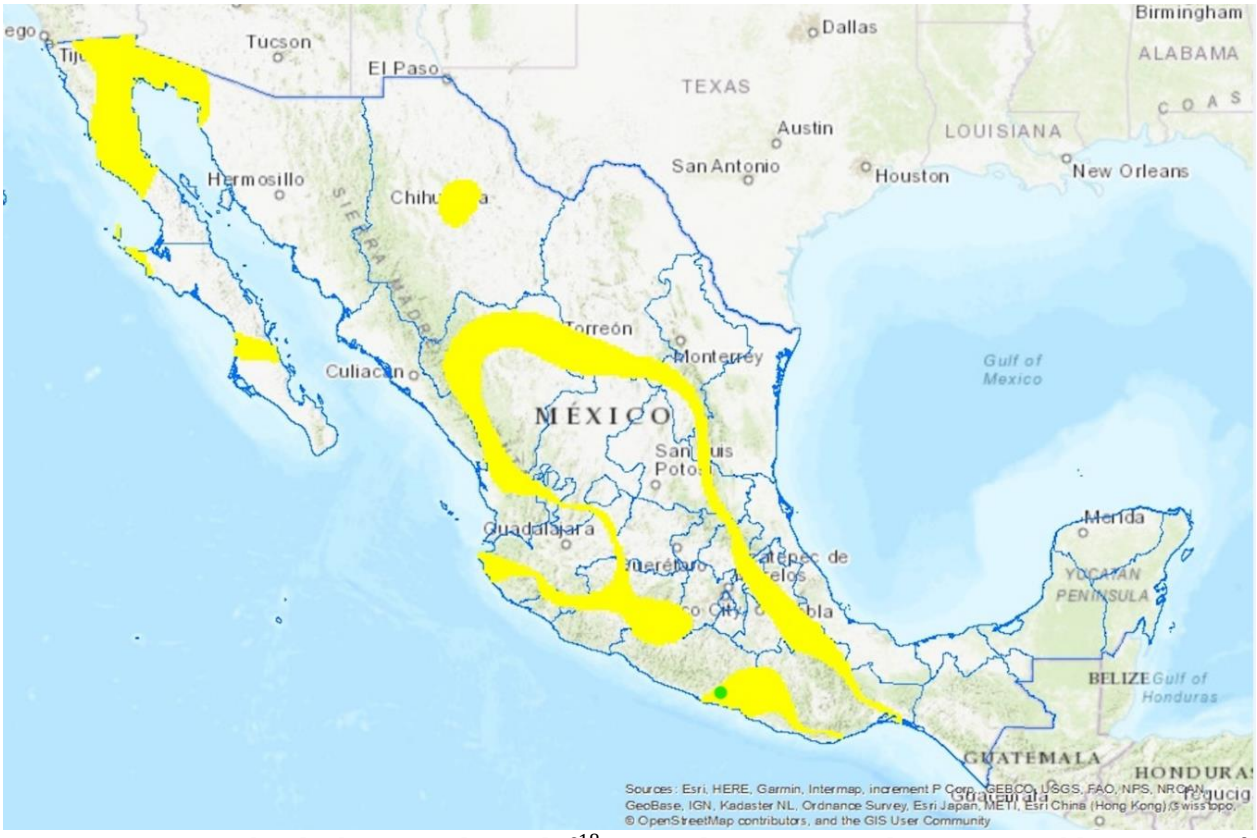

Figure 5.5.3.2. Individual 1- Conditional $\delta^{18}O$ correlation map indicating possible regions of origin. The birthplace of the recently identified individual is marked with the green dot.

Based on the $\delta^{18}O$ values obtained from the stable isotope analysis on the tooth enamel of the two undocumented border crossers, conditional correlation maps were developed. An error of ±0.5‰ was included in the calculations in order to account for the analytical error as well as errors in the interpolation of the isoscape.

Individual 1:

A $\delta^{18}O$ value of -5.37 was obtained for the tooth enamel sample of Individual 1. This value represents VPDBcarbonate in the equations presented above. Therefore, the first equation reads as follows:

1.03091 * -5.37 + 30.91 = 25.37

The result (in the equation above labeled as VSMOWcarbonate is then used in the second equation to calculate VSMOWphosphate:

0.998 * 25.38 - 8.5 = 16.82

Further, the VSMOWphosphate value is used in the last of the three equations to calculate VSMOWphosphate aka the tap water value that is used for the conditional correlation procedure in the Raster Calculator as described above:

1.54 * 16.83 - 33.72 = -7.81

The resulting prediction map explicitly excludes the Yucatan peninsula and the Gulf Coast (Figure 3). The predicted regions of origin include large portions of Baja California and Durango as well as areas various other states, such as Guerrero in which the birthplace of the individual falls (Figure 3, green dot).

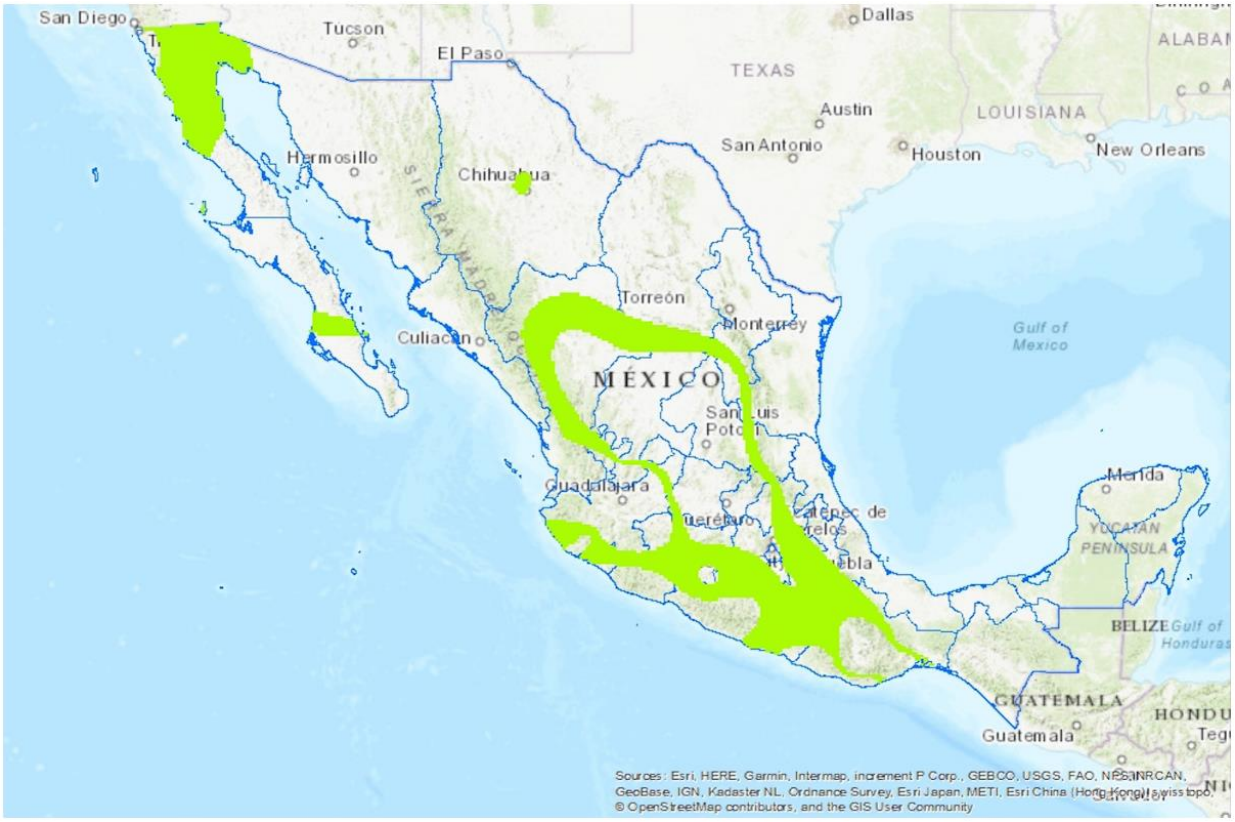

Figure 5.5.3.3. Individual 2- Conditional $\delta^{18}O$ correlation map indicating possible regions of origin.

Individual 2:

A $\delta^{18}O$ value of -5.61 was obtained for the tooth enamel sample of Individual 2. The same procedure to convert VPDBcarbonate to VSMOWphosphate $\delta^{18}O$ values was employed for Individual 2 and the calculations read as follows:

1.03091 * -5.61 + 30.91 = 25.13

0.998 * 25.14 - 8.5 = 16.58

1.54 * 16.59- 33.72 = -8.19

Similarly to Individual 1, the prediction excludes the Yucatan peninsula and the Gulf Coast (Figure 4). It does, however, include the Pacific coastal region from the state of Oaxaca to Jalisco as well as the state of Baja California. Furthermore, it includes several smaller states that are located more inland, such as Puebla, Tlaxcala and Hidalgo. The place of birth is currently being withheld from the first author to ensure the possibility of further blind testing of other isotope

systems and methodologies. Nonetheless, it was confirmed by the Pima County Office of the Medical Examiner (Tucson, Arizona) that this individual's place of birth falls within the predicted regions.

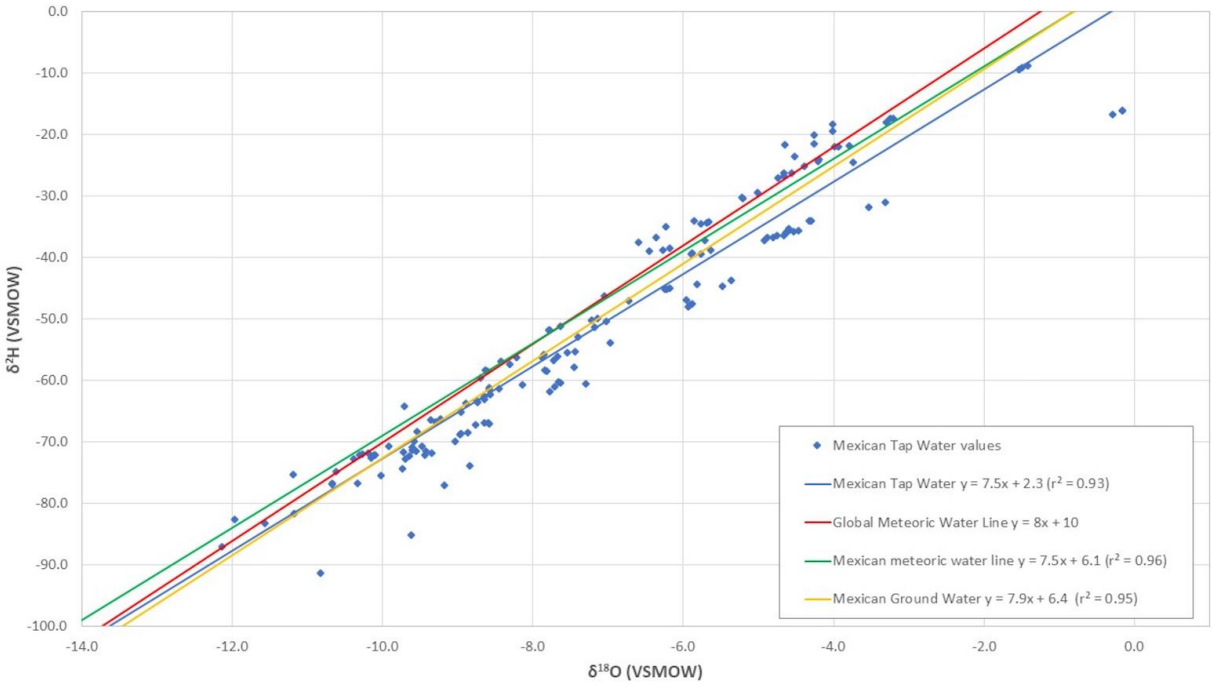

Figure 5.5.3.4. Plot of $\delta^{18}O$ versus $\delta^{2}H$ for Mexican tap water. The regression lines for the Mexican tap water (blue line), the Global Meteoric Water Line (red line, Craig 1961), the previously defined Mexican Meteoric Water Line (green line, 23), and the Mexican Ground Water lines (yellow line, Wassenaar *et al.* 23) are also depicted.

5.5.3.4. Discussion

Overall, the tap water values reported for the 158 samples fall within the range of the data reported by the GNIP stations and the ground water study by Wassenaar *et al.* (2009). The tap water data falls close to the Mexican Meteoric Water Line, which suggests that evaporation occurs in the drinking water sources but that it is not substantial. If evaporation would have a significant effect, it would result in significant isotopic excursions to the right of the meteoric water line as well as shallower slopes. This is rather remarkable since the samples were collected during the summer (high evaporation and high precipitation) (Figure 1).

The Guadalajara, Jalisco area is notable. As one can see in Figure 2, the isotopic $\delta^{18}O$ values fall completely out of the normal regional range. This is possibly be explained by the fact that Guadalajara's main water source is Mexico's largest freshwater lake, Lake Chapala (von Bertrab 2003) and that lakes are known to be very sensitive to precipitation and evaporation.

The resulting isoscape shows sufficient detail and geospatial patterning to be of use for future research as well as first order region of origin predictions. In the upcoming publication,

which will discuss the tap water data in greater detail, ways to further improve the isoscape will be explored. These will include environmental covariates; such as elevation, mean annual temperature, mean annual precipitation, and distance to the ocean; and socioeconomic covariates; including the Human Development Index, the percentage of the population living in poverty in the respective states, and the percentage of the population being of indigenous ancestry.

The $\delta^{18}O$ isoscape has proven to be a solid tool for region of origin prediction for these recently identified undocumented border crossers. Nonetheless, other isotope systems will have to be explored to further narrow down the possible regions of origin since the currently developed prediction maps still include large areas of the country. Several researchers have shown that the application of a multi-isotope approach can successfully aid the identification process in forensic investigations and case work (Bartelink *et al.* 2019; Font *et al.* 2015; Meier-Augenstein 2008; O'Reilly 2007; Chesson *et al.* 2018b). The development of models that include environmental and socioeconomic covariates will be of great use if successful. Furthermore, it is hoped that the improved models will allow the use of a smaller error for the conditional correlations than the currently employed ±0.5‰.

5.5.3.5. Conclusion

Overall, this case study shows the great potential and possible successfulness of the $\delta^{18}O$ isoscape and the conditional correlation procedures. The two recently identified individuals demonstrate that while it is not possible to identify an individual solely by stable isotope analysis, the predicted regions of origin can provide useful investigative leads. There is a need to further explore factors influencing the $\delta^{18}O$ tap water values in Mexico as well as the analytical methodology behind it as recent research has down that mass spectrometry procedures, such as acidification temperatures, may influence $\delta^{18}O$ values of bone and tooth bioapatite samples.

5. 5. 4. Results and Discussion of the Strontium Isotope Analyses of Body Tissues of Undocumented Border Crossers

In Chapter II and the published Chapter 5.4, an overview is given over strontium $^{87}Sr/^{86}Sr$ and its uses in forensic sciences, especially in forensic provenancing. In short, the $^{87}Sr/^{86}Sr$ ratio of an organism's tissues reflects the intake of environmental $^{87}Sr/^{86}Sr$ ratios during the time of tissue formation and can be used as an indicator of residency and to track migration (Beard and Johnson 2000; R. A. Bentley and Knipper 2005; R. Alexander Bentley 2006; Lee-Thorp 2008). This is possible due to the fact that there is little to no mass-dependent fractionation occurring during the ecological, chemical, or biological processes (Åberg 1995; Capo, Stewart, and Chadwick 1998). This fact is utilized when employing $^{87}Sr/^{86}Sr$ for human provenancing. In following, the results of the $^{87}Sr/^{86}Sr$ analyses for the various body tissues and the region of origin predictions are presented and discussed.

A total of 55 samples were analyzed for their $^{87}Sr/^{86}Sr$ ratios. The ratios and the corresponding standard errors are presented in Table 5.5.4.1. The small standard errors give confidence in the values up to the fifth decimal place.

Table 5.5.4.1. Results of $^{87}Sr/^{86}Sr$ analyses in bones, teeth and of sixteen undocumented border crossers housed at the PCOME.

	$^{87}Sr/^{86}Sr$ Tooth	**2xSE**	**$^{87}Sr/^{86}Sr$ Long bone**	**2xSE**	**$^{87}Sr/^{86}Sr$ Rib**	**2xSE**	**$^{87}Sr/^{86}Sr$ Hair**	**2xSE**
17-1466	0.706974	7.83E-06	0.707138	8.71E-06	0.707223	9.62E-06	0.709783	9.31E-06
17-1314	0.705207	1.00E-05	0.708094	7.17E-06	0.708071	8.86E-06	0.710898	9.51E-06
17-2006	0.706284	8.76E-06	0.706856	8.28E-06	0.706987	9.61E-06		
17-1944	0.706949	9.77E-06	0.706987	7.92E-06	0.707028	8.56E-06		
17-2186	0.707411	1.01E-05	0.707331	9.08E-06	0.707310	8.25E-06		
17-1681	0.707519	8.93E-06	0.707598	9.39E-06	0.707945	8.42E-06		
17-1682	0.708071	8.65E-06	0.705962	7.49E-06	0.707982	8.10E-06	0.709309	9.44E-06
16-2623	0.706296	9.63E-06	0.706748	7.26E-06	0.706693	8.45E-06		
16-2688	0.706797	7.41E-06	0.707118	7.78E-06	0.707387	9.21E-06		
17-2469	0.707916	8.68E-06	0.709768	8.25E-06	0.709460	8.54E-06		
16-1585	0.707004	8.94E-06	0.707226	8.05E-06	0.707654	8.94E-06		
16-01822	0.706068	7.48E-06	0.706380	9.15E-06	0.706665	8.72E-06	0.709554	9.75E-06
17-1742	0.707705	9.68E-06	0.707656	9.35E-06	0.707741	7.60E-06	0.710058	1.02E-05
16-01516	0.707156	8.09E-06	0.707190	8.40E-06	0.707730	8.33E-06	0.709375	9.72E-06
16-3187	0.706119	8.51E-06	0.707114	8.53E-06	0.707147	8.88E-06		
16-01616	0.706727	9.31E-06	0.706839	7.91E-06	0.707315	8.87E-06	0.713258	2.52E-05

Figure 5.5.4.1 shows the $^{87}Sr/^{86}Sr$ ratios recorded from the Mexican Reference Hair and the $^{87}Sr/^{86}Sr$ ratios of the undocumented border crosser's hair, long bones, ribs, and teeth. The figure serves as a visual aid of the $^{87}Sr/^{86}Sr$ ratio distribution found in Mexican human hair and as a comparison to the values found in the 16 UBCs sampled for this dissertation. It was decided to present the recorded ratios in form of a violin plot to highlight the probability density of the data at different ratios. As one can see, this is of particular importance for the reference hair samples as the high ratios are only represented by very few samples.

As one can see, the human hair values cover the entire range of $^{87}Sr/^{86}Sr$ ratios seen in the undocumented border crossers bones and teeth. The hair $^{87}Sr/^{86}Sr$ ratios are elevated in comparison to most of the $^{87}Sr/^{86}Sr$ ratios found in the other tissues as well as the reference hairs. This finding will be discussed later in the chapter.

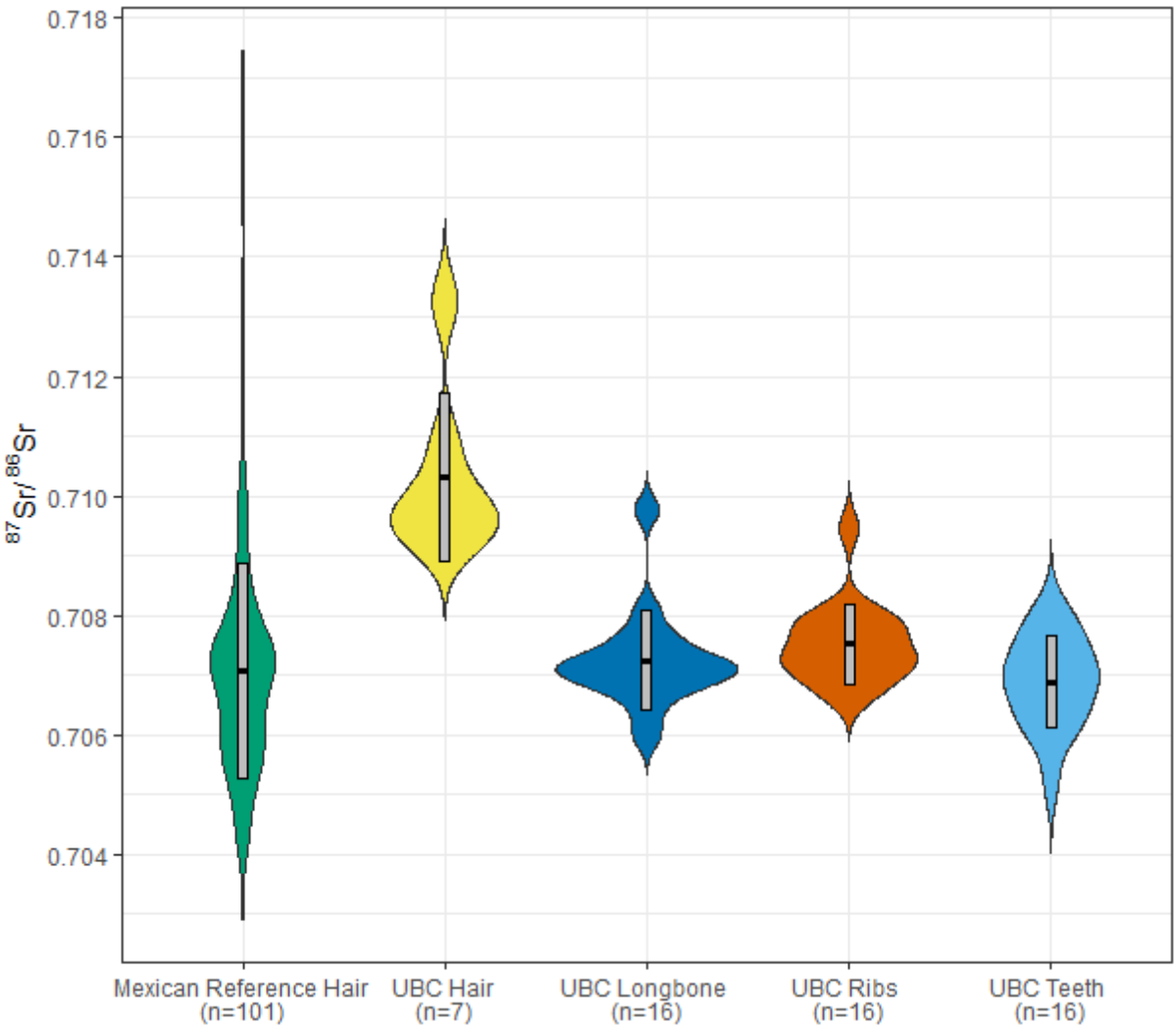

Figure 5.5.4.1. Comparison of Mexican Reference Hair $^{87}Sr/^{86}Sr$ ratios to $^{87}Sr/^{86}Sr$ ratios found in hair, long bones, ribs, and teeth of UBCs shown through the probability density of the data at different ratios.

The visualization of the results of $^{87}Sr/^{86}Sr$ analyses in bones, teeth and hair of sixteen UBCs in Figure 5.5.4.2 shows that several individuals exhibit very similar $^{87}Sr/^{86}Sr$ ratios for all of their available skeletal elements (*e.g.* 17-1944, 17-2186, 17-1742). This fact indicates that these individuals most likely did not move during their lifetime until they started their journey to the United States. The reasoning behind this is that it is rather unlikely to move from one place to another over great distances and remain in the exact same geological $^{87}Sr/^{86}Sr$ signature.

Several individuals (*e.g.* 17-1314, 17-2006, 16-2623, 17-2469, 16-3187) clearly show that they were born in one place but then moved to another and remained there for several years (aka the entire remodeling cycle of the long bone, as this is the bone with the longer remodeling time compared to the rib).

Individual 17-1682 presents an interesting case as the $^{87}Sr/^{86}Sr$ ratios of the sampled tooth and rib are similar but the long bone is much lower, in fact one of the lowest values seen in the analysis of the remains of UBCs. The difference in values underline the fact that this individual moved from his birth/early childhood place of residence. Considering that ribs have a shorter turnover rate than weight-bearing long bones, the $^{87}Sr/^{86}Sr$ ratios at the latest place of residence must have been even higher than the $^{87}Sr/^{86}Sr$ of the sampled root. The mixed signatures obviously further complicate the estimation of the region of origin and more recent movements of this individual.

Individual 17-2469 is particularly interesting as the $^{87}Sr/^{86}Sr$ ratios for the long bone and rib are very high, in the region of the values seen in the United States (Figure 5.5.4.2). Based on the hair reference data it is very possible that this individual was born outside of the US, then moved to the United States and tried to return after being deported.

The visibly elevated $^{87}Sr/^{86}Sr$ ratios in the hair samples will be discussed towards the end of this chapter in greater depth.

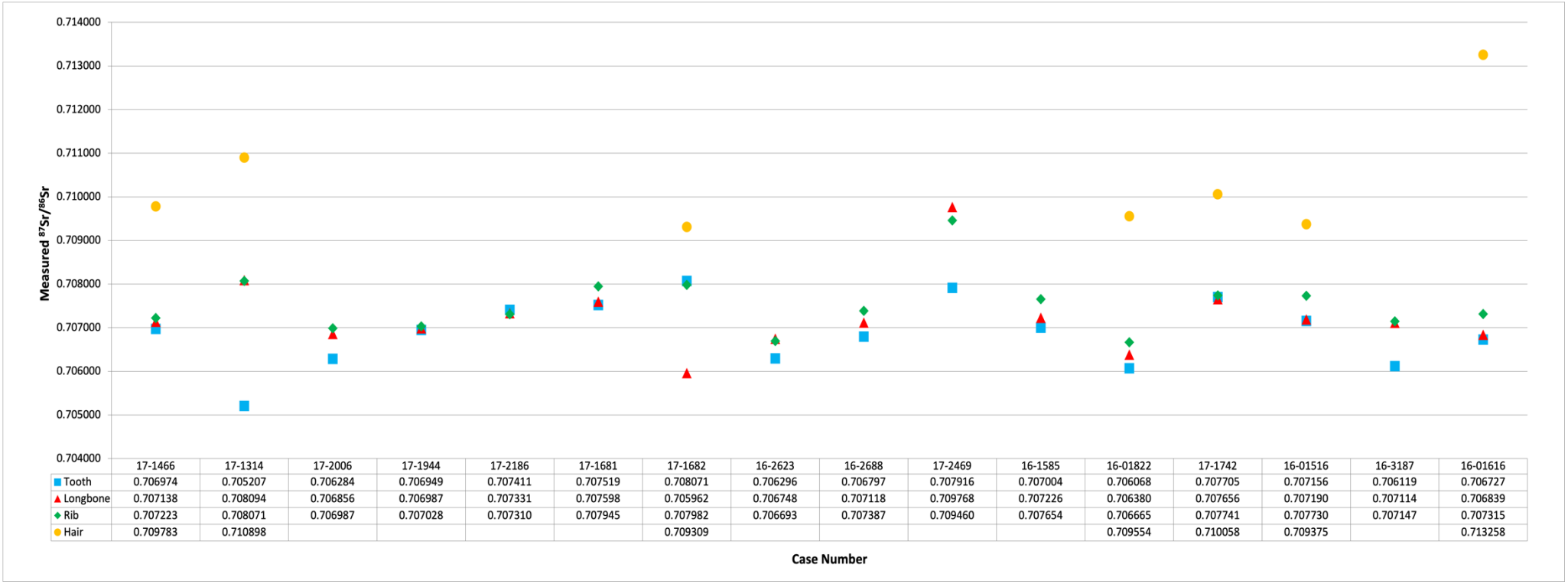

	17-1466	17-1314	17-2006	17-1944	17-2186	17-1681	17-1682	16-2623	16-2688	17-2469	16-1585	16-01822	17-1742	16-01516	16-3187	16-01616
Tooth	0.706974	0.705207	0.706284	0.706949	0.707411	0.707519	0.708071	0.706296	0.706797	0.707916	0.707004	0.706068	0.707705	0.707156	0.706119	0.706727
Longbone	0.707138	0.708094	0.706856	0.706987	0.707331	0.707598	0.705962	0.706748	0.707118	0.709768	0.707226	0.706380	0.707656	0.707190	0.707114	0.706839
Rib	0.707223	0.708071	0.706987	0.707028	0.707310	0.707945	0.707982	0.706693	0.707387	0.709460	0.707654	0.706665	0.707741	0.707730	0.707147	0.707315
Hair	0.709783	0.710898					0.709309					0.709554	0.710058	0.709375		0.713258

Figure 5.5.4.2. Visualization of the results of $^{87}Sr/^{86}Sr$ analyses in bones, teeth, and hair of sixteen undocumented border crossers housed at the PCOME.

UBC Region of Origin Predictions

In the following section, the region of origin predictions for the $^{87}Sr/^{86}Sr$ ratios found in the tissues of UBCs housed at the PCOME are presented. A detailed summary of the samples can be found in Chapter IV. The rationale for the body tissues used in this study as well as information about the tissues structure, composition, and remodeling is detailed in Chapter III.

As the basis for the underlying prediction, a $^{87}Sr/^{86}Sr$ ratio isoscape was used (Figure 5.5.4.3). This isoscape was developed using the Bataille *et al.* (2018) machine learning approach. As a proxy, the $^{87}Sr/^{86}Sr$ ratio of human hair were used. As this is a preliminary isoscape, it will be not be discussed in further detail now. The isoscape was interpolated to the border regions of the United States as well as the Northern Triangle countries (Honduras, Guatemala, El Salvador) and Belize. This was done in order to investigate potential influences of exogenous signatures that may skew with $^{87}Sr/^{86}Sr$ ratios recovered from human tissues, especially human hair as well as to predict potential regions of origins as an increasing number of UBCs come from the Northern Triangle countries. It is important to note here that the interpolation undeniably introduces a greater error because there are no reference data in these countries to base the interpolation on.

Following research by Plomp *et al.* (2020) an error of 0.0002 was used. Thus, the following region-of origin predictions use the $^{87}Sr/^{86}Sr$ ratio documented for the respective human tissue ±0.0002. It is unknown if this error, which was documented for human enamel, is also applicable for bones and hair.

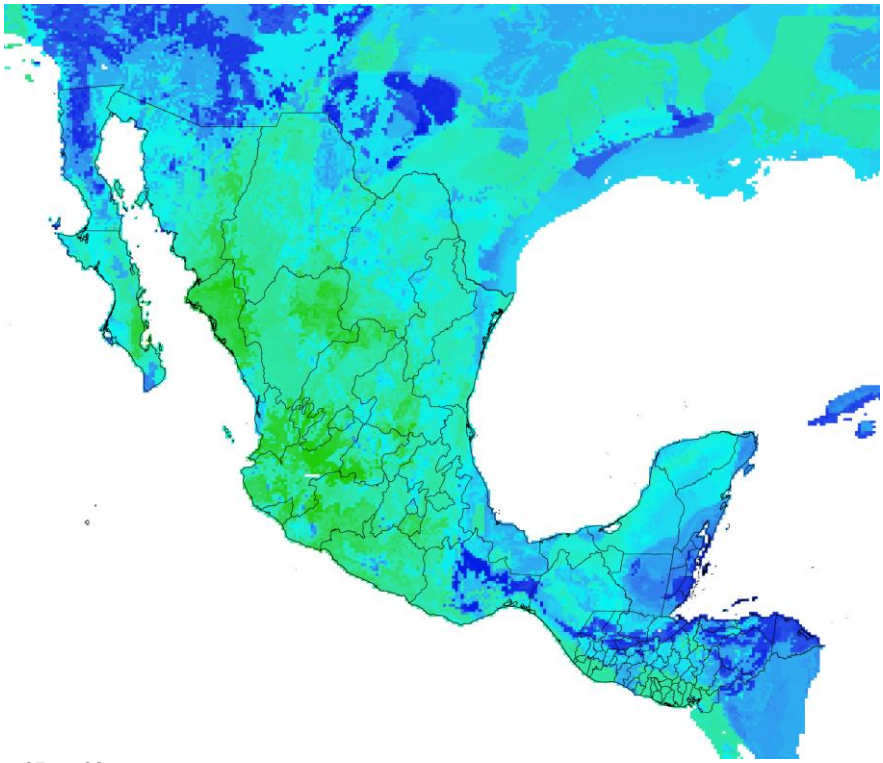

Figure 5.5.4.3. $^{87}Sr/^{86}Sr$ isoscape of Mexico.

Individual 17-1466

Individual 17-1466 shows $^{87}Sr/^{86}Sr$ ratios, which are commonly seen in Mexico based on the collected reference hair (Figure 5.5.4.4 and 5.5.4.22, Chapter 5.4). This makes narrowing down of potential regions of origin challenging. The tooth and femur values are within the inter-person error of ±0.0002 as determined by Plomp *et al.* (2020). The rib, which has a faster turnover rate, is elevated compared to the tooth and femur. Considering that these ratios present mixed ratios, the true ratios of the femur and the rib are likely higher and indicate that this individual moved recently. The hair ratio predicts outside of Mexico and is consistent with the Arizona desert. The $^{87}Sr/^{86}Sr$ ratios in the hair of UBCs will be discussed later in this chapter.

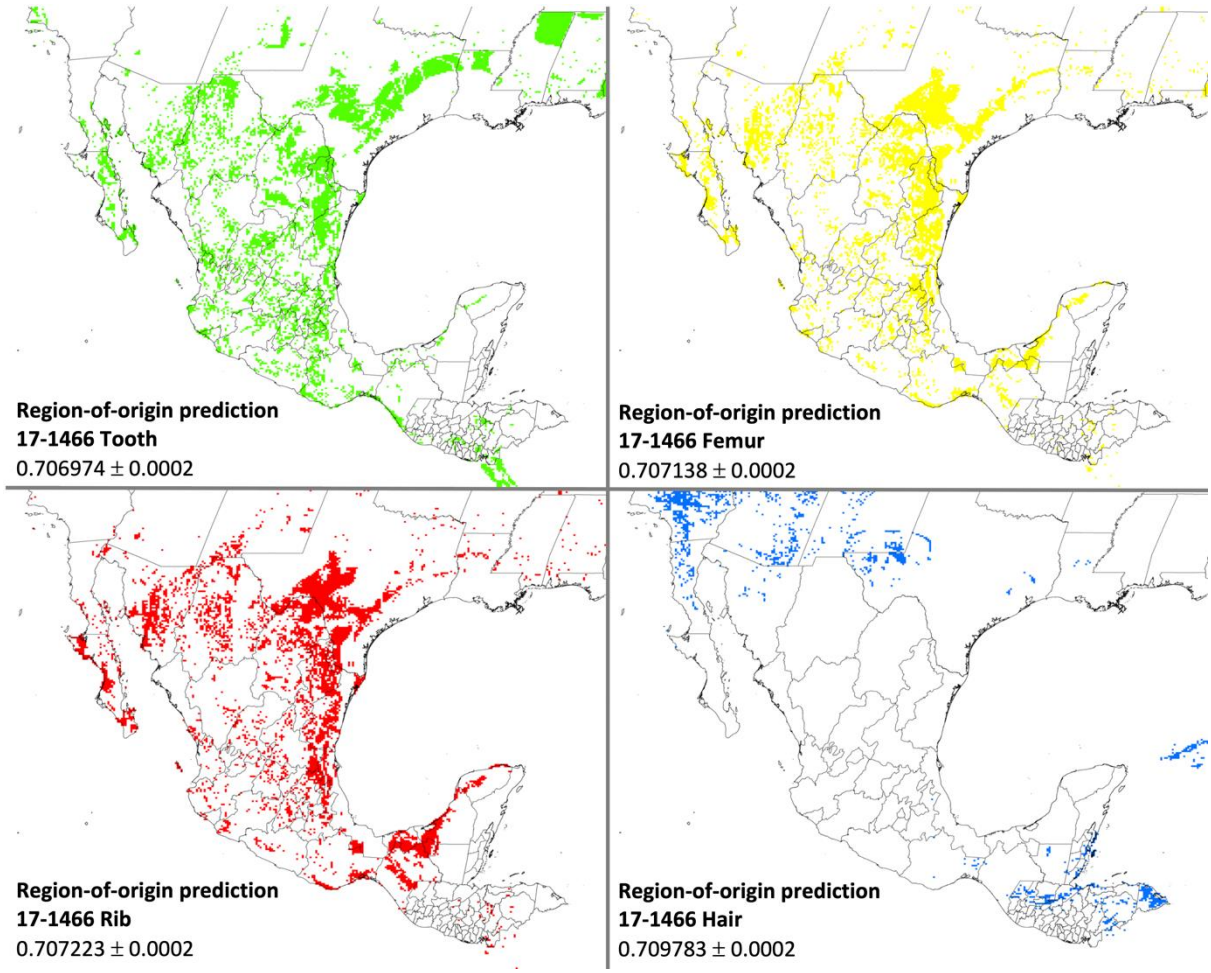

Figure 5.5.4.4. $^{87}Sr/^{86}Sr$ region of origin predictions for individual 17-1466 using the following skeletal elements: tooth, femur, rib, and hair. An error of ±0.0002 was used for the predictions.

Individual 17-1314

Individual 17-1314 shows significantly elevated ratios in the tibia and rib compared to the tooth. The tooth sampled was the left first mandibular molar (19), therefore representing the time around his birth. The $^{87}Sr/^{86}Sr$ ratio predicts an origin within the western part of Mexico, specifically in proximity of the states of Nayarit, Zacatecas, Aguascalientes, and Sinaloa. The $^{87}Sr/^{86}Sr$ ratios of the two bones are very similar, suggesting that this person may not have moved during the last couple of years of his life. Given that this individual was estimated to be between 28-40 years old, this would indicate that they did not move between adolescence and adulthood. The $^{87}Sr/^{86}Sr$ bone ratios are consistent with the coastal areas of the United States (along the Gulf of Mexico) and parts of Texas and New Mexico. Because the map is only interpolated to the most southern parts of the United States, it is unknown if there are other areas that this individual could have been from. The hair values will be discussed at a later point in this chapter.

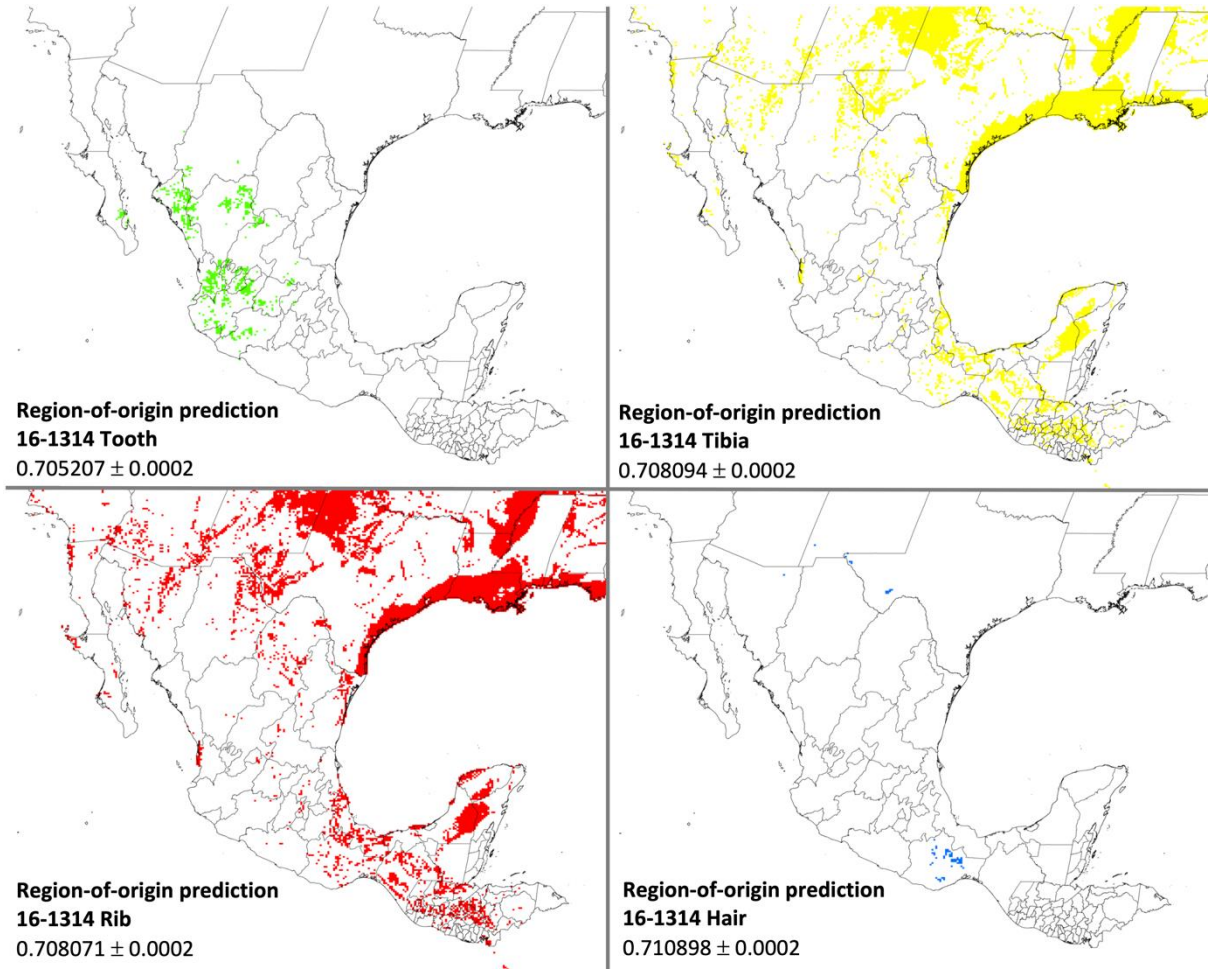

Figure 5.5.4.5. $^{87}Sr/^{86}Sr$ region of origin predictions for individual 16-1314 using the following skeletal elements: tooth, tibia, rib, and hair. An error of ±0.0002 was used for the predictions.

Individual 17-2006

The $^{87}Sr/^{86}Sr$ ratios of Individual 17-2006 indicate that this person moved during his lifetime to an area with elevated $^{87}Sr/^{86}Sr$ ratios. While the tooth (first right maxillary molar, 3) ratio indicates a place of origin within Mexico, the bone ratios unfortunately are not as distinctive and overlap many parts of Mexico and the United States. The fact that the rib $^{87}Sr/^{86}Sr$ ratio is elevated over the femur could indicate that this person moved during the last couple of years of his life but had not remained there long enough before his death in order to fully incorporate the local isotope signature.

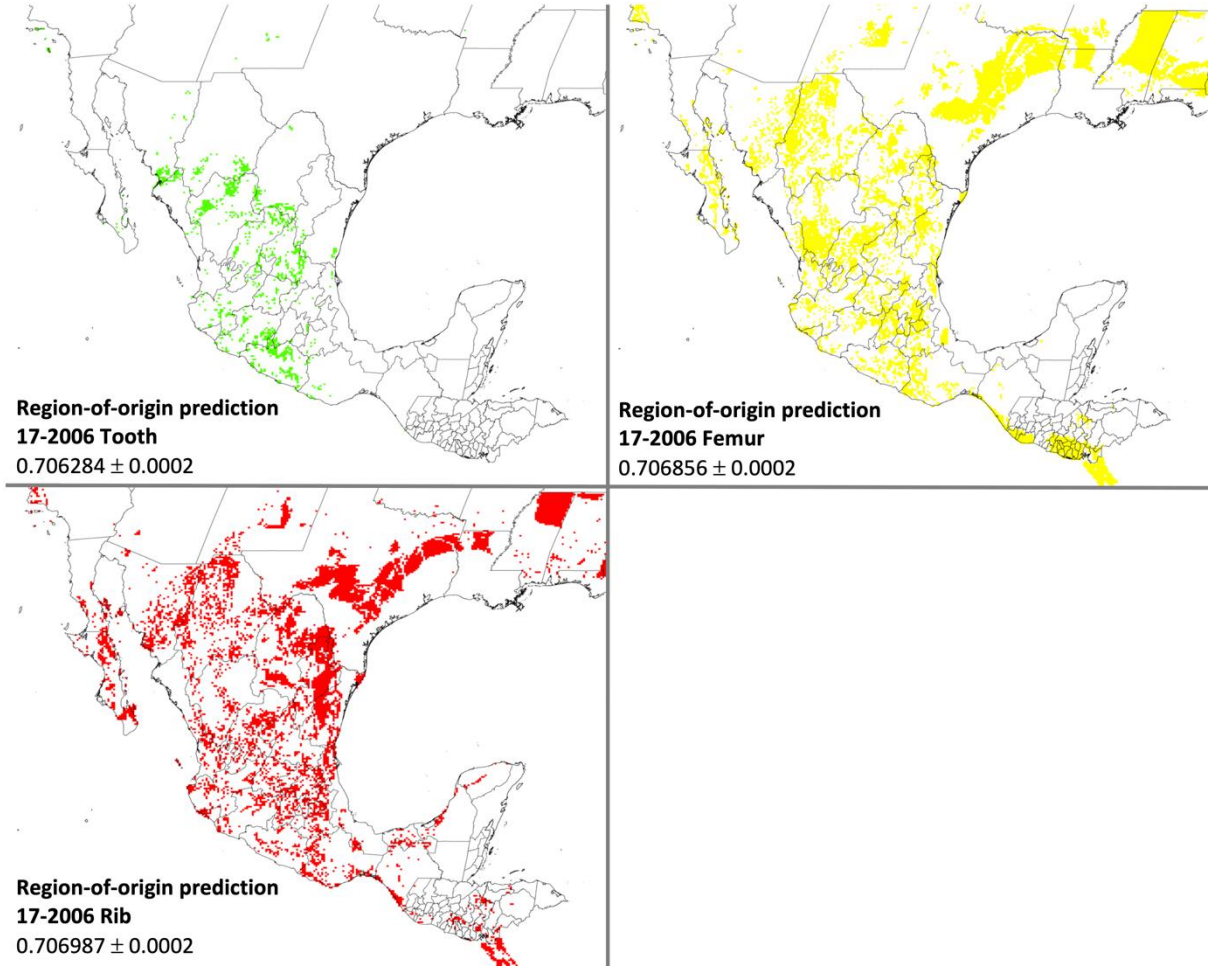

Figure 5.5.4.6. $^{87}Sr/^{86}Sr$ region of origin predictions for individual 17-2006 using the following skeletal elements: tooth, femur, and rib. An error of ±0.0002 was used for the predictions.

Individual 17-1944

The isotopic signatures of Individual 17-1944 were all within the inter-person error of ±0.0002 as determined by Plomp *et al.* (2020). Unfortunately, the values (~0.707) are very common throughout Mexico, limiting the ability to narrow down potential regions of origin. Nonetheless, it can be assumed that this individual did not move from his childhood residence prior to death. The isotopic signature of the place of birth was determined using the left first maxillary molar (#14) as the enamel calcifies around this time.

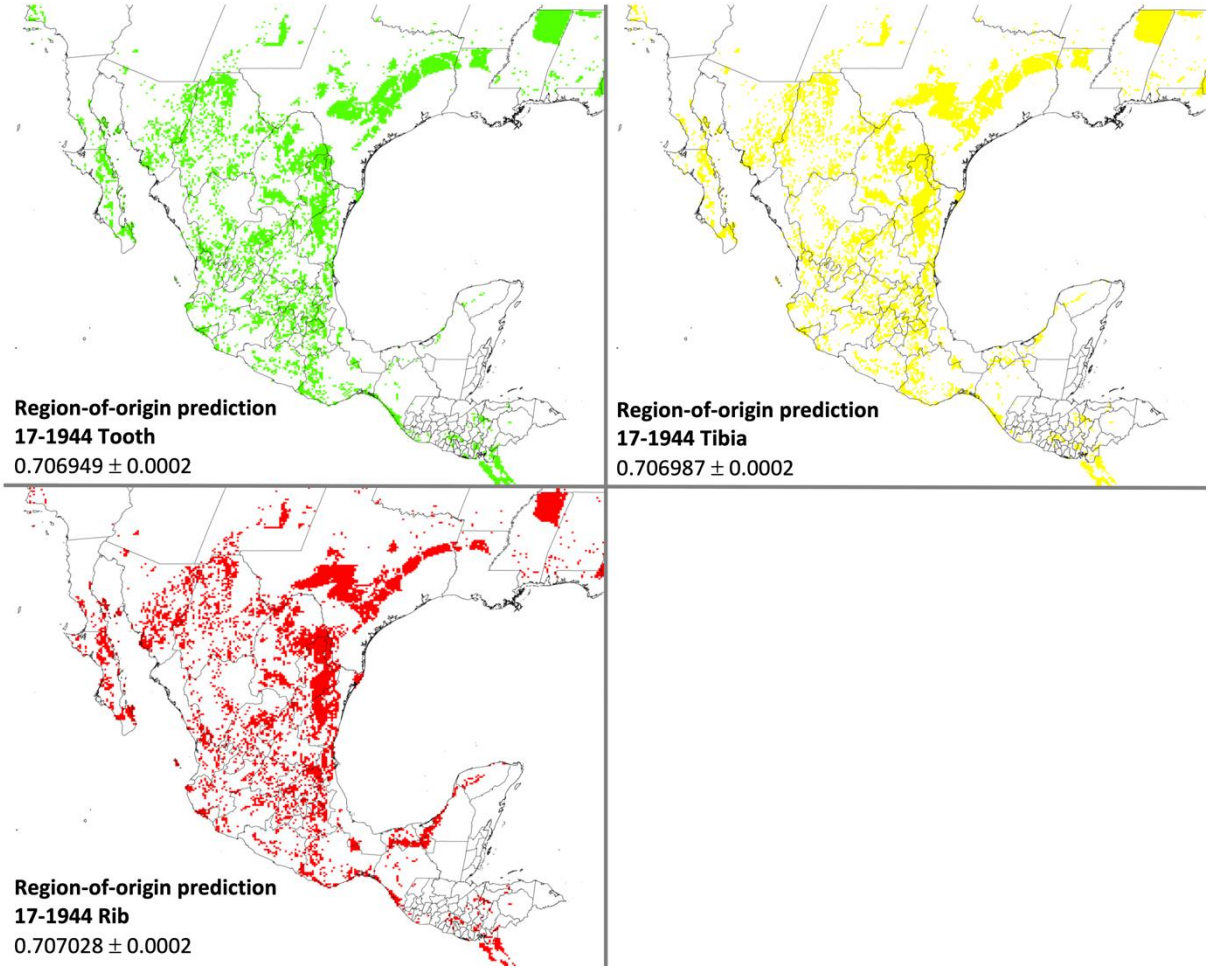

Figure 5.5.4.7. $^{87}Sr/^{86}Sr$ region of origin predictions for individual 17-1944 using the following skeletal elements: tooth, tibia, and rib. An error of ±0.0002 was used for the predictions.

Individual 17-2186

Individual 17-2186 reports $^{87}Sr/^{86}Sr$ ratios, which are all within the inter-person error of ±0.0002 as determined by Plomp *et al.* (2020). A narrowing down of potential regions of origin is not possible because the $^{87}Sr/^{86}Sr$ ratio is common within Mexico. Nonetheless, the maps seem to highlight the states along the Mexico-United States border as well as the coastal area of the Gulf of Mexico south to Chiapas (Figure 5.5.4.8).

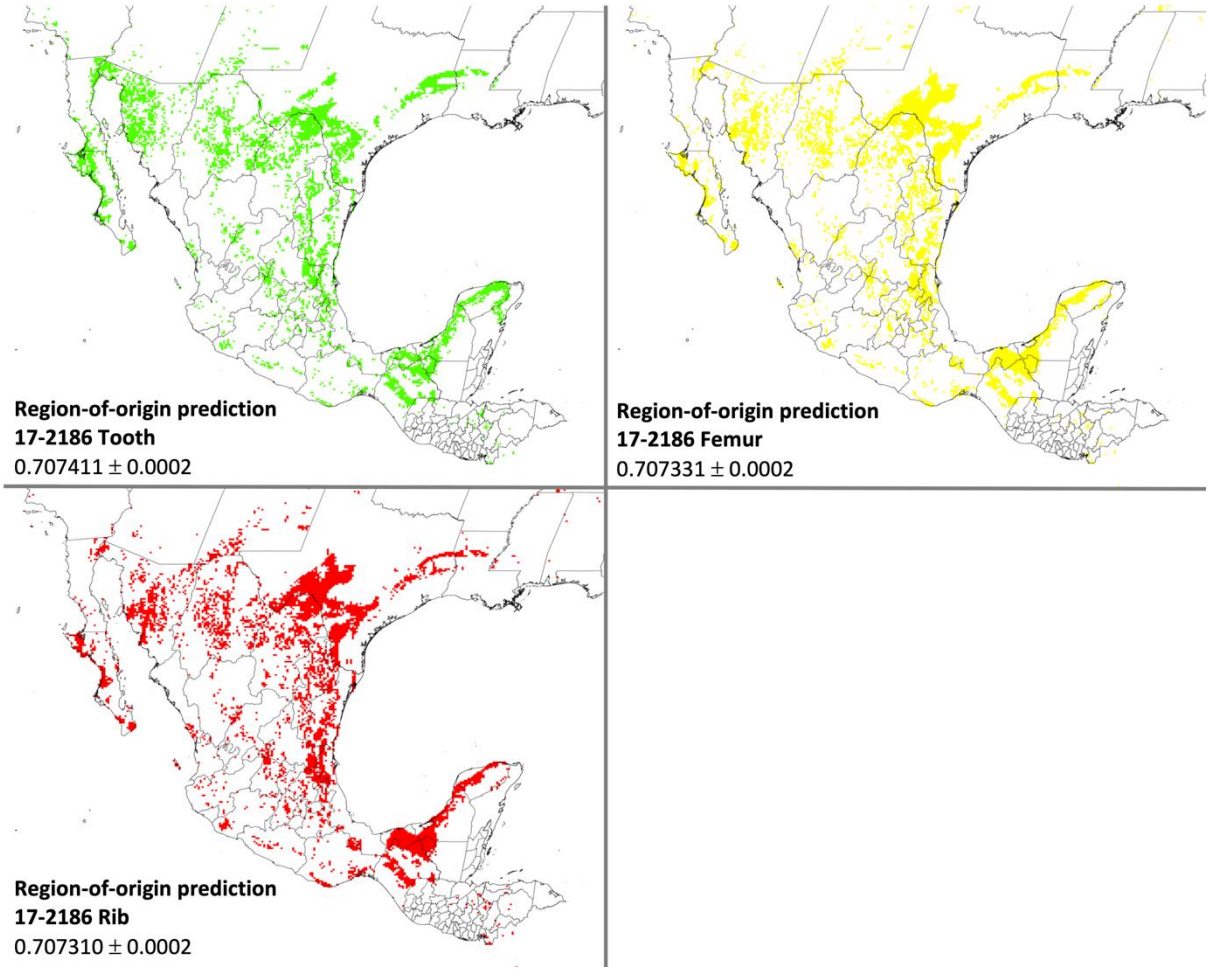

Figure 5.5.4.8. $^{87}Sr/^{86}Sr$ region of origin predictions for individual 17-2186 using the following skeletal elements: tooth, femur, and rib. An error of ±0.0002 was used for the predictions.

Individual 17-1681

The $^{87}Sr/^{86}Sr$ ratios of the tooth and femur of Individual 17-1681 are within the inter-person error of ±0.0002 as determined by Plomp *et al.* (2020). The rib $^{87}Sr/^{86}Sr$ ratio is, however, elevated in comparison, which can be interpreted as movement in the more recent months and years prior to death. As the turnover rate of the rib is much shorter (~17% per year compared to ~3% in the femur (Rummel, Hölzl, and Horn 2007)), it appears as if the rib has started to take on the new regional signature while the femur largely remained the same (slightly elevated but still within error).

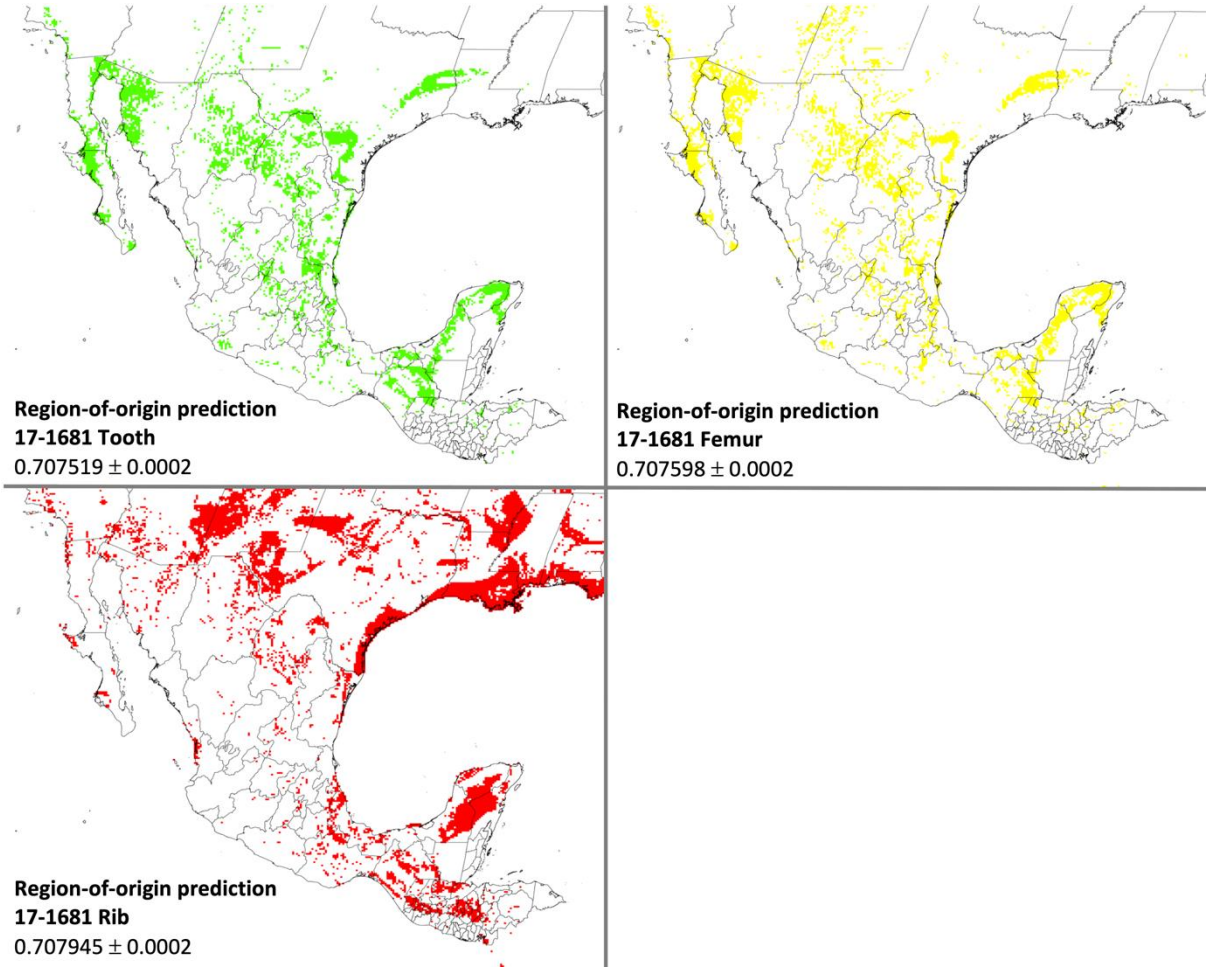

Figure 5.5.4.9. $^{87}Sr/^{86}Sr$ region of origin predictions for individual 17-2186 using the following skeletal elements: tooth, femur, and rib. An error of ±0.0002 was used for the predictions.

Individual 17-1682

Individual 17-1682 shows particularly interesting results for the $^{87}Sr/^{86}Sr$ analyses in the tooth and bones. While the tooth and rib are within error, the $^{87}Sr/^{86}Sr$ ratio of the tibia is much lower. Considering the varying turnover rates of approximately 17% per year for the rib and 3% for the tibia, this individual seemingly must have lived for a long period of time in a region represented by very low $^{87}Sr/^{86}Sr$ ratios (below the reported 0.705962 for the tibia). Furthermore, the individual must have moved in the approximately five years prior to his death to an area with higher isotopic ratios (above the reported 0.707982 for the rib). The hair values will be discussed at a later point in this chapter.

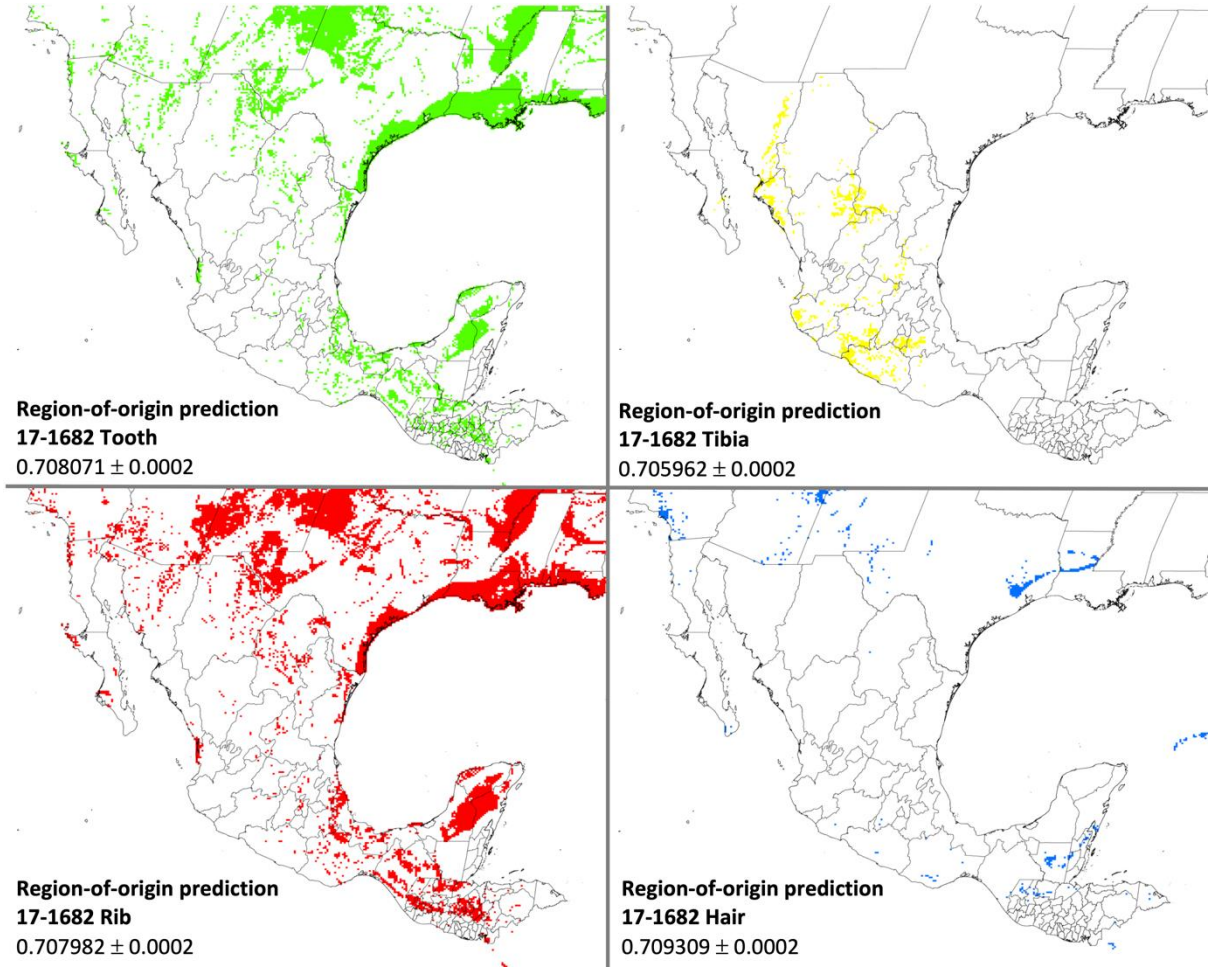

Figure 5.5.4.10. $^{87}Sr/^{86}Sr$ region of origin predictions for individual 17-1682 using the following skeletal elements: tooth, tibia, rib, and hair. An error of ±0.0002 was used for the predictions.

Individual 16-2623

The $^{87}Sr/^{86}Sr$ ratios of Individual 16-2623 of the rib and tibia fall within the inter-person error of ±0.0002 as determined by Plomp *et al.* (2020). Therefore, it can be assumed that this individual had not moved for a significant period given the small difference in $^{87}Sr/^{86}Sr$ ratios between the tibia and rib. The tooth (first left mandibular molar, #19) ratio of 0.706296 indicates a region of origin outside of the Central American countries shown here (Guatemala, Honduras, El Salvador, Belize) as well as further north than the Yucatan peninsula (Figure 5.5.4.11).

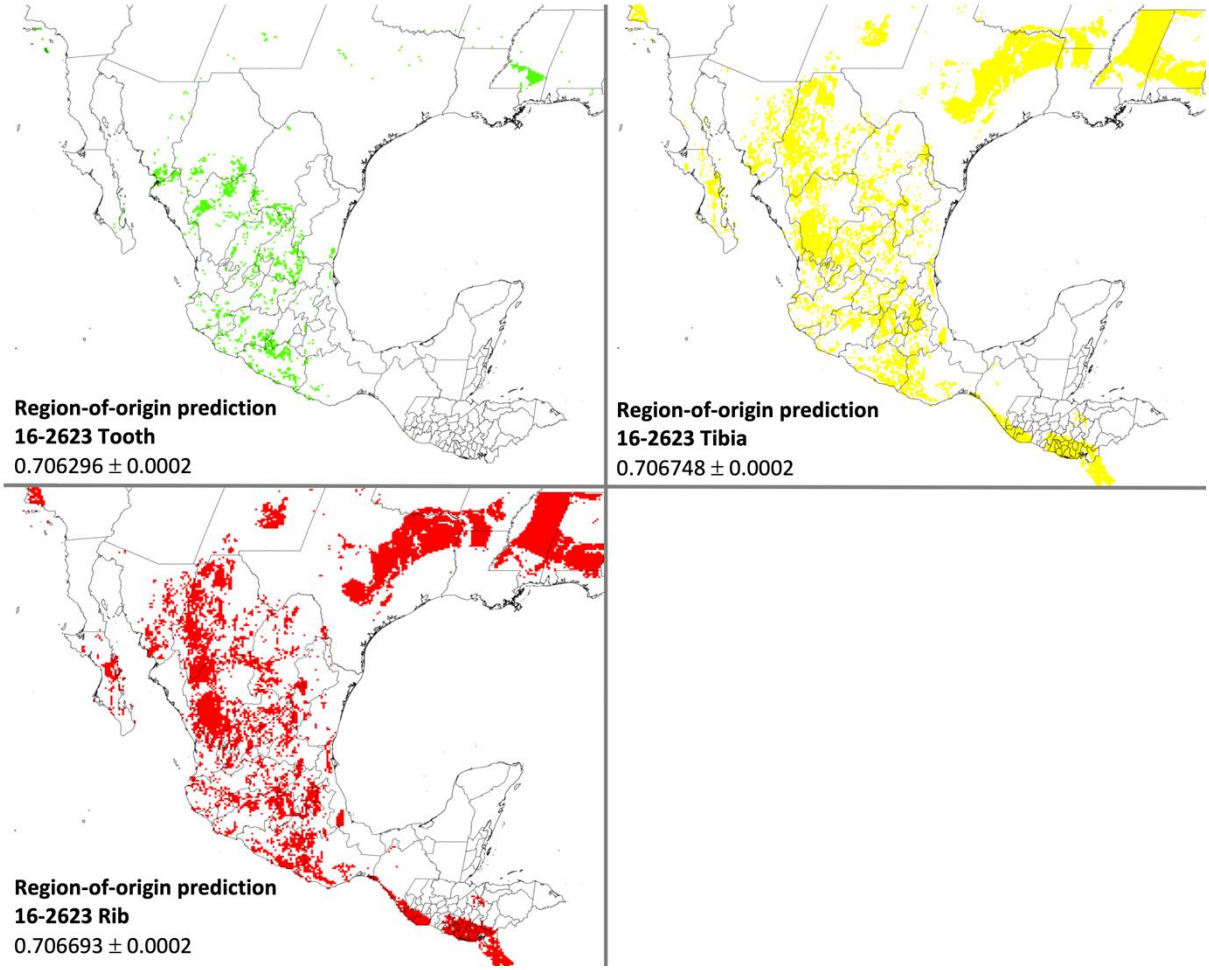

Figure 5.5.4.11. $^{87}Sr/^{86}Sr$ region of origin predictions for individual 16-2623 using the following skeletal elements: tooth, tibia, and rib. An error of ±0.0002 was used for the predictions.

Individual 16-2688

Individual 16-2688 shows indications of more recent movement. The $^{87}Sr/^{86}Sr$ ratio of the rib is elevated in comparison to the $^{87}Sr/^{86}Sr$ ratio of the femur, while the $^{87}Sr/^{86}Sr$ ratio of the femur is elevated compared to the $^{87}Sr/^{86}Sr$ ratio of the tooth (second right mandibular premolar, #29). The second premolar is known to begin calcification at 24-30 months and have completed the crown (enamel) development between 6-7 years. Therefore, this tooth does not represent the place of birth but rather the place where this individual spent his early childhood.

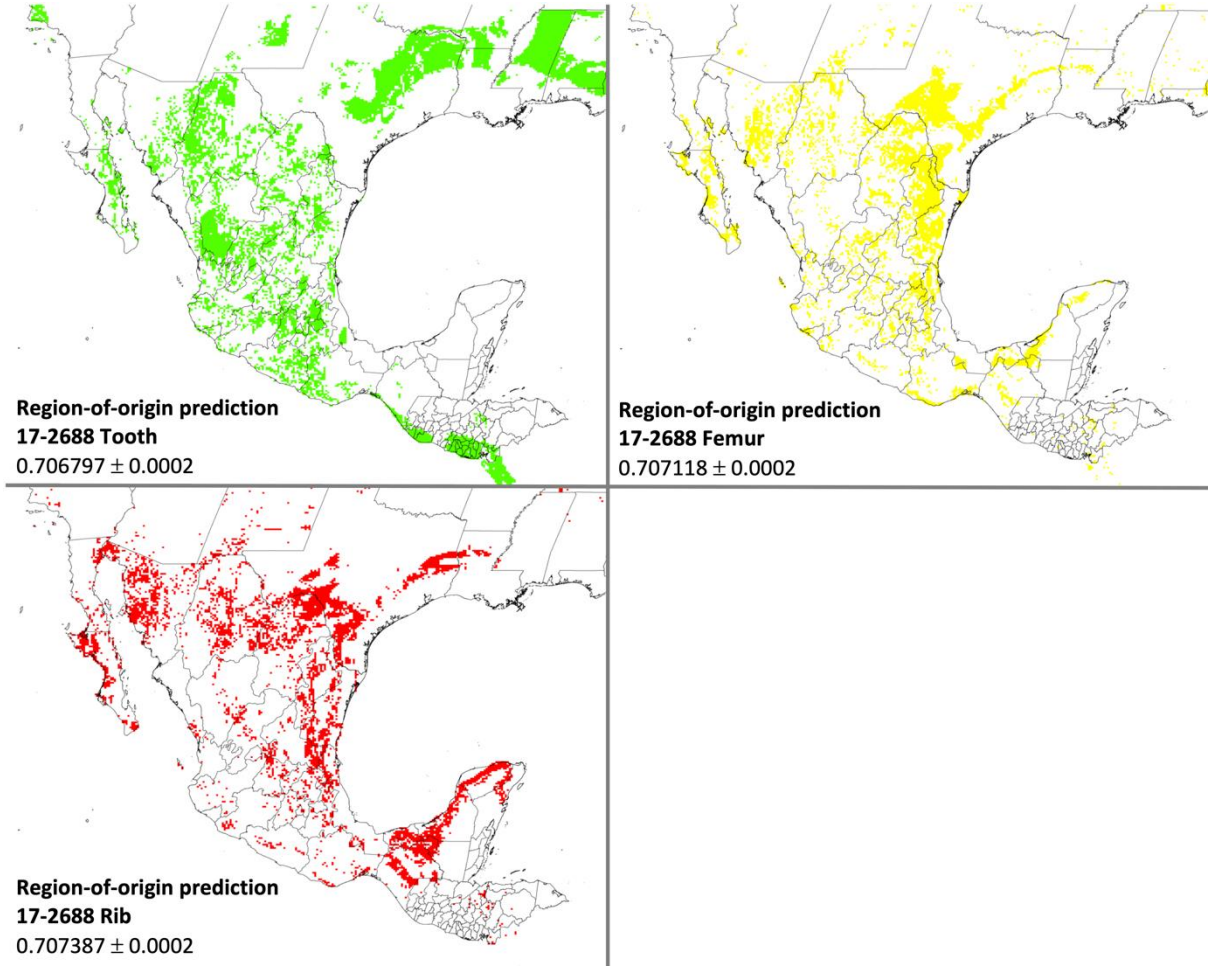

Figure 5.5.4.12. $^{87}Sr/^{86}Sr$ region of origin predictions for individual 17-2688 using the following skeletal elements: tooth, femur, and rib. An error of ±0.0002 was used for the predictions.

Individual 17-2469

Individual 17-2469 shows a range of $^{87}Sr/^{86}Sr$ ratios in the tested skeletal elements. While the tooth (right first mandibular molar, #30) predicts various regions in Mexico, the Central American countries, and the United States, the femur and rib $^{87}Sr/^{86}Sr$ ratios indicate that the individual did not reside in Mexico for an extended period of time. What is particularly interesting about this individual is that the isotopic ratio of the femur is elevated over the rib, which means that the person moved from a region with high $^{87}Sr/^{86}Sr$ ratios to one with lower $^{87}Sr/^{86}Sr$ ratios. These ratios are more consistent with the United States population than the Mexican population (Figure 5.5.4.22 and Chapter 5.4). It is plausible that this person may have lived in the United States for an extended period of time, was then deported back to Mexico or Central America where the mixing (and lowering) of the isotopic signature occurred and then died while trying to cross through the desert back into the United States.

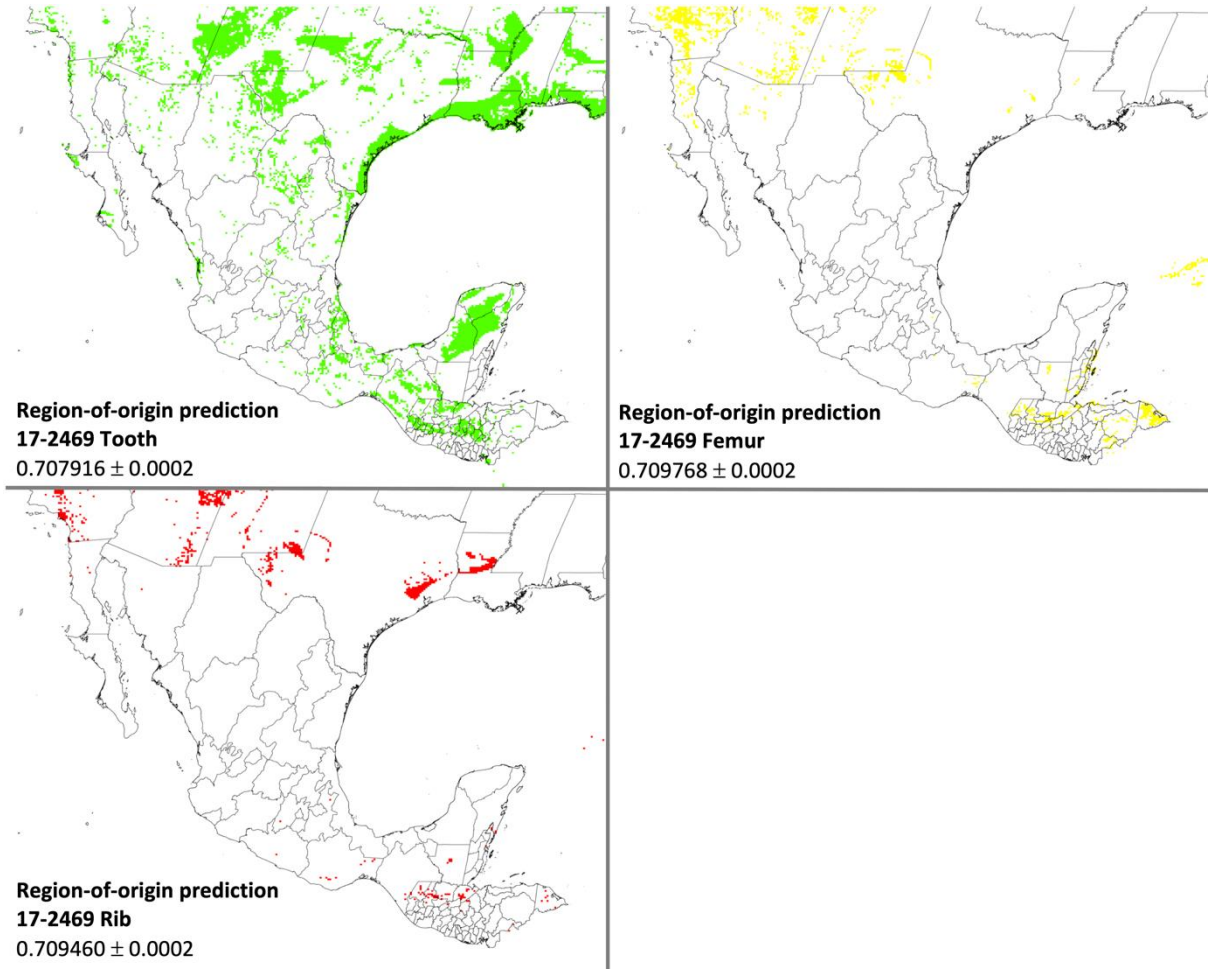

Figure 5.5.4.13. $^{87}Sr/^{86}Sr$ region of origin predictions for individual 17-2469 using the following skeletal elements: tooth, femur, and rib. An error of ±0.0002 was used for the predictions.

Individual 16-1585

Individual 16-1585 unfortunately exhibits isotopic signatures which are commonly seen in the Mexican population (0.707). This makes the narrowing down of potential regions of origin significantly more difficult. For this individual, it appears as if he moved from his place of origin to an area of higher $^{87}Sr/^{86}Sr$ ratios. While the rib $^{87}Sr/^{86}Sr$ ratio is significantly elevated from the tooth $^{87}Sr/^{86}Sr$ ratio, the femur $^{87}Sr/^{86}Sr$ ratio is only slightly outside of the inter-person error of 0.0002. Both the femur and the rib $^{87}Sr/^{86}Sr$ ratios are therefore mixing signatures and the latest region of origin must have been in an area of $^{87}Sr/^{86}Sr$ ratios above 0.707654.

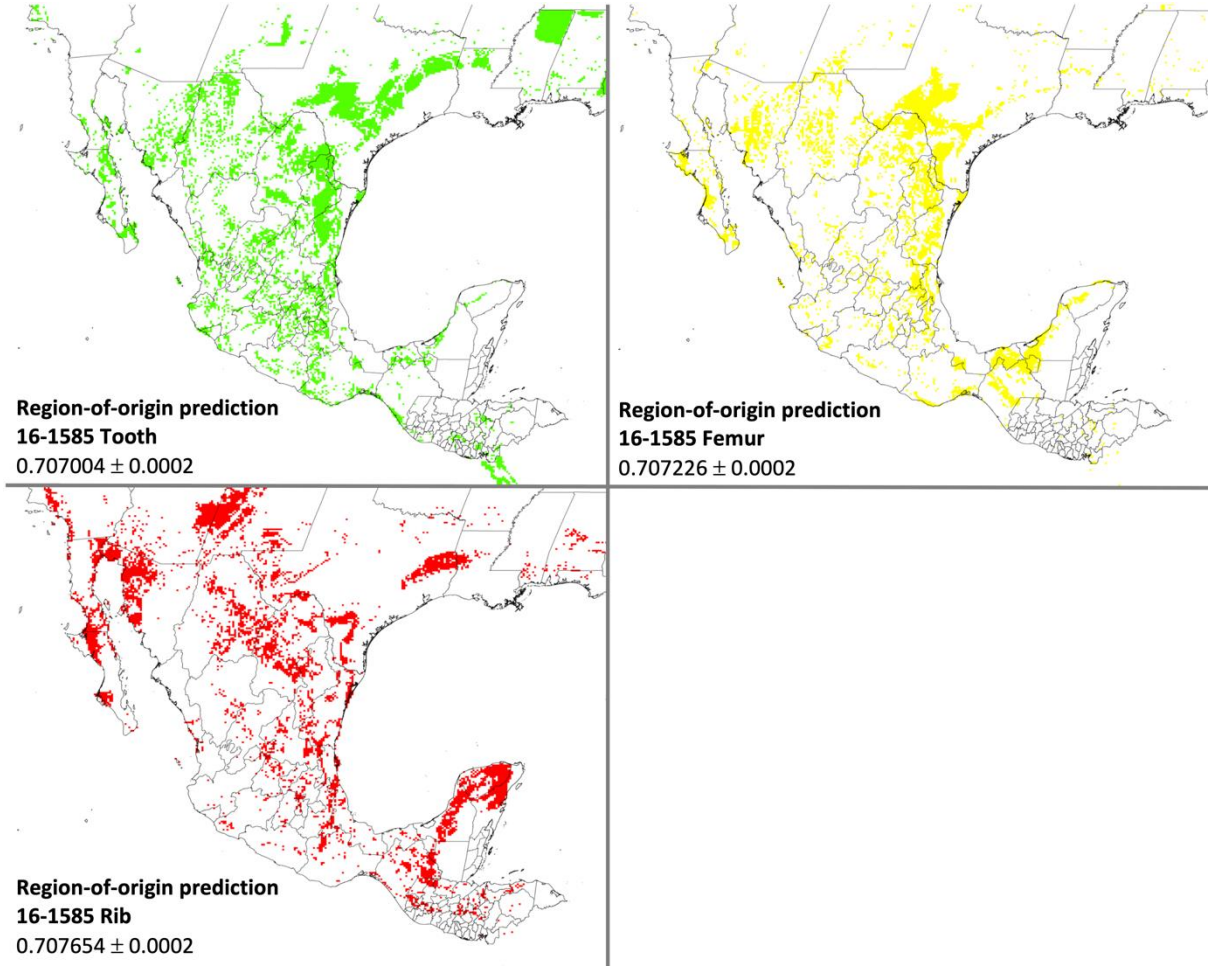

Figure 5.5.4.14. $^{87}Sr/^{86}Sr$ region of origin predictions for individual 16-1585 using the following skeletal elements: tooth, femur, and rib. An error of ±0.0002 was used for the predictions.

Individual 16-01822

The tooth sampled for this individual was the right maxillary canine (#6). Unfortunately, no first molar (which forms around birth) was available for sampling. This canine begins calcifying 4-5 months after birth and the crown (enamel) formation is completed at 6-7 years of age. Therefore, this tooth does not represent the place of birth but rather the individual's place of residence during early childhood. The ratio of the tooth rules out an early childhood residence in the Northern Triangle countries and places him within Mexico.

The $^{87}Sr/^{86}Sr$ bone ratios clearly indicate that the individual moved in the period from the formation of the canine to his time of death. The rib shows a much higher ratio than the tooth and the tibia, indicating that the individual must have moved for a significant period. The tibia $^{87}Sr/^{86}Sr$ ratio falls in between the tooth and the rib ratio, indicating a mixed signature as the turnover rate is longer than in the rib. Again, the hair values are representative of the border region and most likely represent a mixed signature. This observation will be discussed in further detail later in this chapter.

This individual has recently been identified and can therefore be used to test the conditional correlation approach. It is, however, unknown to the author if and where this individual moved to during his lifetime. Furthermore, it is unknown if the known place of origin is the true birthplace or if the next of kin may have reported the last place of residence. The known place of origin is marked with a purple star in Figure 5.5.4.15. For all predictions, except the hair ratio, the place of origin falls within the predicted areas.

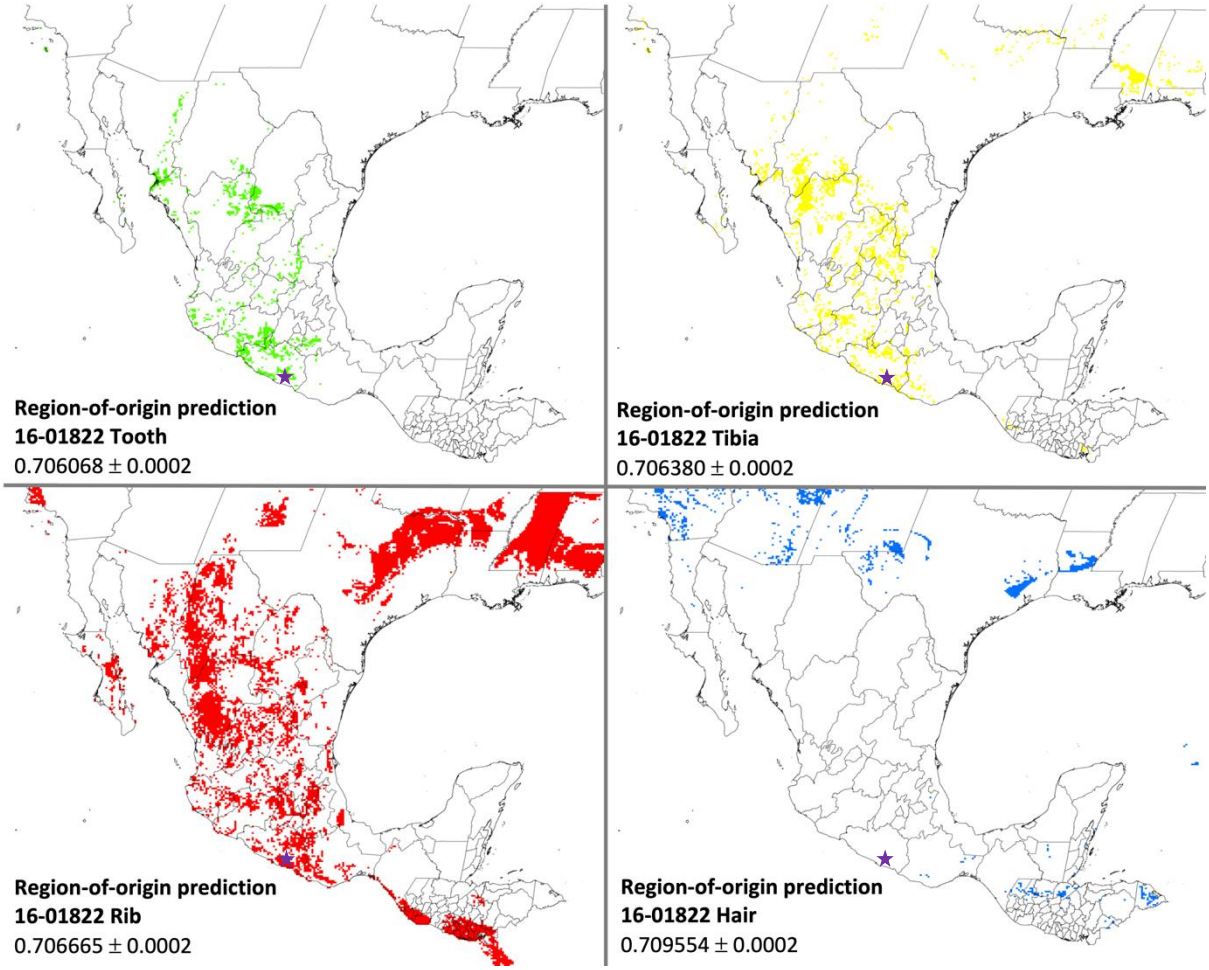

Figure 5.5.4.15. $^{87}Sr/^{86}Sr$ region of origin predictions for individual 16-01822 using the following skeletal elements: tooth, tibia, rib, and hair. An error of ±0.0002 was used for the predictions. The purple star represents the known place of origin for this individual.

Individual 17-1742

Individual 17-1742 exhibits very common $^{87}Sr/^{86}Sr$ values for Mexico (~0.707), which predicts that the individual could have been from various regions in Mexico as well as Guatemala and Honduras. All $^{87}Sr/^{86}Sr$ ratios are within the inter-person error of ±0.0002 as determined by Plomp *et al.* (2020). This indicates that the individual did not move from one region with certain $^{87}Sr/^{86}Sr$ ratios to a new region with different $^{87}Sr/^{86}Sr$ ratios within years prior to his death.

The hair values are representative of the border region and likely present a mixed signature. This observation will be discussed in further detail later in this chapter.

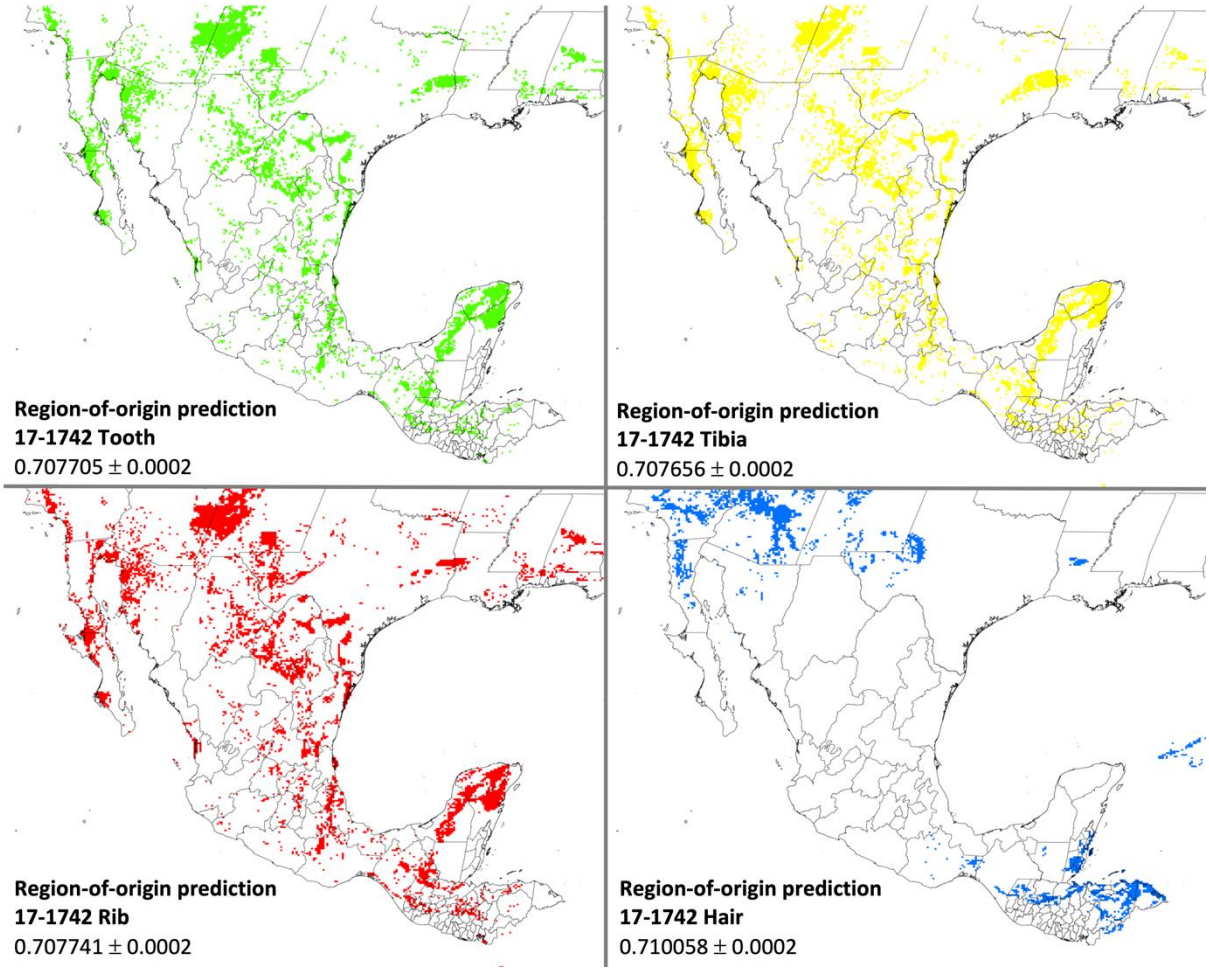

Figure 5.5.4.16. $^{87}Sr/^{86}Sr$ region of origin predictions for individual 17-1742 using the following skeletal elements: tooth, tibia, rib, and hair. An error of ±0.0002 was used for the predictions.

Individual 16-01516

The $^{87}Sr/^{86}Sr$ ratios of Individual 16-01516 indicate that he more recently moved to a region of much higher isotopic ratios compared to his original place of origin. The $^{87}Sr/^{86}Sr$ ratios of the tooth (left first mandibular molar, 19) and the tibia are very similar and within the inter-person error of ±0.0002 as determined by Plomp *et al.* (2020). The rib $^{87}Sr/^{86}Sr$ ratio likely represents a mixed signature based on the original and the new locations. Because the rib $^{87}Sr/^{86}Sr$ ratio is elevated by approximately 0.0006 while the tibia is not significantly elevated over the tooth ratio, it can be assumed that the new isotopic signature must be significantly higher. The hair values will be discussed at a later point in this chapter.

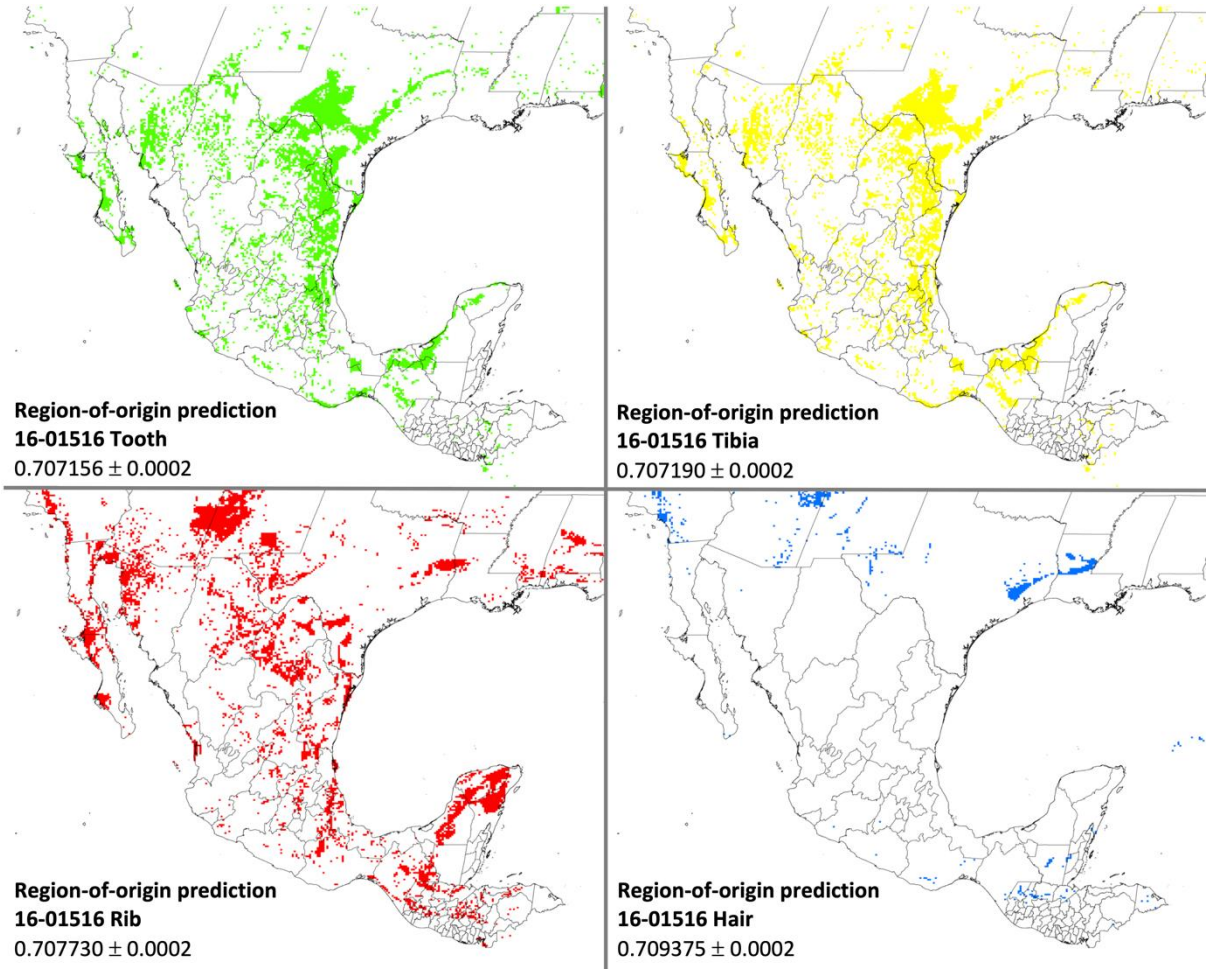

Figure 5.5.4.17. $^{87}Sr/^{86}Sr$ region of origin predictions for individual 16-01516 using the following skeletal elements: tooth, tibia, rib, and hair. An error of ±0.0002 was used for the predictions.

Individual 16-3187

Individual 16-3187 shows very different $^{87}Sr/^{86}Sr$ ratios for the bones than for the sampled tooth. The sampled tooth was a first molar of the left mandible (19) and therefore represents the period from birth to approximately 30 months. The $^{87}Sr/^{86}Sr$ ratio indicates that the individual did not originate from the Central American countries shown here (Figure 5.5.4.18) but may have originated from the western part of Mexico, including the Sierra Mountain range. The $^{87}Sr/^{86}Sr$ ratios of the femur and rib are within the inter-person error of ±0.0002 as determined by Plomp *et al.* (2020) and it can therefore be assumed that the person resided in the last place of origin for an extended and significant period of time. The $^{87}Sr/^{86}Sr$ ratios of the femur and rib are among the most seen ratios seen in the Mexican population (~0.707) which makes it impossible to narrow down potential regions of origin based on the present data.

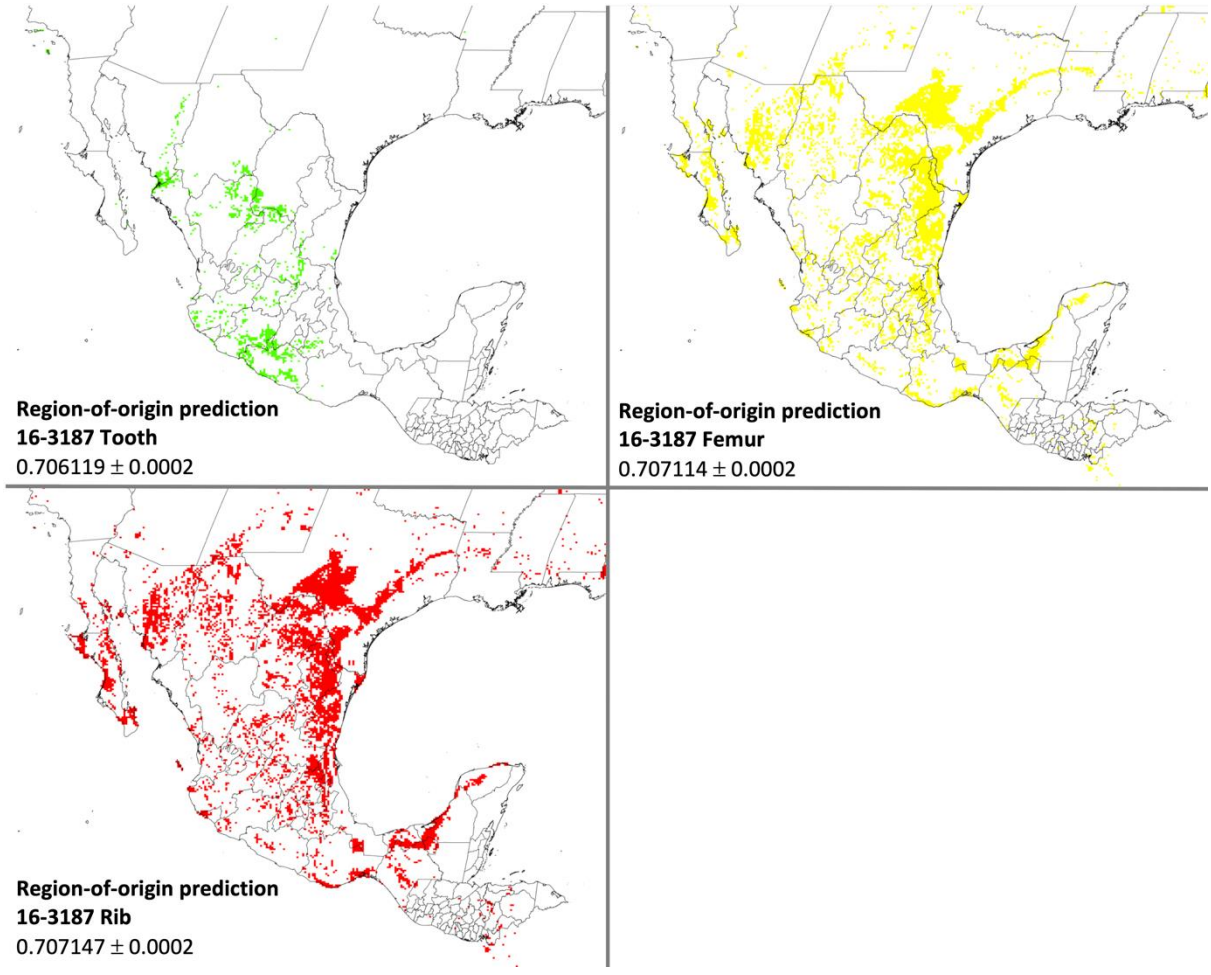

Figure 5.5.4.18. $^{87}Sr/^{86}Sr$ region of origin predictions for individual 16-3187 using the following skeletal elements: tooth, femur, and rib. An error of ±0.0002 was used for the predictions.

Individual 16-01616

The $^{87}Sr/^{86}Sr$ ratios of the tooth and tibia for Individual 16-01616 were within the inter-person error of ±0.0002 as determined by Plomp *et al.* (2020). The rib $^{87}Sr/^{86}Sr$ ratio, on the other hand, is significantly elevated and must represent signatures from the last region that this individual traveled to and is therefore considered a mixed signature. The sampled tooth was a right first maxillary molar (3) and therefore represents the place of birth up until approximately 30 months.

This individual was recently identified and according to the next of kin, was originally from the state of Tlaxcala. The state is highlighted by the circle in Figure 5.5.4.19. As one can see, the tooth and tibia $^{87}Sr/^{86}Sr$ ratio include the individual's state of origin. However, the maps also highlight that the region of origin predictions are still too coarse to narrow them down sufficiently to be of use for the investigators. This fact highlights that a multi-isotope approach is indispensable to assist the forensic investigators in a meaningful way.

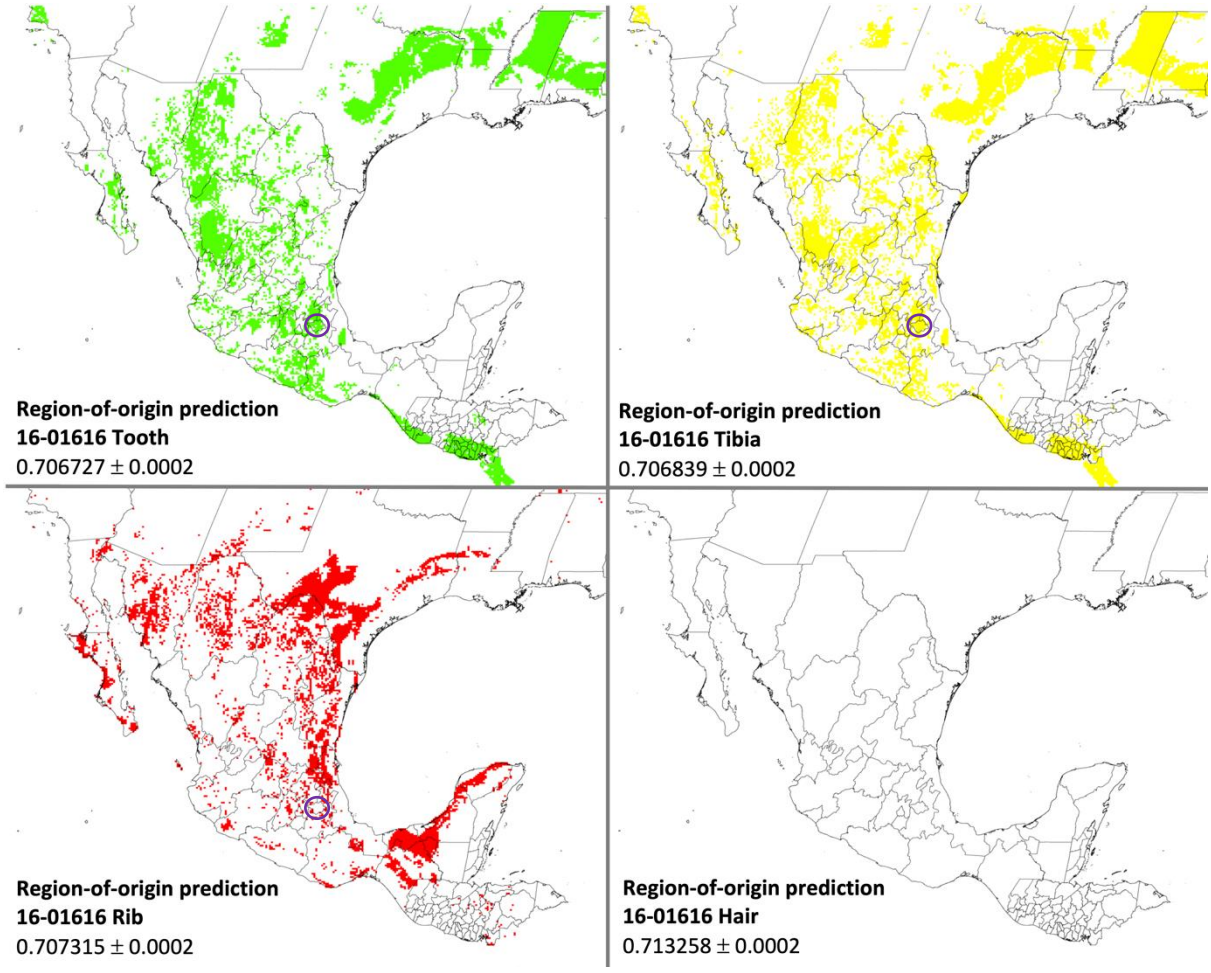

Figure 5.5.4.19. $^{87}Sr/^{86}Sr$ region of origin predictions for individual 16-01616 using the following skeletal elements: tooth, tibia, rib, and hair. An error of ±0.0002 was used for the predictions. The purple circle represents the known state of origin for this individual.

The approach used above merely uses a conditional correlation methodology, which does not take the prediction errors into account. In the future, it will be essential to determine potential regions of origin by underlying the prediction error maps and therefore getting a more confident answer to the research question at hand. A potential tool to rescale isoscapes using known-origin isotope data and assigning origin to the unknown samples is AssignR, a R package which takes into account the likelihood of a certain isotopic value/ratio to occur in any one particular location on the isoscape. Furthermore, it will be pertinent to work on a multi-isotope approach which incorporates all isoscapes and their predication error maps.

Overall, the error of ±0.0002 is not small enough to clearly include or exclude potential regions of origins when the measured $^{87}Sr/^{86}Sr$ ratio is in the range of the most frequently seen ratios (~ 0.707) seen in Mexico. Furthermore, it will be important to further study the mixing of signatures that happens when individuals move from one place to another and the bone turnover integrates the new signature into the old one. The mechanisms of the mixing are, thus far, not studied in great detail but are of utmost importance if those $^{87}Sr/^{86}Sr$ ratios are supposed to be used for interpretations beyond the fact that an individual moved from the former region of origin.

Furthermore, while a significant number of samples were collected throughout Mexico, several regions are still under-sampled and therefore unrepresentative of the true variation. While a machine learning approach, such as the one presented by Bataille *et al.* (2018), provides a much deeper context through the underlying variables, it is still pertinent to input sufficient amounts of data into the model in order to create valuable outcomes.

Elevated $^{87}Sr/^{86}Sr$ ratios in human hair collected from UBCs

The $^{87}Sr/^{86}Sr$ ratios of the hair samples of the undocumented border crossers are clearly elevated over the $^{87}Sr/^{86}Sr$ ratios documented for the other skeletal elements (Figure 5.5.4.20). Figures 5.5.4.21 and 5.5.4.22 show that the ratios of the hair are more like the ratios found in the United States than most of the ratios found in Mexico. The ratios are particularly like those found in the border regions of Arizona. This is also visible in most of the region of origin prediction maps shown above (*e.g.* Figure 5.5.4.4, 5.5.4.15, 5.5.4.16 and 5.5.4.17).

The procedure used to clean the hair was extensively studied and published by Font *et al.* (2012). However, it is important to further investigate the origin of the isotopic ratios found here. To rule out that the ratios measured were not in fact the environmental signatures but truly imbibed in the hair, a progressive leaching study will be conducted. Here, the effect of the cleaning

procedures on the isotope ratios will be investigated to determine whether or not diagenesis affected the hair samples.

Kootker *et al.* (2020) and (Gordon *et al.* 2019) recently showed that the hair strontium composition and signatures of individuals buried in shallow pits as well as surface exposure changed quickly and that it was not possible to retrieve the *in vivo* isotope ratios. Furthermore, the authors were unable to determine a relationship between the hair degradation and isotopic shift. Therefore, it is plausible that the arid environment of the Sonoran Desert has a similar effect on the $^{87}Sr/^{86}Sr$ ratios. Therefore, the signatures found in the hair of the undocumented border crossers are most likely mixed signatures of the "original" place of origin/travel signature and the signatures found in the desert lands of Arizona.

Overall, the digenetic effects of surface burials on $^{87}Sr/^{86}Sr$ ratios in skeletal material needs to be further investigated and yet interpreted with extreme caution. It is not recommended to use hair $^{87}Sr/^{86}Sr$ ratios of decomposed remains found in surface burial contexts for region of origin predictions.

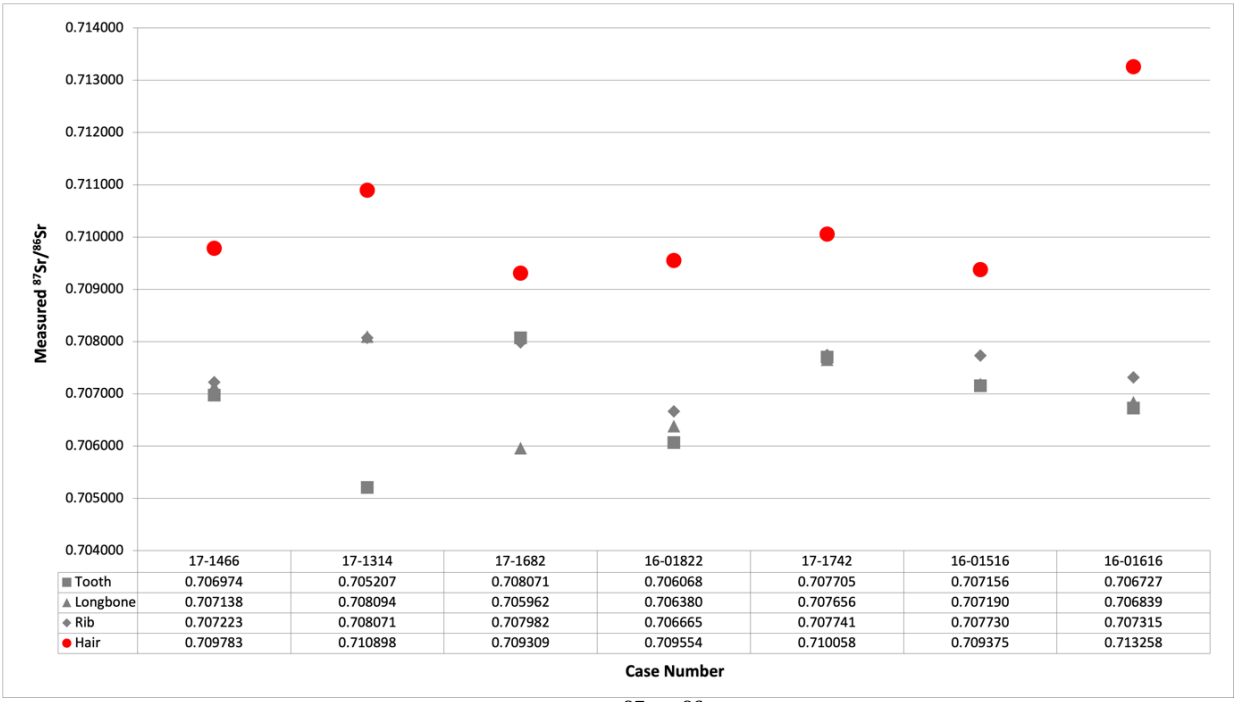

	17-1466	17-1314	17-1682	16-01822	17-1742	16-01516	16-01616
Tooth	0.706974	0.705207	0.708071	0.706068	0.707705	0.707156	0.706727
Longbone	0.707138	0.708094	0.705962	0.706380	0.707656	0.707190	0.706839
Rib	0.707223	0.708071	0.707982	0.706665	0.707741	0.707730	0.707315
Hair	0.709783	0.710898	0.709309	0.709554	0.710058	0.709375	0.713258

Figure 5.5.4.20. Visualization of the measured $^{87}Sr/^{86}Sr$ ratios in the individuals from who hair was sampled. Tooth and bone values in grey color, hair in red.

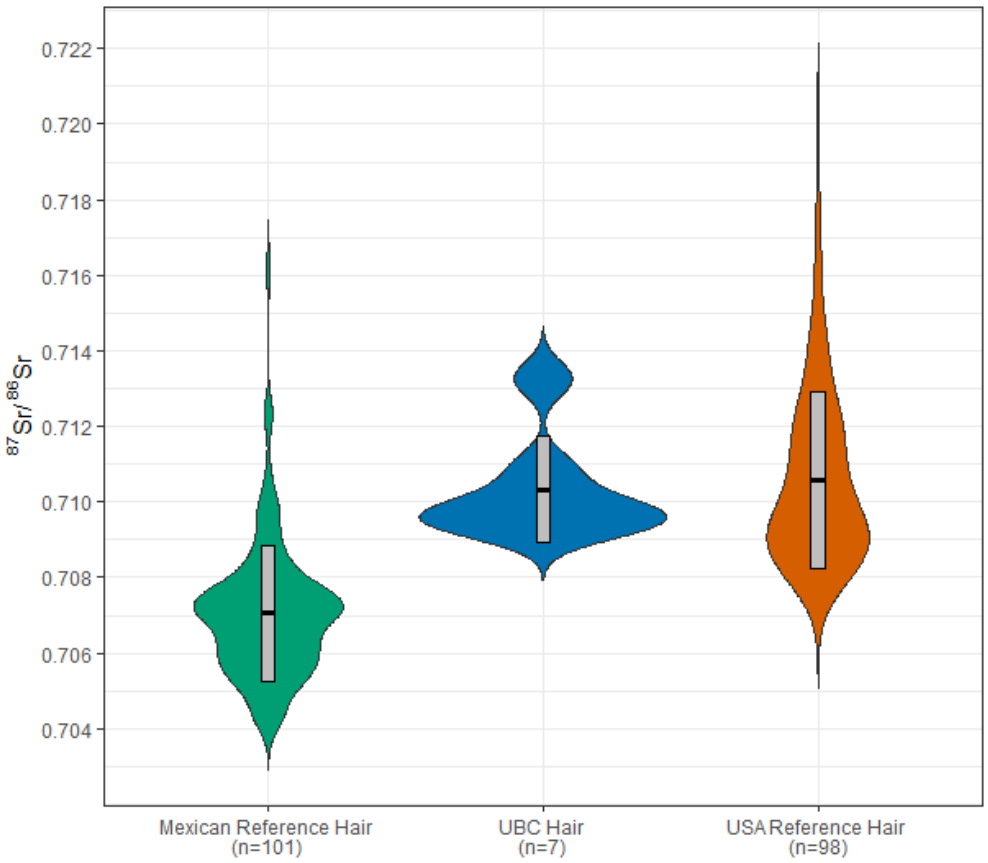

Figure 5.5.4.21. Comparison of the $^{87}Sr/^{86}Sr$ ratios measured in Mexican reference hair, UBC hair, and USA reference hair. The probability density of the data at different ratios is shown through the usage of a violin plot.

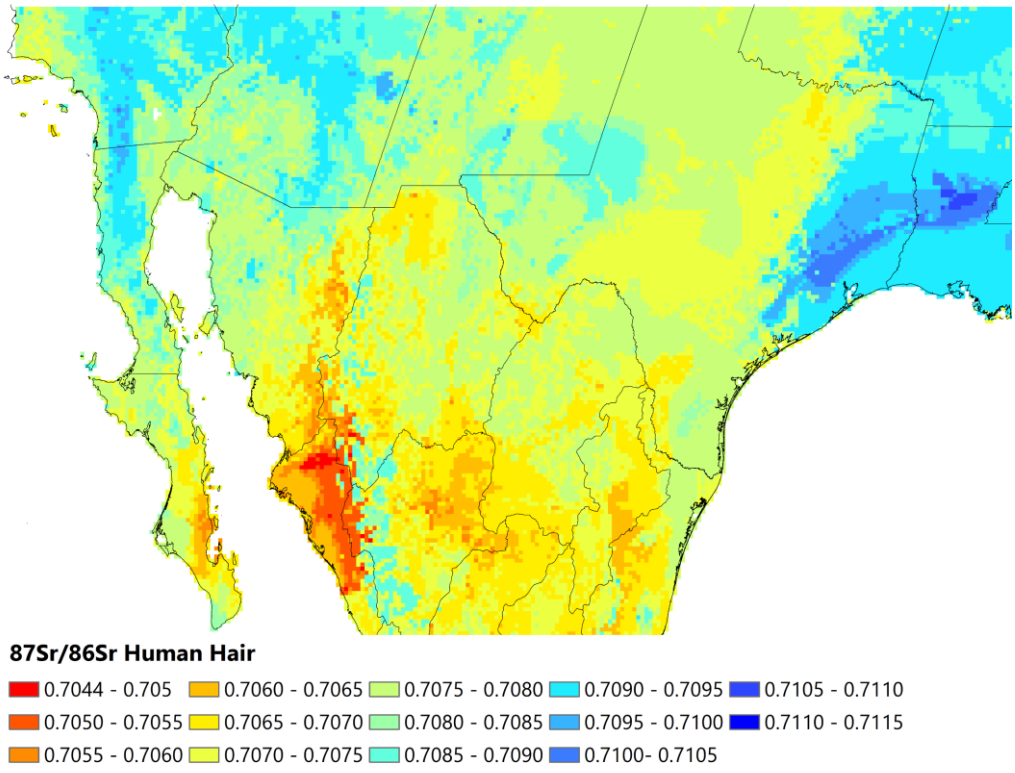

Figure 5.5.4.22. Isoscape of $^{87}Sr/^{86}Sr$ ratios found in the border region of Mexico and the United States.

CHAPTER VI
CONCLUSION

As established in Chapter I of this thesis, a main goal of forensic anthropology is the personal identification of human remains, primarily focusing on establishing a biological profile of deceased individuals and utilizing other identifying aspects such as antemortem trauma, pathological conditions, or other individualizing characteristics. Often, establishing a biological profile and identifying aspects can be difficult as the remains may be significantly fragmented or degraded due to taphonomic processes. Furthermore, undocumented border crossers recovered along the Mexico-U.S. border are considered a rather homogenous group as many of the individuals are male, young and from Latin American countries. A forensic anthropological ancestry assessment for undocumented border crossers, which states some degree of "native American" usually does not add a significant investigative lead to the biological profile. Consequently, the inability to narrow down the search to the most probable geographic locations is a major concern. Therefore, forensic anthropologists are in need of ways that further aid the identification process. They are finding novel information by incorporating biomolecular science (*e.g.* isotope analysis) into their fields of study. Thus, together with the forensic anthropological methods used to establish the biological profile and determine other individualizing factors (antemortem trauma, pathological conditions, anatomical variants *etc.*), isotope analysis can provide investigative leads that may aid the identification process.

This PhD thesis followed two research lines, namely a conceptual line, which aimed to collect essential isotopic baseline data, and an interpretive line, which aimed at a specific interpretation (and consequently the identification of region-of-origin) of the generated data. To achieve this aim, the following objectives were proposed: establish hair and tap water isoscapes of Mexico representing the regional isotopic values; determine the isotopic composition of deceased unidentified border crossers using tissues such as bones, teeth, and hair samples to provide information on probable locations and movements of individuals at different times of their life; match the data obtained from the deceased to the created isoscape (by comparison of the isotopic values); evaluate the precision and accuracy by comparing the isotopic composition data of recently identified remains at the Pima County Office of the Medical Examiner in Arizona to the established isoscape as well as comparing the water isoscapes generated from proxy data to theoretical isoscapes derived from precipitation records and geological maps. While the unidentified undocumented border crossers at the PCOME are the primary concern of this research, it was also an aim to accumulate knowledge of how data collection and analysis should

be performed to assist future large-scale identification missions. In the following, the results of the various isotope systems used in this research will be presented and evaluated in general as well as regarding to its usefulness to aid the identification of undocumented border crossers.

Carbon ($\delta^{13}C$), nitrogen ($\delta^{15}N$), and sulfur ($\delta^{34}S$) in human hair

Data on carbon, nitrogen, and sulfur isotopes of human hair collected throughout Mexico were presented. The recorded values ranged from −18.3‰ to −12.8‰ for δ^{13}C, 6.8‰ to 10.8‰ for δ^{15}N, and from 2.7‰ to 8.0‰ for δ^{34}S.

While previous research showed geographic patterns in the δ^{34}S isotopic values in several countries (Valenzuela *et al.* 2011; Katzenberg and Krouse 1989; Krouse and Grinenko 1991), this study was not able to reproduce these results within Mexico. Further study into the dietary habits of the Mexican population is needed to find potential explanations for these patterns. The findings reinforce the idea that the average Mexican diet is very C_4-plant based as well as terrestrial meat-heavy. Nonetheless, the observation of geographic patterns in the δ^{13}C values is somewhat surprising as they had not been previously documented in human hair studies in Mexico. While the produced isoscape shows clear trends, it is essential to further the research into the farming practices and dietary preferences, especially considering the significant influence of socioeconomic factors on isotope values, given that some socioeconomic correlations were stronger than the geographic correlations.

The Mexican δ^{15}N values were overall in accordance with an omnivore diet with more variance towards a high meat than to a vegetarian or vegan diet (Meier-Augenstein 2018). However, considering that the United States is the highest meat consumer (of the countries evaluated here) with approximately 124 kg/person/year consumed (Food and Agriculture Organization of the United Nations 2017; Ritchie and Roser 2017) versus Mexico's meat consumption that only lies at approximately 64 kg/person/year (Food and Agriculture Organization of the United Nations 2017; Ritchie and Roser 2017). Thus, one must consider other factors that may contribute to elevated isotopic values. Nutritional stress, such as starvation and malnutrition can lead to elevated δ^{15}N values due to breaking down muscle protein to meet the body's amino acid needs (Meier-Augenstein 2018). The data indicated that lower δ^{15}N values can be found in places with higher percentages of indigenous ancestry and language.

A tighter network of samples is needed to strengthen the now established baseline data and employ it in the future as a new tracer from which geographic information can be extracted. Additionally, a more thoroughly documented history of the hair donors would improve the possibility to draw further conclusions.

Overall, the C-N-S data show stronger correlations with socioeconomic covariates than with geographic and environmental ones. The recorded isotopic values have the potential to be used in combination with other isotope systems to narrow potential regions of origin. Furthermore, socioeconomic factors may have an even larger impact on the recorded values than previously thought.

Oxygen ($\delta^{18}O$) and Hydrogen ($\delta^{2}H$) in tap water

δ^{18}O isotopic values in tap water ranged from -12.1‰ to -0.2‰, while the δ^{2}H ranged from -91.3‰ to -8.9‰. The results demonstrate significant spatial variability for in Mexican tap water. The dataset provides important baseline data for extrapolation of values for Mexico, and the associated isoscapes show great potential for usage in hydrological contexts. Isotope analysis has demonstrated its value in identifying travel histories of individuals as well as regions of origin for unidentified remains (Bartelink *et al.* 2018; Chesson *et al.* 2018; E. Bartelink, Berry, and Chesson 2014) and therefore, this study is an important milestone to create a spatially extensive overview of the isotopic values of water in North America.

Nonetheless, this study highlights the need for more water sampling in Mexico (as well as in Central and South America), to provide a tool for understanding hydrological patterning and for predicting region of origin for animals, including unidentified deceased humans. A large-scale baseline database is needed for many hydrological projects but also to help solve humanitarian issues, such as aiding the identification of UBCs found at the Mexico-United States border. An investigation into the social background of Mexican tap water is needed to describe what tap water is used for in everyday life as well as the specific sources of drinking water in different regions.

Oxygen ($\delta^{18}O$) in human hair

This chapter discussed the δ^{18}O isotopic values found in the human hair samples from Mexico. Due to technical issues, the samples had to be reanalyzed which lead to interesting questions regarding quality control and data interpretation. Here, two datasets, the one from September 2019 and the one from March 2020, were presented and discussed. While there is no knowledge of potential issues during the second sample run, the data raise concerns. Specifically, it is very concerning that all statistical and geostatistical tools employed here (and employed for all other isotope systems) performed poorer in the newer March 2020 dataset than in the September 2019 dataset. It is not possible to draw definitive conclusions for the δ^{18}O analyses of Mexican human hair now. Therefore, it is suggested that the samples must be re-run to validate which dataset shows validity and is representative of the Mexican population.

Strontium ($^{87}Sr/^{86}Sr$) in human hair and tap water

This study presents the first large scale modern human tissue based $^{87}Sr/^{86}Sr$ ratios from Mexico and closed a large spatial gap in $^{87}Sr/^{86}Sr$ tap water ratios available in North America. The $^{87}Sr/^{86}Sr$ ratios of the hair samples ranged from 0.70424 to 0.71613 while the tap water samples ranged from 0.70404 to 0.71385. A strong correlation (R^2= 0.80) was observed between $^{87}Sr/^{86}Sr$ of human hair and tap water data and location averages correlated more strongly (R^2= 0.87). This study has shown that the $^{87}Sr/^{86}Sr$ ratios in human hair and tap water from Mexico have great potential to be used for provenancing studies, such as determining potential regions of origin of undocumented border crossers found along the Mexico-United States border. Nonetheless, it is pertinent to expand the research to other known body tissue samples to establish potential relationships of human hair to body tissues more frequently consulted in forensic anthropology.

Because Mexico is one of the highest bottled water consumers per capita in the world, the examination of Mexican bottled water could potentially yield indicators as to what degree the human body tissues are influenced by diet, bottled water, and tap water. Further, this research will serve as a basis for various machine learning regression approaches, which will include multivariate models, to determine regional Sr isoscapes for Mexico.

Summary of UBC Results

Overall, the interpretation of carbon, nitrogen, and sulfur isotopic values present difficulties due to the significant lack of reference data, especially for the collagen and carbonate values of human tissues, such as bones and teeth. The foremost issue with the available hair data is that the correlations of hair keratin to other skeletal tissues is understudied and while the existing studies give indication of the direction of the correlation, no conversion equations to "translate" keratin values to other body tissues could be established thus far. Similarly, some significant correlations were discovered in this study but due to the small sample size, no further conclusions could be drawn. It can be assumed that many variables play into the isotopic values of body tissues and before any conversions can be established, these variables need to be thoroughly studied. Thus far, many questions remain unanswered regarding the interpretation of the carbon, nitrogen, and sulfur isotope values obtained from UBCs.

For the assessment of potential regions of origin based on $\delta^{18}O$ tissue values, the developed tap water $\delta^{18}O$ isoscape was used because no reference database could be created based on human hair data. Furthermore, there were significant differences between the isotopic values recorded from the teeth analyzed at the Stable Isotope Ratio Facility for Environmental Research of the University of Utah and the values documented from the teeth analyzed at IsoForensics. Two cases,

recently identified by the Pima County Office of the Medical Examiner, were successfully used for region of origin predictions. Because the values used for these predictions were produced by Isoforensics, only the cases and the associated region of origin predictions with data from this laboratory were presented. The two recently identified case studies were discussed in detail.

As a proxy for the region of origin predictions of the $^{87}Sr/^{86}Sr$ ratios in the tissues of UBCs, the $^{87}Sr/^{86}Sr$ ratio of human hair were used. This isoscape was developed using a machine learning approach. Overall, the error of ±0.0002 is not small enough to clearly include or exclude potential regions of origins when the measured $^{87}Sr/^{86}Sr$ ratio is in the range of the most frequently observed ratios (~ 0.707) seen in Mexico. The mechanisms of mixed signatures are, thus far, understudied but are of utmost importance if $^{87}Sr/^{86}Sr$ ratios are to be used for interpretations beyond the scope that an individual moved from the former region of origin. Lastly, the $^{87}Sr/^{86}Sr$ ratios of the hair samples of UBCs are clearly elevated over the $^{87}Sr/^{86}Sr$ ratios documented for the other skeletal elements, demonstrating how human hair can easily be influenced by exogeneous sources of contamination.

Overall, the conceptual line, which aimed to collect essential isotopic baseline data, was somewhat more successful that the interpretive line, which aimed at a specific interpretation (and consequently the identification of region-of-origin) of the generated data. As elaborated on above, the regeneration of reference data in human hair was successful for carbon, nitrogen, sulfur, and strontium. Unfortunately, the oxygen reference data collection was not successful, at this point in time, but it is no question that the human hair samples from Mexico will be analyzed for their oxygen isotopic signatures again. Furthermore, the remaining human tissue samples will be used to create hydrogen isotopic reference data. In the initial proposal for this research, lead isotopic analyses were to be conducted on the reference hair samples. Unfortunately, due to methodological difficulties and time constraints, it was not possible to collect these data yet. The amount of work that would be going into these analyses would be another doctoral thesis.

While the region-of-origin assignment method used in this research has proven to be effective, it is pertinent to move towards using methods that take the prediction errors into account. This could, for example, be achieved using AssignR (Ma *et al.* 2020) or a similar approach. The isoscape used for the region-of-origin assignments was developed using the $^{87}Sr/^{86}Sr$ ratios of human hair and yielded very accurate predictions in bioavailable strontium in Mexico ($R^2 = 0.86$ and RMSE = 0.0007). This is especially remarkable considering this isoscape was built upon 101 human hair samples from 32 locations throughout Mexico. Nonetheless, the Sr isoscape will be further developed and an approach used that takes both the tap water and the human hair ratios

into consideration. Furthermore, to serve all countries from where undocumented border crossers are known to originate form, the isoscape will have to be spatially expanded to include Central and South America. Ideally, more human hair and tap water samples will be collected throughout these countries (in conjunction with gathering and employing existing data). Furthermore, to assist the wider research community and answer research questions outside of the scope of this work, the isoscape will be expanded to include the United States of America and Canada. Available data is currently gathered to achieve this goal and significantly expand and improve the currently existing Sr isoscapes of the Americas.

Furthermore, it is essential to establish a multi-isotope approach to further narrow down probable regions of origin. As could be seen in the maps depicting the probable regions of origin for the UBCs, the areas for both isotopes ($\delta^{18}O$ and $^{87}Sr/^{86}Sr$) are still too large to make significant predictions. When combining several isotope systems, such as oxygen and strontium (or any other), the potential arises to further exclude areas from the region of origin prediction maps, further narrowing down potential regions of origin.

It is very concerning that the two datasets received for the $\delta^{18}O$ values of human hair passed the quality control checks and could have confidently been wrongly used as a reference for Mexican hair. These issues show that all scientific analyses and isotopic values need to be analyzed and interpreted with extreme caution to avoid incorrect conclusions. As isotopic analyses in forensic sciences and especially on forensic human remains, which includes human hair, is still relatively new, it is unavoidable to further investigate this issue and draw conclusions as to where the samples preparation, analyses, and interpretation needs advancing. A strong need for international guidelines and standards is given.

Additionally, further research into the relationship of tap water and human tissues is needed. For instances, it is still unknown to which degree drinking water influences human hair versus bones and teeth. It is also pertinent to study how isotopic data may differ if the drinking water consumed is different than the local tap water. Generally, the factors that influence the deposited isotopic signatures in human tissues need to be studied in greater detail as, thus far, only indefinite ideas exist.

Additionally, there is a need to expand the research to other known body tissue samples to establish potential relationships of human hair to body tissues more frequently consulted in forensic anthropology, such as teeth and bones (particularly the ribs, femur/tibia, and first molar). It needs to be investigated how good of a proxy human hair is for the other human tissues commonly employed by forensic anthropologists and scientists working on human identification and region-of-origin assignments. Ideally, hair, bone, and tooth samples will be collected from

individuals and compared. While it would be ideal to always be able to compare values or ratios found in a body tissue to reference data of the same tissue, the current reference data on human tissues other than hair is very limited. In the future, with a combined sample collection effort, isoscapes based on other human tissues (such as teeth) could be developed. This could avoid any conversion errors (from one tissue to another) and would facilitate an easier interpretation of the data.

While most likely not of importance regarding the individuals who cross the border undocumented, it should be investigated how hair products, such as shampoo, conditioner and dye, influence the isotopic signatures of human hair.

- Does the length of the hair influence the usability to track human migration? Specifically, given the growth rate of hair versus the time required to travel from more southern regions of Mexico to the border, will the method be more useful for tracking women, who might keep their hair long, or men with a cropped hair style?
- While this study, as well as Kootker *et al.* (2020) and Gordon *et al.* (2019), showed that certain burial contexts can significantly influence the isotopic signatures of recovered individuals, it remains unknown to which degree these effects take place and what their mechanics are.
- How much does the so-called global supermarket diet influence the isotopic values and ratios of humans?
- This study has shown that socioeconomic factors correlate to isotopic values. However, the exact mechanisms remain unclear as no personal (including socioeconomic) information was gathered from the hair donors. Here, it will be pertinent to conduct large scale studies that not only collect hair samples but also data such as age, sex, occupation, salary etc.

Overall, this research has shown that stable isotope analysis can be an effective geolocation tool and that isotope analysis provides a record of movement and food consumption habits of individuals throughout life. Furthermore, it has highlighted the great potential of isotope analysis but also shown that the use of isotope analysis in forensic anthropology and forensic sciences is still in its baby shoes.

Nonetheless, this research has demonstrated that the approached used here can, in the future and upon further improvements, be used to aid the identification process of not only undocumented border crossers found along the United States-Mexico border, but also in other

cases of humanitarian crises. Millions of people are displaced each year and many have died along their routes to a better life. The humanitarian crisis in the Mediterranean Sea is likely one of the more publicized ones but there are also millions fleeing due to the dire situations in their home countries, including but not limited to the Democratic Republic of Congo, Nigeria, South Sudan, Venezuela, Central African Republic, Syria, Yemen, Afghanistan, the millions of Rohingya fleeing Myanmar, and the general emergency situation in Central America.

While the primary goal of this work was to introduce the reader to the humanitarian crisis along the southern border of the U.S. and show how isotope research can aid in the identification efforts of deceased undocumented border crossers, it is my hope that it will inspire other researchers to push the boundaries of isotope research to further aid the humanitarian catastrophes happening all over the world.

Bibliography

Åberg, Göran. 1995. "The Use of Natural Strontium Isotopes as Tracers in Environmental Studies." *Water, Air, & Soil Pollution* 79 (1–4): 309–22. https://doi.org/10.1007/BF01100444.

Acker, James G., and Gregory Leptoukh. 2007. "Online Analysis Enhances Use of NASA Earth Science Data." *Eos* 88 (2). https://doi.org/10.1029/2007EO020003.

Agarwal, Sabrina C., and Bonnie A. Glencross. 2011. "Building a Social Bioarchaeology." In *Social Bioarchaeology*, edited by Sabrina C. Agarwal and Bonnie A. Glencross. https://doi.org/10.1002/9781444390537.ch1.

Alkass, K., B. A. Buchholz, H. Druid, and K. L. Spalding. 2011. "Analysis of ^{14}C and ^{13}C in Teeth Provides Precise Birth Dating and Clues to Geographical Origin." *Forensic Science International* 209 (1–3): 34–41. https://doi.org/10.1016/j.forsciint.2010.12.002.

Alkerwi, Al A.A., Céderic Vernier, Nicolas Sauvageot, Georgina E. Crichton, and Merrill F. Elias. 2015. "Demographic and Socioeconomic Disparity in Nutrition: Application of a Novel Correlated Component Regression Approach." *BMJ Open* 5 (5): e006814. https://doi.org/10.1136/bmjopen-2014-006814.

Ambrose, Stanley H. 1993. "Investigations of Ancient Human Tissue: Chemical Analyses in Anthropology." *Investigations of Ancient Human Tissue: Chemical Analyses in Anthropology- Volume 10 in Food and Nutrition in History and Anthropology* 10: 59–130.

Ambrose, Stanley H., and Lynette Norr. 1993. "Experimental Evidence for the Relationship of the Carbon Isotope Ratios of Whole Diet and Dietary Protein to Those of Bone Collagen and Carbonate." In *Prehistoric Human Bone- Archaeology at the Molecular Level*, edited by Joseph B. Lambert and Gisela Grupe, 1–37. Springer Berlin Heidelberg. https://doi.org/10.1007/978-3-662-02894-0_1.

Ammer, Saskia. 2019. "IsoMAP Job 74865, Isoscapes Modeling, Analysis and Prediction (Version 1.0). The IsoMAP Project. Http://Isomap.Org."

Ammer, Saskia T.M., and Eric J. Bartelink. 2020. "Spatial Distributions of Isotope Ratios in Tap Water, Hair, and Teeth from Latin America for Region of Origin Predictions of Unidentified Border Crossers." Presented at the American Academy of Forensic Sciences 72nd Annual Scientific Meeting, Anaheim, United States.

Ammer, Saskia T.M., Eric J. Bartelink, Jennifer M. Vollner, Bruce E. Anderson, and Eugénia M. Cunha. 2020a. "Socioeconomic and Geographic Implications from Carbon, Nitrogen and Sulfur Isotope Ratios in Human Hair from Mexico." *Forensic Science International*.

Ammer, Saskia. 2020b. "Spatial Distributions of Oxygen Stable Isotope Ratios in Tap Water From Mexico for Region of Origin Predictions of Unidentified Border Crossers." *Journal of Forensic Sciences*. https://doi.org/10.1111/1556-4029.14283.

Ammer, Saskia. 2020c. "Carbon, Nitrogen and Sulfur Isotopic Values of Human Hair from Mexico." figshare. https://doi.org/10.6084/m9.figshare.12401507.v1.

Ammer, Saskia T.M., Lisette M. Kootker, Eric J. Bartelink, Bruce E. Anderson, Eugénia Cunha, and Gareth R. Davies. 2020. "Comparison of Strontium Isotope Ratios in Mexican Human Hair and Tap Water as Provenance Indicators." *Forensic Science International* 314. https://doi.org/10.1016/j.forsciint.2020.110422.

Anderson, Bruce E. 2008. "Identifying the Dead: Methods Utilized by the Pima County (Arizona) Office of the Medical Examiner for Undocumented Border Crossers: 2001-2006." *Journal of Forensic Sciences* 53 (1): 8–15. https://doi.org/10.1111/j.1556-4029.2007.00609.x.

Anderson, Bruce E., and Bruce O. Parks. 2008. "Symposium on Border Crossing Deaths: Introduction." *Journal of Forensic Sciences* 53 (1): 6–7. https://doi.org/10.1111/j.1556-4029.2007.00608.x.

Anderson, Bruce E., and M. Kate Spradley. 2016. "The Role of the Anthropologist in the Identification of Migrant Remains in the American Southwest." *Academic Forensic*

Pathology 6 (3): 432–38. https://doi.org/10.23907/2016.044.

Bao, Huiming, Xiaobin Cao, and Justin A. Hayles. 2016. "Triple Oxygen Isotopes: Fundamental Relationships and Applications." *Annual Review of Earth and Planetary Sciences* 44 (1): 463–92. https://doi.org/10.1146/annurev-earth-060115-012340.

Bartelink, Eric J. 2020. "Stable Isotopes." In *Oxford Bibliography*. https://www.oxfordbibliographies.com/view/document/obo-9780199766567/obo-9780199766567-0153.xml.

Bartelink, Eric, Rachel Berry, and Lesley Chesson. 2014a. "Stable Isotopes and Human Provenancing." In *Advances in Forensic Human Identification*, edited by Xanthe Mallett, Teri Blythe, and Rachel Berry, 165–92. CRC Press. https://doi.org/10.1201/b16509.

Bartelink, Eric, Rachel Berry, and Lesley Chesson. 2014b. "Stable Isotopes and Human Provenancing." In *Advances in Forensic Human Identification*, 165–92. Taylor and Francis. https://doi.org/10.1201/b16509.

Bartelink, Eric J., Gregory E. Berg, Lesley A. Chesson, Brett J. Tipple, Melanie M. Beasley, Julia R. Prince-Buitenhuys, Heather MacInnes, Amy T. MacKinnon, and Krista E. Latham. 2018. "Applications of Stable Isotope Forensics for Geolocating Unidentified Human Remains From Past Conflict Situations and Large-Scale Humanitarian Efforts." In *New Perspectives in Forensic Human Skeletal Identification*, edited by Krista E. Latham, Eric J. Bartelink, and Michael Finnegan, 175–84. Academic Press. https://doi.org/10.1016/b978-0-12-805429-1.00015-6.

Bartelink, Eric J., and Lesley A. Chesson. 2019. "Recent Applications of Isotope Analysis to Forensic Anthropology." *Forensic Sciences Research* 4 (1): 29–44. https://doi.org/10.1080/20961790.2018.1549527.

Bartelink, Eric J., Amy T. Mackinnon, Julia R. Prince-Buitenhuys, Brett J. Tipple, and Lesley A. Chesson. 2016. "Stable Isotope Forensics as an Investigative Tool in Missing Persons Investigations." In *Handbook of Missing Persons*, edited by Stephen Morewitz and Caroline Sturdy Colls, 443–62. Springer International Publishing. https://doi.org/10.1007/978-3-319-40199-7_29.

Barton, Kate E., David G. Howell, and José F. Vigil. 2003. "The North American Tapestry of Time and Terrain." *U.S. Geological Survey, Geological Investigations Series I-2781*.

Bataille, Clément P., and Gabriel J. Bowen. 2012. "Mapping 87Sr/ 86Sr Variations in Bedrock and Water for Large Scale Provenance Studies." *Chemical Geology* 304–305: 39–52. https://doi.org/10.1016/j.chemgeo.2012.01.028.

Bataille, Clement P., Michelle M.G. Chartrand, Francis Raposo, and Gilles St-Jean. 2020. "Assessing Geographic Controls of Hair Isotopic Variability in Human Populations: A Case-Study in Canada." *PLoS ONE* 15 (8): e0237105. https://doi.org/10.1371/journal.pone.0237105.

Bataille, Clement P., Isabella C.C. von Holstein, Jason E. Laffoon, Malte Willmes, Xiao Ming Liu, and Gareth R. Davies. 2018. "A Bioavailable Strontium Isoscape for Western Europe: A Machine Learning Approach." *PLoS ONE* 13 (5): e0197386. https://doi.org/10.1371/journal.pone.0197386.

Bataille, Clement P., Jason Laffoon, and Gabriel J. Bowen. 2012. "Mapping Multiple Source Effects on the Strontium Isotopic Signatures of Ecosystems from the Circum-Caribbean Region." *Ecosphere* 3 (12): 1–24. https://doi.org/10.1890/es12-00155.1.

Beard, Brian L., and Clark M. Johnson. 2000. "Strontium Isotope Composition of Skeletal Material Can Determine the Birth Place and Geographic Mobility of Humans and Animals." *Journal of Forensic Sciences* 45 (5): 14829J. https://doi.org/10.1520/jfs14829j.

Bender, Richard L., Darna L. Dufour, Luciano O. Valenzuela, Thure E. Cerling, Matt Sponheimer, Julio C. Reina, and James R. Ehleringer. 2015. "Stable Isotopes (Carbon, Nitrogen, Sulfur), Diet, and Anthropometry in Urban Colombian Women: Investigating Socioeconomic Differences." *American Journal of Human Biology* 27 (2): 207–18.

https://doi.org/10.1002/ajhb.22640.
Benson, Sarah, Chris Lennard, Philip Maynard, and Claude Roux. 2006. “Forensic Applications of Isotope Ratio Mass Spectrometry - A Review.” *Forensic Science International* 157 (1): 1–22. https://doi.org/10.1016/j.forsciint.2005.03.012.
Bentley, R. A., and C. Knipper. 2005. “Geographical Patterns in Biologically Available Strontium, Carbon and Oxygen Isotope Signatures in Prehistoric SW Germany.” *Archaeometry* 47 (3): 629–44. https://doi.org/10.1111/j.1475-4754.2005.00223.x.
Bentley, R. Alexander. 2006. “Strontium Isotopes from the Earth to the Archaeological Skeleton: A Review.” *Journal of Archaeological Method and Theory* 13 (3): 135–87. https://doi.org/10.1007/s10816-006-9009-x.
Bentley, R. Alexander, T. Douglas Price, and Elisabeth Stephan. 2004. “Determining the ‘local’ $^{87}Sr/^{86}Sr$ Range for Archaeological Skeletons: A Case Study from Neolithic Europe.” *Journal of Archaeological Science* 31 (4): 365–75. https://doi.org/10.1016/j.jas.2003.09.003.
Bertrab, Étienne von. 2003. “Guadalajara’s Water Crisis and the Fate of Lake Chapala: A Reflection of Poor Water Management in Mexico.” *Environment and Urbanization* 15 (2): 127–40. https://doi.org/10.1630/095624703101286781.
Bethard, Jonathan D., and Elizabeth A. DiGangi. 2020. “Letter to the Editor—Moving Beyond a Lost Cause: Forensic Anthropology and Ancestry Estimates in the United States.” *Journal of Forensic Sciences*. https://doi.org/10.1111/1556-4029.14513.
Bocherens, Hervé, Caroline Polet, and Michel Toussaint. 2007. “Palaeodiet of Mesolithic and Neolithic Populations of Meuse Basin (Belgium): Evidence from Stable Isotopes.” *Journal of Archaeological Science* 34 (1): 10–27. https://doi.org/10.1016/j.jas.2006.03.009.
Bol, Roland, Jen Marsh, and Tim H.E. Heaton. 2007. “Multiple Stable Isotope (^{18}O, ^{13}C, ^{15}N and ^{34}S) Analysis of Human Hair to Identify the Recent Migrants in a Rural Community in SW England.” *Rapid Communications in Mass Spectrometry* 21 (18): 2951–54. https://doi.org/10.1002/rcm.3168.
Bösl, C., G. Grupe, and J. Peters. 2006. “A Late Neolithic Vertebrate Food Web Based on Stable Isotope Analyses.” *International Journal of Osteoarchaeology* 14 (4): 296–315. https://doi.org/10.1002/oa.834.
Bowen G. J., J.B. West, C.C. Miller, L. Zhao, and T. Zhang. 2019. “IsoMAP: Isoscapes Modeling, Analysis and Prediction (Version 1.0). The IsoMAP Project. Http://Isomap.Org.”
Bowen, Gabriel J. 2010a. “Isoscapes: Spatial Pattern in Isotopic Biogeochemistry.” *Annual Review of Earth and Planetary Sciences* 38 (1): 161–87. https://doi.org/10.1146/annurev-earth-040809-152429.
Bowen, Gabriel J. 2010b. “Statistical and Geostatistical Mapping of Precipitation Water Isotope Ratios.” In *Isoscapes: Understanding Movement, Pattern, and Process on Earth through Isotope Mapping*. https://doi.org/10.1007/978-90-481-3354-3_7.
Bowen, Gabriel J., James R. Ehleringer, Lesley A. Chesson, Erik Stange, and Thure E. Cerling. 2007. “Stable Isotope Ratios of Tap Water in the Contiguous United States.” *Water Resources Research* 43 (3): 1–12. https://doi.org/10.1029/2006WR005186.
Bowen, Gabriel J., James R. Ehleringer, Lesley A. Chesson, Alexandra H. Thompson, David W. Podlesak, and Thure E. Cerling. 2009. “Dietary and Physiological Controls on the Hydrogen and Oxygen Isotope Ratios of Hair from Mid-20th Century Indigenous Populations.” *American Journal of Physical Anthropology* 139 (4): 494–504. https://doi.org/10.1002/ajpa.21008.
Bowen, Gabriel J., David A. Winter, Howard J. Spero, Robert A. Zierenberg, Mathew D. Reeder, Thure E. Cerling, and James R. Ehleringer. 2005. “Stable Hydrogen and Oxygen Isotope Ratios of Bottled Waters of the World.” *Rapid Communications in Mass Spectrometry* 19 (23): 3442–50. https://doi.org/10.1002/rcm.2216.
Brettell, Rhea, Janet Montgomery, and Jane Evans. 2012. “Brewing and Stewing: The Effect of Culturally Mediated Behaviour on the Oxygen Isotope Composition of Ingested Fluids and

the Implications for Human Provenance Studies." *Journal of Analytical Atomic Spectrometry* 27 (5): 778–85. https://doi.org/10.1039/c2ja10335d.

Capo, Rosemary C., Brian W. Stewart, and Oliver A. Chadwick. 1998. "Strontium Isotopes as Tracers of Ecosystem Processes: Theory and Methods." *Geoderma* 82 (1–3): 197–225. https://doi.org/10.1016/S0016-7061(97)00102-X.

Cartigny, Pierre, and Vincent Busigny. 2018. "Nitrogen Isotopes." In *Encyclopedia of Geochemistry: A Comprehensive Reference Source on the Chemistry of the Earth*, edited by William M White, 991–1003. Cham: Springer International Publishing. https://doi.org/10.1007/978-3-319-39312-4_197.

Cate, J. M. ten, and J. D.B. Featherstone. 1991. "Mechanistic Aspects of the Interactions between Fluoride and Dental Enamel." *Critical Reviews in Oral Biology and Medicine* 2 (2): 283–296. https://doi.org/10.1177/10454411910020030101.

Chant, Tim De. 2012. "Stable Isotopes in Forensics." *Public Broadcasting Service- NOVA*, October 18, 2012. http://www.pbs.org/wgbh/nova/tech/stable-isotopes.html.

Chau, Thuan H., Brett J. Tipple, Lihai Hu, Diego P. Fernandez, Thure E. Cerling, James R. Ehleringer, and Lesley A. Chesson. 2017. "Reconstruction of Travel History Using Coupled $\delta^{18}O$ and $^{87}Sr/^{86}Sr$ Measurements of Hair." *Rapid Communications in Mass Spectrometry* 31 (6): 583–89. https://doi.org/10.1002/rcm.7822.

Chesson, L. A., M. W. Kenyhercz, L. A. Regan, and G. E. Berg. 2019. "Addressing Data Comparability in the Creation of Combined Data Sets of Bioapatite Carbon and Oxygen Isotopic Compositions." *Archaeometry* 61 (5): 1193–1206. https://doi.org/10.1111/arcm.12480.

Chesson, Lesley A, Brett J Tipple, Lane V Youmans, Michael A O'Brien, and Michael M Harmon. 2018a. "Forensic Identification of Human Skeletal Remains Using Isotopes: A Brief History of Applications from Archaeological Dig Sites to Modern Crime Scenes." In *New Perspectives in Forensic Human Skeletal Identification*, edited by Krista E. Latham, Eric J. Bartelink, and Michael Finnegan, 157–73. Academic Press. https://doi.org/10.1016/B978-0-12-805429-1.00014-4.

Chesson, Lesley A., Brett J. Tipple, James R. Ehleringer, Todd Park, and Eric J. Bartelink. 2018b. "Forensic Applications of Isotope Landscapes ('isoscapes'): A Tool for Predicting Region-of-Origin in Forensic Anthropology Cases." In *Forensic Anthropology: Theoretical Framework and Scientific Basis*, edited by Clifford C. Boyd and Donna C. Boyd, 127–48. John Wiley & Sons Ltd. https://doi.org/10.1002/9781119226529.ch8.

Chesson, Lesley, Brett Tipple, Lane Youmans, Michael O'Brien, and Michael Harmon. 2018c. *Forensic Identification of Human Skeletal Remains Using Isotopes. New Perspectives in Forensic Human Skeletal Identification*. Elsevier Inc. https://doi.org/10.1016/b978-0-12-805429-1.00014-4.

Chesson, L. A., B. J. Tipple, J. D. Howa, G. J. Bowen, J. E. Barnette, T. E. Cerling, and J. R. Ehleringer. 2013. "Stable Isotopes in Forensics Applications." In *Treatise on Geochemistry: Second Edition*, 285–317. https://doi.org/10.1016/B978-0-08-095975-7.01224-9.

Chesson, Lesley A., Brett J. Tipple, Glen N. Mackey, Scott A. Hynek, Diego P. Fernandez, and James R. Ehleringer. 2012. "Strontium Isotopes in Tap Water from the Coterminous USA." *Ecosphere* 3 (7): art67. https://doi.org/10.1890/es12-00122.1.

Chesson, Lesley A., Luciano O. Valenzuela, Shannon P. OGrady, Thure E. Cerling, and James R. Ehleringer. 2010. "Links between Purchase Location and Stable Isotope Ratios of Bottled Water, Soda, and Beer in the United States." *Journal of Agricultural and Food Chemistry* 58 (12): 7311–16. https://doi.org/10.1021/jf1003539.

Colibrí Center for Human Rights. 2018. "Press Kit." https://www.colibricenter.org/press-kit-pdf-download/.

Chisholm, Brian S., D. Erle Nelson, and Henry P. Schwarcz. 1982. "Stable-Carbon Isotope Ratios as a Measure of Marine versus Terrestrial Protein in Ancient Diets." *Science* 216 (4550):

1131–32. https://doi.org/10.1126/science.216.4550.1131.
Consejo Nacional de Evaluación de la Política de Desarrollo Social. 2018. “Medición de La Pobreza- Estados Unidos Mexicanos- Serie 2008.” 2018. https://www.coneval.org.mx/Medicion/MP/Paginas/AE_pobreza_2018.aspx.
Contreras, Delia Montero. 2019. *Instituciones y Actores. Un Enfoque Alternativo Para Entender El Consumo de Agua Embotellada En México*. Universidad Autónoma Metropolitana, Unidad Iztapalapa, Consejo Editorial de Ciencias Sociales y Humanidades.
Coplen, Tyler B. 1988. “Normalization of Oxygen and Hydrogen Isotope Data.” *Chemical Geology: Isotope Geoscience Section* 72 (4): 293–97. https://doi.org/10.1016/0168-9622(88)90042-5.
Cortés, Alejandra, Jaime Durazo, and Robert N. Farvolden. 1997. “Studies of Isotopic Hydrology of the Basin of Mexico and Vicinity: Annotated Bibliography and Interpretation.” *Journal of Hydrology* 198 (1–4): 346–76. https://doi.org/10.1016/S0022-1694(96)03273-8.
Craig, Harmon. 1953. “The Geochemistry of the Stable Carbon Isotopes.” *Geochimica et Cosmochimica Acta* 3 (2–3): 53–92. https://doi.org/10.1016/0016-7037(53)90001-5.
Craig, Harmon. 1961. “Isotopic Variations in Meteoric Waters.” *Science* 133 (3465): 1702–3. https://doi.org/10.1126/science.133.3465.1702.
Cunha, Eugénia, and Douglas H. Ubelaker. 2020. “Evaluation of Ancestry from Human Skeletal Remains: A Concise Review.” *Forensic Sciences Research*. https://doi.org/10.1080/20961790.2019.1697060.
Cunningham, Craig, Louise Scheuer, and Sue Black. 2016. *Developmental Juvenile Osteology*. *Developmental Juvenile Osteology*. 2nd ed. Elsevier Inc.
Daniel Bryant, J., and Philip N. Froelich. 1995. “A Model of Oxygen Isotope Fractionation in Body Water of Large Mammals.” *Geochimica et Cosmochimica Acta* 59 (21): 4523–37. https://doi.org/10.1016/0016-7037(95)00250-4.
Dansgaard, W. 1964. “Stable Isotopes in Precipitation.” *Tellus* 16 (4): 436–68. https://doi.org/10.3402/tellusa.v16i4.8993.
Daux, Valérie, Christophe Lécuyer, Marie Anne Héran, Romain Amiot, Laurent Simon, François Fourel, François Martineau, Niels Lynnerup, Hervé Reychler, and Gilles Escarguel. 2008. “Oxygen Isotope Fractionation between Human Phosphate and Water Revisited.” *Journal of Human Evolution* 55 (6): 1138–47. https://doi.org/10.1016/j.jhevol.2008.06.006.
Deniro, Michael J., and Samuel Epstein. 1981. “Influence of Diet on the Distribution of Nitrogen Isotopes in Animals.” *Geochimica et Cosmochimica Acta* 45 (3): 341–51. https://doi.org/10.1016/0016-7037(81)90244-1.
Dhaliwal, Kirandeep, Carolyn Rando, Hazel Reade, Anne Lise Jourdan, and Rhiannon E. Stevens. 2020. “Socioeconomic Differences in Diet: An Isotopic Examination of Post-Medieval Chichester, West Sussex.” *American Journal of Physical Anthropology* 171 (4): 584–97. https://doi.org/10.1002/ajpa.23984.
Dirkmaat, Dennis C., and Luis L. Cabo. 2012. “Forensic Anthropology: Embracing the New Paradigm.” In *A Companion to Forensic Anthropology*. John Wiley & Sons, Inc. https://doi.org/10.1002/9781118255377.ch1.
Dirkmaat, Dennis C., Luis L. Cabo, Stephen D. Ousley, and Steven A. Symes. 2008. “New Perspectives in Forensic Anthropology.” *American Journal of Physical Anthropology* 137 (S47): 33–52. https://doi.org/10.1002/ajpa.20948.
Drucker, Dorothee, and H. Bocherens. 2004. “Carbon and Nitrogen Stable Istopes as Tracers of Change in Diet Breadth during Middle and Upper Palaeolithic in Europe.” *International Journal of Osteoarchaeology* 14 (3–4): 162–77. https://doi.org/10.1002/oa.753.
Dunn, PJH, and JF Carter. 2018. *Good Practice Guide for Isotope Ratio Mass Spectrometry*. 2nd ed. The FIRMS Network. https://doi.org/10.1016/j.forc.2018.10.005.
Ehleringer, James R., Gabriel J. Bowen, Lesley A. Chesson, Adam G. West, David W. Podlesak, and Thure E. Cerling. 2008. “Hydrogen and Oxygen Isotope Ratios in Human Hair Are

Related to Geography." *Proceedings of the National Academy of Sciences of the United States of America* 105 (8): 2788–93. https://doi.org/10.1073/pnas.0712228105.
Ehleringer, James R., Alexandra H. Thompson, David W. Podlesak, Gabriel J. Bowen, Lesley A. Chesson, Thure E. Cerling, Todd Park, Paul Dostie, and Henry Schwarcz. 2010. "A Framework for the Incorporation of Isotopes and Isoscapes in Geospatial Forensic Investigations." In *Isoscapes: Understanding Movement, Pattern, and Process on Earth through Isotope Mapping*, 357–87. https://doi.org/10.1007/978-90-481-3354-3_17.
Emsley, John. 2011. *Nature's Building Blocks: An A-Z Guide to the Elements*. *Oxford University Press*. https://doi.org/978-0-19-960563-7.
Environmental Systems Research Institute (ESRI). 2018. "ArcGIS Desktop Release 10.6.1." Redlands, CA.
Ezzo, Joseph A., Clark M. Johnson, and T. Douglas Price. 1997. "Analytical Perspectives on Prehistoric Migration: A Case Study from East-Central Arizona." *Journal of Archaeological Science* 24 (5): 447–66. https://doi.org/10.1006/jasc.1996.0129.
Farquhar, James. 2018. "Sulfur Isotopes." In *Encyclopedia of Geochemistry: A Comprehensive Reference Source on the Chemistry of the Earth*, edited by William M White, 1402–9. Cham: Springer International Publishing. https://doi.org/10.1007/978-3-319-39312-4_74.
Faure, Gunter. 1986. *Principles of Isotope Geology*. *John Wiley and Sons*. Second. John Wiley & Sons, Inc.
Faure, Gunter, and James Powell. 1972. *Strontium Isotope Geology*. *Strontium Isotope Geology*. Springer Berlin Heidelberg. https://doi.org/10.1007/978-3-642-65367-4.
Fava, Marcelo, Ii-Sei Watanabe, Flavio Fava-de-Moraes, and Luciane Costa. 1997. "Prismless Enamel in Human Non-Erupted Deciduous Molar Teeth: A Scanning Electron Microscopic Study." *Revista de Odontologia Da Universidade de São Paulo* 11 (4): 239–43. https://doi.org/10.1590/s0103-06631997000400003.
Federal Bureau of Investigation. 2020a. "Combined DNA Index System (CODIS)." 2020. https://www.fbi.gov/services/laboratory/biometric-analysis/codis.
Federal Bureau of Investigation. 2020b. "Frequently Asked Questions on CODIS and NDIS." 2020. https://www.fbi.gov/services/laboratory/biometric-analysis/codis/codis-and-ndis-fact-sheet.
Fejerskov, O., Kaj Josephsen, and Bente Nyvad. 1984. "Surface Ultrastructure of Unerupted Mature Human Enamel." *Caries Research* 18 (4): 302–14. https://doi.org/10.1159/000260781.
Fick, Stephen E., and Robert J. Hijmans. 2017. "WorldClim 2: New 1-Km Spatial Resolution Climate Surfaces for Global Land Areas." *International Journal of Climatology* 37 (12): 4302–15. https://doi.org/10.1002/joc.5086.
Font, Laura, Gerard Van Der Peijl, Carina Van Leuwen, Isis Van Wetten, and Gareth R. Davies. 2015. "Identification of the Geographical Place of Origin of an Unidentified Individual by Multi-Isotope Analysis." *Science and Justice* 55 (1): 34–42. https://doi.org/10.1016/j.scijus.2014.06.011.
Font, Laura, Gerard Van Der Peijl, Isis Van Wetten, Pieter Vroon, Bas Van Der Wagt, and Gareth Davies. 2012. "Strontium and Lead Isotope Ratios in Human Hair: Investigating a Potential Tool for Determining Recent Human Geographical Movements." *Journal of Analytical Atomic Spectrometry* 27 (5): 719–32. https://doi.org/10.1039/c2ja10361c.
Food and Agriculture Organization of the United Nations. 2017. "MEAT FOOD SUPPLY QUANTITY (KG/CAPITA/YR)."
Fraser, I., W. Meier-Augenstein, and R. M. Kalin. 2006. "The Role of Stable Isotopes in Human Identification: A Longitudinal Study into the Variability of Isotopic Signals in Human Hair and Nails." *Rapid Communications in Mass Spectrometry* 20 (7): 1109–16. https://doi.org/10.1002/rcm.2424.
Frei, Karin M., and Robert Frei. 2011. "The Geographic Distribution of Strontium Isotopes in

Danish Surface Waters - A Base for Provenance Studies in Archaeology, Hydrology and Agriculture." *Applied Geochemistry* 26 (3): 326–40. https://doi.org/10.1016/j.apgeochem.2010.12.006.

Freire, German Nicolas, Steven Daniel Schwartz Orellana, Melissa Zumaeta Aurazo, Damasceno Costa Costa, Jonna Maria Lundvall, Martha Celmira Viveros Mendoza, Leonardo Ramiro Lucchetti, Laura Moreno, and Liliana Do Couto Sousa. 2015. "Indigenous Latin America in the Twenty-First Century : The First Decade (English)." Washington, D.C.: World Bank Group. http://documents.worldbank.org/curated/en/145891467991974540/Indigenous-Latin-America-in-the-twenty-first-century-the-first-decade.

Freiwald, C. 2011. "Maya Migration Networks: Reconstructing Population Movement in the Belize River Valley during the Late and Terminal Classic." University of Wisconsin-Madison.

Frost, H. M. 1990. "Skeletal Structural Adaptations to Mechanical Usage (SATMU): 1. Redefining Wolff's Law: The Bone Modeling Problem." *The Anatomical Record* 226 (4): 403–13. https://doi.org/10.1002/ar.1092260402.

Frost, Harold M. 1999. "On the Estrogen-Bone Relationship and Postmenopausal Bone Loss: A New Model." *Journal of Bone and Mineral Research* 14 (9): 1473–77. https://doi.org/10.1359/jbmr.1999.14.9.1473.

Fry, Brian. 2008. *Stable Isotope Ecology*. *Stable Isotope Ecology*. Springer New York. https://doi.org/10.1007-0-387-33745-8.

Fuller, Benjamin T., James L. Fuller, Nancy E. Sage, David A. Harris, Tamsin C. O'Connell, and Robert E.M. Hedges. 2004. "Nitrogen Balance and δ^{15}N: Why You're Not What You Eat during Pregnancy." *Rapid Communications in Mass Spectrometry* 18 (23): 2889–96. https://doi.org/10.1002/rcm.1708.

Geldern, Robert Van, and Johannes A.C. Barth. 2012. "Optimization of Instrument Setup and Post-Run Corrections for Oxygen and Hydrogen Stable Isotope Measurements of Water by Isotope Ratio Infrared Spectroscopy (IRIS)." *Limnology and Oceanography: Methods* 10 (December): 1024–36. https://doi.org/10.4319/lom.2012.10.1024.

Giacaman, R. A., V. A. Perez, and C. A. Carrera. 2016. "Mineralization Processes in Hard Tissues: Teeth." In *Biomineralization and Biomaterials: Fundamentals and Applications*, 147–85. https://doi.org/10.1016/B978-1-78242-338-6.00006-5.

Rubio-Goldsmith, Raquel, Melissa McCormick, Daniel Martinez, and Inez Duarte. 2018. "The 'Funnel Effect' & Recovered Bodies of Unauthorized Migrants Processed by the Pima County Office of the Medical Examiner, 1990-2005." *SSRN Electronic Journal*. https://doi.org/10.2139/ssrn.3040107.

Good, Stephen P., Derek V. Mallia, John C. Lin, and Gabriel J. Bowen. 2014. "Stable Isotope Analysis of Precipitation Samples Obtained via Crowdsourcing Reveals the Spatiotemporal Evolution of Superstorm Sandy." *PLoS ONE* 9 (3). https://doi.org/10.1371/journal.pone.0091117.

Gordon, Gwyneth, Tiffany Saul, Dawnie Steadman, Kelly Knudson, Ariel D. Anbar, and Daniel Wescott. 2019. "Isotopic Taphonomy of Human Remains." https://www.ncjrs.gov/pdffiles1/nij/grants/252506.pdf.

Gordon, Gwyneth W., Tiffany B. Saul, Dawnie Steadman, Daniel J. Wescott, and Kelly Knudson. 2018. "Preservation of Hair Stable Isotope Signatures during Freezing and Law Enforcement Evidence Packaging." *Forensic Chemistry* 11: 108–19. https://doi.org/10.1016/j.forc.2018.10.004.

Gupta, Priya, David Noone, Joseph Galewsky, Colm Sweeney, and Bruce H. Vaughn. 2009. "Demonstration of High-Precision Continuous Measurements of Water Vapor Isotopologues in Laboratory and Remote Field Deployments Using Wavelength-Scanned Cavity Ring-down Spectroscopy (WS-CRDS) Technology." *Rapid Communications in Mass Spectrometry* 23 (16): 2534–42. https://doi.org/10.1002/rcm.4100.

Gwinnett, A. J. 1992. “Structure and Composition of Enamel.” *Operative Dentistry*.
He, Li Hong, and Michael V. Swain. 2007. “Enamel-A ‘Metallic-like’ Deformable Biocomposite.” *Journal of Dentistry* 35 (5): 431–37. https://doi.org/10.1016/j.jdent.2006.12.002.
Hedges, Joshua, Rhiannon Elisabeth Stevens, and Paul Koch. 2006. “Isotopes in Bones and Teeth.” In *Isotopes in Palaeoenvironmental Research*, edited by Melanie J. Leng, 10th ed., 117–45. Springer Netherlands. https://doi.org/10.1007/1-4020-2504-1_03.
Hedges, R. E.M. 2002. “Bone Diagenesis: An Overview of Processes.” *Archaeometry* 44 (3): 319–28. https://doi.org/10.1111/1475-4754.00064.
Hedges, Robert E.M. 2003. “On Bone Collagen - Apatite-Carbonate Isotopic Relationships.” *International Journal of Osteoarchaeology* 13 (1–2): 66–79. https://doi.org/10.1002/oa.660.
Hedges, Robert E.M., John G. Clement, C. David L. Thomas, and Tamsin C. O’Connell. 2007. “Collagen Turnover in the Adult Femoral Mid-Shaft: Modeled from Anthropogenic Radiocarbon Tracer Measurements.” *American Journal of Physical Anthropology* 133 (2): 808–16. https://doi.org/10.1002/ajpa.20598.
Hill, P. A., and M. Orth. 1998. “Bone Remodelling.” *British Journal of Orthodontics* 25: 101–7. https://doi.org/10.1093/ortho/25.2.101.
Hillson, Simon. 1996. *Dental Anthropology*. *Dental Anthropology*. Cambridge University Press. https://doi.org/10.1017/cbo9781139170697.
Hillson, Simon. 2013. *Tooth Development in Human Evolution and Bioarchaeology*. *Tooth Development in Human Evolution and Bioarchaeology*. https://doi.org/10.1017/CBO9780511894916.
Hodell, David A., Rhonda L. Quinn, Mark Brenner, and George Kamenov. 2004. “Spatial Variation of Strontium Isotopes ($^{87}Sr/^{86}Sr$ in the Maya Region: A Tool for Tracking Ancient Human Migration.” *Journal of Archaeological Science* 31 (5): 585–601. https://doi.org/10.1016/j.jas.2003.10.009.
Hoefs, Jochen. 2015. *Stable Isotope Geochemistry: Seventh Edition*. *Stable Isotope Geochemistry: Sixth Edition*. Springer Science & Business Media. https://doi.org/10.1007/978-3-540-70708-0.
Hogan, J. F., J. D. Blum, D. I. Siegel, and P. H. Glaser. 2000. “$^{87}Sr/^{86}Sr$ as a Tracer of Groundwater Discharge and Precipitation Recharge in the Glacial Lake Agassiz Peatlands, Northern Minnesota.” *Water Resources Research* 36 (12): 3701–10. https://doi.org/10.1029/2000WR900233.
Hueb De Menezes Oliveira, Maria Angélica, Carolina Paes Torres, Jaciara Miranda Gomes-Silva, Michelle Alexandra Chinelatti, Fernando Carlos Hueb De Menezes, Regina Guenka Palma-Dibb, and Maria Cristina Borsatto. 2010. “Microstructure and Mineral Composition of Dental Enamel of Permanent and Deciduous Teeth.” *Microscopy Research and Technique* 73 (5): 572–77. https://doi.org/10.1002/jemt.20796.
Huelsemann, Frank, Ulrich Flenker, Karsten Koehler, and Wilhelm Schaenzer. 2009. “Effect of a Controlled Dietary Change on Carbon and Nitrogen Stable Isotope Ratios of Human Hair.” *Rapid Communications in Mass Spectrometry* 23 (16): 2448–54. https://doi.org/10.1002/rcm.4039.
Huelsemann, Frank, Christine Lehn, Sabine Schneider, Glen Jackson, Sarah Hill, Andreas Rossmann, Nicole Scheid, Philip J.H. Dunn, Ulrich Flenker, and Wilhelm Schänzer. 2015. “Global Spatial Distributions of Nitrogen and Carbon Stable Isotope Ratios of Modern Human Hair.” *Rapid Communications in Mass Spectrometry* 29 (22): 2111–21. https://doi.org/10.1002/rcm.7370.
Hughes, Cris E., Bridget F.B. Algee-Hewitt, Robin Reineke, Elizabeth Clausing, and Bruce E. Anderson. 2017. “Temporal Patterns of Mexican Migrant Genetic Ancestry: Implications for Identification.” *American Anthropologist* 119 (2): 193–208. https://doi.org/10.1111/aman.12845.

Humane Borders Inc. 2020. “Arizona Open GIS Initiative for Deceased Migrants.” 2020.
Iacumin, P., H. Bocherens, A. Mariotti, and A. Longinelli. 1996. “Oxygen Isotope Analyses of Co-Existing Carbonate and Phosphate in Biogenic Apatite: A Way to Monitor Diagenetic Alteration of Bone Phosphate?” *Earth and Planetary Science Letters* 142 (1–2): 1–6. https://doi.org/10.1016/0012-821x(96)00093-3.
Illingworth, S. 2015. “Identifying the Bodies of Border Crossers.” *The Huffington Post*, August 4, 2015. http://www.huffingtonpost.com/sarah-illingworth/identifying-the-bodies -of-border-crossers_b_7023596.html.
Instituto Nacional de Estadística y Geografía. 2010. “Censo de Población y Vivienda 2010.” 2010. https://www.inegi.org.mx/programas/ccpv/2010/.
Instituto Nacional de Estadística y Geografía.2015a. “Encuesta Intercensal 2015.” 2015. https://www.inegi.org.mx/programas/intercensal/2015/.
Instituto Nacional de Estadística y Geografía.2015b. “Panorama Sociodemográfico de Mexico.” http://seieg.iplaneg.net/seieg/doc/Panorama_Sociodemografico_2015_1452886126.pdf.
Instituto Nacional de Estadística y Geografía. 2018. “Mortalidad.” 2018. https://www.inegi.org.mx/programas/mortalidad/default.html#Tabulados.
Inter-American Development Bank. 2011. “Latin America’s Other Water Infrastructure.” http://idbdocs.iadb.org/wsdocs/getdocument.aspx?docnum=36984584.
Inter-American Development Bank. 2013. “Increased Water and Sanitation Coverage for Mexico.” https://www.iadb.org/en/news/news-releases/2013-12-18/increased-water-and-sanitation-coverage-for-mexico%2C10708.html.
International Atomic Energy Agency World Meteorological Organization. 2018. “Global Network of Isotopes in Precipitation- The GNIP Database.” http://www.iaea.org/water.
Kamenov, George D., and Jason H. Curtis. 2017. “Using Carbon, Oxygen, Strontium, and Lead Isotopes in Modern Human Teeth for Forensic Investigations: A Critical Overview Based on Data from Bulgaria.” *Journal of Forensic Sciences* 62 (6): 1452–59. https://doi.org/10.1111/1556-4029.13462.
Kamenov, George D., Erin H. Kimmerle, Jason H. Curtis, and Darren Norris. 2014. “Georeferencing a Cold Case Victim with Lead, Strontium, Carbon, and Oxygen Isotopes.” *Annals of Anthropological Practice* 38 (1): 137–54. https://doi.org/10.1111/napa.12048.
Katzenberg, M. Anne. 2007. “Stable Isotope Analysis: A Tool for Studying Past Diet, Demography, and Life History.” In *Biological Anthropology of the Human Skeleton: Second Edition*, edited by Katzenberg MA and Saunders SR, 2nd ed. Hoboken, NJ: John Wiley & Sons, Inc. https://doi.org/10.1002/9780470245842.ch13.
Katzenberg, M. Anne, and H. Roy Krouse. 1989. “Application of Stable Isotope Variation in Human Tissues to Problems in Identification.” *Journal of the Canadian Society of Forensic Science* 22 (1): 7–19. https://doi.org/10.1080/00085030.1989.10757414.
Klinken, Gert J. Van, Mike P. Richards, and Bert E. M. Hedges. 2002. “An Overview of Causes for Stable Isotopic Variations in Past European Human Populations: Environmental, Ecophysiological, and Cultural Effects.” In *Biogeochemical Approaches to Paleodietary Analysis*, 39–63. https://doi.org/10.1007/0-306-47194-9_3.
Knudson, Kelly J., and J. E. Buikstra. 2007. “Residential Mobility and Resource Use in the Chiribaya Polity of Southern Peru: Strontium Isotope Analysis of Archaeological Tooth Enamel and Bone.” *International Journal of Osteoarchaeology* 17 (6): 563–80. https://doi.org/10.1002/oa.916.
Knudson, Kelly J., Tiffiny A. Tung, Kenneth C. Nystrom, T. Douglas Price, and Paul D. Fullagar. 2005. “The Origin of the Juch’uypampa Cave Mummies: Strontium Isotope Analysis of Archaeological Human Remains from Bolivia.” *Journal of Archaeological Science* 32 (6): 903–13. https://doi.org/10.1016/j.jas.2005.01.007.
Knudson, Kelly J., Sloan R. Williams, Rebecca Osborn, Kathleen Forgey, and Patrick Ryan Williams. 2009. “The Geographic Origins of Nasca Trophy Heads Using Strontium, Oxygen,

and Carbon Isotope Data." *Journal of Anthropological Archaeology* 28 (2): 244–57. https://doi.org/10.1016/j.jaa.2008.10.006.

Kohn, Matthew J., Margaret J. Schoeninger, and John W. Valley. 1996. "Herbivore Tooth Oxygen Isotope Compositions: Effects of Diet and Physiology." *Geochimica et Cosmochimica Acta* 60 (20): 3889–96. https://doi.org/10.1016/0016-7037(96)00248-7.

Kootker, Lisette M, Esther Plomp, Saskia T M Ammer, Vera Hoogland, and Gareth R Davies. 2020. "Spatial Patterns in $^{87}Sr/^{86}Sr$ Ratios in Modern Human Dental Enamel and Tap Water from the Netherlands: Implications for Forensic Provenancing." *Science of The Total Environment* 729: 138992.

Kootker, Lisette M., Isabella C.C. von Holstein, Jelle Broeders, Daniel J. Wescott, Gareth R. Davies, and Hayley L. Mickleburgh. 2020. "The Effects of Decomposition and Environment on Antemortem H-Pb-Sr Isotope Compositions and Degradation of Human Scalp Hair: Actualistic Taphonomic Observations." *Forensic Science International* 312 (110336). https://doi.org/https://doi.org/10.1016/j.forsciint.2020.110336.

Kootker, Lisette M., Rowin J. van Lanen, Henk Kars, and Gareth R. Davies. 2016. "Strontium Isoscapes in The Netherlands. Spatial Variations in $^{87}Sr/^{86}Sr$ as a Proxy for Palaeomobility." *Journal of Archaeological Science: Reports* 6: 1–13. https://doi.org/10.1016/j.jasrep.2016.01.015.

Kramer, RT, EJ Bartelink, NP Herrmann, MK Spradley, and CP. Bataille. 2020. "Application of Stable Isotopes and Geostatistics to Infer Region of Geographic Origin for Deceased Unidentified Latin American Migrants. Chapter Submitted." In *Humanitarian Forensic Science: Interacting with the Dead and the Living.*, edited by Roberto C. Parra, Sara C. Zapico, and Douglas H. Ubelaker. Wiley & Sons, Inc.

Krause, Karoline, and Kerstin Foitzik. 2006. "Biology of the Hair Follicle: The Basics." *Seminars in Cutaneous Medicine and Surgery* 25: 2–10. https://doi.org/10.1016/j.sder.2006.01.002.

Krouse, H.R., and V.A. Grinenko. 1991. *Stable Isotopes: Natural and Anthropogenic Sulphur in the Environment*. United Kingdom: John Wiley and Sons.

Krueger, Harold W., and Charles H. Sullivan. 1984. "Models for Carbon Isotope Fractionation Between Diet and Bone." In *Stable Isotopes in Nutrition*, 205–220. https://doi.org/10.1021/bk-1984-0258.ch014.

Lachniet, Matthew S., and William P. Patterson. 2002. "Stable Isotope Values of Costa Rican Surface Waters." *Journal of Hydrology* 260 (1–4): 135–50. https://doi.org/10.1016/S0022-1694(01)00603-5.

Lachniet, Matthew S., William P. Patterson, Steve Burns, Yemane Asmerom, and Victor Polyak. 2007. "Caribbean and Pacific Moisture Sources on the Isthmus of Panama Revealed from Stalagmite and Surface Water $\delta^{18}O$ Gradients." *Geophysical Research Letters* 34 (1). https://doi.org/10.1029/2006GL028469.

Laffoon, Jason E., Till F. Sonnemann, Termeh Shafie, Corinne L. Hofman, Ulrik Brandes, and Gareth R. Davies. 2017. "Investigating Human Geographic Origins Using Dual-Isotope (87 Sr/86 Sr, Ä18 O) Assignment Approaches." *PLoS ONE* 12 (2). https://doi.org/10.1371/journal.pone.0172562.

Lee-Thorp, J. 2002. "Two Decades of Progress towards Understanding Fossilization Processes and Isotopic Signals in Calcified Tissue Minerals." *Archaeometry* 44 (3): 435–46. https://doi.org/10.1111/1475-4754.t01-1-00076.

Lee-Thorp, J. A. 2008. "On Isotopes and Old Bones." *Archaeometry* 50 (6): 925–50. https://doi.org/10.1111/j.1475-4754.2008.00441.x.

Lee-Thorp, Julia A., Judith C. Sealy, and Nikolaas J. van der Merwe. 1989. "Stable Carbon Isotope Ratio Differences between Bone Collagen and Bone Apatite, and Their Relationship to Diet." *Journal of Archaeological Science* 16 (6): 585–99. https://doi.org/10.1016/0305-4403(89)90024-1.

Lehn, C., and M. Graw. 2014. "Stabilisotopenanalysen an Körpergeweben von Unbekannten

Personen: Grundlagen, Probennahme, Analysen, Interpretation." *Rechtsmedizin* 24 (2): 129–43. https://doi.org/10.1007/s00194-014-0946-5.

Lehn, C., and M. Graw. 2016. "Identifizierung Einer Skelettierten „Kofferleiche" Aus Berlin." *Rechtsmedizin* 26 (5): 429–35. https://doi.org/10.1007/s00194-016-0091-4.

Lehn, Christine, Eva Maria Kalbhenn, Andreas Rossmann, and Matthias Graw. 2019. "Revealing Details of Stays Abroad by Sequential Stable Isotope Analyses along Human Hair Strands." *International Journal of Legal Medicine* 133 (3): 935–47. https://doi.org/10.1007/s00414-018-1866-9.

Lehn, Christine, Andreas Rossmann, and Matthias Graw. 2015. "Provenancing of Unidentified Corpses by Stable Isotope Techniques - Presentation of Case Studies." *Science and Justice* 55 (1): 72–88. https://doi.org/10.1016/j.scijus.2014.10.006.

Lehn, Christine, Andreas Rossmann, and Christoph Mayr. 2019. " Stable Isotope Relationships between Apatite Phosphate (δ 18 O), Structural Carbonate (δ^{18}O, δ^{13}C) and Collagen (δ^{2}H, δ^{13}C, δ^{15}N, δ^{34}S) in Modern Human Dentine ." *Rapid Communications in Mass Spectrometry* 26 (3): 2793. https://doi.org/10.1002/rcm.8674.

León, Jason de. 2015. *The Land of Open Graves: Living and Dying on the Migrant Trail*. *The Land of Open Graves*. University of Califrornia Press. https://doi.org/10.1111/ciso.12122.

Longinelli, Antonio. 1984. "Oxygen Isotopes in Mammal Bone Phosphate: A New Tool for Paleohydrological and Paleoclimatological Research?" *Geochimica et Cosmochimica Acta* 48 (2): 385–90. https://doi.org/10.1016/0016-7037(84)90259-X.

Lynnerup, Niels, and Haagen D. Klaus. 2019. "Fundamentals of Human Bone and Dental Biology: Structure, Function, and Development." In *Ortner's Identification of Pathological Conditions in Human Skeletal Remains*, edited by Jane E. Buikstra, 3rd ed., 35–58. Elsevier. https://doi.org/10.1016/C2011-0-06880-1.

Ma, Chao, Hannah B. Vander Zanden, Michael B. Wunder, and Gabriel J. Bowen. 2020. "AssignR : An R Package for Isotope-based Geographic Assignment." *Methods in Ecology and Evolution*, 1–6. https://doi.org/10.1111/2041-210x.13426.

Martin, R. Bruce, David B. Burr, Neil A. Sharkey, and David P. Fyhrie. 2015. *Skeletal Tissue Mechanics*. 2nd ed. Springer New York. https://doi.org/10.1007/978-1-4939-3002-9.

Martínez, Daniel E., Robin C. Reineke, Raquel Rubio-Goldsmith, and Bruce O. Parks. 2014. "Structural Violence and Migrant Deaths in Southern Arizona: Data from the Pima County Office of the Medical Examiner, 1990-2013." *Journal on Migration and Human Security* 2 (4): 257–86. https://doi.org/10.14240/jmhs.v2i4.35.

Martinez, Daniel E., Robin Reineke, Raquel Rubio-Goldsmith, Bruce E. Anderson, Gregory L. Hess, and Bruce O. Parks. 2015. "A Continued Humanitarian Crisis at the Border: Undocumented Border Crosser Deaths Recorded by the Pima County Office of the Medical Examiner, 1990-2012." *SSRN Electronic Journal*. https://doi.org/10.2139/ssrn.2633209.

Massey, Douglas S., Jorge Durand, and Nolan J. Malone. 2002. *Beyond Smoke and Mirrors: Mexican Immigration in an Era of Economic Integration*. Russell Sage Foundation. https://doi.org/10.7758/9781610443821.

Matalová, Eva, Vlasta Lungová, and Paul Sharpe. 2015. "Development of Tooth and Associated Structures." In *Stem Cell Biology and Tissue Engineering in Dental Sciences*, 335–46. https://doi.org/10.1016/B978-0-12-397157-9.00030-8.

McMurry, J., and R. Fay. 2004. "Hydrogen, Oxygen and Water." In *Chemistry*, edited by K.P. Hamann, 4th editio, 575–99. New Jersey: Pearson Education.

Meier-Augenstein, Wolfram. 2018. *Stable Isotope Forensics: An Introduction to the Forensic Application of Stable Isotope Analysis*. *Stable Isotope Forensics: An Introduction to the Forensic Application of Stable Isotope Analysis*. 2nd ed. John Wiley and Sons. https://doi.org/10.1002/9781119080190.

Meier-Augenstein, Wolfram, and Isla Fraser. 2008a. "Forensic Isotope Analysis Leads to Identification of a Mutilated Murder Victim." *Science and Justice* 48 (3): 153–59.

https://doi.org/10.1016/j.scijus.2007.10.010.
Meier-Augenstein, Wolfram, and Isla Fraser. 2008b. “Forensic Isotope Analysis Leads to Identification of a Mutilated Murder Victim.” *Science and Justice*. https://doi.org/10.1016/j.scijus.2007.10.010.
Mekota, Anna Maria, Gisela Grupe, Sandra Ufer, and Ullrich Cuntz. 2006. “Serial Analysis of Stable Nitrogen and Carbon Isotopes in Hair: Monitoring Starvation and Recovery Phases of Patients Suffering from Anorexia Nervosa.” *Rapid Communications in Mass Spectrometry* 20 (10): 1604–10. https://doi.org/10.1002/rcm.2477.
Missing Migrants Project by the United Nations International Organization for Migration. 2018. “Migrant Deaths Remain High Despite Sharp Fall in US-Mexico Border Crossings in 2017,” June 2, 2018. https://www.iom.int/news/migrant-deaths-remain-high-despite-sharp-fall-us-mexico-border-crossings-2017.
Muetzel, Elisabeth, Christine Lehn, Oliver Peschel, Stefan Hoelzl, and Andreas Rossmann. 2009. “Assignment of Unknown Persons to Their Geographical Origin by Determination of Stable Isotopes in Hair Samples.” *International Journal of Legal Medicine* 123 (1): 35–40. https://doi.org/10.1007/s00414-008-0286-7.
Nakamura, K., D. A. Schoeller, F. J. Winkler, and H. -L Schmidt. 1982. “Geographical Variations in the Carbon Isotope Composition of the Diet and Hair in Contemporary Man.” *Biological Mass Spectrometry* 9 (9): 390–94. https://doi.org/10.1002/bms.1200090906.
Nardoto, Gabriela Bielefeld, Steven Silva, Carol Kendall, James R. Ehleringer, Lesley A. Chesson, Epaminondas S.B. Ferraz, Marcelo Z. Moreira, Jean P.H.B. Ometto, and Luiz A. Martinelli. 2006. “Geographical Patterns of Human Diet Derived from Stable-Isotope Analysis of Fingernails.” *American Journal of Physical Anthropology* 131 (1): 137–46. https://doi.org/10.1002/ajpa.20409.
Navarro Chaparro, Karina, Patricia Rivera, and Roberto Sánchez. 2016. “Water Management Analysis of the City of Tijuana Baja California: Critical Factors and Challenges.” *Estudios Fronterizos, Nueva Época* 17 (33): 20.
Négrel, Ph, and E. Petelet-Giraud. 2005. “Strontium Isotopes as Tracers of Groundwater-Induced Floods: The Somme Case Study (France).” *Journal of Hydrology* 305 (1–4): 99–119. https://doi.org/10.1016/j.jhydrol.2004.08.031.
Nehlich, Olaf. 2015. “The Application of Sulphur Isotope Analyses in Archaeological Research: A Review.” *Earth-Science Reviews*. https://doi.org/10.1016/j.earscirev.2014.12.002.
Nelson, Stanley. 2014. *Wheeler’s Dental Anatomy, Physiology and Occlusion*. 10th ed. Elsevier.
Neuberger, Ferdinand M., Eilin Jopp, Matthias Graw, Klaus Püschel, and Gisela Grupe. 2013. “Signs of Malnutrition and Starvation-Reconstruction of Nutritional Life Histories by Serial Isotopic Analyses of Hair.” *Forensic Science International* 226 (1–3): 22–32. https://doi.org/10.1016/j.forsciint.2012.10.037.
Nigro, Angela, Giuseppe Sappa, and Maurizio Barbieri. 2017. “Strontium Isotope as Tracers of Groundwater Contamination.” *Procedia Earth and Planetary Science* 17: 352–55. https://doi.org/10.1016/j.proeps.2016.12.089.
No More Deaths/ No Mas Muertes. June 16th, 2017. “Border Patrol Raids Humanitarian Aid Camp in Targeted Attack.” Press Release. Accessed September 27, 2020. https://nomoredeaths.org/en/.
O’Connell, T. C., R. E.M. Hedges, M. A. Healey, and A. H.R.W. Simpson. 2001. “Isotopic Comparison of Hair, Nail and Bone: Modern Analyses.” *Journal of Archaeological Science* 28 (11): 1247–55. https://doi.org/10.1006/jasc.2001.0698.
O’Connell, T. C., C. J. Kneale, N. Tasevska, and G. G.C. Kuhnle. 2012. “The Diet-Body Offset in Human Nitrogen Isotopic Values: A Controlled Dietary Study.” *American Journal of Physical Anthropology* 149 (3): 426–34. https://doi.org/10.1002/ajpa.22140.
Ortner, Donald J. 2003. *Identification of Pathological Conditions in Human Skeletal Remains*. Edited by Donald J. Ortner. *Identification of Pathological Conditions in Human Skeletal*

Remains. Elsevier Inc. https://doi.org/10.1016/B978-0-12-528628-2.X5037-6.
Pearson, Osbjorn M., and Daniel E. Lieberman. 2004. "The Aging of Wolff's 'Law': Ontogeny and Responses to Mechanical Loading in Cortical Bone." *Yearbook of Physical Anthropology*. https://doi.org/10.1002/ajpa.20155.
Pechey, Rachel, and Pablo Monsivais. 2016. "Socioeconomic Inequalities in the Healthiness of Food Choices: Exploring the Contributions of Food Expenditures." *Preventive Medicine* 88: 203–9. https://doi.org/10.1016/j.ypmed.2016.04.012.
Petzke, Klaus J., Heiner Boeing, and Cornelia C. Metges. 2005. "Choice of Dietary Protein of Vegetarians and Omnivores Is Reflected in Their Hair Protein ^{13}C and ^{15}N Abundance." *Rapid Communications in Mass Spectrometry* 19 (11): 1392–1400. https://doi.org/10.1002/rcm.1925.
Petzke, Klaus J., Benjamin T. Fuller, and Cornelia C. Metges. 2010. "Advances in Natural Stable Isotope Ratio Analysis of Human Hair to Determine Nutritional and Metabolic Status." *Current Opinion in Clinical Nutrition and Metabolic Care* 13 (5): 532–40. https://doi.org/10.1097/MCO.0b013e32833c3c84.
Pima County Office of the Medical Examiner. 2018. "Annual Report 2018."
Plomp, Esther, Isabella C.C. von Holstein, Lisette M. Kootker, Suzanne J.A. Verdegaal-Warmerdam, Tim Forouzanfar, and Gareth R. Davies. 2020. "Strontium, Oxygen, and Carbon Isotope Variation in Modern Human Dental Enamel." *American Journal of Physical Anthropology* 172 (4): 586–604. https://doi.org/10.1002/ajpa.24059.
Price, T. Douglas, James H. Burton, Paul D. Fullagar, Lori E. Wright, Jane E. Buikstra, and Vera Tiesler. 2008. "Strontium Isotopes and the Study of Human Mobility in Ancient Mesoamerica." *Latin American Antiquity* 19 (2): 167–80. https://doi.org/10.1017/S1045663500007781.
Price, T. Douglas, James H. Burton, Paul D. Fullagar, Lori E. Wright, Jane E. Buikstra, and Vera Tiesler. 2015. "Strontium Isotopes and the Study of Human Mobility Among the Ancient Maya." In *Archaeology and Bioarchaeology of Population Movement among the Prehispanic Maya*, 119–132. https://doi.org/10.1007/978-3-319-10858-2_11.
Price, T. Douglas, Clark M. Johnson, Joseph A. Ezzo, Jonathan Ericson, and James H. Burton. 1994. "Residential Mobility in the Prehistoric Southwest United States: A Preliminary Study Using Strontium Isotope Analysis." *Journal of Archaeological Science* 21 (3): 315–30. https://doi.org/10.1006/jasc.1994.1031.
Price, T. Douglas, Linda Manzanilla, and William D. Middleton. 2000. "Immigration and the Ancient City of Teotihuacan in Mexico: A Study Using Strontium Isotope Ratios in Human Bone and Teeth." *Journal of Archaeological Science* 27 (10): 903–13. https://doi.org/10.1006/jasc.1999.0504.
Primrose, S., M. Woolfe, and S. Rollinson. 2010. "Food Forensics: Methods for Determining the Authenticity of Foodstuffs." *Trends in Food Science and Technology* 21 (12): 582–90. https://doi.org/10.1016/j.tifs.2010.09.006.
R Core Team. 2020. "The R: A Language and Environment for Statistical Computing. Vienna, Austria: R Foundation for Statistical Computing." 2020. http://r-project.org/.
Rauch, Elisabeth, Susanne Rummel, Christine Lehn, and Andreas Buettner. 2007. "Origin Assignment of Unidentified Corpses by Use of Stable Isotope Ratios of Light (Bio-) and Heavy (Geo-) Elements-A Case Report." *Forensic Science International* 168 (2–3): 215–18. https://doi.org/10.1016/j.forsciint.2006.02.011.
Regan, L. A. 2006. "Isotopic Determination of Region of Origin in Modern People: Applications for Identification of US War-Dead from the Vietnam Conflict." Florida University, Gainesville.
Reineke, Robin Christine. 2016. "Naming the Dead: Identification and Ambiguity Along the U.S.-Mexico Border." The University of Arizona.
Reitsema, Laurie J. 2013. "Beyond Diet Reconstruction: Stable Isotope Applications to Human

Physiology, Health, and Nutrition." *American Journal of Human Biology* 25 (4): 445–56. https://doi.org/10.1002/ajhb.22398.
Reitsema, Laurie J. 2015. "Laboratory and Field Methods for Stable Isotope Analysis in Human Biology." *American Journal of Human Biology* 27 (5): 593–604. https://doi.org/10.1002/ajhb.22754.
Remien, Christopher H., Frederick R. Adler, Lesley A. Chesson, Luciano O. Valenzuela, James R. Ehleringer, and Thure E. Cerling. 2014. "Deconvolution of Isotope Signals from Bundles of Multiple Hairs." *Oecologia* 175 (3): 781–89. https://doi.org/10.1007/s00442-014-2945-3.
Reynard, Linda M., Nicole Burt, Hannah E.C. Koon, and Noreen Tuross. 2016. "Limits and Possibilities in the Geolocation of Humans Using Multiple Isotope Ratios (H, O, N, C) of Hair from East Coast Cities of the USA*." *Isotopes in Environmental and Health Studies* 52 (4–5): 498–512. https://doi.org/10.1080/10256016.2016.1143821.
Richards, M. P., B. T. Fuller, M. Sponheimer, T. Robinson, and L. Ayliffe. 2003. "Sulphur Isotopes in Palaeodietary Studies: A Review and Results from a Controlled Feeding Experiment." In *International Journal of Osteoarchaeology, Special Issue: Bone Chemistry*, 37–45. https://doi.org/10.1002/oa.654.
Rickard, David. 2012. "Sedimentary Sulfur Isotope Biogeochemistry." In *Developments in Sedimentology*, 419–73. https://doi.org/10.1016/B978-0-444-52989-3.00011-8.
Ritchie, Hannah, and Max Roser. 2017. "Meat and Dairy Production." *Our World in Data*.
Rodan, G. A., and T. J. Martin. 2000. "Therapeutic Approaches to Bone Diseases." *Science* 289 (5484): 1508–14. https://doi.org/10.1126/science.289.5484.1508.
Rodríguez, Francisco A. Bernal. 2005. "Retos Internacionales Para El Manejo Del Agua Del Bajo Río Colorado." In *Seguridad, Agua y Desarrollo: El Futuro de La Frontera México-Estados Unidos*, edited by Alfonso Andrés Cortez Lara, Scott Whiteford, and Manuel Chávez Márquez, 365–415. El Colegio de la Frontera Norte.
Ropp, R.C. 2013. "The Alkaline Earths as Metals." In *Encyclopedia of the Alkaline Earth Compounds*. https://doi.org/10.1016/b978-0-444-59550-8.00001-6.
Ross, Michael H., and Wojciech Pawlina. 2010. *Histology: A Text and Atlas*. 6th ed. Lippincott Williams & Wilkins.
Rozanski, Kazimierz, Luis Araguás-Araguás, and Roberto Gonfiantini. 1993. "Isotopic Patterns in Modern Global Precipitation." In *Climate Change in Continental Isotopic Records*, edited by P. K. Swart K. C. Lohmann J. Mckenzie S. Savin, 78th ed., 1–36. https://doi.org/10.1029/gm078p0001.
Rummel, Susanne, Stefan Hölzl, and Peter Horn. 2007. "Isotopensignaturen von Bio- Und Geo-Elementen in Der Forensik." In *Biologische Spurenkunde, Band 1: Kriminalbiologie*, edited by Bernd Herrmann and Klaus-Steffen Saternus, 381–407. Springer Berlin Heidelberg. https://doi.org/10.1007/978-3-540-71111-7_18.
Santamaria-Fernandez, Rebeca, Justo Giner Martínez-Sierra, J. M. Marchante-Gayón, J. Ignacio García-Alonso, and Ruth Hearn. 2009. "Measurement of Longitudinal Sulfur Isotopic Variations by Laser Ablation MC-ICP-MS in Single Human Hair Strands." *Analytical and Bioanalytical Chemistry* 394 (1): 225–33. https://doi.org/10.1007/s00216-009-2615-1.
Schimmelmann, Arndt, and Peter E. Sauer. 2018. "Hydrogen Isotopes." In *Encyclopedia of Geochemistry. Encyclopedia of Earth Sciences Series*, edited by W. M. White. Springer, Cham. https://doi.org/10.1007/978-3-319-39312-4_326.
Schoeller, Dale A. 1999. "Isotope Fractionation: Why Aren't We What We Eat?" *Journal of Archaeological Science* 26 (6): 667–73. https://doi.org/10.1006/jasc.1998.0391.
Schoeninger, Margaret J, and Katherine Moore. 1992. "Bone Stable Isotope Studies in Archaeology." *Journal of World Prehistory* 6 (2): 247–96. https://doi.org/https://doi.org/10.1007/BF00975551.
Schoeninger, Margaret J., Michael J. Deniro, and Henrik Tauber. 1983. "Stable Nitrogen Isotope Ratios of Bone Collagen Reflect Marine and Terrestrial Components of Prehistoric Human

Diet." *Science* 220 (4604): 1381–83. https://doi.org/10.1126/science.6344217.
Schwarcz, Henry P., and Margaret J. Schoeninger. 1991. "Stable Isotope Analyses in Human Nutritional Ecology." *American Journal of Physical Anthropology* 34 (13S): 283–321. https://doi.org/10.1002/ajpa.1330340613.
Schweissing, Matthew Mike, and Gisela Grupe. 2003. "Stable Strontium Isotopes in Human Teeth and Bone: A Key to Migration Events of the Late Roman Period in Bavaria." *Journal of Archaeological Science* 30 (11): 1373–83. https://doi.org/10.1016/S0305-4403(03)00025-6.
Sealy, J. C., N. J. van der Merwe, A. Sillen, F. J. Kruger, and H. W. Krueger. 1991. "87Sr86Sr as a Dietary Indicator in Modern and Archaeological Bone." *Journal of Archaeological Science* 18 (3): 399–416. https://doi.org/10.1016/0305-4403(91)90074-Y.
Secretariado Ejecutivo del Sistema Nacional de Seguridad Pública. 2018. "Registro Nacional de Datos de Personas Extraviadas o Desaparecidas." *Https://Www.Gob.Mx/Sesnsp/Acciones-y-Programas/Registro-Nacional-de-Datos-de-Personas-Extraviadas-o-Desaparecidas-Rnped*. https://www.gob.mx/sesnsp/acciones-y-programas/registro-nacional-de-datos-de-personas-extraviadas-o-desaparecidas-rnped.
Shand, P., D. P.F. Darbyshire, A. J. Love, and W. M. Edmunds. 2009. "Sr Isotopes in Natural Waters: Applications to Source Characterisation and Water-Rock Interaction in Contrasting Landscapes." *Applied Geochemistry* 24 (4): 574–86. https://doi.org/10.1016/j.apgeochem.2008.12.011.
Sharpe, Ashley E., George D. Kamenov, Adrian Gilli, David A. Hodell, Kitty F. Emery, Mark Brenner, and John Krigbaum. 2016. "Lead (Pb) Isotope Baselines for Studies of Ancient Human Migration and Trade in the Maya Region." *PLoS ONE*. https://doi.org/10.1371/journal.pone.0164871.
Sillen, Andrew, Grant Hall, and Richard Armstrong. 1995. "Strontium Calcium Ratios (Sr/Ca) and Strontium Isotopic Ratios ($^{87}Sr/^{86}Sr$) of Australopithecus Robustus and Homo Sp. from Swartkrans." *Journal of Human Evolution* 28 (3): 277–85. https://doi.org/10.1006/jhev.1995.1020.
Smith, B Holly. 1991. "Standards of Human Tooth Formation and Dental Age Assessment." In *Advances in Dental Anthropology*, edited by M. A. Kelley and C. S. Larsen, 143–68. John Wiley and Sons Ltd. https://doi.org/10.1002/ajhb.1310030624.
Smits, Jeroen, and Iñaki Permanyer. 2019. "The Subnational Human Development Database." *Scientific Data* 6 (1): 190038. https://doi.org/10.1038/sdata.2019.38.
Spradley, M. Katherine. 2014. "Toward Estimating Geographic Origin of Migrant Remains along the United States-Mexico Border." *Annals of Anthropological Practice* 38 (1): 101–10. https://doi.org/10.1111/napa.12045.
Spradley, M. Katherine, Nicholas P. Herrmann, Courtney B. Siegert, and Chloe P. McDaneld. 2019. "Identifying Migrant Remains in South Texas: Policy and Practice." *Forensic Sciences Research* 4 (1): 60–68. https://doi.org/10.1080/20961790.2018.1497437.
Stack, M.V. 1967. "Chemical Organization of the Organic Matrix of Enamel: Volume 2." In *Structural and Chemical Organization of Teeth*, edited by Albert Edward William Miles and John Highet Allan, 317–46. New York and London: Academic Press.
Steele, K. W., and R. M. Daniel. 1978. "Fractionation of Nitrogen Isotopes by Animals: A Further Complication to the Use of Variations in the Natural Abundance of ^{15}N for Tracer Studies." *The Journal of Agricultural Science* 90 (1): 7–9. https://doi.org/10.1017/S002185960004853X.
Stewart, Brian W., Rosemary C. Capo, and Oliver A. Chadwick. 1998. "Quantitative Strontium Isotope Models for Weathering, Pedogenesis and Biogeochemical Cycling." *Geoderma* 82 (1–3): 173–95. https://doi.org/10.1016/S0016-7061(97)00101-8.
Stull, Kyra E., Eric J. Bartelink, Alexandra R. Klales, Gregory E. Berg, Michael W.Ericka N. L'Abbé Kenyhercz, Matthew C. Go, Kyle McCormick, and Carlos Mariscal. n.d. "Commentary on: Bethard JD, DiGangi EA. Letter to the Editor—Moving beyond a Lost

Cause: Forensic Anthropology and Ancestry Estimates in the United States." *Journal of Forensic Sciences*.
The Food and Agriculture Organization of the United Nations. 2014. "AQUASTAT Perfil de País - Mexico." Rome, Italy. http://www.fao.org/3/ca0444es/CA0444ES.pdf.
Thompson, Alexandra H., L. A. Chesson, D. W. Podlesak, G. J. Bowen, T. E. Cerling, and J. R. Ehleringer. 2010. "Stable Isotope Analysis of Modern Human Hair Collected from Asia (China, India, Mongolia, and Pakistan)." *American Journal of Physical Anthropology* 141 (3): 440–51. https://doi.org/10.1002/ajpa.21162.
Thornton, Erin Kennedy. 2011. "Reconstructing Ancient Maya Animal Trade through Strontium Isotope ($^{87}Sr/^{86}Sr$) Analysis." *Journal of Archaeological Science* 38 (12): 3254–63. https://doi.org/10.1016/j.jas.2011.06.035.
Tieszen, Larry L., and Tim Fagre. 1993. "Effect of Diet Quality and Composition on the Isotopic Composition of Respiratory CO2, Bone Collagen, Bioapatite, and Soft Tissues." In *Prehistoric Human Bone*, edited by Joseph B. Lambert and Gisela Grupe, 121–55. Springer Berlin Heidelberg. https://doi.org/10.1007/978-3-662-02894-0_5.
Tipple, B J. 2015. "Isotope Analyses of Hair as a Trace Evidence Tool to Reconstruct Human Movements: Combining Strontium Isotope with Hydrogen/Oxygen Isotope Data," 1–50.
Tipple, Brett J., Luciano O. Valenzuela, Thuan H. Chau, Lihai Hu, Clement P. Bataille, Lesley A. Chesson, and James R. Ehleringer. 2019. "Strontium Isotope Ratios of Human Hair from the United States: Patterns and Aberrations." *Rapid Communications in Mass Spectrometry* 33 (5): 461–72. https://doi.org/10.1002/rcm.8378.
Tipple, Brett J., Luciano O. Valenzuela, and James R. Ehleringer. 2018. "Strontium Isotope Ratios of Human Hair Record Intra-City Variations in Tap Water Source." *Scientific Reports* 8 (1): 3334. https://doi.org/10.1038/s41598-018-21359-0.
Tipple, Brett J., Thuan Chau, Lesley A. Chesson, Diego P. Fernandez, and James R. Ehleringer. 2013. "Isolation of Strontium Pools and Isotope Ratios in Modern Human Hair." *Analytica Chimica Acta* 798 (September 2015): 64–73. https://doi.org/10.1016/j.aca.2013.08.054.
Tykot, Robert H. 2006. "Isotope Analyses and the Histories of Maize." In *Histories of Maize: Multidisciplinary Approaches to the Prehistory, Linguistics, Biogeography, Domestication, and Evolution of Maize*, edited by John E. Staller, Robert H. Tykot, and Bruce F. Benz, 1st ed., 131–42. Elsevier Academic Press. https://doi.org/10.1016/b978-012369364-8/50262-x.
Ubelaker, Douglas H., and Caroline Francescutti. 2020. "The Role of Stable Isotope Analysis in Forensic Anthropology." In *Forensic Science and Humanitarian Action*, 273–84. https://doi.org/10.1002/9781119482062.ch19.
Ubelaker, Douglas H. 2018. "A History of Forensic Anthropology." *American Journal of Physical Anthropology* 165 (4): 915–23. https://doi.org/10.1002/ajpa.23306.
Unger, Kurt. 2005. "Regional Economic Development and Mexican Out-Migration."
United Nations. 2008. "Sustainable Development Goals- Latin American Clean Water Initiative." https://sustainabledevelopment.un.org/partnership/?p=1567.
United Nations General Assembly. 1948. *Universal Declaration of Human Rights (217 [III] A)*. http://www.un.org/en/universal-declaration-human-rights/.
United States Department of the Interior- U.S. Geological Survey. 2007. "North America Elevation 1-Kilometer Resolution." Commission for Environmental Cooperation (Canada), National Atlas of the United States, the Instituto Nacional de Estadística y Geografía (Mexico). https://www.usgs.gov/centers/eros/science/usgs-eros-archive-digital-elevation-global-30-arc-second-elevation-gtopo30?qt-science_center_objects=0#qt-science_center_objects.
United States Supreme Court. 1993. "Daubert v Merrell Dow Pharmaceuticals, Inc [1993]." *The Encyclopedia of Civil Liberties in America*.
Valenzuela, Luciano O., Lesley A. Chesson, Gabriel J. Bowen, Thure E. Cerling, and James R. Ehleringer. 2012. "Dietary Heterogeneity among Western Industrialized Countries

Reflected in the Stable Isotope Ratios of Human Hair." *PLoS ONE* 7 (3). https://doi.org/10.1371/journal.pone.0034234.
Valenzuela, Luciano O., Lesley A. Chesson, Shannon P. O'Grady, Thure E. Cerling, and James R. Ehleringer. 2011. "Spatial Distributions of Carbon, Nitrogen and Sulfur Isotope Ratios in Human Hair across the Central United States." *Rapid Communications in Mass Spectrometry* 25 (7): 861–68. https://doi.org/10.1002/rcm.4934.
Valkovic, V., D. Rendic, and G. C. Phillips. 1975. "Elemental Ratios along Human Hair as Indicators of Exposure to Environmental Pollutants." *Environmental Science and Technology* 9 (13): 1150–52. https://doi.org/10.1021/es60111a006.
Vautour, Geneviève, André Poirier, and David Widory. 2015. "Tracking Mobility Using Human Hair: What Can We Learn from Lead and Strontium Isotopes?" *Science and Justice* 55 (1): 63–71. https://doi.org/10.1016/j.scijus.2014.10.001.
Wadleigh, M. A., H. P. Schwarcz, and J. R. Kramer. 1994. "Sulphur Isotope Tests of Seasalt Correction Factors in Precipitation: Nova Scotia, Canada." *Water, Air, & Soil Pollution* 77 (1–2): 1–6. https://doi.org/10.1007/BF00483047.
Wagner, Thomas, Clayton R Magill, and Jens O Herrle. 2018. "Carbon Isotopes." In *Encyclopedia of Geochemistry: A Comprehensive Reference Source on the Chemistry of the Earth*, edited by William M White, 194–204. Cham: Springer International Publishing. https://doi.org/10.1007/978-3-319-39312-4_176.
Waldron, Tony. 2008. *Palaeopathology*. *Palaeopathology*. Cambridge University Press. https://doi.org/10.1017/CBO9780511812569.
Warner, Monica M., Amber M. Plemons, Nicholas P. Herrmann, and Laura A. Regan. 2018. "Refining Stable Oxygen and Hydrogen Isoscapes for the Identification of Human Remains in Mississippi,." *Journal of Forensic Sciences* 63 (2): 395–402. https://doi.org/10.1111/1556-4029.13575.
Wassenaar, L. I., S. L. Van Wilgenburg, K. Larson, and K. A. Hobson. 2009. "A Groundwater Isoscape (δ^2H, δ^{18}O) for Mexico." *Journal of Geochemical Exploration* 102 (3): 123–36. https://doi.org/10.1016/j.gexplo.2009.01.001.
West, Jason B., Gabriel J. Bowen, Todd E. Dawson, and Kevin P. Tu. 2010. *Isoscapes: Understanding Movement, Pattern, and Process on Earth through Isotope Mapping*. *Isoscapes: Understanding Movement, Pattern, and Process on Earth Through Isotope Mapping*. https://doi.org/10.1007/978-90-481-3354-3.
White, Christine D., T. Douglas Price, and Fred J. Longstaffec. 2007. "Residential Histories of the Human Sacrifices at the Moon Pyramid, Teotihuacan: Evidence from Oxygen and Strontium Isotopes." *Ancient Mesoamerica* 18 (1): 159–72. https://doi.org/10.1017/S0956536107000119.
White, Tim D., Michael T. Black, and Pieter A. Folkens. 2011. *Human Osteology: Third Edition*. *Human Osteology: Third Edition*. 3rd ed. Academic Press.
Wild, E. M., K. A. Arlamovsky, R. Golser, W. Kutschera, A. Priller, S. Puchegger, W. Rom, P. Steier, and W. Vycudilik. 2000. "14C Dating with the Bomb Peak: An Application to Forensic Medicine." *Nuclear Instruments and Methods in Physics Research, Section B: Beam Interactions with Materials and Atoms* 172 (1–4): 944–50. https://doi.org/10.1016/S0168-583X(00)00227-5.
World Bank- World Integrated Trade Solution. 2018. "Mexico Food Products Imports By Country 2018." https://wits.worldbank.org/about_wits.html.
World Bank. 2018. "Mexico- Systematic Country Diagnostics (English)." Washington, D.C.
Wright, Lori E. 2005. "Identifying Immigrants to Tikal, Guatemala: Defining Local Variability in Strontium Isotope Ratios of Human Tooth Enamel." *Journal of Archaeological Science* 32 (4): 555–66. https://doi.org/10.1016/j.jas.2004.11.011.
Wright, Lori E. 2012. "Immigration to Tikal, Guatemala: Evidence from Stable Strontium and Oxygen Isotopes." *Journal of Anthropological Archaeology* 31 (3): 334–52.

https://doi.org/10.1016/j.jaa.2012.02.001.
Wright, Lori E., and Henry P. Schwarcz. 1998. “Stable Carbon and Oxygen Isotopes in Human Tooth Enamel: Identifying Breastfeeding and Weaning in Prehistory.” *American Journal of Physical Anthropology* 106 (1): 1–18. https://doi.org/10.1002/(SICI)1096-8644(199805)106:1<1::AID-AJPA1>3.0.CO;2-W.
Wright, Lori E., and Henry P. Schwarcz.. 1999. “Correspondence between Stable Carbon, Oxygen and Nitrogen Isotopes in Human Tooth Enamel and Dentine: Infant Diets at Kaminaljuyu.” *Journal of Archaeological Science* 26 (9): 1159–70. https://doi.org/10.1006/jasc.1998.0351.
Young Shin, Ji, Tamsin O’Connell, Stuart Black, and Robert Hedges. 2004. “ Differentiating Bone Osteonal Turnover Rates By Density Fractionation; Validation Using the Bomb 14 C Atmospheric Pulse .” *Radiocarbon* 46 (2): 853–61. https://doi.org/10.1017/s0033822200035888.

Impressions from the sampling trip through Mexico

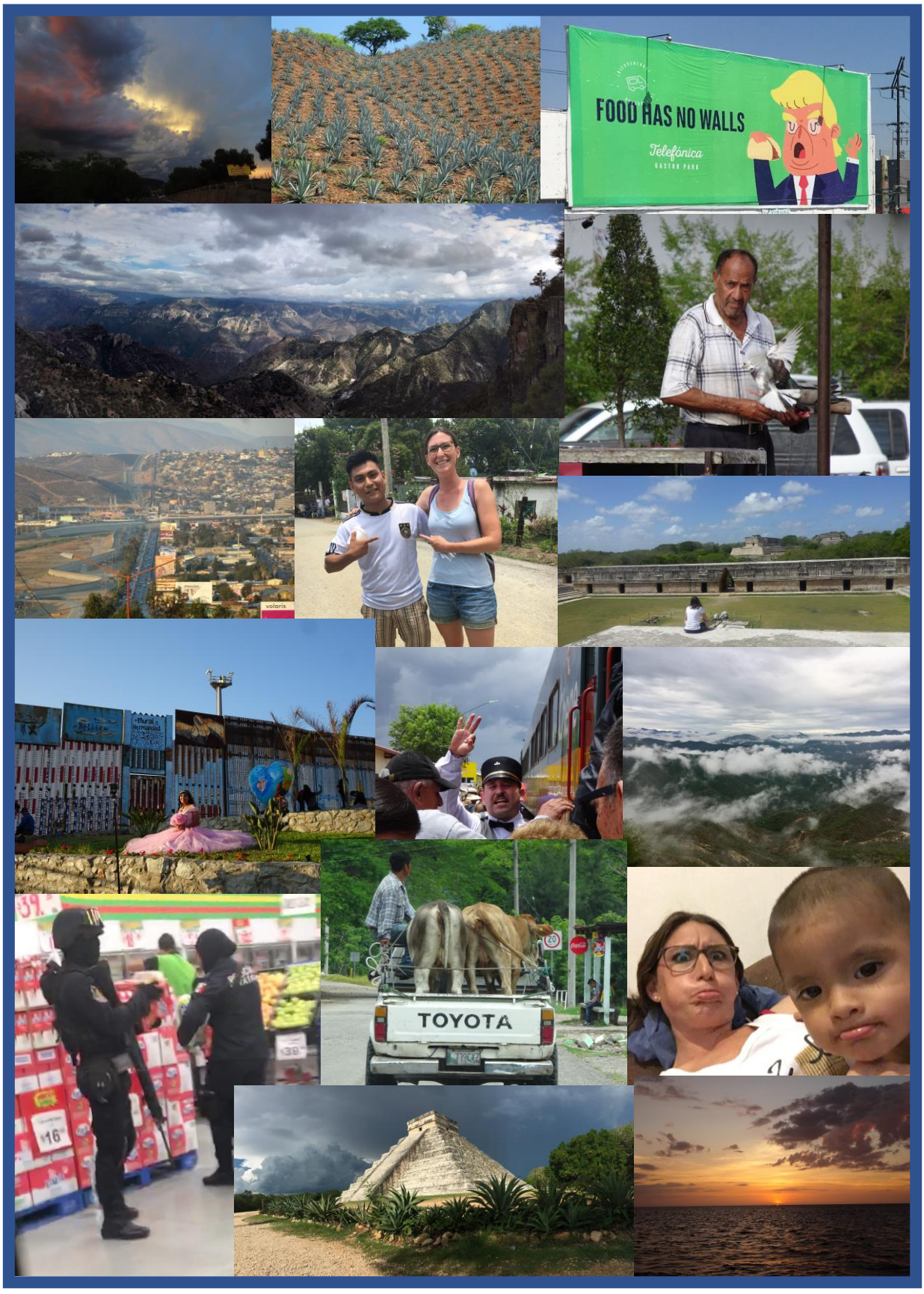

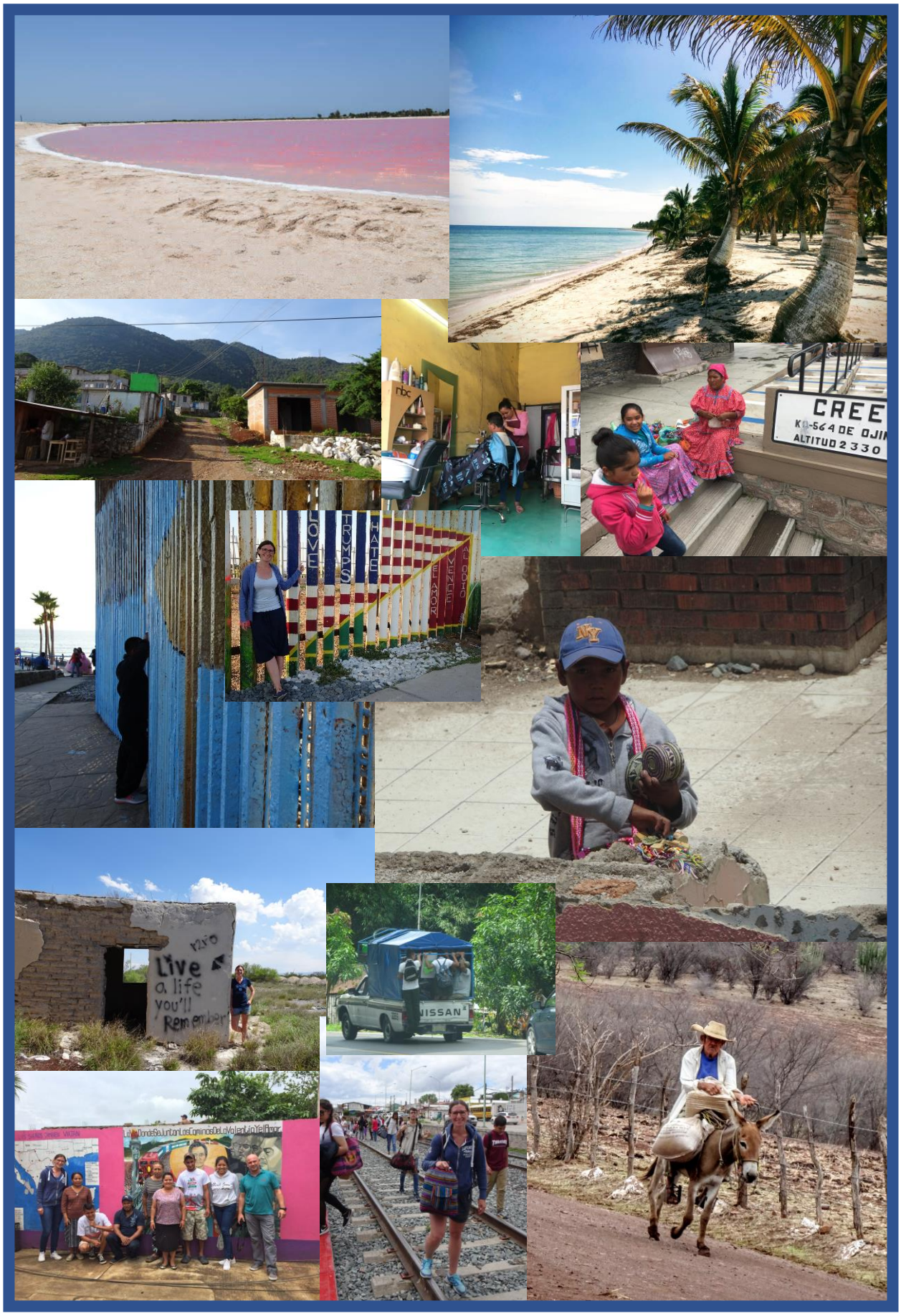
LOVE
HATE
Live
a life
you'll
NISSAN